1-10-2020

# Bioadhesive hydrogel composite cell carrier for the repair of the degenerated intervertebral disc

Thomas Richard Christiani
*Rowan University*

# BIOADHESIVE HYDROGEL COMPOSITE CELL CARRIER FOR THE REPAIR OF THE DEGENERATED INTERVERTEBRAL DISC

by

Thomas Richard Christiani

A Dissertation

Submitted to the
Department of Biomedical Engineering
College of Engineering
In partial fulfillment of the requirement
For the degree of
Doctor of Philosophy
at
Rowan University
April 27, 2018

Dissertation Chair: Andrea Jennifer Vernengo, Ph.D.

## Dedication

This dissertation is dedicated to my parents. I would not have succeeded without their continuous support throughout the doctoral program. Thank you so much for everything, Mom and Dad.

**Acknowledgments**

To my family, I am forever grateful for your continuing support throughout my graduate studies. Mom, Dad, and Vinny, thank you for your kindness, words of encouragement, and reminding me that life doesn't need to be so serious. To my partner Michael, you have been there for me through it all and I am so grateful to have had you with me on this journey. Thank you for listening to me when I needed you most. I love you all so much and I don't know what I would have done without you. I hope I have made you all proud.

To my advisor, Andrea you have been and will always be an amazing teacher, mentor, lab mate, and friend. You have been a huge inspiration to me, and I would not have finished this Ph.D. without your encouragement, guidance, and wisdom. I will miss working with you and I want to wish you the best in the future. To my supportive friends and fellow colleagues: David Brennan, Julian Bello, Laura Osorno, and Trang Vu, you all have been so helpful to me in understanding my own research. Getting to know each and everyone one of you has made me appreciate our different walks in life. I wish you all the best of luck in completing your research and finding what truly makes you happy.

To the technicians: Karl Dyer, Aaron Nolan, and Marvin Harris, you have helped shape my research plans and methods in so many ways. Thank you for helping me tackle aspects of my project that I could not complete on my own. To my committee members: Drs. Cristina Iftode, Mary Staehle, Vince Beachley, Jennifer Kadlowec, and Mark Byrne, thank you for taking the time to be a part of this process. Each of you have been instrumental in the professional development of my career as a student, scientist, or teacher and I really appreciate your guidance.

**Abstract**

Thomas Richard Christiani
BIOADHESIVE HYDROGEL COMPOSITE CELL CARRIER
FOR THE REPAIR OF THE DEGENERATED INTERVERTEBRAL DISC
2017 - 2018
Andrea Jennifer Vernengo, Ph.D.
Doctor of Philosophy

Lower back pain (LBP) affects the worldwide population and can be attributed to the degeneration of the intervertebral disc (IVD). The IVD is composed of a central nucleus pulposus (NP), a peripheral annulus fibrosus (AF), and adjacent cartilage endplates (CEPs). IVD degeneration is characterized by proteoglycan loss, tissue dehydration, and decreased hydrostatic pressure. In this work, the use of an injectable bioadhesive hydrogel composite for replacement of the degenerated NP was investigated. Results indicate that the composite exhibits similar mechanical properties to the NP, adheres to AF tissue, and supports encapsulated mesenchymal stem cell (MSC) differentiation toward an NP-like phenotype in vitro. Additionally, the composite restores biomechanical properties such as range of motion and stiffness and resists expulsion from the injured porcine IVD ex vivo. Lastly, the composite was able to retain viable MSCs which displayed region-specific deposition of biomimetic matrix within the degenerated bovine IVD ex vivo. Tissue engineering scaffolds will play an important clinical role in restoring biomechanical function and prevent transplanted cell leakage, yet none have been designed with adhesive properties to secure the implant in situ. This work is significant in that it represents the development of a novel adhesive that potentially meets the mechanical and adhesive requirements for achieving cellular compatibility, scaffold function, and tissue integration.

## Table of Contents

**Table of Contents (Continued)**

**Table of Contents (Continued)**

**Table of Contents (Continued)**

**Table of Contents (Continued)**

**Table of Contents (Continued)**

## List of Figures

**List of Figures (Continued)**

Figure Page

## List of Figures (Continued)

Figure Page

## List of Figures (Continued)

Figure Page

## List of Figures (Continued)

Figure Page

## List of Figures (Continued)

Figure Page

## List of Tables

# Chapter 1

# Introduction

## 1.1 Motivation

The motivation of this research centers on the repair of the degenerated intervertebral disc (IVD), which is frequently associated with lower back pain (LBP). IVD degeneration is characterized by several changes in morphology such as internal disruption, peripheral tearing, loss in disc height, dehydration, and herniated tissue fragments [1,2,3]. These morphological changes cause nerve root compression, spinal canal narrowing due to stenosis or spondylolisthesis, or facet joint impingement, which ultimately lead to clinical symptoms of neurological deficits, disability, and pain.

At any given time, LBP affects approximately 4 – 33 % of the United States population annually [4]. Approximately 70 – 85 % of individuals will experience some type of LBP within their lifetime [5,6,7]. The estimated mean global lifetime prevalence for LBP is 38.9 % [8,9,10,11]. This type of associated pain is considered one of the leading causes of absence from work compared to any other injury or disease [12,13] and has the greatest impact on the United States health care system due to its high prevalence and influence on disability [14]. Approximately 700,000 spine procedures are performed each year and the rate of these procedures is increasing [15,16,17]. Health care expenditures range from $50 to $90 billion annually [18,19]. Health care demand for treating LBP is on the rise, however disability rates are not improving [20,21].

## 1.2 Project Summary

The IVD is an avascular and alymphatic structure that resembles cartilage tissue. After injury, there is little to no repair activity due to the lack of blood vessels and

immune cells. Further, the tissue is unable to repair itself as the number of viable disc cells declines. Maintenance of the extracellular matrix by disc cells begins to shift from an anabolic to catabolic profile. IVD degeneration is notably characterized by proteoglycan degradation and subsequent dehydration of the nucleus pulposus. Excessive stress is then exerted on the annulus fibrosus leading to the formation of fissures. Consequently, herniation of the nucleus pulposus occurs and impinges on local nerve root endings resulting in radiculopathy.

Treatment for the degenerated disc is dependent on the severity of tissue deterioration. During early stages of degeneration, a conservative approach is implemented to reduce pain and strengthen surrounding back and abdominal muscles to lessen the mechanical demand on the IVD. Conservative treatment typically involves the use of non-steroidal anti-inflammatory drugs or steroidal injections in combination with physical therapy and rest. During moderate stags of degeneration when pain management and rehabilitation become ineffective, fissures in the annulus fibrosus form resulting in nucleus pulposus herniation and ensuing compression of peripheral nerve root endings. A discectomy is performed to remove invading tissue in order to alleviate radiating pain. Late stage degeneration is denoted by a complete loss of biomechanical function and tissue structure and often requires invasive surgery. To stabilize the afflicted joint, a spinal fusion is performed and entails removing the severely degenerated disc tissue and implanting a titanium cage containing a bone graft, thus allowing for the bridging of adjacent vertebrae together. Currently, total disc arthroplasty and nucleus pulposus replacement devices are being investigated as alternative strategies to replace IVD tissues. While these treatment strategies provide some level of pain relief, they are

considered extremely invasive and do not aim to restore natural mechanical or biological function to the joint.

There is an obvious need to improve treatment strategies for repairing the degenerated disc. Tissue engineering is a relatively new area of research that has shown promising results in both animal models and clinical trials in terms of tissue regeneration and functional recovery. Protein delivery can be an effective treatment if disc cells are abundant and present a healthy phenotype, though that is not the case for degenerated tissues. Alternatively, biological function can be substituted by transplanting viable cells into the degenerated disc. The appropriate cell type and origin remains to be determined. Regardless, cell displacement occurs upon injection into the disc. To combat this issue, hydrogels have been proposed as carriers that can encapsulate and deliver cells. Hydrogel carriers are also injectable and can be implanted into the disc in a minimally invasive manner. However, injectable replacements are also prone to dislocation from their implanted site. Therefore, imparting adhesive properties to the cell carrier may have an important impact in the clinical setting and prevent herniation of implanted material.

**1.3 Dissertation Summary**

This work focuses on the evaluation of a bioadhesive hydrogel composite as a tissue engineering replacement for degenerated disc tissues. Chapter 2 describes relevant background information pertaining to LBP and IVD physiology. Existing treatment modalities to repair the degenerated disc and alternative tissue engineering strategies based on protein and cell delivery are also discussed in greater detail. Overall objectives and specific research aims of this project are addressed in Chapter 3.

Chapter 4 focuses on the synthesis and characterization of the bioadhesive hydrogel composite for nucleus pulposus replacement. Composite properties are assessed as a function of microparticle concentration and size. Properties such as swelling, microstructure, degradation, adhesive strength, compressive stiffness, and shear modulus are quantified. Composites that exhibited similar properties to native nucleus pulposus tissue moved on for further biological testing.

Chapter 5 discusses the feasibility of the composites to support the in vitro differentiation of encapsulated adipose-derived mesenchymal stem cells toward a nucleus pulposus phenotype. Cellular viability, metabolic activity, extracellular matrix deposition, and protein and gene expression are analyzed to determine the extent of stem cell differentiation. The composite that exhibited superior mechanical properties from Chapter 4 and supported the differentiation of viable stem cells moved on for further biomechanical testing.

Chapter 6 describes the biomechanical performance of the composite upon injection into an injured ex vivo porcine disc model. Denucleated and mechanically fatigued disc specimen are treated with composite and exposed to cycles of compression-tension. Range of motion and stiffness of the injured and treated disc specimen are analyzed and compared to that of the intact disc. The composite's resistance to expulsion in a denucleated disc during lateral bending is also evaluated.

Chapter 7 highlights the use of the composite as a carrier for the delivery of adipose-derived mesenchymal stem cells into a degenerated ex vivo bovine disc model. First, stem cell viability within the composite after implantation into the degenerated bovine disc is quantified. Site-specific differences in stem cell behavior are compared

between the nucleus pulposus and annulus fibrosus regions. The extent of stem cell differentiation is assessed based on changes in cell morphology and protein expression. Chapter 8 completes the dissertation by providing a summary of conclusions that were drawn from each of the previous chapters.

# Chapter 2

# Background

## 2.1 Spinal Anatomy

The human body is composed of over 200 bones, 33 of which belong to the spine [22]. The spinal column is a complex musculoskeletal structure that is composed of alternating fibrocartilage joints and bony vertebral bodies, which encase and protect the delicate spinal cord. There are five distinct regions of the spinal column: cervical, dorsal (thoracic), lumbar, sacral, and coccygeal (Figure 1). The cervical, dorsal, and lumbar regions each contain 7, 12, and 5 independent vertebrae, respectively. During normal growth and development, the 5 sacral and 4 coccygeal bones fuse together and form the inferior distal units otherwise known as the sacrum and coccyx (Figure 2). When viewed laterally, the spine is an average length of approximately 2 feet and 2 inches and has notable curvatures facing either inward or outward. The shape of the spine also allows for dissipation of compressive load and uniform distribution of body weight [22].

The vertebral bodies of the spine are designed to provide stability under compressive loading. Each vertebral body is unique in that it contains an anterior region called the body and a posterior region called the arch (Figure 3) [22]. Additionally, each arch consists of two pedicles and two laminae which support 7 processes: 4 articular, 2 transverse, and 1 spinous. Bodies of each vertebrae are stacked along the spinal column which support the head and torso. Arches form a hollow cylindrical passageway which allows houses the spinal cord. Vertebrae are connected together by the articular processes and intervertebral discs (Figure 4), while the surrounding back muscles attach to the spinous and transverse processes thus allowing for movement of the trunk (Figure 5)

[23]. Facets joints, also known as zygapophyseal or synovial joints, are formed by the adjacent inferior and superior articular processes. Each of the articular surfaces are covered by a thin layer of hyaline cartilage which permit a sliding motion. The facet joint also contains an inner synovial and outer fibrous membrane, which further lubricates the joint and facilitates movement [24].

Vertebrae are composed of both cortical (compact) and cancellous (trabecular or spongy) bone. Cortical bone is dense, stiff, and provides mechanical strength to support human body weight. Cancellous bone is soft, flexible, and allows for the redirection of applied loads. Vertebral bone is highly vascularized and allows for the diffusion of nutrients to nearby fibrocartilage joints in the spine. Blood supply originates form the aorta and stems from segmental and intercostal arteries [25,26]. Each segmental artery passes through the intervertebral foramina, divides into posterior and anterior radicular arteries, and extends toward the adjacent vertebral body and region of spinal cord. The spinal cord is also supplied by a pair of posterior spinal arteries and a single anterior spinal artery, which originate from the vertebral arteries. These arteries run the length of the surface of the spinal cord [25,26].

**2.2 Intervertebral Disc Anatomy and Biochemistry**

The major constituents of disc tissue are proteoglycans, collagen, and water. Proteoglycans in the IVD are bottlebrush-like structures that contain both glycosaminoglycans (GAG) and aggrecan. GAGs are long chains of unbranched polysaccharide units composed of repeating disaccharide units of an amino acid sugar (N-acetyl glucosamine or N-acetylgalactoseamine) and an uronic acid (D-glucuronic acid or L-iduronic acid). The amino acid sugar unit is usually substituted with a sulfate group,

thus imparting a highly negative charge within the GAG chain. The most common types of GAGs found within proteoglycans of the IVD are chondroitin sulfate, keratin sulfate and heparan sulfate. Aggrecan is a predominant, cartilage-specific protein core that can covalently bond to multiple GAG molecules. The aggrecan core protein has a molecular weight of approximately 250,000 Da and has a high affinity to sequences in hyaluronan and bind via a link protein [27]. Hyaluronan or hyaluronic acid (HA) is a non-sulfated GAG present in connective tissues that exists freely and does not covalently bond as a side chain in proteoglycans [28]. Hyaluronan is an important extracellular matrix component that serves as a ligand for cartilage link protein and aggrecan [29]. A larger proteoglycan complex can form when multiple proteoglycan structures aggregate together and link to a single HA molecule. These complexes increase water retention and provide volume within the ECM to permit diffusion of small molecules and nutrients. Aggregates of PGs can be up to 4 mm long and provide resistance to deformation in load-bearing joints [27].

Collagen is one of the most abundant, insoluble fibrous proteins (25 %) found in mammalian tissues [30]. There are at least 28 types of collagen proteins that have been identified, but roughly 80 – 90 % of collagen in the human body is Type I, II, and III [31]. The collagen proteins are rich in glycine, proline and hydroxyproline amino acid residues. Before the collagen protein is secreted from the cell, the three polypeptide chains twist around one another to form a triple helix secondary structure. Type I collagen is the most abundant protein found in extracellular matrix and is commonly found in skin, tendon, bone and ligaments. The fundamental unit of type I collagen is approximately 300 nm long and 1.5 nm in diameter [32]. Many of these collagen

molecules pack together to form fibrils with a diameter of 50 – 200 nm. Type II collagen is the major fibrous protein found in cartilaginous tissues. Type II fibrils are smaller in diameter compared to Type I and are randomly organized alongside proteoglycans in the ECM. Collagen helices can covalently crosslink through lysine residues, which contributes to changes in mechanical properties and stiffening with age.

The IVD joint is comprised of three tissue regions with distinct biochemical, mechanical and cellular properties (Figure 6) [33]. Each IVD is conjoined to both the superior and inferior vertebral bodies via the cartilage endplates (CEP). In the center of the joint is the nucleus pulposus (NP). The peripheral annulus fibrosus (AF) surrounds and contains the central NP. The IVD is responsible for transmitting loads resulting from body weight or physical activity, while also allowing for flexible motion in bending and twisting. In general, IVDs in the lumbar region are between 8 – 10 mm tall and 4 – 5 cm in diameter [34,35,36]. IVDs constitute approximately one-third of the total spinal column length [37].

The superior and inferior CEPs are responsible for joint attachment and help distribute load evenly across the disc [38]. CEPs are essentially thin layers of cartilage that range from 0.6 to 1 mm in thickness [35]. The CEP covers the entirety of the NP but does not completely interface with the peripheral AF. Proteoglycans, type I and type II collagen have all been identified in the CEPs, with higher proportions of GAG compared to hydroxyproline residues [39]. Due to the avascularity of the disc, the tissue must rely on diffusion of small molecules such as glucose for survival [40]. Nutrient transport and waste removal are hindered processes since the CEPs act as barriers between the vertebral bone and the NP and AF. Blood vessels near the peripheral AF and through

vertebral bone are believed to be important routes for nutrient transport to cells within the IVD [41]. More specifically, disc health strictly relies on diffusion of nutrients from the vascular budding through the subchondral bone to the CEP and into nearby NP and AF tissues [42]. Diffusion can be influenced by factors including solute properties and tissue characteristics such as hydration or calcification [43]. IVD chondrocytes in the CEP are like hyaline cartilage because they are rounded and reside within a lacunar space surrounded by a pericellular matrix. The average density of chondrocytes within the CEP is 15 x $10^6$ cells/$cm^3$ [40].

The NP is a jelly-like viscoelastic tissue that transmits load radially when engaged under compression. NP tissue is roughly 70 – 90 % water and gradually decreases with age [44]. The ECM of the NP is approximately 50 % (dry wt.) proteoglycans and 25 % (dry wt.) collagen. The NP contains a loose network of Type II collagen fibers with interwoven proteoglycan molecules [45]. Type II collagen expression gradually declines moving radially outward from the center of the disc. The NP contains other forms of collagen such as types III, IV, and VI [46] as well as other non-collagenous proteins like elastin [47], versican [48], decorin [49,50], biglycan [49,50], fibronectin [51] and laminin [52], but mainly aggrecan [53,54].

Disc tissue is hypoxic, where oxygen concentration is highest at the periphery and lowest at the center of the NP [55]. Cells closet to the CEPs deplete the oxygen before it reaches cells in the NP. Additionally, lactate concentrations are highest at the center of the NP [55]. Due to the acidic environment within the NP, the proteoglycan content may decrease. NP cells are characteristically chondrocyte-like with varying roundness in shape and exist in discrete clusters. NP cells are highly vacuolated at an early age during

childhood and by adolescence these cells become less swollen and shift toward a more chondrocyte-like population [56,57]. The cytoplasm of NP cells tends to be larger and their shape is more complex compared to AF cells. The cell density of the nucleus pulposus is approximately 4 x $10^6$ cells/$cm^3$ [40].

The AF is composed of concentric lamellae of collagen fibers that are orientated at opposing angles. Approximately 50 % of the layers are discontinuous around the circumference of the disc [58]. Fiber bundle thickness tends to increase with increasing distance from the periphery of the disc. The average number of lamellae in the disc can range from 15 to 25. Fiber bundle orientation ranges from 65 to 70 ° and alternates direction with respect to the sagittal plane. Spaces between lamellae are filled with proteoglycan gel, which help bind the collagen fibers together [58]. The uniquely patterned structure provides increased resistance to tensile forces. Tensile properties of the AF are highly dependent on the radial location within the IVD, where the greatest strength is observed along the outer periphery [59,60].

Water content in AF tissue can range from 65 – 80 % and does not appear to change with age [44]. The inner and outer AF contain 60 – 70 % collagen (dry wt.) and 25 % proteoglycans (dry wt.). Collagen fibers are composed of both type I and type II collagen fibers, which help maintain tensile properties of the IVD [61]. Type I collagen is highly expressed in the outer AF and gradually decreases moving radially inward towards the NP. Conversely, the least amount of type II collagen is found at the periphery and increases moving radially inward toward the NP. The outer AF also contains the most densely packed collagen fibers. Cells in the AF are large and oval-shaped with small nuclei packed with rich chromatin. The size of the cells become smaller and flattened

approaching the interior of the IVD [62]. The AF contains approximately 9 x $10^6$ cells/mL and resemble long, thin fibroblasts that align with the collagen fiber bundles [40].

### 2.3 Intervertebral Disc Biomechanics

The NP, AF, and CEPs each play an important role in weight-bearing activities and biomechanics of the IVD joint. The human disc is considered a flexible, viscoelastic tissue structure that maintains stability and mechanical equilibrium within the functional spinal unit, while also permitting complex combinations of movement. Compressive loads are transferred from adjacent vertebral bodies to the IVD tissues. The CEPs act as mechanical mediators and uniformly distribute load across the entire disc [38]. Both the NP and AF work symbiotically to redirect compressive loads toward the vertebral bodies. Overall this mechanism of action helps to transmit loads along the vertebrae of the spinal column with the discs acting as shock absorbers. Discs are able to protect surrounding vertebrae from excessive loading by slowly diverting compressive forces.

The AF participates in withstanding compressive forces exerted on the disc [63]. A healthy AF can tolerate large bulk forces because of its unique ECM structure that contains thick collagen bundles. These collagen proteins vary throughout the AF and lead to differences in mechanical properties, where the inner lamellae are less stiff compared to the outer lamellae [64]. This tissue can work independently and in unison with the NP core. If the NP were to be removed from the disc, the AF is still able to withstand the same axial forces [63]. However, prolonged weight-bearing can be detrimental to the joint. Sustained pressures can cause the AF tissue to buckle and the proteoglycan gel that adheres the lamellae together will no longer hold.

The NP plays an important role in neutral zone mechanics and dampening forces applied to the disc [36]. Since the NP is mainly composed of water, it can be considered an incompressible semi-solid material. Therefore, when a compressive load is exerted on the NP, the tissue will primarily deform radially against the AF rather than change in volume. Radial expansion causes tension of the AF lamellae and an equal and opposite reactive force is reverted to the NP. Similarly, as the NP vertically deforms, the CEPs and trabecular bone bow into the superior and inferior vertebrae. If the CEPs did not exhibit this type of behavior, the disc would experience decreased height, increased radial bulging, and increased tensile strain on the AF [65,66]. Since the NP is completely encompassed, it will remain highly pressurized during compression. The NP will also migrate to the opposite side during bending motions. Segment stability relies on the pivot point of the joint, which is controlled by the NP's ability to migrate during bending [67]. Radial deformations are much smaller compared to vertical deformations and are indicative of a healthy hydrostatic intradiscal pressure [68].

Maintaining hydrostatic intradiscal pressure is a function of static and dynamic loading and key to healthy biomechanical performance of the IVD [69,70,71,72]. During daily activities such as standing, sitting, or walking, the disc is under continuous compression resulting in disc height loss [70,71,73]. Applying a compressive force will also increase both intradiscal pressure and disc diameter [74]. Other studies have shown that the swelling properties of the NP and AF are affected by loading history and externally applied stresses [75]. During compression, as water diffuses from the tissues to its surroundings, the disc will decrease in volume. Fluid loss is also influenced by the duration of the load and the disc's biochemical composition [76]. Proteoglycans in the

NP tissue are primarily responsible for the retention of water. Monovalent ions are also retained in the disc tissues, which help draw water back into the disc and allow for swelling and disc height recovery [77]. Recovery of disc height after deformation is dependent on fluid exchange within the disc and the removal of load [37]. For example, when the human body lays supine during rest, the disc can relax and imbibe water from its surroundings [73,78,79]. This process of diffusion continues to repeat itself depending on the diurnal events of the day, so long as the disc maintains physiological intradiscal pressure.

While under compressive loading, an IVD joint can bend in multiple directions. IVDs allow for flexion and extension or the forward and backward bending of the spine [80]. The spine's range of motion is greater in flexion compared to extension. Flexion causes compression and tension of the anterior and posterior AF, respectively, whereas extension causes the opposite mechanical effect [81]. Compressive and tensile forces cause a shift in the stress profiles throughout the disc [74]. Therefore, surrounding posterior ligaments and muscles maintain joint balance during flexion or extension by counteracting applied torques. Disc hydration influences the bending motion of the IVD. While laying supine during rest, water diffuses into the disc tissue and improvise the joint's resistance to forward flexion. As the disc is slowly loaded throughout the day, resistance to forward flexion decreases and range of motion increases [82]. The disc's bending mechanical properties exhibit time-dependent behavior. Both repetitive and sustained flexion can lead to reduced resistance to bending [83]. Rapid movements of flexion increase peak bending moments, while creep loading reduces the resistance to bending and increases the range of flexion. The disc is also able to bend laterally from

side to side. Lateral bending, flexion, and compression all cause shear strain on the disc tissue [84]. Lateral bending and flexion place the disc at a greater risk of injury, especially when both motions are combined.

The IVD also permits rotational range of motion in the form of torsion and lateral shear both forward and backward [80]. Torsion applies compressive and tensile forces on different regions of the disc resulting in a distribution of disc height in the anterior, posterior, and lateral sides [85]. Torsional strength is dependent on disc shape, annular integrity, state of degeneration, and loading rate [86]. Discs that are severely degenerated exhibit higher torsional rotation before failure compared to nondegenerate discs. Other surrounding structures also appear to fail before the disc yields to failure, suggesting that torsion alone does not cause severe mechanical trauma [87]. Approximately 35 % of the joint supplies resistance to the applied toque, while 65 % is attributed to the articular processes, capsules, ligaments [86]. Frequent twisting while lifting heavy objects can place a disc at a greater risk of mechanical injury. Torsion places an additional strain on the AF fiber bundles while under compression, thus tensile forces are compounded [88]. Lateral shearing is not one of the predominant motions of the spine but can still occur. Excessive shear loading can cause failure of posterior bony elements, ultimately leading to separation of the AF from the CEPs and vertebral slip [89].

### 2.4 Lower Back Pain and Disc Degeneration

Lower back pain (LBP) is a broad term used to classify several diseases or conditions that plaque the lumbar region of the spine [5]. Pain can be associated with either the vertebrae or disc. For example, spinal stenosis is defined as the narrowing of the spinal canal or IVD foramen that causes compression of spinal nerves or nerve roots,

thus leading to LBP or neurogenic cramping [90]. Narrowing is linked to the hypertrophic cellular behavior of local bone or ligaments. Surgical intervention is highly dependent on the region of narrowing and can include procedures such as laminectomy or facetectomy. Another pain-related condition is spondylolisthesis or the movement of one vertebra slipping over an adjacent vertebra [91]. The motion of slipping can be either forward or backward and results from a degenerated IVD or facet joints. Other causes of spondylolisthesis include congenital abnormalities, lesion in the pars interartciularis, acute fractures in the bone such as the pedicles allowing for instability of the motion segment, bone disease, or aggressive resection of the facet joints or IVD. Treatment options include restriction of physical activities, repair of the pars defect, decompression, or fusion.

Physical injury can initiate a pathway that leads to degenerative disc disease (DDD) resulting in clinical symptoms of LBP and disability [92]. Disc tissue herniation is one of the most common medical issues associated with LBP in the lumbar region of the spine. Herniation can be classified by the subsequent stages of bulging, protrusion, extrusion, and sequestration. Initial depressurization of the NP and weakened AF fibers signal the beginnings of a bulging disc. Protrusion of disc material occurs when the NP tissue seeps through the damaged AF. NP tissue is classified as extruded once the tissue surpasses the outer AF boundary. If the NP becomes dislodged, fragmented from the inside of the disc, and impinges on nearby nerve roots or spinal cord, then the tissue is considered sequestered.

LBP is believed to be associated with the gradual degeneration of the IVD [93]. Healthy IVDs exhibit distinct regions of permeable CEP barriers, aligned AF lamellae,

and a hydrated NP core. However, the morphology and biochemistry of the CEP, NP, and AF dramatically change with age [94]. As the IVD progressively degenerates, disc nutrition and cellularity decline, which lead to alterations in ECM structure and biomechanical properties [95,96]. Degeneration is hastened by additional factors including calcification, shifts in metabolic activity, ECM degradation, and tissue dehydration [97]. The NP loses an appreciable amount of water, shrinks in volume, and can no longer maintain a hydrostatic swelling pressure while under compression (Figure 7) [98]. Degenerated discs contain less water compared to normal discs of the same age and therefore do not maintain hydration when under load [99]. Consequently, the AF bears excessive loading resulting in abnormal tensile stretching and buckling of the lamellae. Therefore, dehydrated disc tissues bulge, decrease in disc height, and lose fluid more rapidly [100]. Additionally, osteophyte formations develop along the periphery of the disc near the vertebrae. Late-stage degeneration is characterized by a complete loss of NP tissue, irregular AF structure, disc thinning, and continuing fusion of adjacent vertebrae [98].

One of the primary causes of disc degeneration is thought to be associated with nutrition of IVD cells [41,42,43]. The disc tissue is large, avascular, and must rely on nearby blood vessels in the CEP and peripheral AF to supply vital nutrients and remove waste [101]. The CEP undergoes several biochemical changes in the matrix structure, gradually thins, and is eventually replaced by bone. Diffusion of nutrients is ultimately hindered by this mineralization process. Even if the blood supply remains undisturbed, nutrients may not reach the inner NP if the CEP calcifies [42,43]. Endplate calcification, mineral deposition, and decreased vascularity can contribute to the beginnings of IVD

degeneration [102,103]. Intense calcification of the endplate has been identified in scoliotic discs and influences the curvature and morphology of the spine [104]. Additional changes including sclerosis (hardening), fracture or vascularity can all be detected through magnetic resonance imaging (MRI) [105]. Biochemical changes such as increasing collagen content, but declining proteoglycan and water content are also signs of disc degeneration, which can lead to the formation of Schmorl's nodes [35]. These nodes occur when the soft NP tissue protrudes through the weakened CEP and into adjacent vertebrae, thus negatively impacting disc biomechanics and furthering degeneration.

Calcification of the CEP hinders the diffusion of nutrients and waste to and from the NP. As a result, cells are unable to obtain nutrients to properly maintain regular metabolic activity. With a build-up of lactic acid in the NP, pH decreases, and cell necrosis occurs. An acidic pH has been found to decrease cellular proliferation and viability, while also upregulating the expression of pro-inflammatory cytokines and pain-sensing factors [106]. Exposure to low pH or glucose concentrations have also shown to be detrimental to native NP cells in vitro [107]. Additionally, the rate of matrix synthesis by disc cells also declines when exposed to low pH and hypoxic conditions [108,109]. The combination of decreasing matrix synthesis and increasing expression of catabolic enzymes result in further degeneration of the disc. Degraded proteoglycan and decreased GAG content are the most identifiable biochemical changes in the degenerated IVD, predominantly in the NP [99]. Chondroitin sulfate and polyanion content decrease throughout the IVD with increasing age and corresponded with decreased water content and increased compressive stiffness [110]. Loss of proteoglycans leads to tissue

dehydration and ultimately depressurization of the NP [76]. Aside from the structural breakdown and loss of proteoglycans and GAGs in the NP, collagen protein expression shifts with degeneration. The overall quantity of collagen changes very little with degeneration, however the type and distribution can vary. Increased type I collagen and denatured type II collagen in the NP have been detected and identified in degenerated human lumbar IVDs [111,112].

The mechanical role of the AF becomes more demanding, once the NP has lost its ability to resist compressive loading. Effects of age-related degenerative changes cause a decline in intradiscal pressure, thus shifting compressive stress distributions from the central NP to the peripheral AF in vitro [113]. Excessive axial strains are distributed along the AF in severely degenerated discs, most likely resulting from the depressurization of the NP [114]. Changes in loading pattern were also detected in patients with degenerated discs who experienced discogenic pain, indicated significantly lower osmotic pressure in the NP, and exhibited a physiologically wider posterolateral annulus [115]. Abnormal loading along the AF can cause changes in the biochemical composition and structure of the native tissue. Although proteoglycans begin to degrade, the presence of collagen within the lamellar structures remains relatively constant [76]. As the AF gradually degenerates, remodeling of the collagen network is only partially retained due to changes in collagen fiber orientation, proportions of expressed collagen proteins, and collagen crosslinking [116,117,118].

Morphological alterations in the AF ultimately lead to inferior mechanical properties. Tensile properties are site dependent and weakened by the inadequately remodeled collagen network [119]. The greatest reductions in tensile stiffness and

strength of severely degenerated human AF tissue were observed in the outer periphery [120]. Decreased tensile properties could potentially be linked to the lack of proper fiber reorientation while under loading [121]. Excessive mechanical loading disrupts the disc's structure and tearing in the AF is considered irreversible [122]. Radial, transverse, and concentric tearing of the AF can occur, which has been diagnosed using magnetic resonance imaging techniques [123]. Radial ruptures in aged human discs are predominantly found in the posterior AF and most frequently occur in the lowest two levels of the lumbar region [62]. One study concluded that the type of AF tearing was linked to either mechanical trauma or natural nuclear degeneration and may be associated with discogenic LBP [124]. It's important to note that alterations in the CEP, nuclear degeneration and annular disorganization progress in tandem and supersede tear and cleft formation in the AF [125].

Healthy IVDs contain degradative enzymes to breakdown matrix and allow for the synthesis of new proteins. On the other hand, degenerated IVDs contain elevated levels of enzymes compared to healthy IVDs. Proteolytic enzymes that exist in the IVD include matrix metalloproteinase (MMP) and aggrecanse, also known as a disintegrin and metalloproteinase with thrombospondin motif (ADAMTS) [126]. MMPs are classified as calcium-dependent zinc-containing endopeptidases. The most commonly active MMPs that become upregulated in the degenerated IVD are MMP-1 (collagenase), MMP-2 (gelatinase), and MMP-3 (stromelysin) [127,128]. Collagenase predominantly cleaves fibrillar collagens. Gelatinase degrades any denatured collagens, laminins, and gelatins. Stromelysin can breakdown not only collagens and gelatins, but proteoglycans as well. The mechanism in which MMPs catabolize collagen is still known, but several protein

domains can unwind triple helices, cleave triple helices, and cleave collagen polypeptide chains [129]. ADAMTSs are classified as multi-domain matrix-associated zinc metalloendopeptidases. The most commonly active ADAMTSs that become upregulated in the degenerated IVD include ADAMTS-1, -4, -5, -7, -9, -12, and -15 [130,131,132,133,134]. Aggrecanses can degrade multiple domains along the aggrecan core protein, thus leaving fragments of the proteoglycan within the disc [135]. Other than the presence of proteolytic enzymes, pro-inflammatory cytokines such as tumor necrosis factor-α (TNF-α) and interleukin-1β (IL-β) are believed to be involved in the progression of DDD [136]. These cytokines play an important role in the natural resolution of herniated tissue, however long-term exposure can negatively impact cell survival and functionality as well as promote a catabolic expression profile.

## 2.5 Strategies for Treating Lower Back Pain

**2.5.1 Conservative treatments.** A conservative strategy is first implemented when treating patients showing signs of acute LBP or early stages of disc degeneration. Physicians will typically recommend a combination of physical therapy and medication to combat pain, depending on the severity of symptoms. A variety of physical therapies are available which include, but are not limited to yoga, inversion, and aquatic exercise. Common forms of medication such as general analgesics, non-steroidal anti-inflammatory drugs (NSAIDs), muscle relaxants and opioids are routinely prescribed. Epidural steroid injections may also be administered to alleviate pain.

Yoga is a physical activity that entails performing postures, breathing exercises, and meditation. If properly and regularly practiced, yoga can impart many beneficial effects for those suffering with LBP. Patients will often notice an immediate

improvement in pain intensity and pain-related disability [137,138,139,140]. An individual's quality of life (QOL) can also vastly improve after performing yoga exercise therapy [139,140]. Pain medication usage can be reduced after 16 weeks of practice [137]. Improvements in sleeping patterns and reduced stress, anxiety, and depression have also been reported [139]. While yoga may improve a patient's psychological and neurological health, other physical benefits have been reported in literature. Flexion and extension of the back are involved in many poses and can increase spinal flexibility after 7 days [138,139]. Yoga can strengthen surrounding muscle tissues, while also enhancing respiratory and cardiovascular function [139]. Yoga can decrease the number of absences from work and is likely to be a cost-effective therapy for treating LBP and other musculoskeletal conditions [140]. This type of physical therapy is also associated with maintaining proper tissue hydration and preventing premature degeneration of the IVDs. Based on MRI readings, those that regularly practiced yoga for more than 10 years showed significantly less DDD in both the cervical and lumbar regions of the spine compared to non-practicing individuals [141].

Another commonly prescribed physical therapy is aquatic exercise. This type of exercise focuses on stretching, walking, and strengthening back, leg, and abdominal muscles while in a pool. The aquatic environment counteracts gravitational pull on the human body by providing a buoyancy force, thus allowing for low-impact exercise and minimizing pressure on joints. Ariyoshi et al. reported that 90 % of patients felt their physical performance improved after 6 months of participation in the program and had less LBP symptoms [142]. Additionally, individuals who practiced two or more days per week showed a significant improvement in their physical performance compared to those

who only exercised once per week. Like yoga, aquatic exercise can reduce LBP and disability, while improving health-related QOL [143,144]. Aquatic exercise can also help patients recover and gain strength after undergoing back surgery [145]. Increasing strength appears to correlate well with other observations such as decreasing body mass index, body fat percentage, waist to hip ratio, and increasing trunk muscle mass [144]. Lastly, an overwhelming number of studies have reported increased strength in individuals who performed aquatic exercises multiple times per week for several weeks [142,143,144,145].

Inversion is another type of physical therapy that does not require any bodily movement. Gravity-facilitated traction, otherwise known as inversion, has been found to increase separation between the posterior, anterior, and foraminal elements of the IVD [146,147,148]. Inversion can counteract the constant compressive forces that are exerted on the disc and may play a role in relieving LBP. A patient is simply held and positioned upside down to stretch the spine. Intradiscal pressure is subsequently reduced as a result of traction. While in the inverted position, a patient will experience decreased heart rate and increased blood pressure [148]. However, these physiological parameters remain relatively unchanged before and after inversion [147, 148]. Electromyography (EMG) can also be measured to assess neuronal activity of skeletal muscle cells before and after inversion. One study found that traction reduced EMG activity indicating relaxed lower back muscle motor function and less LBP [147]. Inversion therapy can improve a patient's flexibility and significantly increase range of motion in flexion [147,149].Additionally, inversion has been found to reduce the mass size of herniated disc tissue and can improve the odds of avoiding surgery for treating lumbar disc diseases

[149,150]. However, it is important to note that inversion may not be suitable for all patients as it may cause persistent headaches or blurred vision due to increase intracranial pressure [148].

One of the main goals of pain treatment for acute LBP is to stay as active as possible. During the chronic stages, pharmacological intervention is crucial in providing pain relief and improving physical function. If severely disabled with chronic LBP, individuals will discontinue exercising. Patients are typically prescribed a variety of medications to combat LBP depending on the severity of their symptoms or dysfunction, preferences, contraindications, and side effects. Prescribed medications include analgesics, nonsteroidal anti-inflammatory drugs (NSAIDs), muscle relaxants and opioids.

NSAIDs such as aspirin and ibuprofen are commonly prescribed to patients suffering from chronic LBP. Arachidonic acid, a polyunsaturated omega-6 fatty acid synthesized in cells, enters the cyclooxygenase (COX) or lipoxygenase pathways to produce prostaglandins. Prostaglandins are cyclic, fatty acid molecules that are implicated in many biological functions like inflammatory processes [151]. NSAIDs subdue the immune system and inhibit the synthesis of prostaglandins by selectively binding to COX-1 or COX-2 [152]. Several types of NSAIDs have been investigated to treat LBP which include, but are not limited to valdecoxib, etoricoxib, and piroxicam [153,154,155]. Valdecoxib, a COX-2 specific inhibitor, provided rapid relief within 1 week and sustained relief for a total of 4 weeks [153]. Improvement in function and decreased disability were observed, yet the number of adverse effects did appear to be significantly higher for those receiving treatment compared to the placebo group.

Etoricoxib, a COX-2 specific inhibitor, was investigated for its efficacy in treating LBP and disability in a 3-month trial [154]. Low and high dosages were both effective relative to the placebo group. Significant relief of symptoms and disability were observed after the first week of treatment, maximized after 4 weeks, and maintained for 3 months. A patch containing piroxicam, a non-selective COX inhibitor, can be applied to the lower lumbar and deliver a continuous dosage of NSAID [155]. After 8 days, pain was reduced by approximately 40 %, while the placebo patch group reduced pain by nearly 25 %.

Muscle relaxants are also prescribed to patients to decrease muscle function and alleviate symptoms of pain and spasms. One study reported that nearly 50 % of patients will utilize muscle relaxants for acute LBP, yet this type of medication alone does not appear to be associated with a faster functional recovery [156]. Muscle relaxants appear to be more effective when paired with NSAIDs. In terms of pain relief, patients taking both types of medication had the best outcomes after 1 week [157]. Patients that report more severe symptoms or dysfunctions are more likely to receive opioids. Prior exposure to taking opioid medications for chronic LBP increases both opioid and non-opioid medication use compared to first time users [158]. Prior opioid users were also found to have scored higher with respect to mental health disorders, chronic pain, and insomnia, indicating detrimental side effects of the medication. In a survey administered to U.S. adults, it was found that opioids are the most commonly prescribed pain medication for chronic LBP and lead to addiction [159]. Opioid misuse continues to be a major public health crisis in the United States. Aside from addiction, prolonged use of NSAIDs or opioids can lead to extensive kidney, liver, gastrointestinal, or central nervous systems problems. There is also increasing evidence that opioids are no more effective than non-

opioid medications when treating either acute or chronic LBP [160]. Psychological factors should also be considered when pursuing a pharmacological treatment. Many studies showed improvements in pain for control groups, suggesting that the placebo effect plays a role in treatment strategies.

Corticosteroids are a class of organic molecular compounds that suppress the immune system and provide an anti-inflammatory effect. Patients can receive these corticosteroid injections for a variety of health issues including bulging, herniation, stenosis, spondylolisthesis, or general degeneration. Those suffering from LBP caused by nerve root irritation can benefit from epidural steroid injections. Patients experiencing acute radiculopathy respond better to this type of treatment compared to those with chronic symptoms [161]. Upon receiving a steroid injection, more than 70 % of patients will experience immediate pain relief within one week [162,163,164,165]. However, less than half of these individuals will experience lasting pain relief ranging from six months to one year [162,163,165]. Multiple injections tend to provide pain relief, but some patients may report no improvement and will need to undergo decompression or spinal fusion surgery [163,164,165]. Epidural steroid injections can end the need for pain medication [163]. With regards to radicular pain due to IVD herniation, a long-term follow-up revealed that a majority of patients will still experience recurring symptoms within five years after treatment with steroids [165]. Some studies have compared steroid injections against saline or water injections. Vad et al. compared transforaminal epidural steroid injections to saline injections when treating lumbar radiculopathy [166]. After more than one year of treatment, the use of steroids has a higher rate of clinical success (84 %) compared to saline (48 %). Injecting water or saline may provide similar pain

relief yet does not act as quickly as steroids [164]. Saline injections may flush pain-related substances out of the disc and create a guided path through herniated tissue into the epidural space, allowing phagocytes to clean up debris, damaged tissue, or dead cells hence reducing pain [167]. Steroid injections are not a cure for LBP and solely serve to mitigate and alleviate pain.

**2.5.2 Discectomy.** When pharmacological intervention does not prove to be successful and disc herniation occurs, surgery may be required. Herniated disc tissue compresses nearby nerve roots and can cause radicular pain. Discectomy is a surgical technique that involves removing imposing disc tissue and alleviates pressure on surrounding nerve processes [168]. One of the first approaches to performing standard lumbar open discectomy (OD) was described by Love in 1939 [169]. First, a large unilateral 5-cm incision is created and the intertransverse space is exposed. Then, the intertransverse fascia is removed and both herniated disc tissue and nerve root are exposed. The hernia is excised or ablated, and the incision is closed.

The surgical technique of performing discectomy has dramatically improved by decreasing the size of the incision to gain access to the herniated disc, minimizing trauma to back muscle tissue, and improving field of vision. A minimally invasive technique of lumbar microdiscectomy (MD) was described by Caspar [170] and Williams [171] in 1977. The disc space is accessed through a smaller 3-cm incision and a guide wire is inserted to locate the herniated disc under fluoroscopy. A dilator is inserted over the guide wire to expand the viewing area. A microscope is used to illuminate the disc space and remove herniated tissue. Then, in 1988, a percutaneous endoscopic discectomy (PED) was performed by Kambin and Sampson [172]. The endoscope contains a canal

that allows for the introduction of forceps and an irrigation system to rinse away blood. In 1997, microendoscopic discectomy (MED) was employed by Foley and Smith [173] to remove all types of disc herniations. A 2-cm incision is made, and a series of tubular retractors are used to push apart the muscle tissue to gain a clear field of vision of the herniated tissue using a light source.

Due to the significant advancements in discectomy, a few reviews have sought to identify a superior technique amongst the different approaches. He et al. [174] compared the outcomes of studies that performed OD or MED on patients with lumbar disc herniation and found no significant differences in visual analog scale (VAS) for pain, Oswestry Disability Index (ODI), or complications between both groups. However, MED was associated with less blood loss, shorter length of hospital stays, and longer operation times. Ruan et al. [175] compared MD to PED and could not identify significant differences in terms of functional outcomes, complications, or reoperation rates, although PED was associated with shorter operation times and length of hospital stay. Zhang et al. [176] also found no significant differences in leg pain improvement, functional recovery, or incidence of complications between individuals that received MD or PED. However, PED was superior to MD in terms of length of hospital stay. Rasouli et al. [177] compared OD and MD to other minimally invasive techniques of interlaminar or transforaminal discectomy, transmuscular tubular MD, and automated PED, but findings weren't profound. There were no clear superior differences between techniques with respect to functional disability or persistence of motor or sensory neurological deficits. Minimally invasive strategies in performing discectomy may be advantageous in terms of

a lower risk of surgical site infection and shorter hospital stays, but each technique still provides the same level of pain relief.

Since the 1980s, rates for performing lumbar discectomy in the United States have continued to increase [178,179]. Even though discectomy provides immediate pain relief, the procedure is associated with inferior, long-term consequences. Once the offending tissue is removed, the biomechanics of the afflicted disc and adjacent segments are altered [180]. Disc degeneration is further hastened [181,182], and scar tissue can form near the epidural space and nerve roots, thus causing recurrent radicular pain [183]. If a partial discectomy is performed, residual tissue can herniate once more requiring revision surgery. On a national scale, the rate of revision discectomy after primary discectomy has been estimated to range from 5.1 % to 7.9 % [184,185,186]. Additionally, patients who had received a lumbar discectomy are approximately three times more likely to undergo a lumbar fusion compared to patients who had a lumbar diagnosis but did not undergo discectomy [187].

**2.5.3 Spinal fusions.** During advanced stages of degeneration, a spinal fusion is performed when the disc tissue can no longer be repaired, or the vertebral bodies become damaged. Spinal fusion aims to eliminate pain associated with degenerated discs by removing the diseased tissue, decompressing nerves, and restrict segment movement. Lumbar interbody fusion (LIF) was first described by Cloward et al. in 1953 [188]. Today, LIF is performed through anterior, posterior, transformainal, lateral and oblique approaches [189]. First, an incision is made through tissue to reach the spinal segment. The joint is decompressed, and a laminectomy may be performed to remove arthritic bone. Once the disc space is accessible, herniated disc tissue is excised. A titanium or

polyether ether ketone (PEEK) cage containing natural or synthetic bone graft material is inserted between the vertebral bodies and the joint is stabilized using plates, rods, and screws [190]. The graft promotes the bridging of the superior and inferior bone together.

Biologically-derived bone grafts are isolated from different sources and each have their own advantages, disadvantages, and limitations on bone healing for spinal fusion [191,192,193]. An autograft is bone harvested from the iliac crest of the hip, distal radius, or tibia and implanted into another site within the same individual [191,192]. Autologous grafts are advantageous in that they lack immunogenicity or disease transmission, contain living cells and osteogenic proteins that promote bone formation, and are efficient mechanical structures that support implanted devices. One major disadvantage of using an autograft is performing additional surgery resulting in increased operation time, blood loss, and risk of infection. Bone tissue is also limited in supply and donor site pain and morbidity are common [191,192]. Allografts are obtained from cadavers or living donors and implanted into an individual of the same species [191,193]. Allogeneic material can be fresh or preserved in tissue banks, cortical or cancellous bone, and vary in shape or form. Allografts are readily available and avoid the need to sacrifice host tissue, however they have limited osteogenic properties, lack viable cells, may induce an immune response, and carry the risk of transmitting bacterial infections or viral diseases [191,193]. Xenografts are obtained from the donor of a particular species and implanted into a recipient of a different species [191,193]. Xenogeneic material could be potentially harvested from an unlimited number of sources but pose a more serious threat to the transmission of diseases and immune response. Naturally-derived polymers such as collagen, elastin, chitosan, alginate, and cellulose or synthetic compounds such as

calcium sulfate, calcium phosphate ceramics, and bioactive glass have also been commonly used as bone graft substitutes [191,193].

Many studies have compared the different approaches in performing LIF surgery in order to determine if there is a superior technique. In 1997, Hacker et al. [194] compared the clinical outcomes of patients who underwent anterior or posterior LIF. A higher fusion rate was observed for the posterior LIF group compared to the anterior approach. In addition, blood loss, operation time, hospital stay, and total costs were all significantly lower for posterior compared to anterior LIF. Over the years, surgical technique was improved and differences in these clinical outcomes became minimal.

Kim et al. [195] compared the clinical outcomes of patients who underwent transforaminal or anterior LIF for treatment of spondylolisthesis. Overall, VAS and ODI scores were not significantly different. At the L5-S1 level, anterior was superior to transformainal LIF in restoring disc height, lumbar lordosis, and sacral slope. Similar radiographic evidence was reported in a previous study by Hsieh et al. [196]. Other studies by Humphreys et al. [197] and Park et al. [198] reported a higher complication rate for patients receiving posterior compared to transformainal LIF. Audat et al. [199] and Sakeb et al. [200] reported similar findings but observed no significant differences in fusion rates between posterior and transformainal LIF. Lateral LIF is relatively new and may provide several advantages over other approaches, which include preserving posterior or anterior ligamentous structures, reduced risk of vascular injuries, dural tearing, or perioperative injections [201]. Lateral LIF also appears to equally improve sagittal contour compared to other approaches and is superior to the posterior approach with respect to disc height restoration [202]. Clinical results for the oblique technique are

also promising and potentially present several advantages over other LIF approaches but require further investigation [203].

Although spinal fusion is an accepted approach to treating degenerated joints or herniated discs, LIF procedures are not always successful and may produce inferior outcomes resulting in revision surgeries. One of the most significant issues associated with LIF is the increased risk of adjacent segment disease (ASD). ASD is the accelerated degeneration of the superior or inferior IVDs relative to the fused joint due to stiffness of the interbody fixtures and bone graft cage. Lee et al. [204] performed a retrospective study in which risk factors associated with ASD after lumbar fusion were investigated. Out of 1,069 patients who underwent fusion, 28 (2.62 %) required revision surgery because of ASD. Facet degeneration was found to be a significant factor and the incidence of proximal ASD was significantly higher compared to distal ASD. Heo et al. [205] also confirmed that facet degeneration increased the risk of ASD, as well as other factors including low segmental lordosis and laminectomy-treated isthmic spondylolisthesis. Additionally, authors concluded that there is an approximately 25 % greater risk of ASD following 10 years post-surgery. Pseudoarthrosis, also known as the improper healing of bone across the spinal motion segment due to the misalignment of the vertebra, can also occur. Suh et al. [206] performed a retrospective study on patients receiving posterior LIF revision surgery due to complications associated with ASD or pseudoarthrosis. Fusion rates after revision surgery were 71 % and 95 % successful for the pseudoarthrosis and ASD groups, respectively. This study demonstrated that pseudoarthrosis can be a tenacious clinical symptom to resolve.

Additional clinical issues have been reported to arise after performing LIF surgery. Since LIF requires removing the IVD, joint flexibility is lost and range of motion decreases [207]. Wang et al. [208] performed a retrospective study and determined that persistent LBP had an incidence rate of 7.2 %. Bai et al. [209] reported that 3.8 % of patients developed contralateral neurological symptoms after performing LIF. Symptoms of numbness or pain may be linked to the malposition, loosening, and migration of the bone graft cage or metal fixtures, and subsequent mechanical compression and damage to surrounding nerves. In fact, bone graft migration continues to be a problem and has been reported in several cases over the past 30 years [210,211,212], which can lead to perforation of the colon or misdirected bone formation. Implant subsidence is yet another inferior clinical outcome [213]. The metal interbody cage needs to maintain space between vertebra to allow for bone fusion and subsequent foraminal decompression.

**2.5.4 Total disc replacements.** One alternative to spinal fusion is total disc replacement (TDR). This type of procedure aims to conserve the natural biomechanics of the joint by replacing the entire diseased lumbar disc with an artificial disc prosthesis [214]. Compared to LIF, TDR can restore physiological motion, balance, and curvature of the lumbar spine by mimicking the mechanical properties of the native NP and AF. Prosthetic devices must bond to the adjacent vertebra, restore disc height, accommodate high loads without breaking, reduce wear under fatigue, and enable flexible motion. Due to the numerous inventions of TDR devices, only FDA approved implants will be discussed hereon [214].

One of the first designed lumbar TDRs was the SB Charité artificial disc (DePuy Spine, Raynham, MA) (Figure 8A). In 1982, Schellnack and Büttner-Janz developed the

SB Charité I in Berlin, Germany at the Charité Hospital [215]. Following mechanical testing, the artificial TDR was implanted into patients. In 1985, the TDR underwent axial migration, which led to the development of the SB Charité II. The stainless-steel endplates were enlarged to improve contact with the vertebral bodies. However, the endplates were prone to fractures and subsidence. In 1987, Waldemar Link marketed the SB Charité III outside of the US and DePuy Spine acquired the product rights in 2004 [215]. The current design of the TDR contains an ultra-high molecular weight polyethylene core positioned between two metal endplates [216]. The core is unconstrained and allowed to freely move during bending. The endplates are composed of a cobalt chromium molybdenum alloy with three anchoring teeth positioned on both the dorsal and ventral side of each endplate. To promote the mineralized connection between the vertebra and device, the endplate surfaces are sprayed with a porous coating of titanium and calcium phosphate [216]. The SB Charité III was approved by the US FDA in 2004 and introduced to the US market in 2006.

The SB Charité III has a long history of use in the clinical setting. One of the first clinical experiences with the TDR was reported by Griffith et al. [217]. The TDR was implanted into 93 patients suffering from DDD. After one year, patients noted a significant improvement in pain intensity, walking distance, and lumbar mobility. Only 6 patients exhibited signs of device failure, migration, or dislocation. Cinotti et al. [218] also reported short-term results of 46 patients who received TDR after a two-year follow up period. Many patients were satisfied with the procedure and experienced pain relief; however, seven patients underwent posterolateral fusion without TDR removal and two patients required removal of the prosthesis.

Long-term evaluations are essential in determining the efficacy of TDR devices in resolving DDD and LBP. Findings from a 10-year follow-up of 100 patients who received the SB Charité III were first reported by Lemaire et al. [219]. Clinical outcomes were reported as "excellent" or "good" by 90 % of patients and 91.5 % returned to work. ASD and facet joint degeneration were observed in 2 % and 11 % of patients, respectively. Another 10-year follow-up retrospective study was performed on 106 patients [220]. Clinical outcomes were reported as either "excellent" or "good" by 82.1 % of patients and 89.6 % returned to work. Eight patients required fusion and other minor complications occurred including facet arthrosis (4.6 %), subsidence (2.8 %), ASD (2.8 %), and implant dislocation (1.9 %). Putzier et al. [221] provided outcomes after 17 years for 53 patients implanted with the SB Charité types I - III. Interestingly, 32 patients (60 %) exhibited signs of spontaneous ankylosis or joint stiffening due to bone fusion, regardless of implant type.

Results from these earlier clinical trials are polarizing. Ultimately, long-term outcomes for TDR should be compared to spinal fusion. Therefore, Guyer et al. [222] compared the use of the SB Charité III to anterior LIF and published findings from a prospective, randomized, multicenter FDA investigational device exemption study. Authors concluded that both procedures produced similar clinical outcomes. Patients that received a TDR were statistically less disabled and more likely to return to full-time employment. Recently published findings from China [223] and Australia [224] support the notion that TDR provides satisfactory clinical results, reduce pain and disability, maintain intradiscal height at both surgical and adjacent levels, and potentially reduces the risk of ASD.

Another example of a lumbar TDR is the ProDisc (Synthesis Spine, West Chester, PA). The first prototype of the ProDisc was developed in the 1980s in France. The ProDisc has two titanium endplates with notched keels to allow for mechanical interlocking with the vertebra. The surfaces of the endplates are sprayed with titanium to allow for bony ingrowth and attachment. An ultra-high molecular weight polyethylene core is inserted between the two plates, which permits motion. ProDisc I was first implanted into a total of 64 patients from 1990 to 1993 and proved to be a safe and effective treatment for symptomatic DDD [225,226]. Since then, the ProDisc I evolved in design resulting in the production of ProDisc II and ProDisc-L (Figure 8B). The endplate material for the ProDisc-L was changed to a cobalt chromium molybdenum alloy. Unlike the free-floating core of the SB Charité III, the ProDisc-L contains a fixed core that permits partial movement which minimizes the risk of subsidence or fracturing [227].

Preliminary clinical studies compared the efficacy of TDR using the ProDisc and spinal fusion to treat DDD. Delamarter et al. [228] found that patients that received TDR reported significantly less pain and disability compared to fusion, however these differences were insignificant after 6 months. Zigler et al. [229] found that implantation of the ProDiscII was superior to spinal fusion in that the procedure allowed for quicker recovery times and decreased hospital stay, operation time, and intraoperative blood loss. Both studies were able to conclude that TDR was more effective in preserving motion compared to spinal fusion.

The ProDisc-L was US FDA approved in 2006 and several clinical trials were performed thereafter. One clinical trial performed in Plano, Texas showed excellent outcomes using the ProDisc-L after 2 and 5 years [230,231]. TDR was considered non-

inferior to fusion and both treatments observed significant improvements in disability and decreased pain scores. None of the devices developed spontaneous ankylosis and segment range of motion remained within the normal physiological range. Many FDA trials reported mixed results after comparing the outcomes of single-level to multiple-level TDR in patients. The ProDisc-L has also been implanted at two adjacent levels in patients and showed similar success as single-level replacement TDR [232,233,234]. Multiple-level TDR preserves motion and can provide similar levels of pain relief and decreased disability compared to single-level TDR. Other studies have reported that multiple-level TDR is inferior to single-level TDR due to significantly higher complication rates, even though similar trends in functional scores were observed [235,236].

The activL Artificial Disc (Aesculap Implant Systems, Breinigsville, PA) is a next-generation motion-preserving TDR that was approved by the US FDA in 2015 (Figure 8C) [237]. The endplates are composed of a cobalt chromium alloy coated with titanium and dicalcium phosphate. There are spikes that protrude perpendicular to the endplates and allow for fixation to the vertebra. The endplates are designed in a variety of sizes and lordotic angles to accommodate anatomical differences in patients. The core is composed of an ultra-high molecular weight polyethylene that is available in different height sizes [237]. Compared to SB Charité and ProDisc-L, the activL was the only TDR that provided an ideal implant size for 87 % of patients in a recent clinical trial [238].

ActivL has been mechanically tested in vitro [237]. While under axial compression, a maximum shear force of 1,259 ± 60 N caused activL to dislodge from a simulated dense bone substrate. The activL exhibited enough resistance to endplate expulsion based on the maximum shear force of 400 N, which is encountered in the

lumbar spine [239]. The maximum observed subsidence load into the simulated dense bone substrate was 5,761 ± 391 N, well above the accepted in vivo axial force of 3,400 N [240]. ActivL also surpassed accepted values of static and dynamic compressive shear based on in vivo loads [240,241]. The maximum observed displacement after exposure to creep-like conditions of 3,000 N cyclic loading was 0.5 mm, which are below the diurnal changes exhibited by the IVD of 1.5 mm [242]. The average cumulative wear produced by the activL after 1 million cycles of fatigue was 2.7 mg of polyethylene debris.

Due to the recent US FDA approval, the activL has very few reported outcomes from clinical trials. Garcia et al. [238] assessed the use of the activL in patients with symptomatic DDD. Patients in the control group received either the ProDisc-L or SB Charité III. Both treatment groups reported improved mean back pain severity and decreased ODI scores, but no significant differences were detected. Patient satisfaction was over 90 % for both treatment groups and those that received activL TDRs returned to work approximately 1 month sooner versus the control group. The number of device-related adverse effects and surgical reinterventions were not significantly different between both groups. ActivL is considered a safe and effective device for treatment of DDD compared to other FDA approved TDRs.

**2.5.5 Nucleus pulposus replacements.** Early intervention and treatment of degenerative discs can avoid the need for invasive surgeries of discectomy, LIF, or TDR. The gradual breakdown of NP tissue significantly contributes to disc degeneration. Therefore, much research has led to the development of acellular devices for replacing NP tissue [243,244,245,246,247]. There are several requirements that must be met for the implant to successfully restore mechanical function to the degenerated disc. The

replacement must have similar mechanical properties to the native NP. Exerted compressive stresses produced by the device should not exceed the failure strength of the adjacent CEPs, otherwise subsidence may occur. The device must be well integrated with the surrounding CEPs and AF to promote proper load transfer, thus minimizing device migration or extrusion. Implant durability and fatigue life are important to evaluate as the disc undergoes cycles of diurnal loading. The device should generate as little material debris as possible and should not elicit a host immune response. NP replacement devices can be classified as either mechanical or elastomeric in nature. Mechanical devices are further subdivided into single or multiple component devices. Elastomeric devices are naturally-derived hydrogels or synthetic compounds that are either injected or pre-formed and inserted into the disc space.

The NuBac (Pioneer Surgical Technology, Marquette, MI) is a two-piece, unconstrained device composed entirely of polyether ether ketone (PEEK), and designed with an internal articulation and endplates that prevent movement inside the disc (Figure **9**A). The rigid implant was biomechanically assessed in a human cadaver IVDs under compression, torsion, and bending [248]. Disc height was restored and there was no statistical difference in range of motion between the implant and intact conditions. One out of six implants failed due to specimen failure and a few showed signs of slight migration. Regardless, all constructs completed 100,000 cycles without extruding or causing damage to the CEPs. Devices were proven to be biodurable after exposure to gamma irradiation, accelerated aging using oxygen, and physiological saline solution at supraphysiological temperatures [247]. The biocompatibility of implants was also evaluated in a rabbit model and PEEK debris elicited a mild immune response compared

to surgical controls [249]. Bao et al. reported excellent device biocompatibility, restoration of disc height and range of motion in a human cadaver disc, and no adverse or local or systematic tissue reaction in a baboon model [250]. Furthermore, 39 patients were implanted with the device and examined after 2 years [251]. No complications arose and a significant decrease in ODI and VAS scores were observed.

Another type of rigid implant designed for NP replacement is Regain (EBI Medical Systems, Parsippany, NJ). Regain is a one-piece device made of a graphite compound coated with pyrolytic carbon (Figure **9**B). The geometric profile of the Regain was optimized using an electromagnetic motion tracking system [243]. Upon insertion into a spinal motion segment, changes in the implant position during dynamic bending cycles were recorded. Regain has convex outer surfaces in order to conform to the shape of the vertebral bodies [246].

The prosthetic disc nucleus (PDN) is an example of a pre-formed synthetic hydrogel, which has a long-standing clinical history [252,253,254]. The PDN (RayMedica, Minnetonka, MN) is a hydrogel pellet composed of polyacrylonitrile and polyacrylamide encased in a polyethylene jacket (Figure **9**C) [253]. This device is implanted in a dehydrated state, absorbs 80 % of its weight in water, and maintains a swelling pressure within the disc. The polyethylene jacket prevents excessive swelling that can cause damage to the CEPs and minimizes horizontal spreading allowing for disc height retention when compressed axially. The device also contains platinum-iridium markers wires that allows for visualization using radiography [253]. Eysel et al. evaluated the biomechanical performance of the PDN in human cadaver lumbar spinal motion segments and found that the device restored disc height after nucleotomy [255].

In 1996, the PDN was first implanted in ten patients in Germany [252,256]. Eight patients returned to full working capacity, whereas two patients experienced adverse side effects of implant migration or sensory disturbances. Four patients exhibited disc height loss and implant subsidence into the CEPs. After a two-year follow up, all ten patients showed excellent clinical and functional outcomes with reduced disability and increased range of motion. From 1996 to 1997, an additional eight patients from Sweden and five patients from South Africa were implanted with the same PDN [252]. However, from 1997 to 1998, a group of 17 patients received a new iteration of the PDN. To prevent implant migration or subsidence, the shape of the device was angled to conform to the curvature of the CEPs and the hydrogel's stiffness was decreased by altering water absorptivity. However, only a 62 % success rate was reported for this clinical trial due to the high rate of device migration and revision surgeries. From 1998 to 1999, twenty-six patients were implanted with devices varying in both shape and size. The success rate for this group of patients increased to 79 %. The evolution in the design of the PDN has emphasized the importance of minimizing damage to the AF, improving surgical technique, and device conformity within the intradiscal space [252,253,254].

Another example of a pre-formed hydrogel is the Aquarelle. Unlike the PDN, the Aquarelle (Stryker Howmedica Osteonics, Allendale, NJ) is composed of pre-hydrated poly (vinyl alcohol) (PVA) that is allowed to freely swell within the disc (Figure **9**D). Aquarelle was effective in maintaining disc height under axial loading in an ex vivo human cadaver model [257]. The device was also implanted in baboons that underwent lumbar discectomy [258]. Five out of fifteen devices extruded from the disc space and either compressed nearby nerve roots or slipped within the spinal canal. Implants were

difficult to image using X-ray but showed increased water content. The biomaterial was deemed non-cytotoxic; however, hydrogel particulates were in the subchondral bone, thus producing an inflammatory reaction. Damage to the CEPs occurred, which may have been associated with the incorrect sizing of the implants.

The Newcleus (Centerpulse Orthopaedics, Winterthur, Switzerland) is another uniquely shaped intradiscal implant. The device is a polycarbonate urethane elastomer that is curled into a spiral and absorbs water up to 35 % of its weight (Figure **9**E). Biomechanical testing showed that the implant restores cranio-caudal distance of the lumbar facet joint and the cranio-caudal distance between adjacent endplates [259,260]. Endplate deformations between the spiral implant and the intact conditions were not statistically different. In addition, the Newcleus was implanted into five patients. After 24 months, patients experienced decreased radicular pain and device migration was not observed.

Another pre-formed NP replacement is the NeuDisc (Replication Medical, Cranbury, NJ), which is composed of hydrolyzed polyacrylonitrile and reinforced with a polyester Dacron mesh (Figure **9**F). NeuDisc is implanted in a dehydrated state and swells primarily in the axial direction with limited radial expansion upon absorbing water. Bertagnoli et al. [261] evaluated the NeuDisc in an ex vivo extrusion model using discs from human cadavers. Discs received an annular incision and NP tissue was excised using rongeurs. Specimen were tested until failure in compression, lateral bending, and flexion. Implant extrusion was observed for one specimen during compression (n = 12), one specimen during lateral bending (n = 12), and none during flexion (n = 8). Device

biocompatibility was tested in vivo using New Zealand rabbits and did not elicit a cytotoxic response [243,244].

The DASCOR Disc Arthroplasty System (Disc Dynamics, Eden Prairie, MN) is an example of an injectable synthetic polymer that cures in situ. The device consists of a catheter-based polyurethane (PUR) balloon that conforms to the intradiscal space and is filled with a PUR core optimized for resilience, flexibility, and mechanical strength (Figure **9**G) [246,247]. A two-part pre-polymer system is mixed and injected into the disc space using a custom injection system. Once the polymer cures, the PUR balloon adheres to the polymer. Tsantrizos et al. [262] evaluated the mechanical properties of the DASCOR and its biomechanical performance in discs from human cadavers. The static compression and shear moduli of the devices were between 4.2 – 5.6 MPa, and 1.4 – 1.9 MPa, respectively. The maximum axial fatigue strength of the tested device is approximately 3 MPa. Overall, the device restores segment flexibility to a level comparable to the intact condition and produces a uniform contact stress along the CEP.

NuCore Injectable Disc Nucleus (Spine Wave, Shelton, CT) is another injectable polymer that is composed of synthetic silk and elastin (Figure **9**H). The copolymer cures within minutes, restores disc height under load, and resists extrusion during mechanical testing in a cadaver model [263]. Additionally, the NuCore was implanted in several animal species and showed no evidence of irritation, cytotoxicity, or neurotoxicity [264]. The NuCore injectable implant was evaluated in a 2-year long pilot clinical study [265]. Patients experienced significantly less leg and back pain upon receiving microdiscectomy and implantation with the NuCore. No adverse events were reported, and radiographic measurements confirmed implant stability within the intradiscal space.

There are several additional examples of injectable polymers that have been developed for NP replacement [246,247]. For example, the Biodisc (Cryolife, Kennesaw, GA) is a protein hydrogel consisting of albumin crosslinked with glutaraldehyde that polymerizes within 30 seconds, solidifies after 2 minutes, and restores disc height and motion to the IVD. The risk of transmitting diseases is reduced since the protein polymer is created through DNA bacterial synthesis fermentation and does not contain biological compounds from a human or animal species. SINUX ANR (J&J DePuy, Raynham, MA) is a liquid polymethylsiloxane (silicone) that cures in approximately 15 minutes. Hydrafil (Synthes, West Chester, PA) consists of hydrophilic polyvinyl alcohol (PVA) and polyvinyl pyrollidine (PVP). Each of these devices are still being investigated using pre-clinical models.

**2.6 Tissue Engineering Strategies**

Tissue engineering can be defined as "an interdisciplinary field that applies the principles of engineering and the life sciences toward the development of biological substitutes that restore, maintain, or improve tissue function [266]. This field aims to replace, repair or regenerate damaged tissues depending on the desired approach and application. The triad of tissue engineering and regenerative medicine includes the use of cells, scaffolds, and signals. The limitations and consequences of using autologous, allogeneic, or xenogeneic cells should be carefully considered when repairing human IVD tissue. The choice of cell line can vary from using stem cells, progenitor cells, or even fully differentiated cells. The scaffold used to deliver cells can be a synthetic biomaterial or a naturally derived extracellular matrix component or a combination

thereof. Signaling with growth factors, chemotactic factors, or mechanical stimuli can be utilized to direct a desired cellular response.

IVD tissue engineering has evolved over the decades to improve strategies for treating the degenerated joint. Spinal fusion can be considered one of the most proven surgical treatments to eliminate joint pain. Although pain subsides several months post-surgery, the patient's range of motion is potentially lost. Therefore, disc replacements have been investigated as potential implants to restore joint function and mobility. Additionally, acellular replacements, specifically for the nucleus pulposus, have been designed to treat patients with low grade degeneration. All the aforementioned procedures are considered invasive, which has led to the growing number of minimally invasive tissue engineering strategies in repairing the NP or AF with a cell-seeded biomaterial or growth factor injections.

There are several factors to consider when applying a tissue engineering strategy to the degenerated IVD. Metabolic activity of native disc cells and overall composition and structure of surrounding ECM tissue dictate the type of treatment strategy whether delivering steroids, cells, proteins, or a scaffold [267]. Tissue engineering strategies should be implemented during early stages of degeneration when the AF tissue is still competent to sustain swelling pressure [268]. Increased intradiscal pressure will lead to restoration of disc height and AF tissue will undergo tensile strain allowing for fibril repair. Protein therapy may serve as a viable option if native disc cells are still responsive and metabolically active. Injection of proteins into the NP can stimulate endogenous ECM formation and improve tissue hydration. Alternatively, introducing new cells into the disc space could provide a means of generating new tissue. Due to the low cell

density and senescent state of degenerated IVD tissues, autologous cell transplantation may prove to be a challenge and should be avoided [269]. Therefore, stem cells may serve as an alternative cell source for regenerative therapies. The use of a biomaterial scaffold can also play an important role in the retention and delivery of stem cells and growth factors to the degenerated disc.

**2.6.1 Protein-based therapies.** Growth factors are known to influence morphogenesis or the biological process of forming musculoskeletal structures by controlling the growth and differentiation of cells and tissues. Moreover, disc cells modulate their activity through a variety of signals using growth factors, cytokines, enzymes, and inhibitors [270]. Protein administration has been studied to stimulate native disc cells and upregulate the production of key ECM molecules such as aggrecan and collagen. The transforming growth factor-beta (TGF-β) superfamily is responsible for regulating cell growth, proliferation, differentiation, and apoptosis. Bone morphogenetic proteins (BMPs) and cartilage-derived morphogenetic proteins (CDMPs) are cytokines within the TGF-β superfamily. BMPs are known to initiate, promote, and sustain osteogenesis and chondrogenesis. CDMPs were identified as critical proteins involved in cartilage and joint morphogenesis and stimulate proteoglycan synthesis [271]. BMPs and CDMPs are often referred to by other names such as osteogenic proteins (OPs) or growth differentiation factors (GDFs). Other biologics have also been used to downregulate pro-inflammatory cytokines such as TNF-α [272,273,274,275,276] and interleukin (IL) [272,273,274,277], or matrix-degrading enzymes such as MMPs [274,276,277,278,279] and aggrecanases [276,277,278,279,280] to slow the degenerative cascade.

***2.6.1.1 In vitro studies.*** Many in vitro studies have demonstrated the influence of growth factors and other biologics on cells derived from disc tissues. For example, human AF cells were isolated, expanded and encapsulated in alginate and agarose [281] or grown in micromass [282] and cultured in conditioned media containing TGF- β1. Gruber et al. identified newly synthesized type I and type II collagen as well as chondroitin sulfate and keratin sulfate [281,282]. Two additional studies also isolated and cultured degenerated NP cells in alginate [283] or healthy NP cells in micromass [284] in the presence of TGF- β3. Healthy NP cells showed an upregulation of type I, II, III, IX collagen and aggrecan [283]. Degenerated NP cells exhibited an anti-catabolic gene expression profiles with a decrease in ADAMTS-5, MMP-1, type I collagen, type III collagen and an increase in SRY Box 9 (SOX9) [284]. Interestingly, another study was able to culture viable degenerated AF cells in a three-dimensional mesh but failed to stimulate an anabolic response with TGF-β1 [285]. Therefore, growth factors may not be a suitable treatment for patients with severely degenerated AF tissue. Additionally, several of these studies showed increased cell proliferation over time [281,283,284].

BMPs have also been extensively studied as a potential therapeutic agent for human disc cells. Kim et al. encapsulated human IVD cells in alginate beads and exposed cells to recombinant human BMP-2 [286]. Cultures treated with BMP-2 exhibited a dose-dependent response and protein concentration is directly correlated with proteoglycan synthesis. Aggrecan, type I, and type II collagen were upregulated, while osteocalcin did not. In this study however, both NP and AF cells were seeded together and the effects BMP-2 on each cell type were not studied. Another study aimed to identify region specific responses of BMP-2 on IVD cells in the NP, AF, and transitional zone [287].

Cells were isolated from each region and encapsulated in alginate beads. In response to BMP-2 administration, NP cells showed a significant increase in proteoglycan synthesis, yet AF cells only proliferated and did not produce significant amounts of ECM. Gilbertson et al. also showed that NP cells in monolayer produced proteoglycan, collagen, and other non-collagenous proteins when exposed to BMP-2 for two days, AF cells showed little activity in terms of ECM synthesis, and that growth factor efficacy is dose-dependent [288]. TGF- β has been shown to induce type I collagen deposition and re-differentiation of cells toward a fibroblast-like phenotype, whereas BMP-2 induces more type II collagen deposition [289]. Both grown factors were reported to increase proteoglycan deposition, increase cell number, and upregulate the Smad1 gene, which is an important transcriptional modulator.

BMP-7 was studied for its potential to stimulate ECM production and prevent apoptosis [290]. Apoptosis can be induced using tumor necrosis factor-α (TNF- α) or hydrogen peroxide. BMP-7 helped inhibit apoptosis and decreased the activity of caspase-3, a regulator for programmed cell death. Interestingly, NP cells produced ECM macromolecules even in an apoptotic environment. While TNF- α can upregulate catabolic enzymes like ADAMTS-4 and ADAMTS-5, BMP-7 can reverse this pathway and suppress phosphorylation and nucleus translocation of nuclear factor kappa-light-chain-enhancer of activated B cells (NF-κB) protein p65 [291]. The NF-κB protein is involved in the transcription of DNA into messenger RNA (mRNA) and associated with inflammatory and immune response. The regenerative potential of BMP-7 is donor dependent and requires very high doses, which may increase the incidence of complications [292]. In general, these studies have demonstrated that BMPs specifically

support chondrogenic behavior and do not upregulate osteogenic expression [286,287,290].

***2.6.1.2 Animal models.*** The efficacy of growth factor administration, specifically the delivery of BMP-2, BMP-7, and BMP-14, has been studied in vivo [293]. Huang et al. [294] injected BMP-2 into discs of New Zealand white rabbits that received an annular stab injury with a width of 7 mm and a depth of 5 mm. Discs that were treated with growth factor were compared to a saline control. Radiographic images revealed more severe degenerative changes in discs that received saline versus BMP-2. Histological findings showed bone formation in both groups, however fibroblast proliferation and vascularization were highly evident in discs that received BMP-2. Authors concluded that BMP-2 may play a role in tissue repair after a disc has been injured and undesired stimulation of bone production may occur in vivo. Inoue et al. [295] also injected BMP-2 into discs of a rat tail. Two coccygeal discs from each rat were punctured with an 18-gauge needle and degeneration progressed for 4 weeks. Discs received an injection of either PBS or BMP-2 at 4, 6, or 8 weeks post-injury. Injection of BMP-2 significantly improved degeneration grade at the 4-week time point as evidenced by MRI. Additionally, improvements in disc height index were observed at 4 and 6 weeks for discs that received a BMP-2 injection. Immunohistochemical staining identified signs of cartilage-like tissue formation and cellular behavior.

Kawakami et al. [296] injected BMP-7, also known as osteogenic protein-1 (OP-1), into discs of a rat tail. Disc were exposed to chronic compression to induce hyperalgesia (increased sensitivity to pain) for 4 weeks, followed by an injection of either saline or BMP-7. As a control, a sham group was also included where tails were

immobilized in the apparatus, but not compressed. Discs that received injections of BMP-7 were either continuously compressed for an additional 4 weeks or released. Progressive mechanical hyperalgesia in all groups, except for discs that received BMP-7. Overall, compressed discs showed a decrease in NP size and a substantial loss of proteoglycans in the NP and CEP. However, BMP-7 was able to restore the morphology of the tissue in comparison to the control. NP cells in the saline group appeared spindle in shape, whereas BMP-7 caused NP cells to become swollen showing signs of increased ECM production. Authors concluded that BMP-7 may play a role in inhibiting pain-related behavior.

An et al. [297] delivered BMP-7 into uninjured discs of New Zealand white rabbits. Three consecutive discs in each rabbit received only injections of saline or BMP-7. Disc heights were measured using lateral plain radiographs after 2, 4, and 8 weeks. DNA, proteoglycan, and collagen content were analyzed at the end of the study. After 2 weeks, proteoglycan content was higher and disc height index was 15 % greater for discs that received BMP-7 versus the saline control group. After 4 weeks, there was a significant increase in DNA content of the AF in discs treated with BMP-7 compared to the saline group, however no significant differences were detected in the NP. Authors concluded that BMP-7 may act to stimulate protein synthesis in the NP and proliferation in the AF.

Masuda et al. [298] treated degenerated discs from New Zealand white rabbits with BMP-7. Degeneration was induced by puncturing the AF with an 18-gauge needle. Four weeks after injury, 5% lactose or BMP-7 was injected into the center of the NP. Disc height was measured radiographically for up to 24 weeks and spinal columns were

harvested for histological assessment, biochemical composition, and grading of disc degeneration. After 4 weeks, disc narrowing occurred following annular injury. Injection of BMP-7 induced a restoration of disc height at 6 weeks and was sustained. MRI grading indicated a significantly higher water content in the NP for discs that received BMP-7 compared to 5 % lactose. Histological findings also revealed a significantly higher proteoglycan content in the NP and AF and lower degeneration grades in the BMP-7 group compared to the 5 % lactose group.

Alternatively, Imai et al. [299] induced disc degeneration in New Zealand white rabbits through chemonucleolysis using chondroitinase ABC. Four weeks after enzyme injection, discs received either BMP-7 or 5 % lactose as a control. Disc heights were measured every 2 weeks and rabbits were sacrificed for histological and biochemical analyses. Disc space narrowing was observed for both groups; however, BMP-7 injection caused a significant increase in disc height index at 6 weeks and was sustained for up to 16 weeks. Proteoglycan content was higher for the BMP-7 group, yet histologic changes after BMP-7 injection were not observed.

Walsh et al. [300] statically compressed discs to induce disc degeneration in a mouse model. This study tested the efficacy of several growth factors including BMP-14 (GDF-5), TGF-β1, insulin-like growth factor 1 (IGF-1), and basic fibroblast growth factor (bFGF) with PBS serving as the control group. After 1-week, static compression was removed, and multiple groups of rats were treated immediately with a single injection of a growth factor or PBS. At the 4-week time point, discs received either a single injection or multiple injections of a growth factor or PBS. Disc morphology, AF cell density, cell proliferation, disc height, and gene expression for aggrecan and type II

collagen were assessed at 1 week or 4 weeks after treatment. Following static loading, NP volume and disc height were significantly reduced, and outward bulging of the AF and disorganization of collagen fibers were evident. Compared to the PBS group, a single injection of BMP-14 or IGF-1 at the 4-week time point showed abundant cluster of AF fibrochondrocytes. BMP-14 was the only growth factor that significantly increased disc height. Cells in the NP, and inner AF showed expression for both type II collagen and aggrecan. This study suggests that BMP-14 plays a major role in fostering mitosis of AF cells and recruitment into the degenerated NP.

Chujo et al. [301] reported similar findings with the use of BMP-14 to treat degenerated discs in a rabbit model. An annular puncture was performed using an 18-gauge needle to induce degeneration. Two non-contiguous lumbar discs were injured while the IVD between injured discs was left intact as a control. Four weeks later, an injection of PBS or BMP-14 was administered into the disc space. Radiographs were taken every two weeks after the injury in order to calculate disc height index. MRI was performed to grade the level of disc degeneration. Histological sections of tissue were scored by a blind observer. Twelve weeks post-treatment, rabbits were sacrificed and IVDs were harvested for analysis. Overall, a single injection of BMP-14 into the NP resulted in a restoration of disc height, improved water content in the NP, and reduced the graded level of degeneration.

***2.6.1.3 Clinical trials.*** DePuy Spine has sponsored several clinical trials for treating early lumbar disc degeneration using recombinant human GDF-5 (rhGDF-5). All these phase I/II trials are completed and have not published results. Primary outcomes of clinical trials include a neurological assessment for motor function and reflexes and

determining adverse side effects. Secondary outcomes of clinical trials include assessment in changes of ODI, VAS pain scores, and QOL after 12 months from baseline.

Data for clinical trial NCT01158924 [302] was collected from multiple locations in Australia. A total of 40 subjects were enrolled in the study. Patients received either 1.0 mg (n = 14) or 2.0 mg (n = 26) of rhGDF-5. None of the patients experienced neurological or motor function problems after 12 months. Both groups showed a decrease in ODI, VAS pain scores, and an increase in overall QOL. Five out of 40 patients reported some type of serious adverse side effects, which may or may not be associated with growth factor administration. No placebo control group was used in this study. The influence of growth factor dosage on pain relief remains unknown.

Clinical trial NCT00813913 [303] performed a similar study located at centers across the United States. A total of 32 patients received either 0.25 mg (n = 7) or 1.0 mg of rhGDF-5. None of the patients experienced neurological or motor function problems after 12 months. Four out of 32 patients experienced serious adverse side effects. Overall, both groups reported decreased ODI and VAS pain scores and increased QOL. Interestingly, more than half of the number of patients still reported LBP (19 out of 32). This clinical trial also did not have a placebo control group.

Clinical trial NCT01182337 [304] was performed in several areas of Korea. A total of 31 patients were enrolled. Patients received either 1.0 mg of rhGDF-5 (n = 22) or a vehicle control consisting of trehalose, glycine, HCl and water for injection (n = 9). Neurological or motor function symptoms were not reported. Both groups reported a decrease in ODI and VAS pain scores with growth factor administration showing slightly

larger reductions. Improvements in QOL were higher for the placebo group compared to the rhGDF-5 group. Two out of 22 patients experienced IVD protrusion and 9 out of 31 patients still experienced LBP after 12 months. The clinical trial demonstrates that the placebo effect most likely plays a role in perception of pain relief.

Finally, data for clinical trial NCT01124006 [305] was collected throughout several centers in the United States. A total of 24 patients were enrolled and received either 1.0 mg of rhGDF-5 (n = 10), 2.0 mg of rhGDF-5, or water for injection (n = 10). Like the previous clinical trial, patients experienced similar levels of decreased ODI, and VAS pain scores compared to the placebo control group. QOL improved for all patients in the study, however 14 out of 24 subjects still experienced LBP.

Growth factor administration has proven to be an effective therapy for repairing the degenerated disc. In vitro models have shown that a wide variety of BMPs can promote cell proliferation and ECM production. Each growth factor plays a specific role in cellular response to repair. In the presence of growth factors, healthy disc cells produce discogenic ECM, whereas the catabolic behavior of degenerated disc cells is reversed in order to regain a healthy phenotype. Animal models have demonstrated increased disc height, water content, and proteoglycan synthesis after delivering growth factors to the degenerated disc. Additionally, growth factor delivery promotes discogenic phenotype. On the contrary, BMPs can also stimulate undesired bone formation in vivo. In the clinical setting, growth factor injections decrease patient pain or disability and improve overall QOL, however the placebo effect should not be overlooked. It is also difficult to determine the exact mechanisms in which human disc cells respond to protein therapy in vivo. Lastly, protein therapy relies on the presence of metabolically active NP and AF

cells to stimulate an anabolic response, which may not be effective if disc tissues are degenerated [306]. New cells may be implanted into the disc if there aren't enough native disc cells to produce newly synthesized ECM.

**2.6.2 Stem cell therapy.** Stem cell therapy has been investigated as an additional type of treatment for repairing the degenerated disc. Stem cells are self-renewing and have the potential to differentiate toward any cell type in the human body. Self-renewal is an important property in which a single stem cell can proliferate and generate daughter cells that are identical to the dividing parent cell [307]. These unspecialized cells do not perform any tissue-specific tasks, until instructed to differentiate through signaling pathways. Stem cells can be classified as totipotent, pluripotent, or multipotent. Totipotent cells are found in a zygote and form the beginnings of an embryo and placenta. Pluripotent cells such embryonic stem cells (ESCs) or induced pluripotent stem cells (iPSCs) can further differentiate to the three germ layers: endoderm, mesoderm, and ectoderm. Multipotent stem cells such as mesenchymal stem cells (MSCs) can differentiate toward an osteogenic, chondrogenic, myogenic, or adipogenic lineage. MSCs secrete extracellular vesicles such as exosomes as well as cytokines and growth factors that suppress immune system response [308]. Populations of MSCs are heterogeneous and exhibit varying degrees of multipotency, which are most likely controlled via autocrine or paracrine signaling mechanisms [309]. MSCs also exhibit plasticity, which is the ability to dedifferentiate or transdifferentiate from one cell phenotype into another [310].

Bone marrow-derived MSCs (BMDMSCs) have been isolated and evaluated for their differentiation potential [311,312,313]. Donor site morbidity or pain, and low cell

yield are all existing obstacles to overcome when isolated MSCs from bone marrow [313,314]. Therefore, alternative sources of tissue for MSC isolation have been explored which include, but is not limited to trabecular bone [315,316], muscle [317,318,319], adipose [320,321], articular cartilage [322,323,324], and skin [317,325]. Although MSCs show similar phenotypic behavior, many factors such as yield, proliferative ability, differentiation propensity, multipotency, and ease of accessibility and isolation can vary depending on the tissue source. Kern et al. [326] compared properties of MSCs derived from umbilical cord blood, bone marrow, and adipose tissue. This study demonstrated that all three stem cell populations exhibited differences in total yield, culturing duration, and proliferative capacity. Extracted MSCs were the highest and lowest in adipose and umbilical cord blood, respectively. Additionally, MSCs derived from umbilical cord blood showed the highest proliferative capacity, while bone marrow derived MSCs exhibited the lowest proliferative capacity. Sakaguchi et al. [327] found significant differences in differentiation potential amongst MSCs derived from bone marrow, synovium, adipose, skeletal muscle, and periosteum. Overall, bone marrow, synovium, and periosteum derived MSCs showed superior differential capacity for chondrogenesis compared to adipose and muscle derived MSCs.

Other contributing factors that may impact MSC properties are donor age and disease state. Quarto et al. [328] showed that MSC yield, proliferation rate, and differential ability decreased with increasing donor age. Bone marrow derived MSCs were isolated from osteoporotic women and showed significantly reduced ability to proliferate and differentiate toward an osteogenic lineage when compared to healthy donors of the same age [329]. Similar findings were observed by Murphy et al. [330]

when MSCs from patients with advanced osteoarthritis exhibited inferior properties in terms of chondrogenic and adipogenic activity. Although autologous tissue sources are considered ideal in the clinical setting, donor age and disease should be carefully considered as well as allogeneic cell sources.

Adipose-derived MSCs (ADMSCs) have gained much interest in the field of tissue engineering. One benefit of adipose-derived stem cells is that they are easily obtained in large quantities with minimal donor site morbidity [331]. In general, adipose-derived MSCs have been proven to be feasible and effective in treating disease and injury in both the pre-clinical and clinical settings [332,333]. This stem cell type exhibits the ability to self-renew and proliferate based on telomere length and relative telomerase activity [334] and show immunosuppressive properties [335]. Stromal cells can be isolated from lipoaspirate with greater than 95 % purity [336]. Additionally, the number of fibroblast colony-forming units isolated from one gram of adipose tissue (5,000) is greater than from one milliliter of bone marrow (1,000) [337]. This result suggests that donor site morbidity plays a critical role in stem cell isolation and can limit the yield of viable cells. Adipose-derived MSCs have been shown to undergo adipogenesis [338,339,340], osteogenesis [341], chondrogenesis [341,342,343], myogensis [343,344,345], angiogenesis [346,347] and form pre-cursor neuronal cells [348] under the appropriate culturing conditions with growth factors, external stimuli, and three-dimensional scaffold support or combination thereof.

***2.6.2.1 In vitro studies.*** The effects of MSCs on resident cells isolated from disc tissues have been well characterized in vitro. In general, proliferative capacity and ECM expression of disc cells are enhanced when co-cultured with MSCs

[349,350,351,352,353]. However, the ratio of co-cultured MSCs to NP or AF cells can either inhibit or promote disc cell growth and protein accumulation [350,352,354]. Watanabe et al. [351] compared the monoculture of NP cells to co-cultures of NP cells and MSCs with or without direct contact. NP cells that were in direct contact with MSCs showed significantly higher levels of proliferation and proteoglycan production compared to indirect co-cultures. Strassburg et al. [349] co-cultured non-degenerate or degenerate NP cells with MSCs in monolayers at a ratio of 1:1. Interestingly, non-degenerate NP cell phenotype did not change, however degenerate NP cells exhibited an enhanced matrix gene expression. Further, Shim et al. [353] demonstrated that MSCs can downregulate the expression of pro-inflammatory cytokines such as IL-1α, IL-6, and TNF-α in NP and AF cells.

Co-cultured disc cells can also influence MSC behavior. MSCs will undergo differentiation toward an NP [355,356] or AF-like [357] phenotype when in direct contact with the corresponding cell type. The proliferative capacity of MSCs increases when co-cultured with either NP or AF cells compared to monocultures [353]. MSCs have also been shown to produce significantly more proteoglycan when co-cultured with AF cells [358]. Several studies have identified increased expression in MSCs for trophic factors such as TGF- β [349,353], CDMP-1 [349], BMP-7 [353], GDF-7 [353], and IGF-1 [304,353]. The release of these growth factors enables degenerate disc cells to regain a healthy phenotype. In addition, MSC matrix gene expression levels for type I collagen [354], type II collagen [308,354,357], type VI collagen [304,308,354], aggrecan [304,308,354,357], and versican [304,308] are elevated when in co-culture with disc cells. These findings suggest that MSCs may be able to stimulate the endogenous disc

cell population and initiate self-repair of disc tissue. Alternatively, MSCs can produce their own disc-like ECM and potentially restore biological functions within the IVD if degeneracy cannot be reversed or endogenous cell anabolism remains inadequate.

***2.6.2.2 Animal models.*** The benefits of intradiscal injection of MSCs into degenerated discs have been widely studied using animal models. For example, Feng et al. [359] injected autologous BMDMSCs into rabbit discs that received a nucleotomy via needle puncture and aspiration. After two weeks, degenerated discs received an injection of either cell culture medium containing $2 \times 10^4$ BMDMSCs or medium alone as a control. Disc tissues treated with BMDMSCs exhibited increased concentrations of sulfated GAG, significant improvements in disc height index, and elevated gene expression levels for aggrecan and type II collagen compared to the control group. Cai et al. [360] injected autologous BMDMSCs into rabbit discs that were degenerated via needle puncture. Two weeks post-injury, degenerated discs received an injection of either $2 \times 10^4$ cells in saline or saline alone as a control. During the 10-week study, disc height decreased more slowly for discs that received cells compared to the control group. Additionally, discs treated with MSCs exhibited increased water content. Tissues also exhibited a significant increase in gene expression levels for aggrecan and type II collagen.

While the previous studies demonstrated beneficial outcomes of cell transplantation, it is important to note that MSC location nor survival were assessed. To gain a better understanding of cellular behavior in vivo, MSCs are labeled or stained with a marker to identify their location within the disc. Several animal models have observed cell leakage after MSC transplantation into IVDs.

Wei et al. [361] transplanted fluorescently labeled human BMDMSCs into uninjured rat coccygeal discs. Discs injected with human MSCs did not contain any T or B cells, suggesting minimal immune system response in this xenogeneic transplantation model. Immunohistochemical staining of human MSCs was positive for SOX-9 and type II collagen, indicating that the microenvironment induced differentiation. After 42 days, labeled MSCs were detected in only 6 out of 9 discs.

Jeong et al. [362] injected human ADMSCs in a rat disc degeneration model induced by puncture with a 26-gauge needle. Two weeks later, discs were each treated with an injection of $5 \times 10^4$ cells. As a control, discs received an injection of saline. Discs that received an MSC injection exhibited a smaller reduction in height and a healthier inner AF morphology compared to the saline control group. MSCs were detected using anti-human nucleic monoclonal antibody at two weeks post-implantation, however staining was negative after 4 and 6 weeks.

Sobajima et al. [363] implanted $10^5$ allogeneic BMDMSCs into healthy nucleus pulposi of New Zealand white rabbits. MSCs were retrovirally transduced with the lacZ marker gene for tracking purposes. Cells remained viable for 24 weeks after implantation. At 12 weeks post implantation, cells were in the NP and exhibited a round morphology. However, after 24 weeks, cells migrated toward the inner AF and exhibited an elongated morphology.

Ho et al. [364] explored how the severity of disc degeneration affects the regenerative capability of MSCs in a rabbit model. A 21-gauge needle was used to puncture the AF and the disc could degenerate for either 1 month or 7 months. At each

time point, $10^5$ MSCs were labeled with bromodeoxyuridine (BrdU) and injected into degenerated discs. Transplanted cells were found in the AF or CEP, but not in the NP.

Vadala et al. [365] implanted $10^5$ allogeneic BMDMSCs into degenerated IVDs of New Zealand white rabbits. Discs were stabbed in the AF with a 16-gauge needle to a depth of 5 mm and allowed to degenerate for 3 weeks. MSCs were transduced with retrovirus expressing enhanced green fluorescent protein (eGFP) for tracking purposes. Radiographic images and histological analysis revealed that MSCs had migrated toward the vertebral bone and formed osteophytes. Authors concluded that the disc's high intradiscal pressure forced MSCs to leak from the central NP.

Marfia et al. [366] injected 8 x $10^4$ human ADMSCs into bigylcan deficient mice. Over the course of 16 months, mice began to develop disc degeneration and was confirmed using MRI. Immunohistochemistry was performed to locate human ADMSCs using anti-human nucleic monoclonal antibody. ADMSCs survived 12 weeks post implantation and acquired a positive expression for biglycan. ADMSCs were identified in treated and adjacent discs, thus indicating cell migration.

Overall, the results of these animal models point toward the feasibility of cell transplantation and have led to insights into how to optimize the strategy as an approach in achieving disc regeneration. Injection of MSCs increases the disc's water content, height, and gene expression of ECM. Furthermore, the disc microenvironment will induce MSC differentiation toward a specific phenotype as evidenced by changes in cell morphology and gene or protein expression. Despite these successes, cell retention has proven to be a common occurrence and can have negative clinical consequences. Implanted MSCs tend to migrate from the injection site toward the peripheral AF, CEP,

or vertebral bone. Osteogenic differentiation is an undesirable side effect of MSC transplantation and can lead to the formation of osteophytes instead of disc-like tissue.

***2.6.2.3 Clinical trials.*** Several clinical trials have investigated the efficacy of cell transplantation into degenerated discs. This type of treatment is considered relatively new; therefore, results are limited, and sample sizes are low. Different approaches were taken to repair degenerated discs with stem cells. Some studies expanded isolated cells in vitro prior to implantation, whereas others injected bone marrow aspirate directly into IVDs. A few cell types were selected for transplantation including hematopoietic stem cells, BMDMSCs, or reactivated NP cells after coculture with MSCs.

Haufe et al. [367] injected 1 mL of autologous bone marrow aspirate containing hematopoietic precursor stem cells into painful discs of 10 patients. Following stem cell injection, patients were provided a daily treatment of hyperbaric oxygen for two weeks. One year after surgery, none of the patients reported a reduction in VAS scores, signifying no pain relief. Authors hypothesized that stem cells were not able to survive in the degenerated discs due to the low oxygen concentration. Disc height and water content were also not evaluated using radiography or MRI. It is possible that stem cells should be expanded in vitro prior to delivering to the degenerated disc. Exposure to hypoxia may also better prepare stem cells to the disc's low oxygen tension.

Orozco et al. [368] performed a cell therapy based clinical study on 10 patients who had disc pain with a preserved AF. MSCs were isolated from bone marrow aspirate and cultured in vitro for 7 days until confluent. A total of $10^7$ BMDMSCs were injected into the NP with a 20-gauge needle. After 3 months, there was an 85 % improvement in pain and parallel improvements in disability and QOL.

Pettine et al. [369] injected approximately 2 – 3 mL of autologous bone marrow concentrate into symptomatic discs of 26 patients. Bone marrow concentrate contained both hematopoietic stem cells and MSCs. ODI and VAS scores drastically decreased over a 12-month period. Discs appeared to be less degenerated and more hydrated as evidenced by improved Pfirrmann grading and MRI scores, respectively. It's important to note that MSCs were not expanded in vitro prior to delivery in the degenerated disc, however bone marrow concentrate contains important cytokines and growth factors that may aid in tissue repair.

Mochida et al. [370] performed a 3 year-long study on 9 candidates who exhibited a Pfirrmann's grade III disc degeneration. BMDMSCs from the iliac crest and NP cells from symptomatic discs were extracted from patients. NP cells were co-cultured with MSCs to reestablish a healthy phenotype. Approximately 7 x $10^5$ NP cells were transplanted into the IVDs. Japanese Orthopaedic Association (JOA) scores increased, signifying improvement in (PAIN?) after receiving an injection of NP cells. Pfirrmann grading scores were maintained after a 3-year follow up. This study demonstrates that reactivated NP cells can also be used instead of MSCs.

Elabd et al. [371] treated 5 patients exhibiting signs of degenerative disc degeneration with an intradiscal injection of autologous BMDMSCs. Extracted MSCs were populated under hypoxic conditions prior to delivery into symptomatic discs. Approximately 15.1 – 51.6 million cells were delivered into each IVD. No adverse effects were reported from 4 – 6 years after injection. Four out of five patients reported a 40 – 90 % improvement in strength and mobility. Interestingly, authors observed a linear

correlation between increasing cell number and increasing improvement, however conclusions cannot be drawn due to the study's low sample size.

These clinical studies have shown promising results in treating disc degeneration using cell transplantation. The superior cell type used for transplantation, whether reactivated NP cells or MSCs, remains to be determined. MSCs may be advantageous as they can provide immunomodulatory mechanisms, promote anabolism, and stimulate native disc cells to regain a healthy phenotype. After receiving MSC transplantation, patients experienced decreased pain and disability, as well as increased strength and mobility. These clinical improvements may be associated with the rehydration of degenerated discs. It is believed that MSCs are responsible for the production of proteoglycans, which aids in water retention. Interestingly, the increased water content does not produce a sufficient hydrostatic pressure to restore disc height. Cell retention also continues to be a challenge in the field of IVD tissue engineering. To combat these potential issues, the use of an encapsulating polymeric biomaterial may prove useful in restoring disc height and ensuring the retention of delivered MSCs.

**2.6.3 Polymeric biomaterials and scaffolds.** Use of a polymeric biomaterial that encapsulates and localizes cells within the disc is considered a beneficial addition to disc tissue engineering strategies. A carrier would provide a matrix for cell attachment, making them less prone to dislocation after injection. Injectable carriers represent the only practical option for intradiscal cell transplantation because they are implantable through small gauge needles. This lowers the degree of damage to the AF, thus helping to prevent cell leakage. In addition, polymeric carriers can aid in the restoration of disc height and reestablish intradiscal pressure. Polymeric materials are largely derived from

natural sources for reasons of biocompatibility. BMDMSCs and ADMSCs have been suspended in polymers based on hyaluronic acid (HA) [372,373,374,375,376,377,378,379], collagen [380,381,382,383], fibrin [384,385,386], alginate [387], chondroitin sulfate [388], and protein [389,390].

***2.6.3.1 Animal models.*** A strategy to locate and quantify enzymatic activity of transplanted MSCs was developed by Omlor, Bertram et al. [384]. A partial nucleotomy was performed on minipigs using a 16-gauge cannula equipped with suction. Fibrin hydrogel containing $Al_2O_3$ particles and autologous BMDMSCs retrovirally labeled with luciferase gene was injected into the denucleated disc. $Al_2O_3$ particles were added to identify the fibrin hydrogel with microCT. MSCs were transfected with the luciferase gene in order to gauge enzymatic activity. Three days post-injection, the volume of detected $Al_2O_3$ particles declined to 9 % of the original measured value upon implantation. Similarly, only 7 % of cellular luciferase activity was quantified. Authors hypothesized that the implant extruded from the injection site during motion. In a follow-up study, Omlor, Fischer et al. [379] switched the hydrogel carrier from fibrin to an in situ forming albumin and hyaluronan hydrogel. The crosslinked hydrogel is designed to fill irregularly shaped defects in the disc and exhibits a higher compressive strength compared to fibrin. The same methods of tissue injury, cell transfection, and particle suspension were applied in this model. Three days post-injection, the volume of detected $Al_2O_3$ declined to 61 % of the original measured value. Implant retention was significantly improved compared to the previous study. Only 38 % of cellular luciferase activity was quantified after accounting for implant loss, therefore cellular viability or metabolic activity may have declined. These studies demonstrate that the mechanical and

adhesive properties of a hydrogel carrier must be high enough to endure loading and resist expulsion from the IVD.

Crevensten et al. [372] tested the feasibility of implanting BMDMSCs into rat coccygeal IVDs to test whether injected cells survive, differentiate, and produce disc-like ECM in vivo. To test this hypothesis, autologous BMDMSCs were suspended at a density of $10^7$ cells/mL in a 15 % HA solution and injected into uninjured discs. MSCs were clearly localized in the central NP at the beginning of the study. After 7 and 14 days, the cell number had reduced appreciably and MSCs were in the AF. After 28 days, MSCs were able to proliferate within the rat disc and exhibited 100 % viability. Authors concluded that the decrease in the number of injected cells may have resulted from the expulsion of NP tissue or HA carrier from the needle tract. Therefore, cell carriers must exhibit high viscosity to resist expulsion upon injection into the disc. This model also represents the best-case scenario in which disc degeneration has not occurred and MSCs are able to thrive in a healthy IVD microenvironment.

Revell et al. [373] evaluated the use of two different HA derivatives for autologous BMDMSC delivery into nucleotomized porcine discs. The D-glucuronic acid residues of HA were conjugated with an ester or dodecylamide, which facilitates self-assembly and cell encapsulation. Cells were encapsulated at a density of $10^6$ cells/mL and a total volume between 0.5 – 1 mL was injected into each disc. Discs that received no treatment after nucleotomy exhibited a loss in IVD structure with narrowing, fibrosis, and bony endplate disruption. Injection of the HA derivatives resembled the biconvexity of the native NP tissue and preserved disc architecture. Upon histological examination,

MSCs appeared chondrocyte-like in nature and produced ECM. Both HA carriers were effective in transplanting MSCs into the nucleotomized discs.

Ganey et al. [374] evaluated the use of HA for autologous ADMSC delivery into nucleotomized canine discs. Three discs in each dog underwent a nucleotomy and received either an injection of HA containing ADMSCs, HA only, or no intervention. One year after transplantation, gene expression and protein deposition of type II collagen and aggrecan were significantly higher in discs treated with ADMSCs compared to those that received only HA or no intervention. Measureable differences in disc height recovery and water content assessed through MRI between the treated and untreated groups did not reach significance. Authors concluded that treatment with ADMSCs can potentially retard disc degeneration after nucleotomy and replace lost disc tissue.

Ghosh et al. [375] treated degenerated ovine discs with mesenchymal precursor cells encapsulated in HA. Discs were enzymatically degenerated using chondroitinase ABC. Chondroitinase ABC specifically cleaves the glycosidic bond of chondroitin sulfate polymer chains found in the IVD. Sheep were treated with HA containing either a low ($0.5 \times 10^6$) or high ($4 \times 10^6$) dosage of cells. As controls for comparison, superior and inferior discs remained untreated or were injected with HA. Enzymatic degeneration caused disc height index to decrease by 45 – 50 %. Degenerated discs treated with cells exhibited improvements in MRI scores and disc height index recovered toward baseline values. Histopathology scores confirmed that discs treated with low and high doses of cells were significantly different compared to discs that remained untreated or received HA only. A higher cell dose can potentially hasten the regeneration of IVD-like tissue.

Chun et al. [376] transplanted ADMSCs into a degenerated lapine disc model. Discs in New Zealand white rabbits were degenerated via a 19-gauge needle puncture and was verified with MRI. Nineteen weeks post-injury, human ADMSCs were suspended in hyaluronic acid at a density of 2 x $10^6$ cells/mL and injected into the disc. As a control, saline was injected into the adjacent injured disc. Eighteen weeks after treatment, discs injected with ADMSCs regained a lamellar structure between the NP and inner AF. Increased cellularity and a dense ECM rich in proteoglycan were also observed in treated discs compared to the untreated controls. Grafted ADMSCs were not rejected by the host and bone formation was not observed.

Reitmaier et al. [377] used an ovine degeneration model to study the effects of MSC transplantation. Partial nucleotomies were performed on sheep discs and subjected to a variety of treatments. Discs received either an injection of HA containing BMDMSCs at a density of $10^6$ cells/mL, HA alone, or no treatment. The AF defect was closed with sutures, sealed with 2-octyl-cyanoacrylate, and covered with a collagen sponge. Discs implanted with MSCs were not superior to untreated discs in terms of disc height recovery, biomechanics, and histology. Authors suggested that the implanted HA hydrogel may have extruded from the nuclear cavity, however MSCs were not tracked in this animal model. This study emphasizes the importance of minimizing annular damage to minimize the risk of extrusion.

Barczewska et al. [378] emphasized the importance of cell retention upon delivering MSCs into a degenerated porcine disc model. Dehydration and subsequent degeneration of the IVD was induced through laser vaporization. Autologous BMDMSCs were encapsulated at a density of 1 x $10^6$ cells/mL in HyStem. HyStem is a hydrogel

composed of modified components of hyaluronan and gelatin, which in the presence of a crosslinker, forms a biocompatible resorbable hydrogel. MSCs were labeled with superparamagnetic iron oxide nanoparticles for tracking purposes. After two weeks, transplanted MSCs were successfully confirmed within the central NP using both MRI and histological staining. While the technique used for tracking purposes is unique, the authors did not report the behavior of MSCs in vivo.

Sakai, Mochida, Yamamoto et al. [380] hypothesized that maintaining the integrity of the central nucleus pulposus will preserve the structure of the AF and decelerate IVD degeneration. Authors suggested that NP tissue can be fortified by injecting a hydrogel carrier containing MSCs. Autologous BMDMSCs were isolated from New Zealand white rabbits and labeled with recombinant Adenovirus vector expressing E. coli lacZ gene to confirm the viability after transplantation. Discs were punctured and NP tissue was aspirated through a 21-gauge needle. Two weeks following NP removal, MSCs were embedded in Atelocollagen® matrices and transplanted into degenerated discs. Atelocollagen was selected as the hydrogel carrier for its anti-immunogenic properties and potential degradability. Additionally, atelocollagen behaves as an injectable liquid at 4 °C and solidifies into a hydrogel at physiological temperature of 37 °C. Histology revealed significant structural changes in degenerated discs compared to normal control discs. Eight weeks following nucleotomy, cells in the NP were sparse, lamellae of the inner AF collapsed, and connective tissue formation occurred. In contrast, discs treated with collagen hydrogel containing BMDMSCs prevented the collapse of the inner AF and connective tissue invasion. Newly synthesized ECM replaced the previously removed NP tissue. Positive immunostaining for proteoglycans and beta-

galactosidase were detected in discs treated with MSCs, thus indicating ECM synthesis and cell survival, respectively. Sakai, Mochida, Iwashina, Hiyama et al. [382] performed an identical study in which autologous BMDMSCs were implanted into degenerated rabbit discs. However, this study presented morphological findings as well as gene and protein expression analyses. After 24 weeks following MSC transplantation, authors reported a restoration in disc height and water content as shown by x-ray and MRI. Immunohistochemistry and gene expression analyses demonstrated that MSCs were able to replenish proteoglycan content in degenerated discs. In a similar study, Sakai, Mochida, Iwashina, Watanabe et al. [381] injected autologous BMDMSCs labeled with green fluorescent protein (GFP) into degenerated rabbit discs and results were evaluated after 2 and 48 weeks after transplantation. The percentage of GFP-positive cells located in the NP rose from 15 ± 8 % (2 weeks) to 55 ± 7 % (48 weeks). In addition, transplanted MSCs were positively stained for keratin sulfate, chondroitin sulfate, and type II collagen, but lacked expression for type I collagen. These studies suggest that MSCs differentiated toward an NP-like phenotype and were influenced by the surrounding IVD microenvironment.

Li et al. [383] implanted collagen microspheres containing autologous BMDMSCs into degenerated rabbit discs. Similar to other studies, discs were punctured with a 21-gauge needle and NP tissue was removed to induce degeneration. One month after injury, 2.5 x $10^5$ MSCs were either suspended in saline or encapsulated in collagen microspheres and injected into the degenerated discs. Results demonstrated that the use of a collagen carrier for transplanting MSCs reduced the incidence of osteophyte formation, relative to the saline control. It is believed that the natural adhesive behavior

of the collagen helped to anchor the carrier within the disc space, thus aiding in cell retention. However, improvements could still be made to reduce that incidence even further.

Allon et al. [385] studied the use of bilaminar coculture pellets (BCPs) combined with hydrogel carrier delivery for treating degenerated discs. In brief, human MSCs form the center of the BCP and NP cells isolated from adult bovine tails surround the MSCs. Each pellet contains a total of 250,000 cells with a 3:1 ratio of MSCs to NP cells. Rat discs were injured via stab and denucleation. Discs were treated with a single BCP encapsulated in a fibrin hydrogel. For comparison, the same number of total cells, MSCs, NP cells, or a mix, were suspended in fibrin and injected into degenerated discs. Control groups included injured discs that were untreated or treated with acellular fibrin. Disc height and grade, as determined by x-ray and histology, improved over time for discs that received fibrin hydrogel and a BCP. After 35 days, proteoglycan was only detected in discs treated with fibrin and a BCP. Cells were not traced nor assessed for viability in this study, however BCP appeared to retain more cells overall compared to other groups. Immunogenic response was not evaluated in this xenogeneic model which involved three different species. Pellet cultures may provide an improved means of retaining and sustaining cellular performance in vivo.

Yang et al. [386] implanted autologous BMDMSCs into a degenerated lapine disc model. Disc degeneration was induced in New Zealand white rabbits by puncture with a 21-gauge needle and NP tissue was aspirated. MSCs were suspended at a density of $10^8$ cells/mL in fibrin hydrogel carrier containing TGF-β1. Treated discs were compared with degenerated discs that received acellular hydrogel or no treatment. Discs that were

transplanted with MSCs exhibited a slower rate of decrease in both DHI and cell apoptosis. BMDMSCs were also able to synthesize type II collagen in vivo.

Wang et al. [387] compared the regenerative properties of human BMDMSCs to MSCs derived from the NP, CEP, and AF in a rabbit degeneration model. Disc degeneration was induced by puncture with an 18-gauge needle to a depth of 5 mm and NP tissue was aspirated. Degenerated discs were treated with alginate solution containing MSCs derived from bone marrow, NP, CEP, or AF. MSCs were fluorescently labeled for tracking purposes. Calcium chloride solution was injected into the disc to crosslink the alginate hydrogel. Treated discs were compared to degenerated discs that received acellular alginate hydrogel or no treatment. Discs that were not manipulated served as a normal control group. Interestingly, MSCs derived from the CEP exhibited the greatest MRI signal intensity compared to all other treatment groups. After 6 months, there were no statistical differences detected between the discs treated with CEP derived MSCs and the normal control group. BMDMSCs and NP derived MSCs appeared to have similar regenerative capacity, whereas MSCs derived from the AF produced inferior results and resembled the untreated disc. The use of allogeneic MSCs derived from the IVD is appealing, however autologous isolation of cells from CEP may not be clinically feasible.

Zhang et al. [388] utilized a semi-synthetic hydrogel carrier for the delivery of allogenic BMDMSCs in a caprine degeneration model. The hydrogel is composed of poly (ethylene glycol)-diacrylate, acrylated chondroitin sulfate, and HA. Crosslinking was achieved using a redox initiation system. Discs were stabbed with a scalpel blade to a depth of 15 mm in order to induce differentiation. After one month, discs were treated with hydrogel containing 2.5 x $10^5$ MSCs, hydrogel, or saline. Compared to the control

IVDs, discs treated with cells showed increased proteoglycan content in the NP, yet no statistically significant changes in collagen, MRI grade, or histology were detected. MSCs were not tracked nor was viability ascertained in this study. The presence of a redox initiator could potentially compromise MSC viability in vivo.

Henriksson et al. [389] compared the delivery of MSCs into discs with and without the use of a hydrogel carrier. Puramatrix ®, a synthetic polypeptide sequence consisting of 16 amino acids, was used to encapsulate and deliver human BMDMSCs into degenerated discs of minipigs. NP tissue was aspirated from the disc using a 20-gauge needle. Two weeks later, $0.5 \times 10^6$ MSCs were encapsulated in the peptide hydrogel and injected into each disc. For comparison, discs were also treated with MSCs suspended in culture media or left untreated. MSCs were detected in 90 % and 80 % of discs treated with a hydrogel and media carrier, respectively. Cells delivered in a media carrier were located within the transition zone and regions of the NP, whereas cells delivered in the peptide hydrogel were distributed throughout the NP and AF. MSCs differentiated toward a discogenic phenotype as evidenced by enhanced gene expression for SOX9, type I collagen, type II collagen, aggrecan, and versican, however this study did not quantify cell survival. The use of a hydrogel carrier can potentially facilitate cell differentiation and protein formation by providing a three-dimensional network.

Bendsten et al. [390] compared the use of HA to PhotoFix, a protein-based hydrogel. Minipigs received a full thickness annular incision to induce disc degeneration over a 12-week period. Autologous BMDMSCs were isolated and labeled intracellularly with quantum dots. Discs were treated with cell-seeded hydrogels or left untreated as a control. Twelve weeks after treatment, MSCs were in the disc. Discs treated with MSCs

delivered in both HA or PhotoFix exhibited significantly higher signal intensities on MRI and significantly lower Pfirrmann scores compared to untreated controls.

Hydrogel carriers are beneficial in that they entrap MSCs within a three-dimensional network, thus improving retention. Once the carrier has successfully anchored to surrounding disc tissue, MSCs become localized within the disc and are able to replace lost tissue by producing new discogenic ECM. In addition, studies have noted that the microenvironment directs MSC differentiation toward an NP-like phenotype. Ultimately, the delivery of a carrier with MSCs can retard disc degeneration after nucleotomy. However, the carrier must demonstrate high viscosity, mechanical, and adhesive properties to endure loading and resist expulsion from the injection site. It is important to note that annular damage should minimized to reduce the risk of implant extrusion.

***2.6.3.2 Clinical trials.*** Few clinical trials have been published that describe the use of polymeric carriers for the encapsulation and delivery of cells to treat patients with degenerated discs and LBP. Since a superior cell line has yet to be identified for transplantation, various types have been utilized to treat DDD. The sources in which these cells have been derived from are strictly autologous or allogeneic, as xenogeneic origins pose potential risks of disease transmission and immune response. In addition, both synthetic and naturally-derived polymeric carriers have been evaluated as potential three-dimensional cultures systems for the delivery of cells in vivo.

Autologous IVD cells can be potentially isolated from surgically removed tissue, expanded in vitro, and reinserted into the degenerated disc. Tschugg et al. [391] investigated the use of a product called Novocart Disc Plus, which contained 3 – 4

million autologous IVD cells encapsulated in a carrier (NDisc). The NDisc is a two-part injectable system. One solution is composed of modified human albumin, serum, chondroitin sulfate, and hyaluronic acid. The other solution is a bis thio-polyethylene glycol. When combined, the solutions polymerize in situ to form a hydrogel. Results from this study have yet to be published.

Another cell type that has been clinically investigated to treat DDD and LBP are chondrocytes. Coric et al. [392] performed a phase II clinical study to evaluate the safety and effectiveness of allogeneic juvenile chondrocytes. Chondrocytes were encapsulated in NuQu, a fibrin-based carrier, at a density of approximately $10^7$ cells/mL. A total of 15 patients were enrolled in this study. All functional scores significantly improved from pre-operative baseline readings. Out of thirteen patients, ten individuals exhibited improvements in MRI and three showed improvements in disc height and contour. None of the patients experienced neurological deterioration, infection, or adverse events. However, three out of 15 patients underwent TDR at the one-year follow-up due to persistent LBP.

Yoshikawa et al. [393] was one of the first to report implanting collagen sponges containing autologous MSCs into two patients with LBP. The MSCs were obtained from bone marrow isolated from the iliac crest. BMDMSCs were first expanded in culture for either 2 or 4 weeks in vitro and seeded onto collagen sponges at a density of $10^5$ cells/mL. Sponges were grafted percutaneously into the central region of the IVD. Two years post-surgery treated discs exhibited high moisture content and lumbar disc instability improved. While these results seem promising, the sample size for this study was small.

Kumar et al. [394] performed one of the first phase I clinical studies to utilize ADMSCs combined with a hyaluronic acid derivative for the treatment of chronic LBP. A total of ten patients were enrolled in this study. Three weeks prior to delivery, MSCs were isolated from adipose tissue gathered via liposuction, expanded in vitro, and encapsulated within the hyaluronic acid hydrogel. The hyaluronic acid was derived from a nonanimal origin and is cross-linked with butanediol diglycidyl ether. Patients were split into two groups and received either $2 \times 10^7$ or $4 \times 10^7$ ADMSCs per disc. After one year, six out of ten patients, three from each cell dose group, exhibited significantly improved functional scores. Cell dosing did not cause any significant differences in improvements. Three patients also exhibited increased water content in the disc. Authors noted that other diseases that cause chronic LBP such as spondylolisthesis, spinal stenosis, facet joint arthritis, decreased disc height, and herniation may have prevented successful treatment. This study demonstrates that early intervention in treating disc degeneration is key to clinical success. The total number of delivered cells may be an important variable that impacts patient outcomes, however this study could not conclude whether a low or high dose was more effective.

Several clinical trials have been initiated by numerous companies around the world. Hydrogels based on fibrin [395] and hyaluronic acid [396,397,398,399,400] have been proposed as potential polymeric cell carriers. Hyaluronic acid is frequently selected over fibrin as the carrier of choice, most likely because it is a naturally occurring GAG within the IVD. Clinical trials have also proposed to isolate a variety of cell types including mesenchymal precursor cells [396,397], IVD cells [398], juvenile chondrocytes [395], BMDMSCs [399], and ADMSCs [400] from either allogeneic [395,396,397,399]

or autologous [398,399,400] origins. The status of each study has been deemed as completed [396], active, but not recruiting [397,398], unknown due to inactivity [399,400], or terminated due to changes in clinical approach [395]. Results from these studies have not been published but will potentially answer important questions concerning the advantages and disadvantages of cell origin, type, dosage, and use of polymeric carriers.

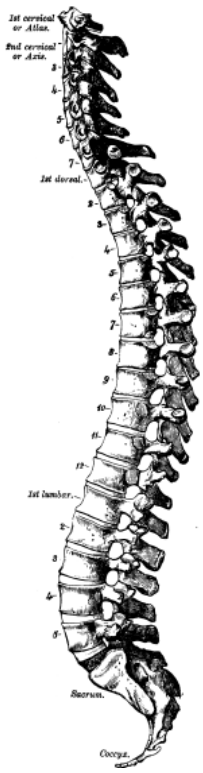


*Figure 1.* Lateral view of the human spinal column illustrating the cervical, dorsal, lumbar, sacral, and coccygeal regions.

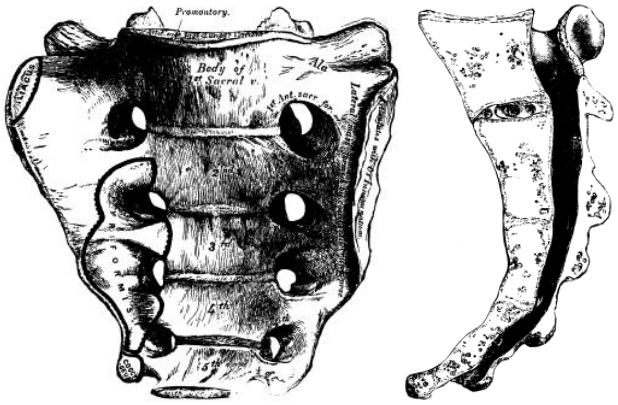


*Figure 2.* The distal fused regions of the spine: sacrum (left) and coccyx (right).

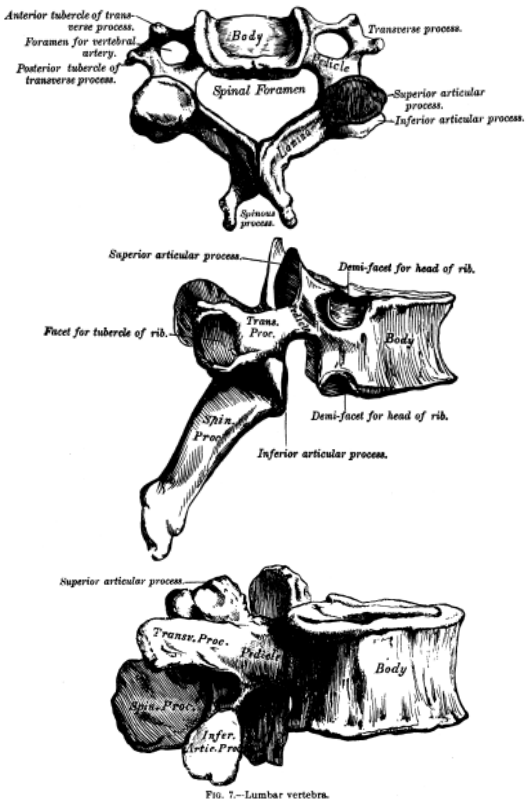


FIG. 7.—Lumbar vertebra.

*Figure 3.* Examples of the various vertebral bodies of the cervical (top), dorsal (middle), and lumbar (bottom) regions.

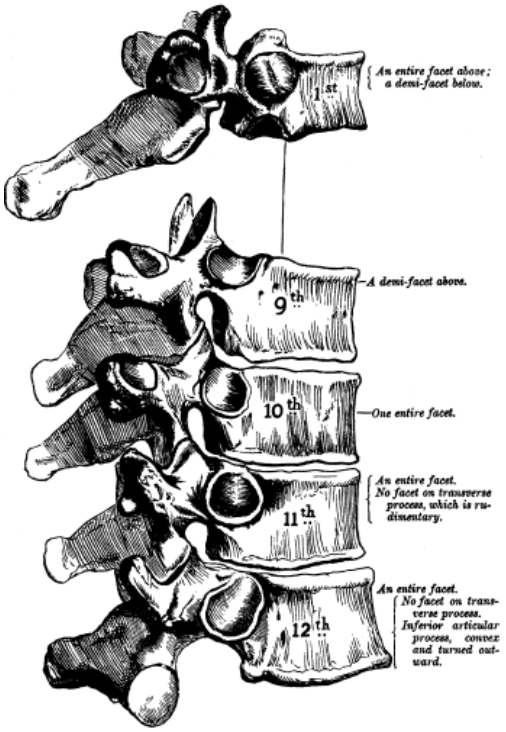


*Figure 4.* Stacked arrangement of the dorsal vertebral bodies.

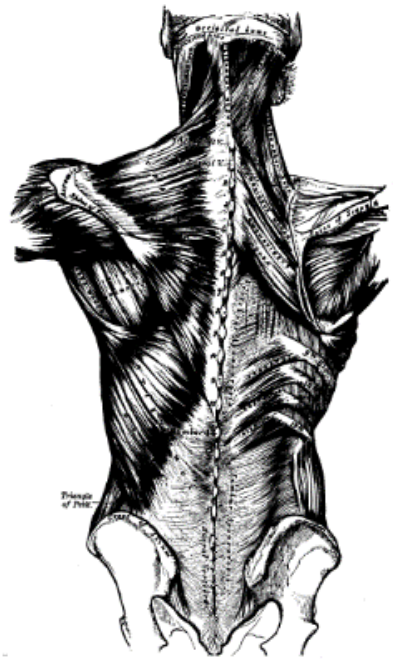

*Figure 5.* The intricate network of back muscles that attach to the spinal column of the human body.

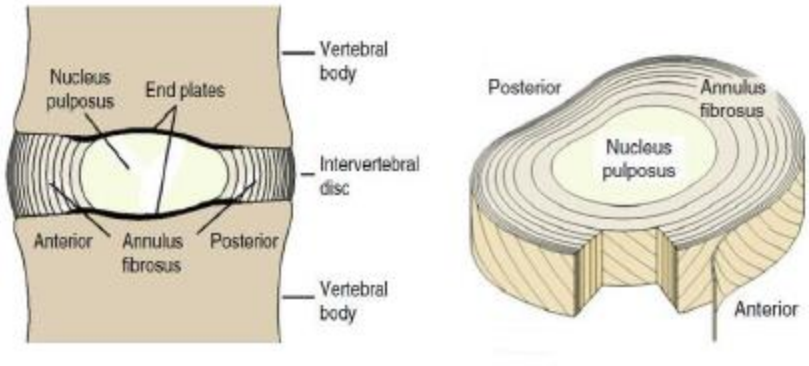


*Figure 6.* Intervertebral disc. The disc resides between two adjacent vertebral bodies (left) and is composed of the cartilage endplates, annulus fibrosus, and nucleus pulposus (right).

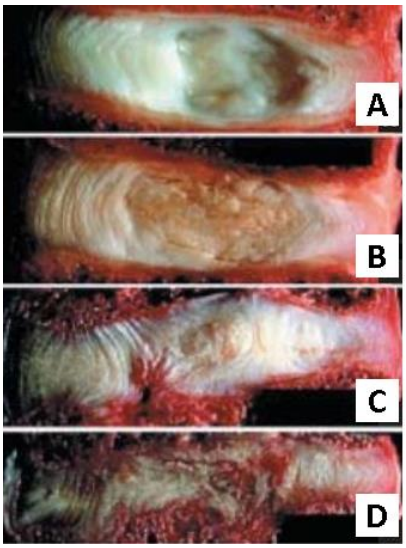


*Figure 7.* Progressive degeneration of the intervertebral disc. (A) healthy IVD characterized by a hydrated NP and highly aligned, concentric AF, (B) degeneration begins with the dehydration of the NP, (C) NP volume dramatically decreases, collagen fibers in the AF begin to buckle inward, and osteophyte infiltration occurs, (D) complete loss of NP, disc thinning, and transverse bone fusion occurs during late-stages of degeneration.


*Figure 8.* Lumbar total disc replacements include the (A) SB Charit**é** III, (B) ProDisc-L, and (C) activL.

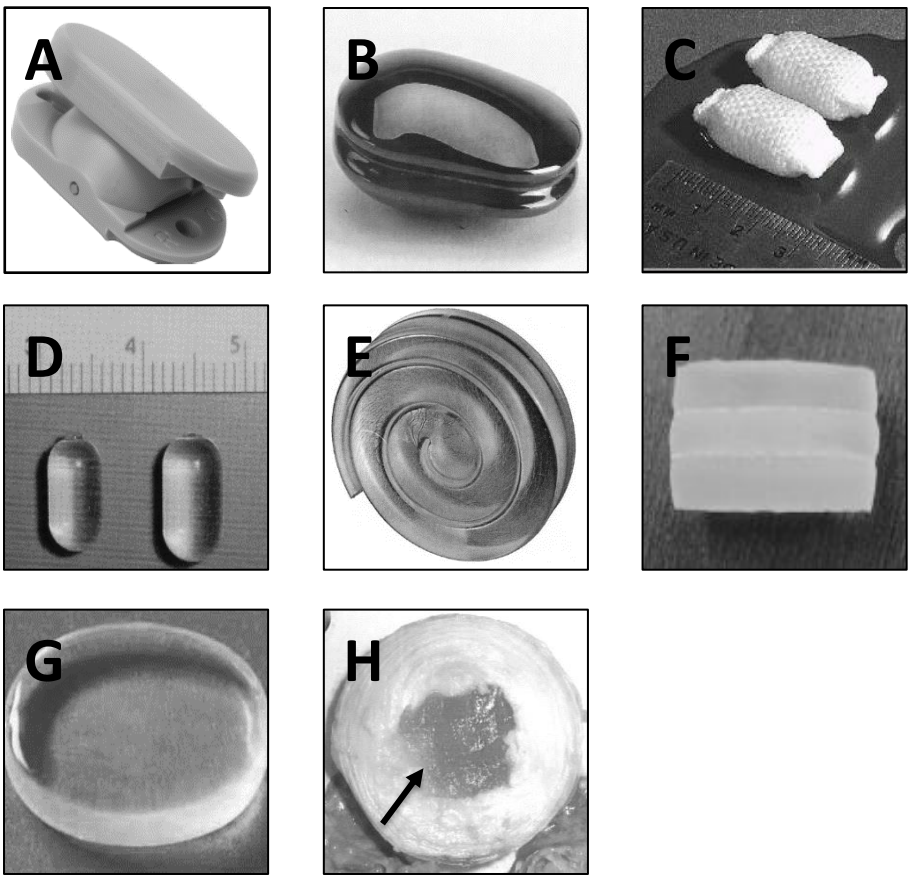


*Figure 9.* Synthetic nucleus pulposus replacement devices including: (A) NuBac, (B) Regain, (C) PDN, (D) Aquarelle, (E) Newcleus, (F) NeuDisc, (G) DASCOR, and (H) NuCore.

# Chapter 3

## Research Aims

This work focuses on the development and evaluation of a bioadhesive hydrogel composite cell carrier for the repair of degenerated IVD tissue.

The first objective was to synthesize an injectable adhesive composite consisting of a thermally sensitive hydrogel, poly(N-isopropylacrylamide)-graft-chondroitin sulfate (PNIPAAm-g-CS), and calcium-crosslinked alginate microparticles. Composite mechanical properties and adhesion to a tissue substrate were primarily evaluated and compared to native nucleus pulposus tissue. Additional scaffold properties such as swelling, porosity, degradability, shear stiffness, viscosity, and compressive stiffness were examined as a function of MP concentration and diameter.

The second objective focused on characterizing the differentiation of encapsulated ADMSCs toward an NP-like phenotype within the adhesive cell carrier in vitro. Cytotoxicity of PNIPAAm-g-CS and calcium-crosslinked alginate microparticles were primarily investigated to prevent cell death. Cells were then cultured and primarily assessed in terms of viability and metabolic activity. Lastly, extracellular matrix deposition and NP-specific markers on both the gene and protein level were evaluated.

The third objective was to evaluate the adhesive's ability to restore biomechanical properties and resist expulsion after performing a partial nucleotomy in an ex vivo porcine disc. Two types of loading schemes were performed: compression-tension and lateral bending. Disc tissue and implant properties were measured throughout the different stages of mechanical testing. A histological approach was used to determine implant stability and adherence within the nuclear disc space.

The fourth objective was to demonstrate that the adhesive supports the differentiation of transplanted ADMSCs in an ex vivo bovine disc. Intact and degenerative disc models were first established to determine the feasibility of implanting the adhesive. Finally, we investigated the site-specific differentiation and protein deposition by implanted ADMSCs within the composite.

The specific aims of this project are as follows:

Specific Aim 1: Engineer injectable copolymers based on PNIPAAm-g-CS combined with alginate microparticles that demonstrate adhesion to tissue and the requisite mechanical properties for nucleus pulposus replacement.

Specific Aim 2: Demonstrate the in vitro differentiation of encapsulated ADMSCs toward nucleus pulposus phenotype in order to establish the feasibility of the adhesive as a three-dimensional culture system for IVD regeneration.

Specific Aim 3: Test ex vivo the hypothesis that the adhesive, when used to fill defects in the nucleus pulposus, will restore biomechanics after partial nucleotomy without the risk of herniation.

Specific Aim 4: Test ex vivo the hypothesis that the adhesive supports differentiation of transplanted ADMSCs toward nucleus pulposus or annulus fibrosus phenotype and deposition of region-specific discogenic proteins in a degenerated microenvironment.

# Chapter 4

## Synthesis & Characterization of the Bioadhesive Composite

### 4.1 Introduction

The characterization of the bioadhesive NP replacement begins with the synthesis of the thermosensitive hydrogel composite. The hydrogel, poly(N-isopropylacrylamide)-graft-chondroitin sulfate (PNIPAAm-g-CS), was developed in previous work and can be injected in a minimally invasive manner [401]. PNIPAAm-g-CS rapidly gels in situ and exhibits a phase transition above its lower critical solution temperature (LCST) and below physiological temperature [401]. Below the LCST, PNIPAAm-g-CS behaves as a hydrophilic liquid that retains water. Upon heating above the LCST, PNIPAAm-g-CS expels water and behaves as a compact, hydrophobic polymer network. In subsequent studies, calcium crosslinked alginate microparticles (MPs) were blended with PNIPAAm-g-CS to improve adhesive strength to tissue [402,403]. Alginate was selected because it is an inexpensive, biocompatible, and hydrophilic polymer that can be easily crosslinked to form MPs without the use of toxic solvents. When combined, PNIPAAm-g-CS hydrogel and alginate MPs form a unique viscous bioadhesive composite.

The addition of MPs within a hydrogel can potentially impart new or enhanced characteristics upon forming a composite. Several studies have found that both MP concentration and diameter influence composite properties. For example, Holland et al. observed that the concentration of gelatin MPs in an oligo(poly(ethylene glycol) fumarate) hydrogel varied the swelling rate [404]. Qi et al. showed that incorporating alginate MPs within a thermosensitive chitosan hydrogel influences a scaffold's topography by creating a rough surface [405]. DeVolder et al. demonstrated that

poly(lactic-co-glycolic acid) MPs exhibited interconnectivity and bonding with a collagen hydrogel phase [406]. Encapsulation of MPs in hydrogel systems has also been shown to increase a composite's viscosity [405] and stiffness [406]. Subsequent changes in rheological behavior are correlated with the composite's ability to adhere to tissue [407]. In the following work, composite properties were evaluated as a function of MP concentration and diameter and compared to PNIPAAm-g-CS. Properties such as scaffold swelling, porosity, degradation behavior, shear moduli, viscosity, adhesive strength, and compressive moduli were determined.

## 4.2 Methods

**4.2.1 Purification of N-isopropylacrylamide.** N-isopropylacrylamide (NIPAAm) (Acros Organics) monomer was purified to remove any stabilizers that prevent polymerization. Approximately 15 g of NIPAAm was combined with 500 mL of n-hexane (Sigma Aldrich) and heated to 60 °C until fully dissolved. The solution was allowed to recrystallize in a freezer overnight. A vacuum-filtration apparatus was used to remove excess solvent and the recrystallized monomer was dried for 24 h under vacuum. Purified NIPAAm monomer was ground and stored at 4 °C until further use.

**4.2.2 Methacrylation of chondroitin sulfate.** Chondroitin sulfate (CS) (Sigma Aldrich) was substituted with methacrylate functional groups to impart reactivity through the presence of the vinyl bond (Figure 10). First, 6 g of CS was dissolved in 24 mL of deionized water to create a 25 % w/v solution. The solution was initially heated and stirred at 60 °C to facilitate solvation. The pH of the solution was adjusted to 10 using 50 % w/w sodium hydroxide (NaOH). Then, 894 µL of methacrylic anhydride (MAA) (Sigma Aldrich) was added dropwise to the solution. The reaction proceeded for a total of

24 h at 60 °C under constant reflux and the pH was periodically adjusted to 10 with 50 % w/w NaOH. In parallel, 500 mL of acetone was chilled overnight in the freezer. After 24 h, the solution was poured and precipitated into the chilled acetone. A vacuum-filtration apparatus was used to remove excess solvent and methacrylated chondroitin sulfate (mCS) was dried for 24 h under vacuum. Once dry, mCS was ground and stored at 4 °C until further use.

**4.2.3 Synthesis and purification of PNIPAAm-g-CS.** Poly(N-isopropylacrylamide-graft-chondroitin sulfate) (PNIPAAm-g-CS) was synthesized by performing a free radical copolymerization with purified NIPAAm monomer and mCS (Figure 11). First, 10 g of NIPAAm and 2.2 g of mCS were dissolved in 192 mL of deionized water. Oxygen was purged from the solution by continuously bubbling with nitrogen. After 5 minutes of purging, the rate at which free radicals were generated was controlled by adding 976 µL of the accelerator, tetramethylenediamine (TEMED) (Sigma Aldrich). Polymerization was initiated by introducing 97.6 mg of ammonium persulfate (APS) (Sigma Aldrich). The reaction mixture was mixed for 30 seconds, blanketed with nitrogen gas, sealed, and allowed to polymerize for 24 h under fluorescent light. After the reaction reached completion, the hydrogel was placed in a 40 °C oven and allowed to gel. PNIPAAm-g-CS was submerged in pre-heated 0.01 M phosphate buffered saline (PBS) for 1 week. PBS was refreshed daily to remove unreacted components such as monomer, accelerator, or initiator. Once purified, the hydrogel was freeze dried, ground, and stored at 4 °C until further use.

**4.2.4 Synthesis of calcium crosslinked alginate microparticles.** A water-in-oil emulsion was performed to produce calcium-crosslinked alginate microparticles (MPs). First, 2 % w/v alginic acid (Acros Organics) and 2 % w/v calcium chloride ($CaCl_2$) (Fisher Scientific) were prepared. Next, 100 mL of vegetable oil, 1 mL of surfactant or Tween 20 (Sigma Aldrich), and 10 mL of 2 % w/v alginate solution were combined and blended. Alginate droplet size within the emulsion was varied using low (400 rpm) and high (1,200 rpm) stir speeds, thus generating large and small MPs, respectively. After 5 minutes of emulsification, 10 mL of $CaCl_2$ was added dropwise to the mixture. The emulsion was stirred for an additional 5 minutes to allow for crosslinking of the MPs. Bulk vegetable oil was first removed by centrifugation at 500 x g for 2 minutes and decanting the top oil phase. MPs were purified by removing residual oil through a series of washing steps with 70 % v/v isopropanol and centrifugation at 500 x g for 2 minutes. Residual isopropanol was removed through a series of washing steps with deionized water and centrifugations at 500 x g for 2 minutes. An average size for each batch was calculated by measuring the diameters of 50 randomly selected MPs using inverted light microscopy. Alginate MPs were then frozen at – 80 °C, lyophilized until dry, and stored at 4 °C until further use.

**4.2.5 Formulations and factorial design.** Freeze dried PNIPAAm-g-CS was dissolved in 0.01 M PBS at a concentration of 5 % (w/v) and blended with MPs to create different composites. The same batches of PNIPAAm-g-CS hydrogel and alginate MPs were used for each individual study. Batch consistency between studies was maintained by monitoring hydrogel viscosity and MP diameter. A 2 x 2 factorial design was

employed to study the effects of low and high MP concentration and diameter on scaffold properties compared to PNIPAAm-g-CS (P-0) alone (Table 1).

**4.2.6 Swelling properties.** Formulations were evaluated for their swelling ability and water retention. Approximately 0.5 mL of each formulation (n = 5) were weighed in a vial, gelled, immersed in 0.01 M PBS at 37 ºC for 14 d. PBS solutions were refreshed every other day. Samples were weighed and freeze dried to obtain wet and dry masses on days 0 and 14. The swelling ratio for each sample was calculated as the wet weight divided by the dry weight.

**4.2.7 Scanning electron microscopy.** Scaffold architecture and pore morphology were imaged using a Phenom Pure scanning electron microscope (SEM) (Nanoscience Instruments) equipped with a cryostage cooled to -20 ºC. Samples (n = 3) were formed in a 96 well plate, pre-heated on a slide warmer, submersed in 0.01 M PBS and incubated at 37 °C. PBS solutions were refreshed every other day. Samples were removed from the wells, placed on pre-warmed foil wraps, flash frozen in liquid nitrogen, and stored at – 80 °C. Cross sections were compared on days 0 and 14.

**4.2.8 Rheological characterization.** The rheological properties of each formulation were characterized using a Texas Instrument DHR-3 rheometer. A 20 mm parallel plate configuration with a 500 µm gap (160 µL sample volume) was used for each test (n = 5). A strain sweep was first performed to confirm that the observed data was within the linear viscoelastic region. Temperature ramps were performed within the range of 25 to 37 °C using a rate of 1 °C/min at a constant 1 % strain and frequency of 1 Hz. Gel points were identified as the crossover of the storage modulus (G') and loss modulus (G''). Frequency sweep tests were performed within the range of 0.01 to 15 Hz

with a constant 1 % strain and temperature of 37 °C to understand trends in G', G'', complex modulus (G*), complex viscosity (η*), and phase shift angle (δ).

**4.2.9 Enzyme degradation study.** The degradation behavior of P-0 and S-50 were examined in the presence of enzymes purchased from Sigma Aldrich. The wet and dry masses of formulations on day 0 were measured before and after lyophilization. An average water content was calculated to estimate the theoretical initial dry masses for day 7 enzymatic samples by using Equation 1:

$$\text{Water Content } (\%) = 100 * \frac{M_w - M_d}{M_w} \quad (1)$$

where, $M_w$ and $M_d$ are the wet and dry masses of the sample on day 0, respectively.

Approximately 0.3 mL of each sample (n = 5) was immersed in 2 mL of 0.01 M PBS containing either 0.1 mg/mL collagenase P, 50 ng/mL aggrecanase 2, or 0.1 U/mL chondroitinase ABC. Enzyme solution was maintained at 37 °C and refreshed each day for 7 days. As a control, formulations were exposed to 0.01 M PBS without enzyme. The dry mass of samples on days 0 and 7 were compared for differences. The percent mass loss was also calculated using Equation 2:

$$\text{Mass Loss } (\%) = 100 * \frac{M_i - M_f}{M_i} \quad (2)$$

where, $M_i$ and $M_i$ are the initial and final dry masses of the sample, respectively.

**4.2.10 Mechanical characterization.** All mechanical in vitro studies were performed on a Shimpo E-Force Test Stand. A 2 N load cell (FGV-0.5XY) was used for tensile, shear, and unconfined compression tests and a 200 N load cell (FGV-50XY) was used for confined compression tests. AF tissue was isolated from porcine IVDs (Tissue

Source, LLC, Lafayette, Indiana) and utilized for adhesion tests. The adhesive strength of each formulation was compared to a fibrin hydrogel, known for its high biocompatibility, but weak mechanical properties [408,409,410,411]. The fibrin hydrogel used in this study was formed from 100 mg/mL fibrinogen, 500 U/mL thrombin, and 5 mg/mL $CaCl_2$ [412]. All mechanical tests were performed at a rate of 5 mm/min in a 37 °C saline bath.

***4.2.10.1 Adhesive tensile tests.*** Adhesive tensile tests, as described by ASTM F2258-05, were performed to observe the adhesive behavior of the composites on a porcine AF substrate (n = 5). AF tissue was cut to dimensions of approximately 0.5 $cm^2$ and glued to the top and bottom fixtures. A sample volume of 25 µL was applied to the AF surface, spaced approximately 1 mm apart, and a preload of 0.01 N was applied for 5 minutes. Ultimate tensile strength was determined from the data and normalized to the cross-sectional area of the AF tissue.

***4.2.10.2 Adhesive Lap Shear Tests.*** Adhesive lap shear tests, as described by ASTM F2255-05, were performed to observe the adhesive behavior of the composites on a porcine AF substrate (n = 5). 3-D printed fixtures composed of polylactic acid (PLA) were used to grip tissue samples for vertical shear movement. AF tissue was cut to dimensions of approximately 0.5 cm x 1 cm and affixed to the PLA fixtures. A sample volume of 50 µL was injected between both tissue substrates, spaced approximately 1 mm apart, and gelled for 5 minutes. Ultimate shear strength was determined from the data and normalized to the cross-sectional area of the AF tissue.

***4.2.10.3 Unconfined compression tests.*** Unconfined compression tests (n = 5) were performed on pre-formed, cylindrical gels (n = 5) in a 48 well plate. A preload of 0.05 N was applied to the composites for 5 minutes. Data was normalized to stress and

strain using the initial cross-sectional area and height of each composite. Tangential modulus was calculated at 25 % strain.

***4.2.10.4 Confined compression tests.*** Confined compression tests (n = 7) were performed using a custom-built apparatus. A vertical, stainless steel cylinder, mounted on a base plate, guided a Teflon™ coated piston to minimize frictional contact along the cylinder walls. To allow entrapped air to escape, a sintered stainless-steel metal filter (Mott 50 U-PXX-002-A-10, 0.2 µm pore size, ½" diameter, 1/16" thick) was cut and inserted onto the end of the piston. Based on ASTM F2789-10, a surrogate AF mold composed of RTV-630 silicone elastomer (Momentive Performance Materials Inc.) was inserted into the cylinder to allow for confinement of the composite. A false bottom in the base plate was created to allow for easy insertion and removal of the surrogate mold. The apparatus is encased in plexiglass to contain heated saline and maintain physiological temperature. Approximately 100 µL of sample was injected into the mold for testing. Data was normalized to stress and strain using the initial cross-sectional area and height of each composite. Tangential modulus was calculated at 25% strain.

**4.2.11 Adhesive bonding to tissue.** The bonding interface between P-0, S-50, and fibrin hydrogel to porcine AF tissue was histologically assessed. AF tissues were first isolated from porcine IVDs and wrapped in saline soaked gauze to prevent dehydration. Formulations were applied to the surfaces of AF tissue and gelled at 37 °C. Samples were then embedded in frozen section compound (VWR), flash frozen in liquid nitrogen, and sectioned on a cryostat at 30 µm. Sections were stained with alcian blue and Wiegert's hematoxylin to identify the adhesive and native porcine cells, respectively. Bonding

interfaces between the various adhesives and tissues were imaged on an upright light microscope.

**4.2.12 Statistical analysis.** SPSS software was used to perform a statistical analysis between data sets. A one-way analysis of variance (ANOVA) was conducted to compare means over time or between formulations. Assuming equal variance, Tukey's post-hoc test was applied for all comparisons. Significance was set at the 95 % confidence level ($p < 0.05$). All values are reported as the mean ± standard deviation (SD).

## 4.3 Results

**4.3.1 Synthesis of PNIPAAm-g-CS.** Methacrylation of chondroitin sulfate was performed to impart potential reactivity through the vinyl bond in the methacrylate functional group (Figure 10). In previous work, the degree of methacrylate substitution to CS was previously demonstrated to be 0.1 [401,402]. Free radical copolymerization of NIPAAm monomer and mCS yielded the thermosensitive hydrogel PNIPAAm-g-CS (Figure 11). At room temperature, approximately 25 °C, PNIPAAm-g-CS is soluble in water and behaves as a hydrophilic polymer network (Figure 12). Upon heating above the lower critical solution temperature (LCST) to a physiological temperature of 37 °C, the polymer behaves as hydrophobic compact polymer network.

**4.3.2 Characterization of calcium crosslinked alginate microparticles.** Alginate MPs were successfully crosslinked with calcium chloride and visualized using inverted light microscopy. Both small and large MPs were generated using different stir speeds (Figure 13). A low stir speed (400 rpm) and high stir speed (1,200 rpm) generated MPs with a diameter of 120 ± 39.0 µm and 20.0 ± 5.9 µm, respectively (Figure 14).

There was a statistically significant difference between the mean diameters of each MP batch ($p < 0.05$).

**4.3.3 Swelling properties.** Swelling study results (Figure 15) indicated differences in swelling ratio for formulations after 14 days in PBS. P-0 exhibited a significant decrease ($p < 0.05$) in swelling ratio by 37 %, thus indicating water loss. S-25 and L-25 exhibited a slight significant increase ($p < 0.05$) in swelling ratio by 22 % and 17 %, respectively, suggesting that the addition of alginate MPs combats the shrinking behavior of PNIPAAm-g-CS and imbibes water. Doubling the MP concentration causes (S-50 and L-50) further swelling of the composite scaffold by 152 % and 157 % ($p < 0.05$). MP diameter did not significantly influence the swelling ratio ($p > 0.05$).

**4.3.4 Scanning electron microscopy imaging.** SEM imaging (Figure 16) revealed microscopic features such as pore shape, size and number for each formulation and reinforced findings from the swelling study. Pore sizes ranged from approximately 10 – 40 µm at the beginning of the study. No immediate differences in microscopic structure were observed between formulations. After 14 days, P-0 showed an appreciable decrease in porosity and pore diameter due to its hydrophobic behavior above 37 °C. Addition of 25 mg/mL of alginate MPs to PNIPAAm-g-CS (S-25 and L-25) counteracts shrinking and improves pore retention. Composites that contained 50 mg/mL of alginate MPs (S-50 and L-50) exhibited the greatest number of pores. MP diameter did not cause any obvious differences in scaffold porosity.

**4.3.5 Rheological characterization.** The rheological behavior of each formulation was assessed under shear oscillatory loading. Temperature sweep tests (Figure 17A) revealed a gel point of 33.4 ± 0.4 °C for P-0. However, gel points for all

other formulations (Figure 17C) could not be identified by the crossover of G' and G'' due to their predominantly elastic behavior over the entire temperature range. Frequency sweep tests revealed typical viscoelastic behavior and strain-rate dependency for all formulations (Table 2). G' and G'' increased with increasing strain-rate over the entire frequency range for all sample types except P-0 (Figure 17B and D). In general, inclusion of MPs increases the drag force on PNIPAAm-g-CS, causes a resistance to flow, and significantly increased G* and η* compared to P-0 ($p < 0.05$). S-50 exhibited the highest viscosity and shear moduli due to the combined effect of high MP concentration and small MP size.

**4.3.6 Enzyme degradation study.** Formulations P-0 and S-50 were each examined for potential to enzymatically degrade (Table 3). P-0 and S-50 showed no significant loss in dry mass between 0 and 7 days in PBS ($p > 0.05$). Exposure to enzymes such as aggrecanase or collagenase did not significantly degrade the samples compared to the PBS control ($p > 0.05$). These results were expected since these enzymes degrade the core protein aggrecan and collagen, neither of which are present within the hydrogel or MPs. However, chondroitinase ABC caused a significant mass loss of 7.6 ± 0.8 % and 8.9 ± 0.8 % 1.0 % for P-0 and S-50, respectively ($p < 0.05$).

**4.3.7 Adhesive tensile and shear tests.** Adhesive strength to AF tissue was evaluated for each formulation in tension and shear and compared to a fibrin hydrogel (Table 4). Only S-50 and L-50 outperformed the fibrin hydrogel in adhesive tensile strength ($p < 0.05$). S-50 exhibited the highest adhesive tensile strength (2.79 ± 0.23 kPa) but was not significantly different than E (2.62 ± 0.53 kPa) ($p > 0.05$). All formulations except for P-0 outperformed the fibrin hydrogel in adhesive shear strength ($p < 0.05$). S-

50 presented the highest adhesive shear strength (7.43 ± 1.23 kPa) compared to all other formulations ($p < 0.05$). Increased concentration of smaller MPs caused a significant difference in adhesive tensile and shear strength ($p < 0.05$), while MP diameter did not ($p > 0.05$).

**4.3.8 Unconfined and confined compression tests.** Compressive modulus was calculated for each formulation in unconfined and confined testing conditions (Table 5). P-0 exhibited the lowest unconfined (6.84 ± 1.27 kPa) and confined compressive moduli (203 ± 113 kPa) compared to all other formulations. S-50 exhibited the highest unconfined (15.15 ± 1.08 kPa) and confined compressive moduli (894 ± 78 kPa) compared to P-0 ($p < 0.05$). In general, increasing the concentration of alginate MPs results in increased compressive modulus ($p < 0.05$) in unconfined and confined testing conditions, regardless of MP diameter. MP diameter only caused significant changes in modulus for unconfined compression ($p < 0.05$) and not confined compression ($p > 0.05$).

**4.3.9 Adhesive bonding to tissue.** Differences in flow characteristics of the formulations were immediately observed after applying to porcine AF tissue substrates (Figure 18). P-0 and fibrin hydrogel appeared thin and dispersed along the tissue surface. However, S-50 was thick and did not flow as easily. Each sample adhered to the tissue surface and filled irregular spaces. Aside from tissue adherence, S-50 appeared reinforced by the anchoring of PNIPAAm-g-CS to alginate MPs. Embedded MPs enhance the adhesive and mechanical properties of PNIPAAm-g-CS hydrogel by structurally interfacing with the network. Interaction between adjacent MPs with one another or with the tissue surface may also influence adhesive and mechanical properties.

### 4.4 Discussion

An ideal carrier for cell delivery should remain porous and hydrated to allow for the exchange of nutrients and metabolic waste products. In previous work, hydrophobic PNIPAAm was grafted with chondroitin sulfate to increase the LCST and allow for greater water retention [401]. Alginate MPs are hydrophilic and have been shown to uptake large proportions of water [413]. Therefore, alginate MPs were added to PNIPAAm-g-CS to further improve water retention and increase scaffold porosity. Degradation properties of the carrier should also be considered for IVD cell therapy. Although the composite is susceptible to degradation by chondroitinase ABC, this enzyme is not found in the human IVD. Formulations were not degraded by native disc enzymes such as collagenase or aggrecanase and may be considered non-degradable, however other factors such as low pH may cause acid hydrolysis of glycosidic linkages found in chondroitin sulfate or alginate. A non-degradable composite may be beneficial in the localization and retention of cells for delivery.

Overall, the shear mechanical properties of the composite are strengthened by the addition of alginate MPs. Decreasing the MP diameter while holding concentration constant increases the surface area to volume ratio, thus allowing for greater distribution of MPs throughout the PNIPAAm-g-CS phase. The rheological properties of the PNIPAAm-g-CS phase dominate at a low MP concentration of 25 mg/mL, independent of size (S-25 and L-25). However, at 50 mg/mL, a distribution of smaller MPs (S-50) resulted in a significantly higher increase in $\eta^*$ and $G^*$ compared to larger MPs (L-50) due to a higher particle surface area to volume ratio. Similar behavior has been reported for hydrogels with suspended MPs [405,406]. Vibrations within the tested frequency

range and below 1 % strain have been reported to induce degenerative changes in the IVD [414]. At high frequencies, the gel appears to be more elastic and less viscous. This stiffening at high frequencies is coincident with reported behavior for the native human NP [415] and indicates that the various formulations have potential to prevent or minimize degeneration that can occur at high frequencies and low deformation [416]. Only S-50 and L-50 approached the minimum measured value of G' and G'' that have been reported for NP tissue in shear at low frequencies, starting at 7 kPa [415]. Furthermore, the phase shift angle (δ) increases with frequency but remains below 45 °. This behavior is consistent with the NP and indicates that S-50 and L-50 behave as viscoelastic solids under dynamic shear [415].

S-50 and L-50 demonstrated superior tensile and shear adhesive strength compared to fibrin hydrogel and P-0. Fibrin glue adhesives have been studied for IVD tissue engineering applications and are considered extremely biocompatible, yet its use has several disadvantages: high degradation rate [417], low mechanical properties [408,409], and low cohesive strength [410,411]. Additionally, the load-bearing activity of the IVD would make a fibrin hydrogel more susceptible to dislodging from the nuclear cavity after injection. In the clinical setting, residual disc tissue can also herniate after performing discectomy and requires future revision surgery [418,419]. Hence, imparting adhesive properties to a cell carrier is necessary in order to prevent implant migration or extrusion from the disc.

One of the most frequent types of loading exerted on the IVD tissue is compression. In general, increased MP concentration and surface area to volume ratios increased compressive moduli. Decreased MP diameter allowed for a greater distribution

of MPs throughout the PNIPAAm-g-CS hydrogel, thus increasing composite stiffness. All formulations either meet or exceed mechanical properties of the native NP tissue in unconfined compression, which ranges from 3 – 5 kPa [420]. However, the NP is physiologically confined and surrounded by the AF and CEP. Therefore, the confined compressive moduli of formulations were subsequently measured. Trends from confined compression testing were nearly identical to unconfined conditions, yet moduli varied in magnitude. Restricted movement within the rubber surrogate AF caused over a 50-fold increase in confined compressive moduli compared to unconfined testing. S-50 and L-50 reached just below 1 MPa at 25 % strain, which is slightly below the reported range of native NP tissue [421].

**4.5 Conclusions**

The successful treatment of the degenerated IVD using an injectable cell carrier relies on several key prerequisites. Since tissue herniation has been reported in the clinical setting post-discectomy, implant migration or extrusion can potentially occur in the load-bearing IVD. Therefore, imparting adhesive properties to a cell carrier are vital. An implant's ability to endure repetitive compressive or shear loading are desirable to allow for proper load dissipation to surrounding spinal tissues. Blending a high concentration of small alginate MPs in PNIPAAm-g-CS significantly enhanced rheological properties such as viscosity and shear modulus, thus increasing adhesive tensile and shear strength on AF tissue. These results are also coincident with previous findings in literature [405,406,407]. More importantly, the IVD endures complex combinations of load, hence the composite's adhesive behavior and resistance to extrusion will need to be further tested using an ex vivo disc model or an in vivo animal

model. If extrusion occurs, properties of PNIPAAm-g-CS can be altered to improve stiffness and viscosity [401] alginate MPs can be conjugated with dopamine to improve adhesive strength with tissue [422]. Modifications to the cell carrier in order to meet mechanical design criteria would consequently affect ADMSC response and would require further investigation.

Table 1

*Formula Designations of Factorial Design*

| Formulation Designation | MP Diameter (µm) | MP Concentration (mg/mL) |
|---|---|---|
| P-0 | n/a | 0 |
| S-25 | 20.0 ± 6.0 | 25 |
| S-50 | 20.0 ± 6.0 | 50 |
| L-25 | 120.0 ± 39 | 25 |
| L-50 | 120.0 ± 39 | 50 |

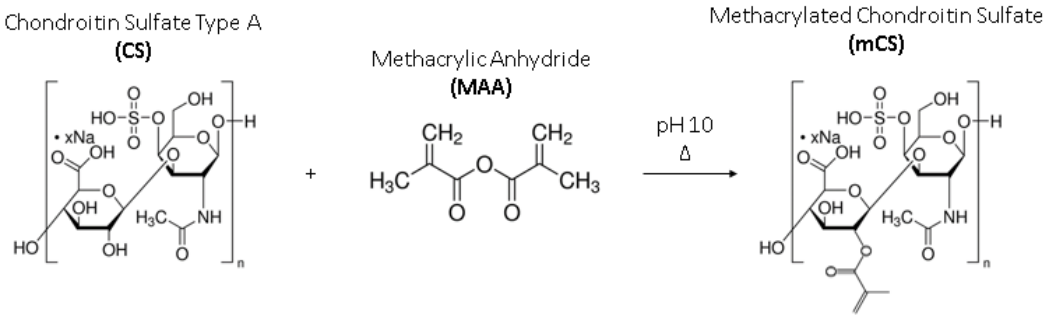


*Figure 10.* Reaction mechanism for the substitution of a methacrylate group on CS using MAA to create MCS.

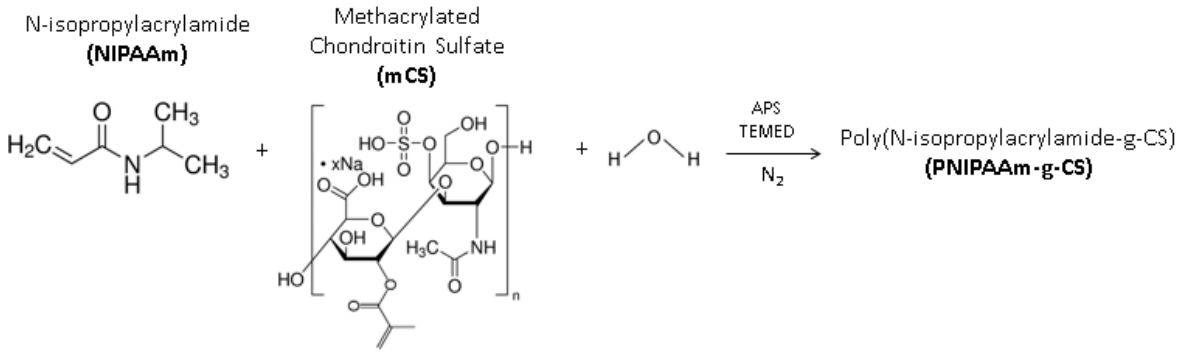


*Figure 11.* Free radical polymerization of NIPAAm and mCS in deionized water with TEMED and APS to create PNIPAAm-g-CS.

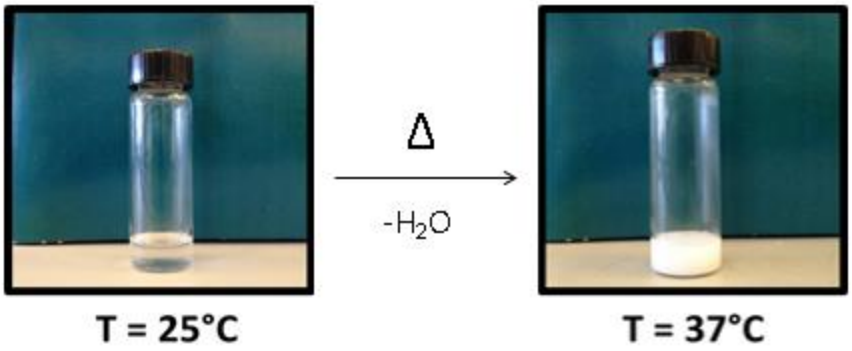


*Figure 12.* Phase transition of PNIPAAm-g-CS. The copolymer behaves as a liquid at room temperature (25 °C). Upon heating to physiological temperature (37 °C), the copolymer becomes hydrophobic and forms a compact hydrogel.

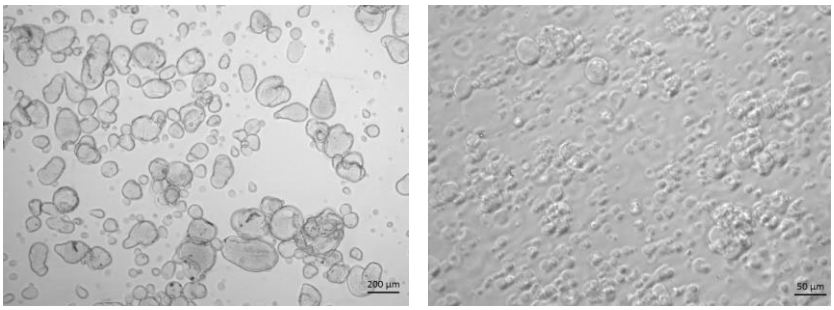


*Figure 13.* Light micrographs of hydrated alginate MPs that are 120 ± 39.0 µm (left) and 20.0 ± 5.9 µm (right), respectively.

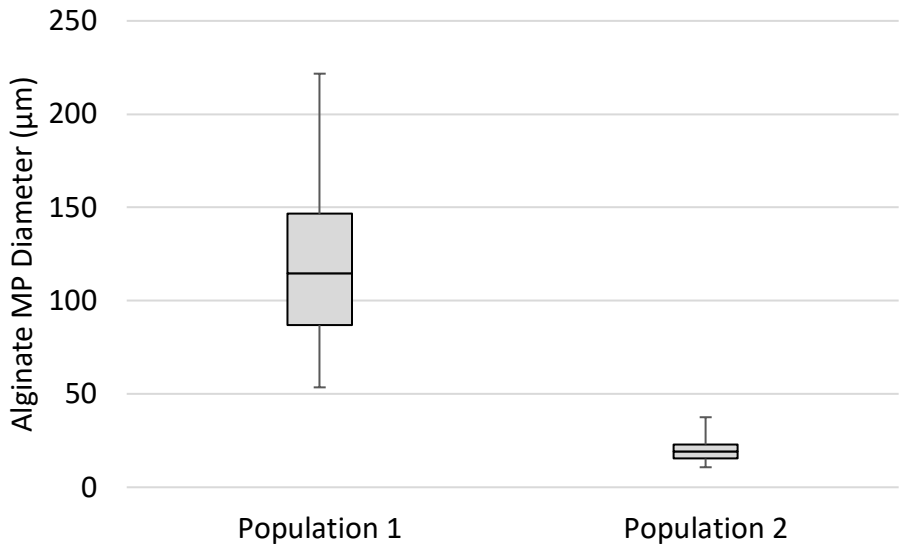


*Figure 14.* Box and whisker plot illustrating the two populations of alginate MPs with statistically different means of 120 ± 39.0 µm and 20.0 ± 5.9 µm.

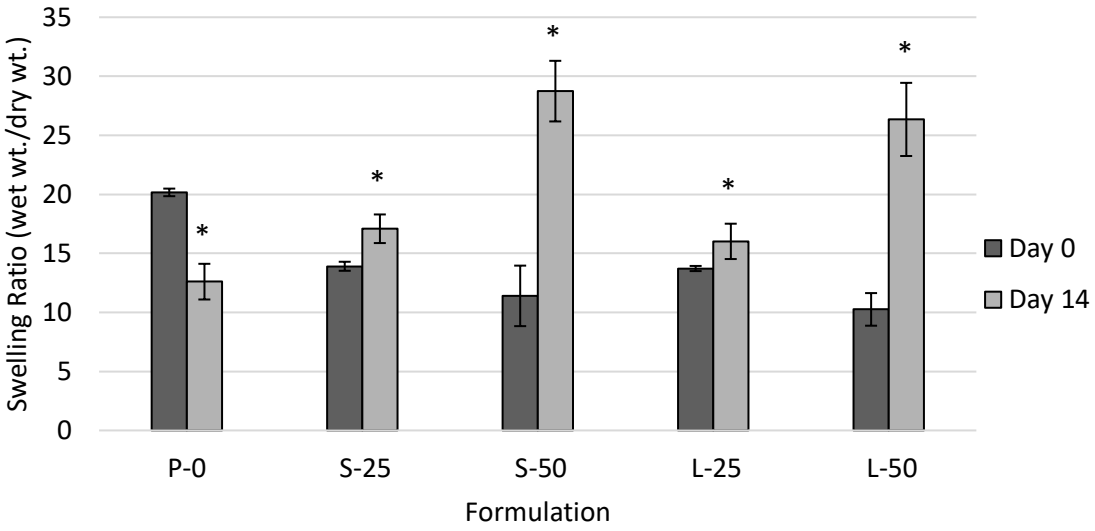


*Figure 15.* Swelling ratios of formulations incubated in PBS at 37 °C after 0 and 14 days (n = 5). An asterisk (*) indicates a statistically significant difference ($p < 0.05$) compared to day 0. Swelling ratio increased with increasing MP concentration but did not vary with MP diameter.

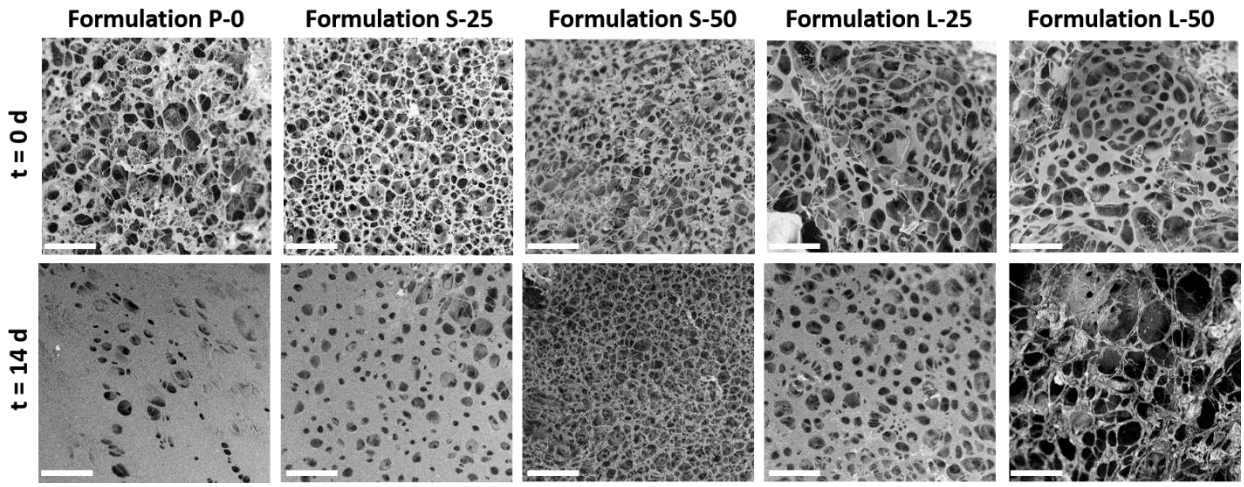


*Figure 16.* SEM images of formulations incubated in PBS at 37 °C after 0 and 14 days (n = 3). P-0 exhibited decreased porosity due to its hydrophobic behavior at physiological temperature. S-25 and L-25 counteracted shrinking from the hydrophilic addition of 25 mg/mL of alginate MPs. Increasing MP concentration to 50 mg/mL (S-50 and L-50) further improved pore retention. Scale bars = 50 µm.

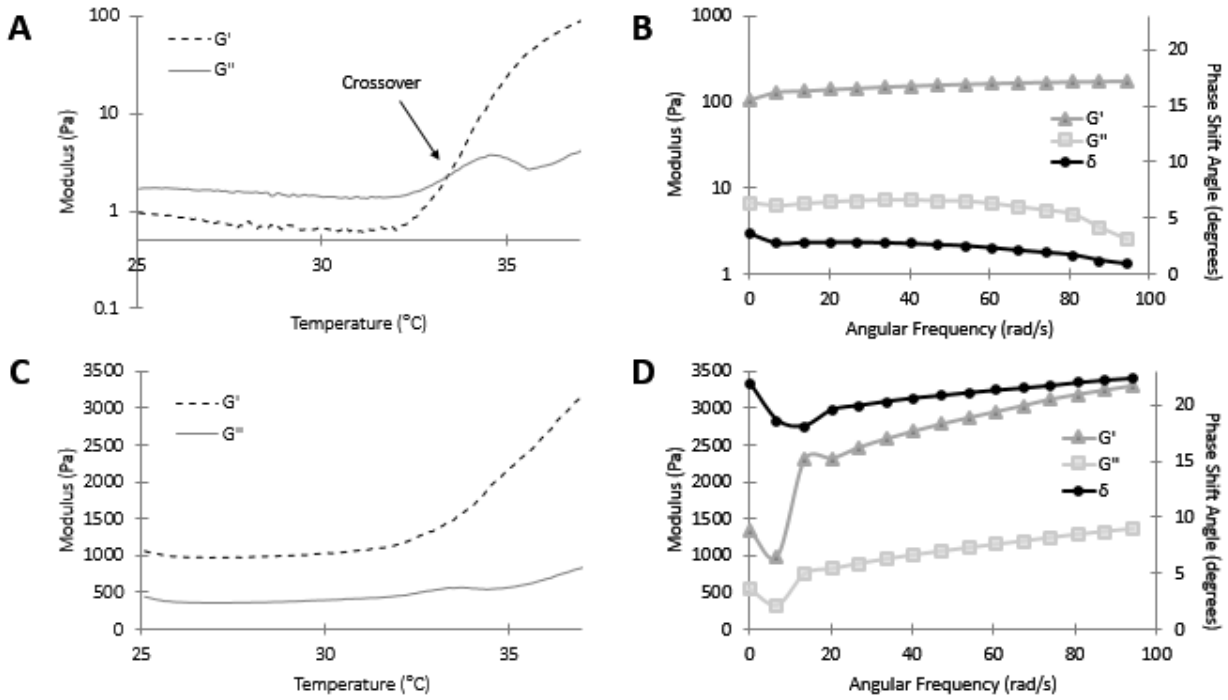


*Figure 17.* Representative plots from rheological testing of (A, C) temperature and (B, D) frequency sweep tests for formulations P-0 and S-50, respectively. Note that P-0 exhibits a crossover of G' and G'' and S-50 does not. With increasing frequency, S-50 stiffens, whereas P-0 does not.

Table 2

*Complex Modulus (G*) and Phase Angle (δ) as a Function of Frequency*

| | | ω (Hz) | |
|---|---|---|---|
| **Property** | **Formulation** | **0.1** | **15** |
| G* (Pa) | P-0 | 129 ± 20 | 194 ± 33 |
| | S-25 | 268 ± 61 | 565 ± 152 |
| | S-50 | 1454 ± 263 | 3637 ± 806 |
| | L-25 | 183 ± 39 | 426 ± 38 |
| | L-50 | 814 ± 97 | 2215 ± 331 |
| δ (°) | P-0 | 3.7 ± 0.1 | 1.7 ± 0.6 |
| | S-25 | 9.6 ± 1.3 | 10.7 ± 1.5 |
| | S-50 | 20.9 ± 1.2 | 21.3 ± 1.5 |
| | L-25 | 12.6 ± 1.3 | 13.6 ± 1.7 |
| | L-50 | 21.0 ± 1.4 | 26.9 ± 1.8 |

Table 3

*Enzymatic Degradation and Mass Loss*

| | Mass Loss with Enzyme Exposure (%) | | | |
|---|---|---|---|---|
| **Formulation** | **PBS** | **Aggrecanase 2** | **Collagenase P** | **Chondroitinase ABC** |
| P-0 | 0.16 ± 0.9 | 0.09 ± 0.7 | 0.21 ± 1.1 | 7.55 ± 0.80 |
| S-50 | 0.1 ± 1.1 | 0.15 ± 0.9 | 0.19 ± 1.6 | 8.88 ± 1.0 |

Table 4

*Adhesive Strength to AF Tissue in Tension and Shear*

| | Adhesive Test | |
|---|---|---|
| **Formulation** | **Tensile Strength (kPa)** | **Shear Strength (kPa)** |
| Fibrin Hydrogel | 1.83 ± 0.52 | 2.66 ± 0.81 |
| P-0 | 1.30 ± 0.12 | 0.96 ± 0.17 |
| S-25 | 1.72 ± 0.30 | 4.88 ± 0.83 * |
| S-50 | 2.79 ± 0.23 * | 7.43 ± 1.23 * |
| L-25 | 1.95 ± 0.36 | 4.37 ± 0.45 * |
| L-50 | 2.62 ± 0.53 * | 5.47 ± 0.64 * |

*Note.* An asterisk (*) indicates a statistically significant difference ($p < 0.05$) compared to the fibrin hydrogel.

Table 5

*Unconfined and Continued Compressive Moduli at 25 % Strain*

| | Compressive Test | |
|---|---|---|
| **Formulation** | **Unconfined Modulus (kPa)** | **Confined Modulus (kPa)** |
| P-0 | 6.84 ± 1.27 | 203 ± 113 |
| S-25 | 10.31 ± 2.14 * | 537 ± 181 * |
| S-50 | 15.15 ± 1.08 * | 894 ± 78 * |
| L-25 | 7.56 ± 1.16 | 613 ± 88 * |
| L-50 | 9.00 ± 0.64 | 810 ± 57 * |

*Note.* An asterisk (*) indicates a statistically significant difference ($p < 0.05$) compared to P-0.

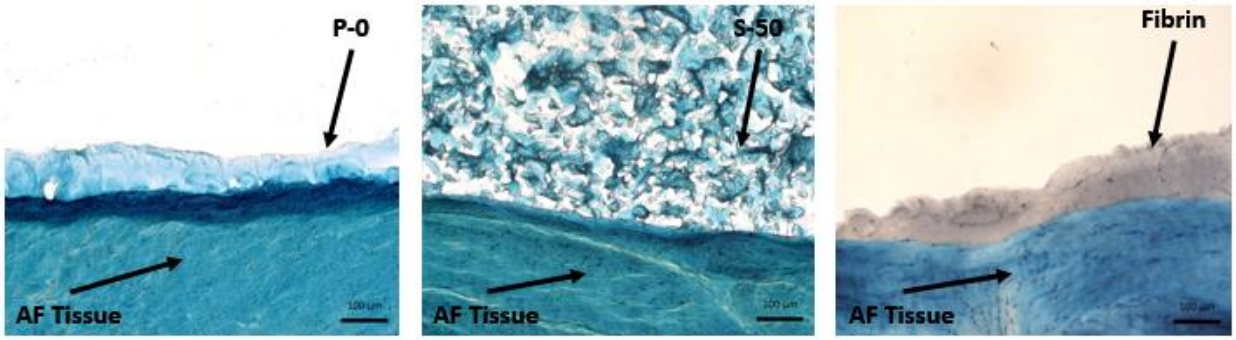


*Figure 18.* Adherence of formulations P-0, S-50, and fibrin hydrogel along the AF tissue substrate. GAGs and cell nuclei were stained with alcian blue and Weigert's hematoxylin, respectively. Scale bars = 100 µm.

# Chapter 5

## Differentiation of Mesenchymal Stem Cells Toward an NP Phenotype

### 5.1 Introduction

The differentiation of human ADMSCs and BMDMSCs has been extensively studied in vitro [423,424,425,426]. Exposing MSCs to solubilized proteins from the TGF-β and GDF families is one method to induce discogenic differentiation. MSC differentiation toward an NP-like phenotype has been characterized by changes in protein and gene expression. One feature that differentiates NP cells from other chondrogenic cell lines is the amount of synthesized proteoglycan and collagen. Compared to articular chondrocytes, healthy NP cells produce higher proportions of proteoglycans containing aggrecan (ACAN) compared to type II collagen (COL2) [424,427]. Therefore, MSCs must also produce a proteoglycan rich matrix upon differentiation. Additional discogenic proteins of interest that should be produced and expressed by MSCs include type I collagen (COL1), SOX9, and hypoxia inducible factor 1α (HIF1α). Studies have also identified significant increases in the expression of NP-specific genetic markers like paired box 1 (PAX1) [423,424], forkhead box 1 (FOXF1) [423,424,425,426], cytokeratin 19 (KRT19) [424,425,426], carbonic anhydrase 12 (CA12) [425,426] after growth factor exposure.

Clarke et al. [426] compared the influence of TGF- β3, GDF-5, and GDF-6 on both BMDMSCs and ADMSCs. Authors concluded that GDF-6 stimulation caused MSCs to produce more sulfated GAG, express a higher ACAN to COL2 gene ratio, and upregulate NP-specific genes compared to TGF- β3 and GDF-5. All these effects were more prominent for ADMSCs relative to BMDMSCs. Additionally, Minogue et al. [423]

determined that ADMSCs may be more suitable for differentiation toward an NP-like phenotype because they lack articular chondrocyte gene expression for integrin binding sialoprotein (IBSP) and fibulin 1 (FBLN1). The combination of GDF-6 and ADMSCs may be ideal for IVD tissue engineering strategies.

Prior in vitro work demonstrated that PNIPAAm-g-CS [401] and a preliminary composite [402] supported the viability of human embryonic kidney (HEK) 293 cells. Even though these formulations supported the survival of this model cell line, HEK-293 cells would not be grafted into the IVD for regenerative purposes. In the previous chapter, S-50 and L-50 exhibited superior swelling, rheological, adhesive, and mechanical properties compared to PNIPAAm-g-CS. Based on these findings, S-50 and L-50 were evaluated and compared to PNIPAAm-g-CS as potential three-dimensional culture systems for ADMSC delivery. The subsequent work describes the survival, behavior, and differentiation of ADMSCs toward an NP-like phenotype. PNIPAAm-g-CS hydrogel and alginate MPs were first screened for potential cytotoxic leachable byproducts that may illicit cell death. Then, ADMSCs were encapsulated within the formulations, cultured in vitro with exposure to GDF-6, and evaluated in terms of viability, metabolic activity, and secretion of sulfated GAG and collagen. ADMSC differentiation toward an NP-like phenotype was assessed on both the gene and protein level using qRT-PCR and immunofluorescence analyses, respectively.

## 5.2 Methods

**5.2.1 Culturing and passaging ADMSCs.** Normal human ADMSCs (ScienCell, female donor, 30 years old) were stored in liquid nitrogen until needed. ADMSCs were grown in tissue culture treated plates using MSC complete medium (ScienCell)

containing basal medium, 5 % fetal bovine serum (FBS), 5 % MSC growth supplement, and 5 % penicillin and streptomycin solution. ADMSCs were kept in a water-jacketed incubator at 37 °C with 5 % $CO_2$. Once 80 % confluency was reached, ADMSCs were detached with trypsin (VWR) for 5 minutes and rinsed with complete medium. ADMSCs were then split and passaged at a plating density of 5,000 cells/cm$^2$. Cell number and viability was checked using a hemocytometer and 0.4 % trypan blue (Thermo Fisher Scientific). Media was changed every other day to remove waste byproducts and refresh available nutrients. Stem cells used for future assays were passage 4.

**5.2.2 Biomaterial cytotoxicity.** Prior to seeding ADMSCs in composites, extract tests were performed following the guidelines of ISO 10993-5 Biological Evaluation of Medical Devices - Part 5: Tests for In Vitro Cytotoxicity. As described previously, ADMSCs were expanded to 80% confluency in advance in a 48 well plate. In parallel, 5% w/v PNIPAAm-g-CS (n = 3), 20 µm alginate MPs (n = 3), and 120 µm alginate MPs (n = 3) were immersed in complete medium for 24 h. Culture media was removed from the ADMSC monolayers, replaced with media exposed to hydrogel or MP material, and exposed for a total of 3 h at 37 °C and 5 % $CO_2$. Control monolayers were also included to identify both living and killed cells. The living control monolayer was given fresh complete medium. The killed control monolayer was exposed to 70 % methanol for 15 minutes, washed with PBS and replaced with fresh complete medium. Cytotoxicity was evaluated using the Live/Dead™ Viability/Cytotoxicity Kit for Mammalian Cells (Thermo Fisher Scientific) as prescribed by the manufacturer. Images were taken with an inverted fluorescent microscope.

**5.2.3 ADMSC encapsulation in formulations.** P-0, S-50, and L-50 were examined for their ability to support the viability and differentiation of ADMSCs toward an NP-like phenotype using GDF-6. NP differentiation medium was prepared based on Clarke et al. [426] and consisted of high-glucose Dulbecco's Modified Eagle Medium (DMEM) (Thermo Fisher Scientific) supplemented with 1 % FBS, antibiotics/antimycotics (Thermo Fisher Scientific) containing 100 U/mL penicillin, 100 µg/mL streptomycin, 0.25 µg/mL amphotericin B, 1.25 mg/mL bovine serum albumin (Sigma Aldrich), 5.4 µg/mL linoleic acid (Sigma Aldrich), 100 µM L-ascorbic acid-2-phosphate (Sigma Aldrich), 40 µg/mL L-proline (Sigma Aldrich), $10^{-7}$ M dexamethasone (Sigma Aldrich), and 100 ng/mL GDF-6 (PeproTech). The differentiation medium was then sterilized through a 0.2 µm filter, protected from light, and stored at 4 °C. Freeze-dried alginate MPs were sterilized by soaking in 70% isopropanol and allowed to dry overnight under vacuum. PNIPAAm-g-CS was dissolved in NP differentiation medium overnight at a concentration of 5 % w/v and 4 °C. Both alginate MPs and PNIPAAm-g-CS were exposed to UV light for 3 h. Alginate MPs were mixed with the PNIPAAm-g-CS solution using a positive displacement pipette to form composites. ADMSCs were then suspended in either PNIPAAm-g-CS or composites at a density of 5 x $10^6$ cells/mL. Approximately 100 µL samples were dispensed into a 48 well plate and gelled before adding 500 µL of NP differentiation medium. Media was refreshed every other day and ADMSCs were cultured for 14 days.

**5.2.4 Cellular viability.** Live/Dead™ Viability/Cytotoxicity Kit was used to assess ADMSC viability. Hydrogel composites (n = 3) were first dissolved in 0.01 M PBS containing 50 mM citrate (Sigma Aldrich) and 20 mM EDTA (Sigma Aldrich).

Sodium citrate-EDTA buffer dilutes the hydrogel and reverses ionic alginate-$Ca^{2+}$ crosslinks for complete removal of composite material. Suspended cells were pelleted at 300 x g for 5 minutes at 4 °C and resuspended in Live/Dead™ reagent containing 2 µM calcein AM and 4 µM ethidium homodimer-1 in high glucose DMEM for 1 hour at 37 °C and 5 % $CO_2$. Cells were isolated from the Live/Dead™ reagent, rinsed with 0.01 M PBS, dispensed in a 48 well plate, and imaged using an inverted fluorescent light microscope. Cellular viability was quantified using ImageJ software.

**5.2.5 Metabolic activity.** ADMSC metabolic activity was tracked over 14 days using the alamarBlue® Cell Viability Assay (Bio-Rad). Media was removed from samples (n = 5), replaced with 300 µL of 10 % alamarBlue reagent in NP differentiation medium, and incubated for 5 hours at 37 °C and 5 % $CO_2$. Blank wells containing solely alamarBlue reagent served as a reference negative control. Reduced reagents were removed from the samples, dispensed in a 96 well plate and absorbance readings were measured using a spectrophotometer at 570 and 600 nm. Percent reagent reduction was calculated as described by the manufacturer's instructions.

**5.2.6 Protein expression.** GAG and collagen production were visualized using a histological approach. P-0, S-50, and L-50 (n = 3 each) were fixed for 10 minutes with 4 % formaldehyde (Fisher Scientific), embedded in frozen section compound, snap-frozen in methylbutane chilled with liquid nitrogen, and sectioned to 20 µm sections. PNIPAAm-g-CS and alginate MPs were dissolved using sodium citrate-EDTA buffer to identify ECM produced solely by ADMSCs. GAGs or collagen were stained for using 1 % w/v alcian blue or 0.1 % w/v picrosirius red, respectively. Cell nuclei were

counterstained with Weigert's hematoxylin. ECM deposition was compared on days 0 and 14.

An indirect immunofluorescent labeling technique was also used to detect the presence of discogenic and NP-specific proteins. Discogenic proteins include type I collagen (COL1), type II collagen (COL2), aggrecan (ACAN), and SRY-BOX 9 (SOX9). NP-specific proteins include cytokeratin 19 (KRT19), carbonic anhydrase 12 (CA12), hypoxia-inducible factor 1-α (HIF1α), and forkhead box F1 (FOXF1). S-50 (n = 3) was sectioned to 20 µm, washed with sodium citrate-EDTA buffer, permeabilized for 10 minutes with tris-buffered saline (TBS) containing 0.3 % Triton X-100 (Fisher Scientific), and blocked with 10 % v/v goat serum in TBS for 10 minutes. Primary antibodies (Table 6) were applied for 1 hour at room temperature and rinsed off with TBS. Secondary antibodies conjugated with Alexa Fluor 647 were applied for 30 minutes at room temperature and rinsed off with TBS. Sections were counterstained with 4',6-diamidino-2-phenylindole dihydrochloride (DAPI) and imaged on a confocal microscope (Model A1+, Nikon Instruments Inc.). Immunofluorescent staining performed on sections without primary, secondary, or any antibodies from either mouse or rabbit species served as controls to check for non-specific staining or endogenous autofluorescence. Primary antibodies were monoclonal to increase specificity of the target cite on the protein. Secondary antibodies were polyclonal to increase binding capacity to the respective primary antibody. Primary and secondary antibodies were raised in either mouse or rabbit and goat, respectively. Immunofluorescent protein expression was compared on days 0 and 14.

**5.2.7 Gene expression.** Gene expression profiles of ADMSCs in S-50 on days 0 and 14 were examined using quantitative real-time polymerase chain reaction (qRT-PCR). Seeded cells were isolated from samples (n = 3, 5 constructs each). As described previously, gels were treated with sodium citrate-EDTA buffer and centrifuged to isolate ADMSCs. Total RNA was extracted using the Pure Link™ RNA Extraction Mini Kit (Ambion®, Life Technologies™) and quantified in terms of concentration and purity with a nanodrop (Applied Biosystems). RNA integrity was verified by performing gel electrophoresis and checking for the presence of the 28S and 18S ribosomal bands. RNA samples were combined with loading dye containing formamide, bromophenol blue and xylene cyanol and electrophoresed on a 1 % agarose gel containing 3.7 % formaldehyde in MOPS running buffer at 90 V and 4 °C. A 9.0 kB RNA ladder (Lonza) was used to compare the size of the bands. The gel was stained with 0.5 µg/mL of ethidium bromide for 30 minutes and imaged with an Azure Biosystems c600.

RNA was then reverse transcribed to cDNA using the High Capacity cDNA Reverse Transcription Kit (Applied Biosystems). Target genes (Table 7) were amplified in 20 µL reactions using 20 ng of cDNA, Fast SYBR® Green Master Mix (Fisher Scientific), 500 nM primer concentrations, and an Applied Biosystems 9800 Fast Thermal Cycler. Discogenic genes include COL1, COL2, ACAN, and SOX9. NP-specific genes include CA12, HIF1α, FOXF1, and paired box 1 (PAX1). Relative gene expression was calculated using the delta-delta Ct method ($2^{-\Delta\Delta Ct}$) and normalized to ADMSCs on day 0 and the housekeeping gene glyceraldehyde 3-phosphate dehydrogenase (GAPDH). Size of DNA products were estimated using Basic Local Alignment Search Tool (BLAST) through the National Center for Biotechnology

Information (NCBI) database and verified using gel electrophoresis. DNA samples were combined with loading dye containing bromophenol blue and xylene cyanol and electrophoresed on a 2 % agarose gel in TBE running buffer at 90 V and 4 °C. A 500 bp DNA ladder (Lonza) was used to compare the size of the bands. The gel was stained with 0.5 µg/mL of ethidium bromide for 30 minutes and imaged with an Azure Biosystems c600.

**5.2.8 Statistical analysis.** SPSS software was used to perform a statistical analysis between data sets. A one-way analysis of variance (ANOVA) was conducted to compare means over time or between formulations. Assuming equal variance, Tukey's post-hoc test was applied for all comparisons. Significance was set at the 95 % confidence level ($p < 0.05$). All values are reported as the mean ± SD.

## 5.3 Results

**5.3.1 Biomaterial cytotoxicity.** Any potential toxic byproducts that may have leeched from the PNIPAAm-g-CS hydrogel or alginate MPs did not elicit cell death (Figure 19). Therefore, both biomaterial components were deemed non-cytotoxic. The living control showed a healthy monolayer of metabolically active cells as shown in green. After exposure to 70 % methanol, the killed control showed compromised cell membranes and nuclear staining as shown in red. Cell monolayers exposed to extracts from PNIPAAm-g-CS, 20 µm MPs, and 120 µm MPs exhibited characteristics of the living control and were greater than 95 % viable.

**5.3.2 Cellular viability.** After 14 days of culture, ADMSCs showed cellular viability within the different adhesive formulations (Figure 20). The number of living cells in P-0, S-50, and L-50 were estimated to be 91.8 ± 1.7 %, 92.0 ± 6.5 %, and 93.4 ±

1.8 %, respectively. The presence or size of MPs did not significantly influence cell survival.

**5.3.3 Metabolic activity.** ADMSCs exhibited significant increases in metabolic activity during the differentiation period (Figure 21). P-0 showed the greatest increase in percent reagent reduction after 14 days by 123 ± 7.5 % ($p < 0.05$). Reagent reduction also significantly increased for S-50 (45 ± 9.8 %) and L-50 (23 ± 4.9 %) ($p < 0.05$), but not as considerably as P-0.

**5.3.4 Protein expression.** ADMSCs seeded in P-0, S-50, and L-50 synthesized GAGs and collagen after 14 days of culture (Figure 22). Cells remained round in morphology and intensity of intracellular and extracellular staining increased for all formulations relative to day 0. Interestingly, diffuse ECM appeared to form around large MPs in L-50, while concentrated striations bridged gaps between encapsulated cells in S-50. Overall, P-0, S-50, and L-50 all supported ADMSC survival for 14 days and retained secreted ECM for NP tissue regeneration.

ADMSC differentiation toward an NP-like phenotype was further examined in S-50, since this composite exhibited superior adhesive, mechanical, and rheological behavior compared to P-0 and L-50. A progressive induction of discogenic and NP-specific proteins was confirmed by immunofluorescent staining. Discogenic proteins such as COL1, COL2, ACAN, and SOX 9 were detected after 14 days (Figure 23). Intracellular staining for the NP-specific proteins, CA12, FOXF1, HIF1α, and KRT19 were also identified (Figure 24). ADMSCs showed minor intracellular staining of discogenic or NP-specific proteins prior to culture. Controls did not stain positive for any

protein markers ensuring target specificity and absence of non-specific antibody binding or endogenous autofluorescence (Figure 25).

**5.3.5 Gene expression.** Total RNA was successfully extracted from ADMSCs on days 0 and 14 and quantified in terms of purity and concentration using a nanodrop. Gel electrophoresis revealed that all samples showed the presence of the 28S and 18S human ribosomal bands, which are 5.0 kB and 1.9 kB long, correspondingly (Figure 27). Intact RNA was used to synthesize cDNA for qRT-PCR to identify changes in gene expression in discogenic and NP-specific markers. PCR results (Figure 26) indicate the upregulation of all tested discogenic and NP-specific markers normalized to day 0 and GAPDH. Among all of the tested genetic markers, ACAN showed the highest upregulation (≈ 250-fold change) followed by COL2 (≈ 50-fold change). Both COL1 and SOX9 exhibited a relatively smaller upregulation (≈ 5-fold change). KRT19, FOXF1, and PAX1 were the highest upregulated NP-specific markers compared to HIF1α and CA12. Amplified PCR product sizes were confirmed using gel electrophoresis (Figure 28). Target genes exhibited the correct base pair sizes and did not contain genomic DNA or non-specific amplified products.

**5.4 Discussion**

After 14 days of encapsulation, the long-term survival of ADMSCs were corroborated by both Live/Dead and alamarBlue results. Interestingly, ADMSCs appeared to proliferate more rapidly in P-0 relative to S-50 and L-50. Cells may prefer to grow inside thin versus viscous carriers [428,429], nonetheless at least 90 % of ADMSCs remained viable in each formulation. One potential contributor to decreased cell survival is nutrient deprivation. An ischemic microenvironment with limited protein availability

has been shown to induce ADMSC death [430,431], but fosters differentiation potential [432].

Histological analysis revealed that ADMSCs produced GAG and collagen after 14 days in vitro. Minimal protein staining was observed in P-0 and may be associated with a carrier's water retention, as ADMSCs may have been prevented from depositing ECM due to the hydrogel's constrictive and hydrophobic behavior above the LCST [433]. ECM in L-50 appeared diffuse throughout the hydrogel with concentrated striations around alginate MPs. S-50 exhibited finer and more connective tissue formation throughout the carrier due to the presence of smaller alginate MPs. Therefore, MP diameter will influence the pattern and distribution of newly synthesized tissue throughout the carrier [443]. ADMSCs remained round after 14 days of culture indicating a NP-like phenotype.

Immunofluorescent staining and qRT-PCR were performed on encapsulated ADMSCs in S-50 to confirm the presence of discogenic and NP-specific proteins and genes. Extracellular proteins such as COL1, COL2, and ACAN were detected, confirming the production of connective disc-like ECM. Higher proportions of aggrecan to collagen protein (27:1) in the NP tissue of young adult disc with no signs of degeneration have been previously reported in literature [427]. Similarly, ACAN gene expression was approximately 5 and 50 times higher than COL2 and COL1 expression, respectively, indicating NP-like phenotype. Intracellular staining of NP-specific proteins FOXF1 and KRT19 were also identified. KRT19, FOXF1, and PAX1 have been recently identified as novel NP markers [423,434,435] and were among the highest upregulated genes. CA12 and HIF1α showed limited intracellular staining and upregulation, which

may be stabilized by MSCs in vitro and linked to glycolysis [436]. Exposure to a hypoxic environment would most likely enhance the upregulation of these genes [425,437].

**5.5 Conclusions**

ADMSCs were successfully encapsulated in each formulation and survived for a total of 14 days in vitro. ADMSCs exhibited increased metabolic activity over time within all tested formulations, potentially indicating cellular proliferation however DNA content was not measured. Histology revealed that P-0, S-50, and L-50 retained newly synthesized sulfated GAG and collagen produced by ADMSCs. Since S-50 demonstrated superior mechanical properties and supported the survival of ADMSCs, gene and protein expression were evaluated further using this formulation. Discogenic proteins (ACAN and COL2), and NP-specific proteins (KRT19, FOXF1, and PAX1) were positively identified using immunostaining techniques. These markers were also the top five most upregulated genes detected using qRT-PCR. Results presented here indicate that ADMSCs differentiated toward an NP-like phenotype after encapsulation in S-50 and exposure to GDF-6.

One important limitation in this study was that the degenerative state was not completely recapitulated in vitro. Factors such as low pH [438], reduced nutrient supply [430,431], low oxygen tension [425,437], hydrostatic pressure [439,440], or mechanical loading [441,442] were not implemented. Each of these factors may detrimentally impact MSC retention or survival upon injection into the degenerated disc. To improve cell survival, ADMSCs can be cultured in vitro under degenerative-like conditions prior to delivery into the harsh disc microenvironment. If intradiscal pressure or loading causes displacement of ADMSCs, functional groups can be incorporated into the hydrogel

composite network to improve cell adhesion. It should also be noted that the influence of composite properties on MSC behavior was not explored in this work. Characteristics of PNIPAAm-g-CS such as polymer concentration, degree of methacrylate substitution on CS, and molar ratio of NIPAAm to CS were held constant but can be modified if need be [401]. Bertolo et al. [424] demonstrated that MSC survival and protein expression varied depending on the type of encapsulating biomaterial. Studies have also reported that diameter and concentration of MPs within a hydrogel affect interstitial space, which impact cell to cell interactions, viability, morphology, aggregation, and protein deposition [443,444]. These variables should be further investigated in future work.

Table 6

*Target Proteins Identified Using Immunofluorescent Labeling*

| **Protein** | **Antibody Type** | **Species** | **Clonality** | **Dilution** |
|---|---|---|---|---|
| COL1 | Primary | Mouse anti-human | Monoclonal | 1:100 |
| COL2 | Primary | Mouse anti-human | Monoclonal | 1:200 |
| ACAN | Primary | Mouse anti-human | Monoclonal | 1:50 |
| SOX9 | Primary | Mouse anti-human | Monoclonal | 1:100 |
| KRT19 | Primary | Mouse anti-human | Monoclonal | 1:200 |
| CA12 | Primary | Rabbit anti-human | Monoclonal | 1:50 |
| HIF1α | Primary | Rabbit anti-human | Monoclonal | 1:100 |
| FOXF1 | Primary | Rabbit anti-human | Monoclonal | 1:100 |
| Alexa Fluor 647 | Secondary | Goat anti-mouse | Polyclonal | 1:200 |
| Alexa Fluor 647 | Secondary | Goat anti-rabbit | Polyclonal | 1:200 |

Table 7

*Genes of Interest Amplified Using qRT-PCR*

| Gene | Forward Primer (5' – 3') | Reverse Primer (5' – 3') |
|---|---|---|
| COL1 | CCTGCTGGCAAGAGTGGTGAT | GAAGCCACGGTGACCCTTTATG |
| COL2 | GGCAATAGCAGGTTCACGTACA | CGATAACAGTCTTGCCCCACTT |
| ACAN | TCGAGGACAGCGAGGCC | TCGAGGGTGTAGCGTGTAGAGA |
| SOX9 | AGCGAACGCACATCAAGAC | CTGTAGGCGATCTGTTGGGG |
| KRT19 | GATAGTGAGCGGCAGAATCA | CCTCCAAAGGACAGCAGAAG |
| CA12 | CGTGCTCCTGCTGGTGATCT | AGTCCACTTGGAACCGTTCACT |
| HIF1α | GGGTTGAAACTCAAGCAACTGTC | GTGCTGAATAATACCACTCACAACG |
| FOXF1 | AAGCCGCCCTATTCCTACATC | GCGCTTGGTGGGTGAACT |
| PAX1 | TGGCCCTCGGCACACTC | GCCCCTGTTTGCTCCATAAA |
| GAPDH | CAGCGACACCCACTCCTC | TGAGGTCCACCACCCTGT |

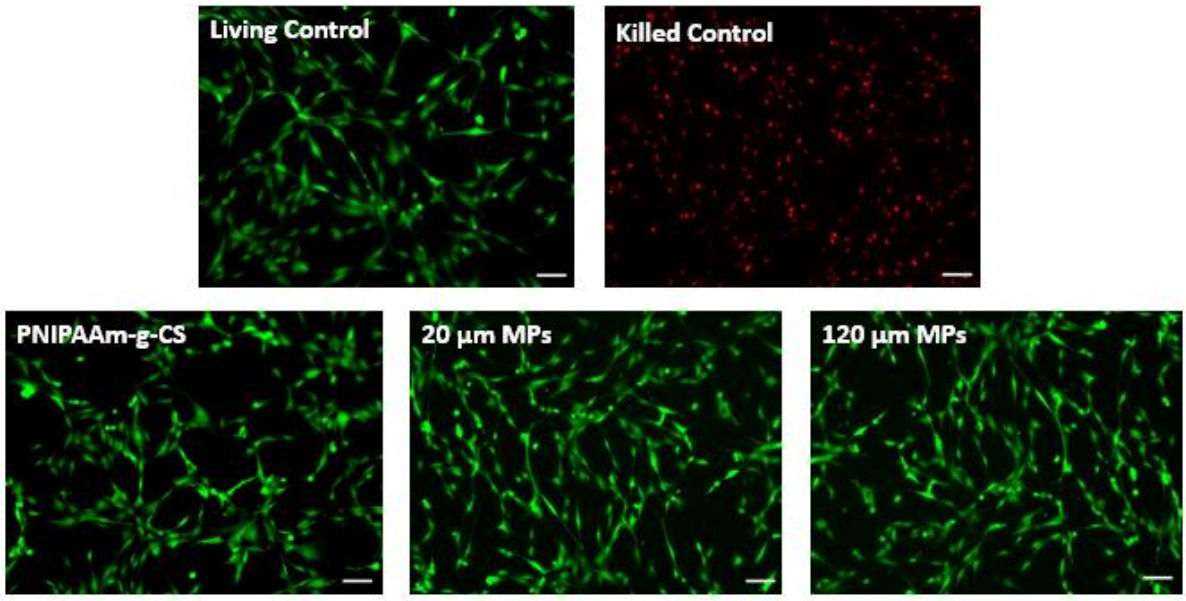


*Figure 19.* Representative Live/Dead images illustrating the non-cytotoxicity of PNIPAAm-g-CS and alginate MPs. Living cells that metabolized calcein-AM are shown in green. Cells death was induced with 70 % methanol and are shown in red. Scale bars = 100 µm.

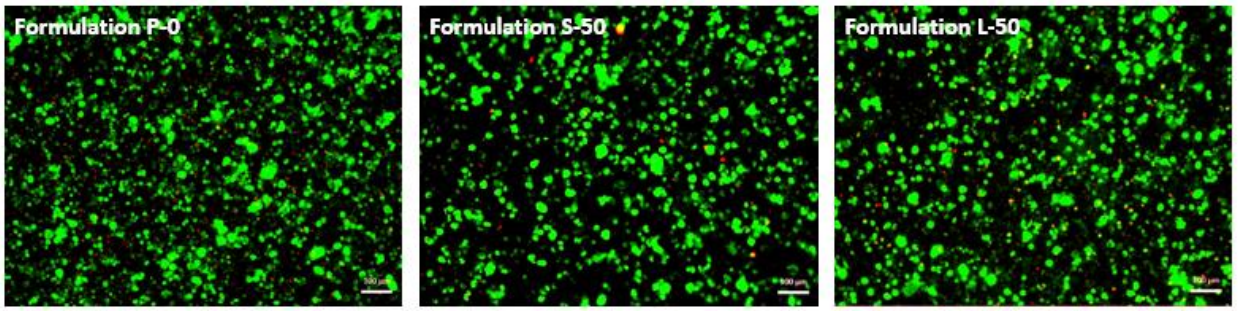


*Figure 20.* Representative Live/Dead images illustrating the viability of ADMSCs in formulations P-0, S-50, and L-50 after 14 days (n = 3). Living and dead cells are shown in green and red, respectively. Scale bars = 100 µm.

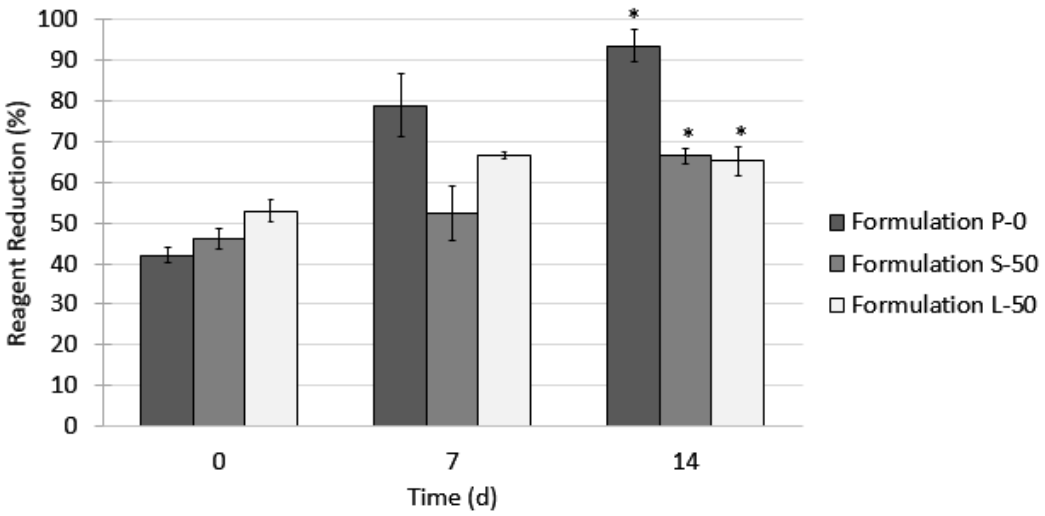


*Figure 21.* Reagent reduction values calculated from alamarBlue assay results illustrating the metabolic activity of ADMSCs in formulations P-0, S-50, and L-50 on days 0, 7, and 14 (n = 5). An asterisk (*) indicates a statistically significant difference ($p < 0.05$) compared to day 0.

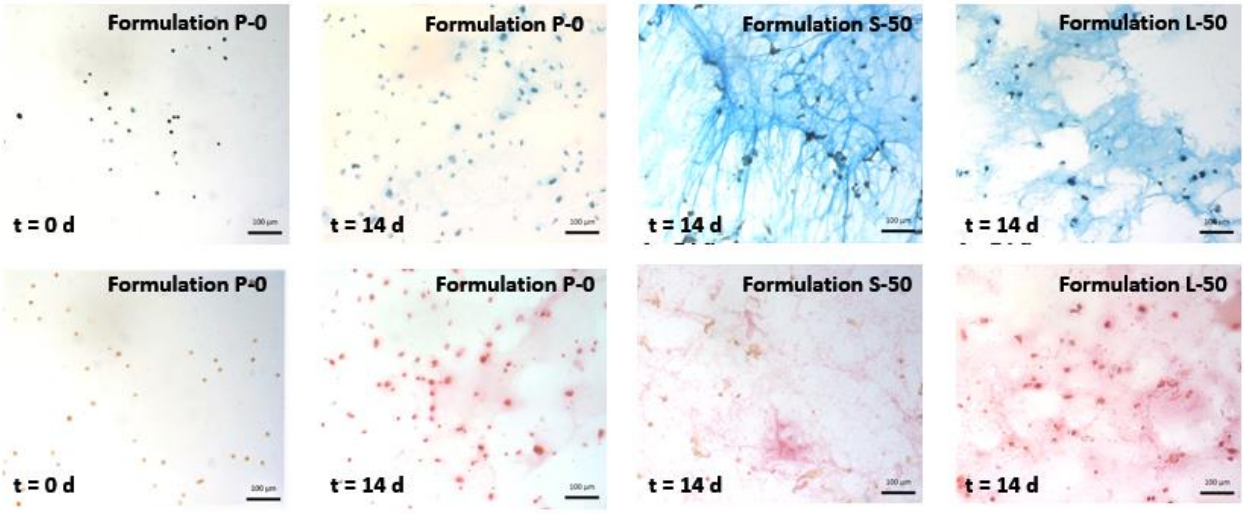


*Figure 22.* Representative histological images illustrating the ECM produced by ADMSCs in formulations P-0, S-50, and L-50 after 0 and 14 days (n = 3). GAGs (top row in blue) and collagen (bottom row in red) were stained with alcian blue and picrosirius red, respectively. Nuclei were counterstained with Weigert's hematoxylin and are shown in black. Scale bars = 100 µm.

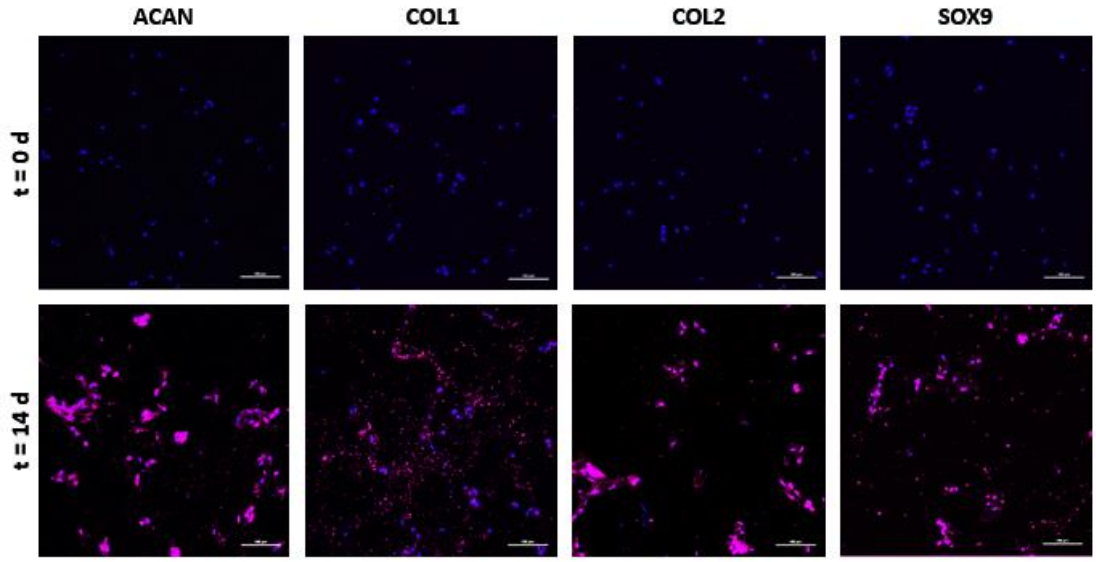


*Figure 23.* Representative immunofluorescent staining of proteins (magenta) produced by ADMSCs in formulation S-50 after 14 days (n = 3). Discogenic proteins include ACAN, COL1, COL2, and SOX9. Cell nuclei were counterstained with DAPI (blue). Scale bars = 100 µm.

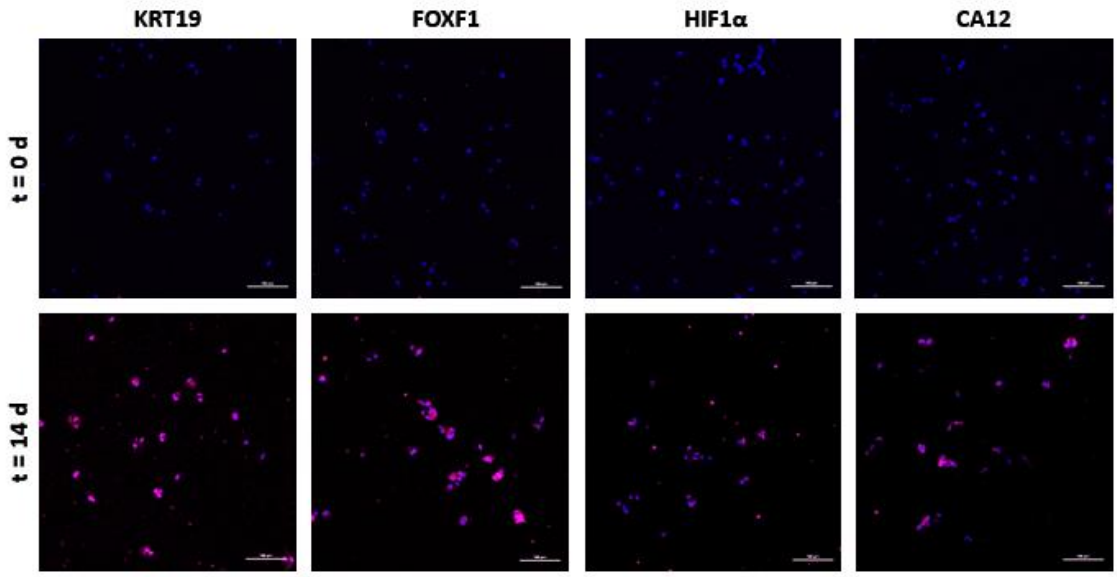


*Figure 24.* Representative immunofluorescent staining of proteins (magenta) produced by ADMSCs in formulation S-50 after 0 and 14 days (n = 3). NP-specific proteins include KRT19, FOXF1, HIF1α, and CA12. Cell nuclei were counterstained with DAPI (blue). Scale bars = 100 µm.

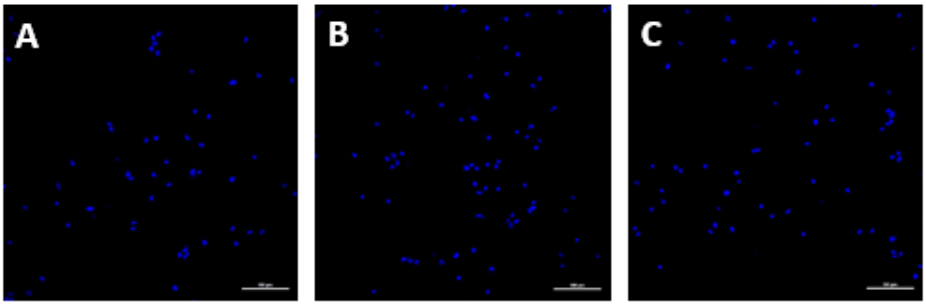


*Figure 25.* Representative immunofluorescent staining of negative control samples in formulation S-50 after 14 days (n = 3). Negative control samples were routinely stained with no primary antibody and (A) secondary mouse antibody, (B) secondary rabbit antibody, or (C) no secondary antibody. Cell nuclei were counterstained with DAPI (blue). Scale bars = 100 µm.

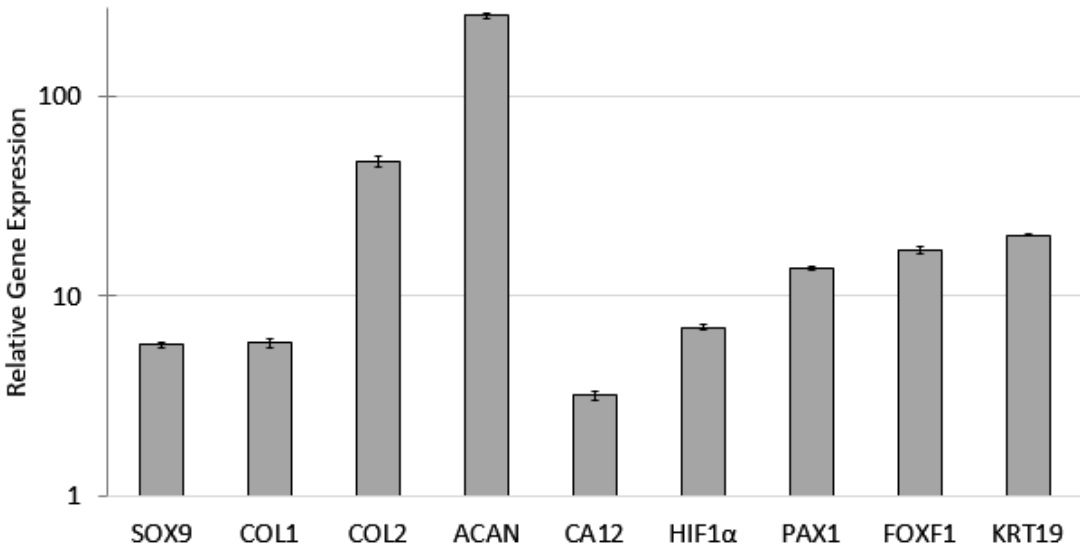


*Figure 26.* Relative gene expression profiles of ADMSCs in formulation S-50 after 14 days using qRT-PCR (n = 3). Discogenic genes include SOX9, COL1, COL2, and ACAN. NP-specific genes include CA12, HIF1α, PAX1, FOXF1, and KRT19. Data was normalized to ADMSC gene expression on day 0 and the housekeeping gene GAPDH.

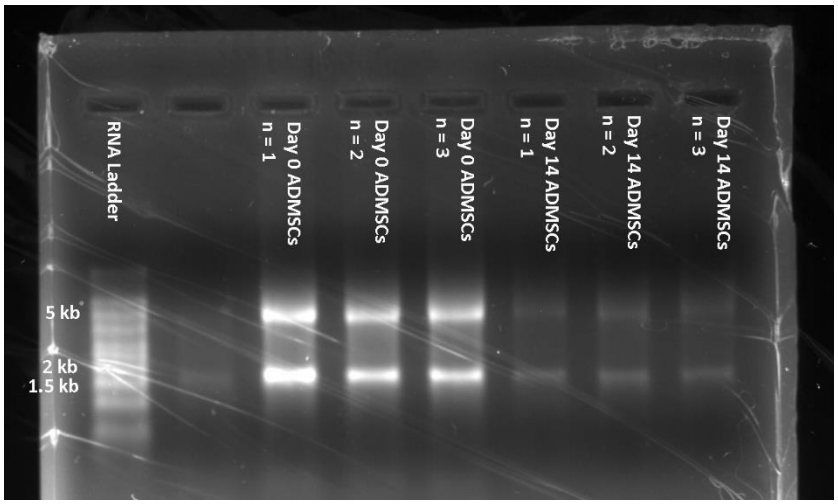


*Figure 27.* An agarose gel with RNA products isolated using the Pure Link™ RNA Extraction Mini Kit. Total RNA from ADMSCs after 0 days and 14 days of incubation in NP differentiation media were electrophoresed to detect the 28S and 18S ribosomal bands with sizes of 5.0 kB and 1.9 kB, respectively. An RNA ladder is provided to estimate the size of the bands.

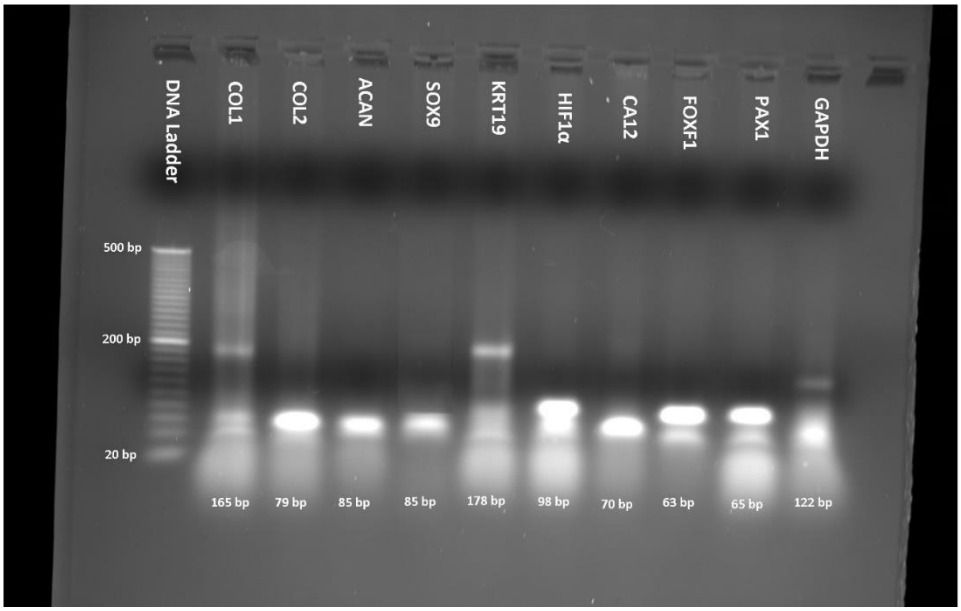


*Figure 28.* An agarose gel with DNA products amplified from qRT-PCR. Amplified DNA from ADMSCs after 14 days in NP differentiation medium were electrophoresed to observe quality and approximate size of the products. A DNA ladder is provided to estimate the size of the bands. Estimated product sizes are listed below each lane.

# Chapter 6

## Biomechanical Restoration of the Injured Porcine Disc

### 6.1 Introduction

The IVD must maintain a healthy hydrostatic pressure to withstand diurnal static and dynamic loading [69,70,71,72]. Mechanical injury from tissue herniation or dehydration of the NP due to proteoglycan degradation can cause a significant decline in intradiscal pressure, thus result in decreased disc height, subsequent nerve root compression, and increased LBP [92]. Current strategies for treating these conditions such as discectomy [168], LIF [189], or TDR [214] can resolve LBP, but ultimately do not restore the healthy biomechanics to the afflicted joint. Therefore, a clinical need exists for an injectable implant that can restore normal physiological function to the injured or degenerated disc.

Preemptive augmentation of the NP, while the AF is still competent, may be key in preventing further disc degeneration [268]. Therefore, research has shifted towards developing NP replacements that can be injected in a minimally invasive manner. In situ forming hydrogels have gained popular interest as replacements, since they have been shown to restore disc height and decrease radial bulge [445]. Additionally, the implant should match the mechanical properties of the native NP, conform to the intradiscal space, and adhere to the surrounding disc tissue to minimize the risk of expulsion. Other studies have also emphasized the importance of restoring biomechanical parameters such as stiffness and range of motion (ROM) [416,446,447,448,449,450], which are key to achieving pain relief and joint mobility in the clinical setting.

In the previous chapters, S-50 was identified as a composite with superior mechanical and adhesive properties and supported the survival and differentiation of encapsulated ADMSCs in vitro. Therefore, S-50 moved on for further mechanical testing as a potential NP replacement in an ex vivo porcine disc model. An injury model was developed by removing NP tissue and exposing each disc to mechanical fatigue. The first objective was to assess the bioadhesive composite's ability to restore range of motion and stiffness during axial compression relative to that of the intact condition. The second objective was to observe the composite's resistance to expulsion during lateral bending.

## 6.2 Methods

**6.2.1 Dissection, isolation, casting of porcine IVDs.** Lumbar spines from healthy male and female porcine donors (5 – 6 months old, 250 – 300 lb.) were purchased from Tissue Source, LLC (LaFayette, IN) and IVDs were isolated for biomechanical testing (Figure 29A). External tissue was removed from the surrounding joints using scalpels to reveal motion segments. All bony posterior and transverse elements were removed from each motion segment using shears. Individual motion segments were isolated by cutting through the midline of each vertebral body using a bone band saw (Mar-Med Inc.). Motion segments were wrapped with saline soaked gauze to prevent dehydration, while each vertebral body was cast in a polyurethane mold (Smooth Cast) (Figure 29B). Potted specimens were kept frozen at -20 °C.

**6.2.2 Histology.** Histology was performed to assess implant conformation to the inner cavity of the porcine IVD. Discs were either (1) intact, (2) denucleated, or (3) denucleated and injected with composite. After subjected to treatment, discs were fixed with 4% formaldehyde in PBS for 24 h at 37°C. Bone segments were decalcified using

5% v/v HCl in PBS for 24 h at 37°C. Discs were embedded in frozen section compound and 30 µm sagittal cross sections were obtained on a cryostat. GAGs and collagen were stained with alcian blue and picrosirius red, respectively. Cross sections were imaged using a stereoscope.

**6.2.2 Compression-tension and biomechanical restoration.** IVDs (n = 7) were compressed and tensed based on previously reported literature by Cannella et al. using human lumbar IVDs [36]. Image J software was used to approximate the average cross-sectional area (8.2 ± 0.4 $cm^2$) for discs (Figure 29C). IVDs were compressed to -1000 N and tensed to 100 N for 10 cycles at a rate of 0.1 Hz. The peak compressive and tensile forces were selected to represent physiological pressures of jogging or climbing stairs [71,72] and were scaled for differences in cross-sectional area between human and porcine species [36,451]. The first nine cycles were performed as preconditioning to establish a repeatable hysteresis response and the slow rate allowed for complete transfer of load to the specimen. Range of motion (ROM) and stiffness were calculated using the 10th cycle (Figure 30). ROM was measured as the end-to-end displacement of the hysteresis curve. A linear regression was used to calculate the compressive (0 to -200 N) and tensile stiffness (0 to 50 N). Specimens were tested on an MTS 831 elastomer test system and maintained at 37°C in saline.

Each disc was subjected to compression-tension after the following conditions to detect differences in ROM and stiffness. First, properties were measured for the intact specimen to obtain a baseline reference. Next, the specimen was then punctured approximately 15 – 30° from the coronal plane with an 18-gauge needle (Figure 31). Third, NP tissue was removed using the needle attached to a syringe with vacuum.

Fourth, an excessive fatigue compressive load from -1800 N to 0 N for 50 cycles at a rate of 0.1 Hz was applied to mechanically overload the disc. Last, the specimen was injected with composite until the syringe's plunger could no longer be depressed. The composite was dyed blue for identification purposes, kept cold at 4°C, and allowed to set for 10 minutes. ROM and stiffness for the punctured, denucleated, fatigued, and injected conditions were all normalized to that of the intact disc.

**6.2.3 Lateral bending and resistance to expulsion.** Lateral bending tests were performed to observe the composite's resistance to expulsion (n = 7). Custom-designed mechanical fixtures were created to allow for bending of the IVD specimen (Figure 32). The rod is offset 25.4 mm from the center of the top stainless-steel fixture (3 ° from the vertical) and connected to a hinge, thus allowing for rotational movement. Specimens were denucleated, injected with composite, and subjected to lateral bending (- 3 to + 3°) along the injury axis for 10 cycles at a rate of 0.5°/s by applying a vertical displacement (- 4 to + 4 mm) located 25.4 mm from the center of the specimen (Figure 33A). This was followed by an expulsion test where the bending angle was continuously increased at a rate of 0.1 °/s on the side opposite of the injection site (Figure 33B). The test was stopped manually when the maximum bending angle was reached due to geometric constraints of the tissue. Angles were tracked using a video camera recording at a rate of 30 frames per second. Torque was calculated as the applied force multiplied by the perpendicular distance from the axis of rotation. Specimens were tested on an MTS 831 elastomer machine and maintained at 37 °C using a saline bath.

**6.2.5 Statistical analysis.** SPSS software was used to perform a statistical analysis in identifying significant differences of biomechanical parameters between

experimental conditions. A repeated-measures, one-way analysis of variance (ANOVA) was conducted to compare means and a post-hoc Bonferroni correction was applied. Significance was set at the 95 % confidence level ($p < 0.05$). All values are reported as the mean ± SD.

## 6.3 Results

**6.3.1 Histology.** The composite's ability to completely fill, conform, and adhere to surrounding disc tissue was confirmed using a histological approach (Figure 34). Specimen height varies across the disc, ranging from 2 – 5 mm, with a noticeably taller NP and shorter AF. The native porcine disc exhibits a strong presence of sulfated GAGs and slight staining of collagen in the NP. The lamellar collagenous structure of the AF and thin CEPs can also be identified in the disc. Puncturing the disc with an 18-gauge needle does not cause large-scale morphological damage. Conversely, denucleation causes disorganization of NP tissue and leaves behind a large void in the nuclear cavity. Injection of the composite fills the void and contacts native NP, AF, and CEP.

**6.3.2 Compression-tension and biomechanical restoration.** Restoration of biomechanical parameters was first assessed by performing compression and tension on the porcine IVDs. Approximately 294 ± 41 mg or 44 ± 8.9 % of NP tissue were removed from IVDs. The average mass of composite hydrogel that was injected into the IVD was 340 ± 43 mg. ROM (Figure 35) and stiffness (Figure 36) were calculated for each condition and normalized to the intact disc. Relative to the intact condition, needle puncture did not cause a significant increase in ROM ($p > 0.05$), yet resulted in a small decrease in compressive and tensile stiffness ($p < 0.05$). Denucleation caused a significant increase in ROM by approximately 20 ± 10 % ($p < 0.05$) and decrease in both

compressive and tensile stiffness ($p < 0.05$). Excessive mechanical fatigue caused a further significant increase in ROM by 35 ± 18 % ($p < 0.05$) and caused compressive and tensile stiffness to drop by nearly 28 ± 5 % and 47 ± 10 %, respectively. Upon injection of the hydrogel composite, ROM and stiffness were restored relative to the intact condition ($p > 0.05$). The implant remained within the disc space and expulsion through the annular defect was not observed during loading (Figure 37).

**6.3.3 Lateral bending and resistance to expulsion.** Lateral bending tests were performed to evaluate the composite's ability to resist migration and expulsion from within the disc space. The average mass of NP removed from the IVD was 357 ± 78 mg or 47 ± 9.3 %. The average mass of composite hydrogel that was injected into the IVD was 449 ± 157 mg. Specimens were bent to an average maximum angle of 11.2 ± 1.2 °, exhibited an average maximum torque of 5.3 ± 1.4 Nm and showed no evidence of expulsion during testing.

**6.4 Discussion**

Ex vivo biomechanical testing can offer important preliminary findings when evaluating an injectable implant for NP replacement. Several laboratories have investigated replacements in cadaver models including human [446,447,452,453], ovine [448,454,455], porcine [456,457], bovine [416,449], caprine [450], and murine [458]. Partial denucleation increased ROM and decreased stiffness, which has been consistently reported in literature [416,446,447,448,449,450]. Peak compressive stress values for excessive fatigued loading without NP augmentation surpassed intradiscal pressures of regular physiological activity [71,72]and caused further degenerative changes. Composite injection restored ROM and stiffness relative to the intact condition and expulsion was

not observed. Several ex vivo studies in literature have also demonstrated that an injectable replacement can restore ROM and stiffness [416,446,447,448,449,450]. Expulsion of the composite was also not observed within the limits of physiological bilateral bending or hyperphysiological unilateral bending.

One difference between the presented work and other cadaver models was the method of inducing degeneration. For example, other studies have augmented disc biomechanics through nucleus disruption [455], forced herniation [457,458], or enzymatic degradation [450]. In our model, aspiration of NP tissue using a needle was feasible due to its mucous-like rather than fibrous texture, which is typically observed across other animal species including humans. Conversely, others created vertical [448], oblique [454], or cruciate [452,449] incisions in the AF and physically excised NP tissue with rongeurs. Accessing the intradiscal space by creating a large annular incision increases the risk of implant herniation [377]. While the bioadhesive did not expel through the needle tract, resistance to expulsion through alternative annular defects such as an incision should be explored further.

Biomechanical assessment was modeled after repetitive physiological activity to determine if properties of ROM and stiffness could be restored, however additional types of in vivo behavior should also be considered. For example, the IVD undergoes continuous cycles of creep-recovery during diurnal activity [459,460], which was not modeled in this study. Creep is indicative of the disc's poroelasticity in which fluid flows from the tissue during loading and returns due to the presence of proteoglycans. The composite's performance should also be evaluated during other twisting or bending motions such as axial rotation or flexion-extension with superimposed compressive

loading [446,455,456,457]. Other properties such as hysteresis [446], neutral zone [446,447,455,449,450], hydraulic permeability [458], and DH [447,456,457,449] can also be measured to assess physiological function in future work.

There are several key factors to achieving clinical success in restoring mechanical function. Maximizing an implant's adhesive strength to host tissue is important in preventing implant migration [402,403]. Histology revealed that the composite was able to completely fill void space within the denucleated disc. If implant dislocation were to occur, the hydrogel's stiffness or viscosity can be increased [401], or alginate microparticles can be conjugated with dopamine or cysteine to enhance adhesion [422, 461]. The amount of NP removed from the disc [447] and injected replacement [446] influence ROM, NZ, stiffness, and DH. In this work, the removed mass of NP tissue was completely substituted with excess composite, whereas inadequate filling can lead to incomplete biomechanical restoration. Delivery of an injectable NP implant requires injuring the AF by needle puncture, and we showed potential of the implant to resist expulsion through the defect. Importantly, needle puncture may initiate long-term degenerative changes [462] which should be considered when evaluating implant resistance to expulsion. Sealing annular defects with a bioadhesive can help prevent expulsion, maintain implant hydration, and promote healing of the AF [458,463,464,465,466]. Therefore, simultaneously replacing the NP and AF should be considered when repairing the disc. Lastly, the host's immune response and whether the body will accept or reject the bioadhesive composite material will need to be evaluated.

## 6.5 Conclusions

Compression-tension tests were performed to assess changes in the disc's mechanical properties during different experimental conditions. Puncturing with an 18-gauge needle did not significantly alter disc biomechanics. Artificial degeneration was induced to the porcine IVD through partial denucleation followed by excessive mechanical fatigue. Consequently, a significant increase in ROM and decrease in stiffness were observed. Upon injection of the composite, biomechanical properties were restored and did not significantly differ from the intact condition. Denucleated IVDs injected with composite were then exposed to cyclic bilateral bending followed by a unilateral expulsion test. No evidence of implant herniation was observed during lateral bending tests. Histological results confirm that the composite is space-filling and adheres to native disc tissue. Results presented in these ex vivo studies demonstrate the bioadhesive composite's ability to restore mechanical properties and resist expulsion from a denucleated and mechanically fatigued porcine IVD.

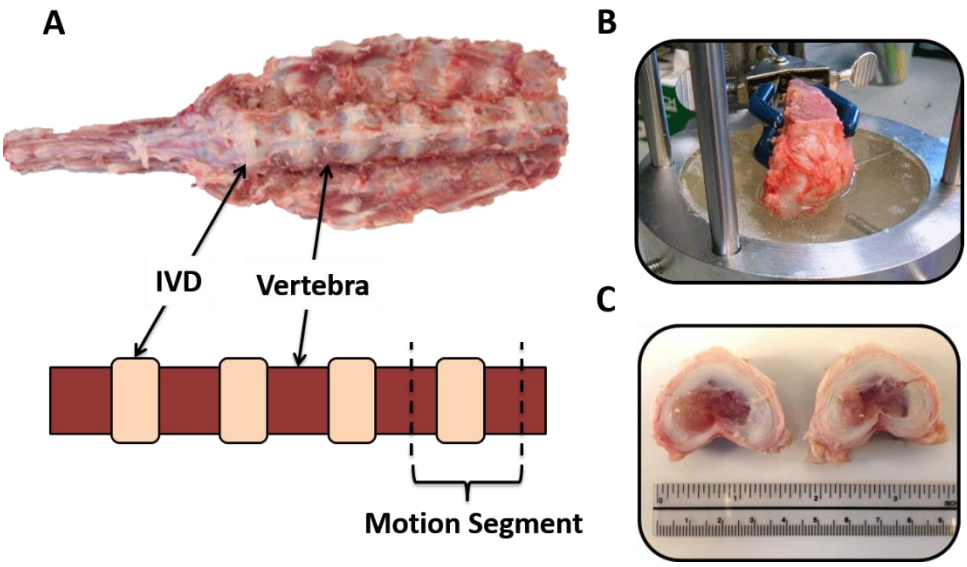


*Figure 29.* Dissection, isolation, and casting of porcine IVDs. (A) Macroscopic view of the porcine lumbar spine, (B) casting of a motion segment in polyurethane, and (C) a transverse cross section of an IVD.

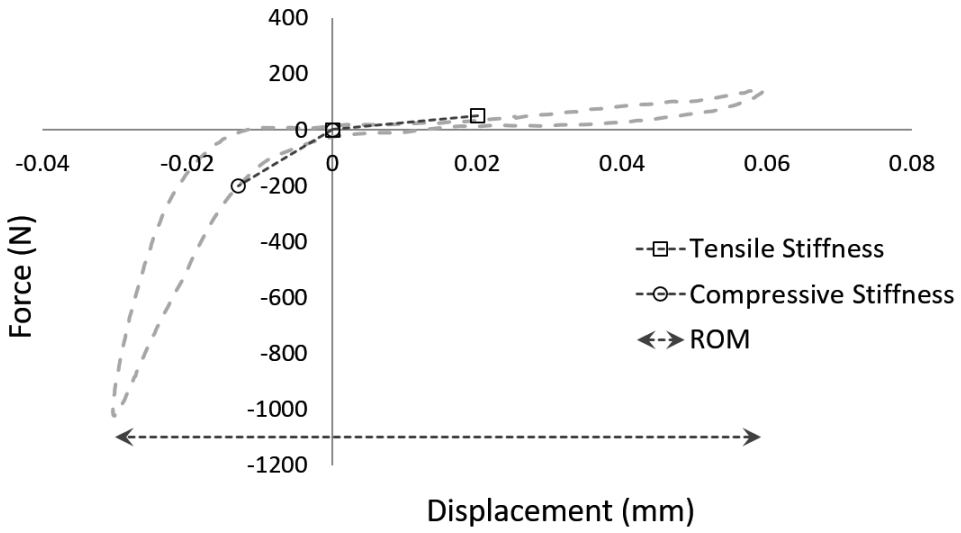


*Figure 30.* A representative hysteresis plot of an intact disc from compression-tension testing. Range of motion (ROM) and stiffness, represented by the linear dashed lines, were calculated from measured data.

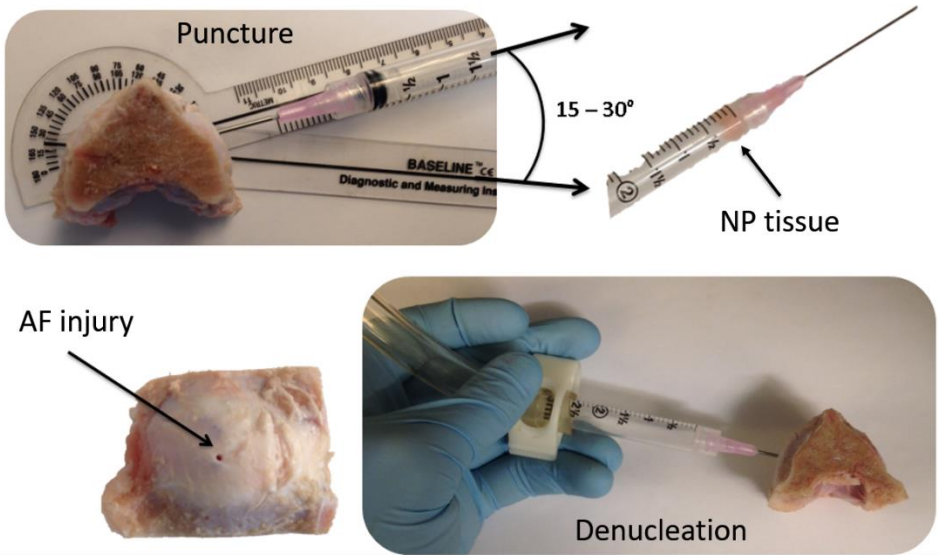


*Figure 31.* Denucleation process. An 18-gauge needle attached to a syringe and vacuum was used to puncture the porcine IVD and remove NP tissue.

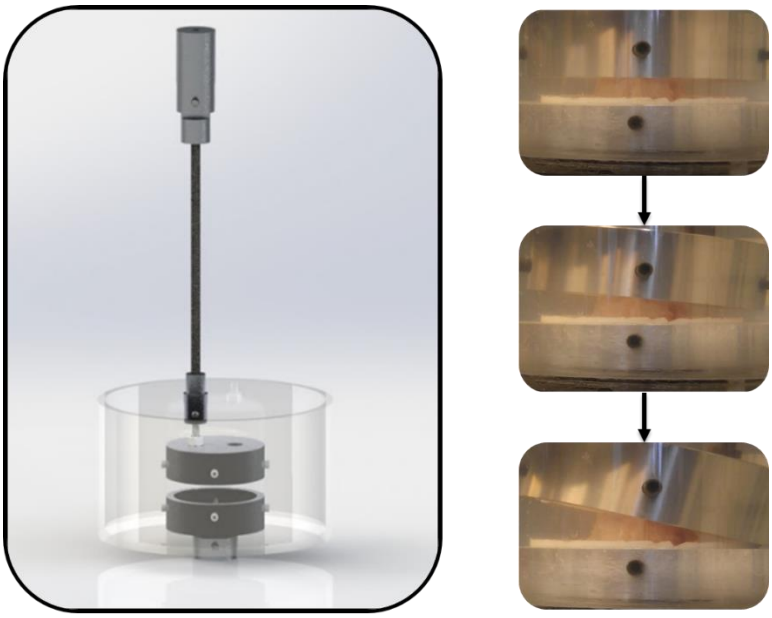

*Figure 32.* Custom-made mechanical fixtures designed to induce bending of the IVD specimen. The vertical rod is offset 25.4 mm from the center of the stainless-steel cup and affixed to a hinge allowing for rotational movement.

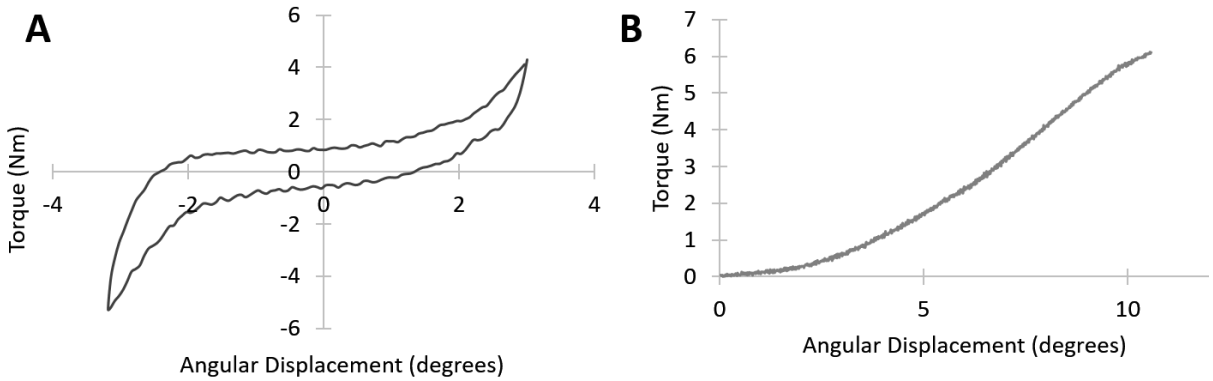


*Figure 33.* IVD specimens were punctured, denucleated, injected with composite and bent to observe potential risks for implant extrusion. (A) Representative bilateral bending hysteresis curve followed by a (B) unilateral bending expulsion test until the maximum angle of rotation was reached.

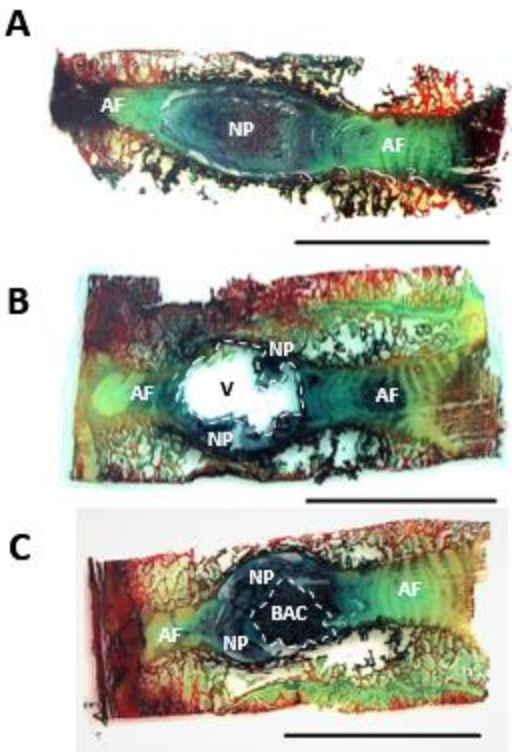


*Figure 34.* Histological sagittal cross sections of IVDs subjected to different treatments and stained with alcian blue and picrosirius red. IVDs were (A) intact, (B) denucleated, or (C) denucleated and injected with implant. The location of the void (V) and the bioadhesive composite (BAC) have been identified within the white dashed lines. The implant fills void space and interfaces with both the native NP and AF in the porcine disc. Scale bars = 1 cm.

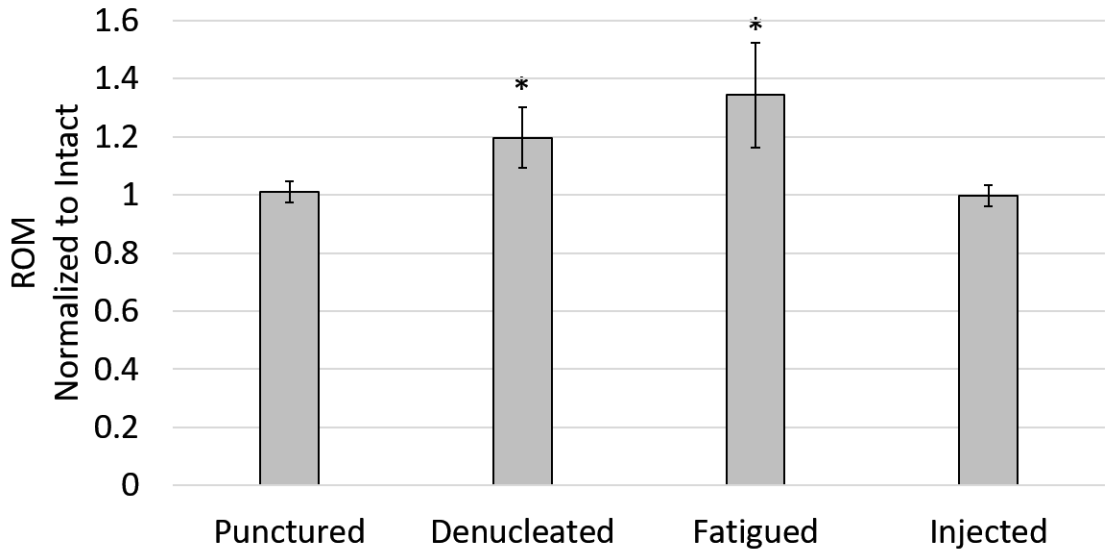


*Figure 35.* Range of motion (ROM) normalized to the intact disc for each test condition. An asterisk (*) indicates a statistically significant difference ($p < 0.05$) compared to the intact disc.

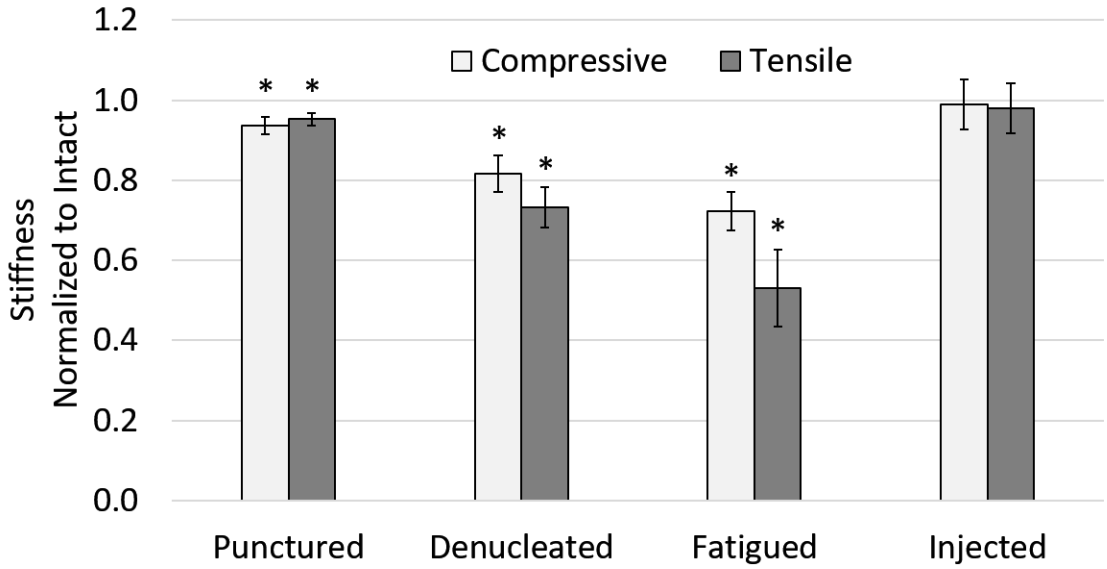


*Figure 36.* Compressive and tensile stiffness normalized to the intact disc for each test condition. An asterisk (*) indicates a statistically significant difference ($p < 0.05$) compared to the intact disc.

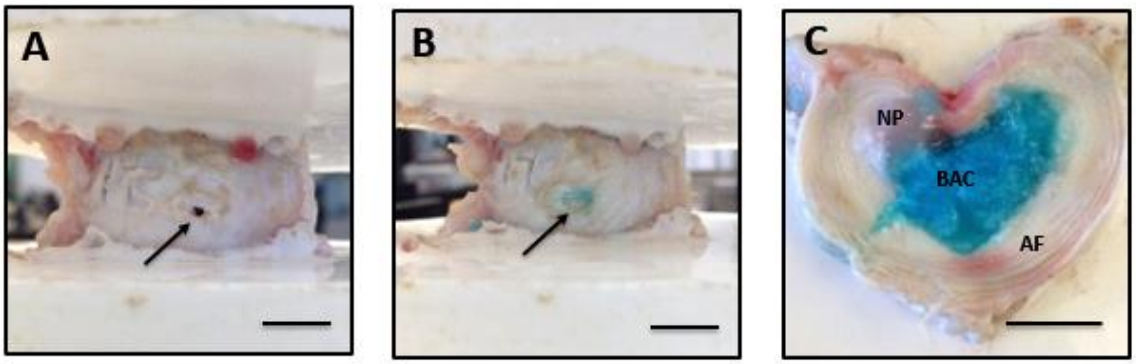


*Figure 37.* The porcine IVD after (A) puncture with an 18-gauge needle, (B) denucleation and injection of the bioadhesive composite (BAC) filling the annular defect, and (C) transverse cross section of the IVD containing the implant within the nuclear cavity post-mechanical testing. Scale bars = 1 cm.

# Chapter 7

## Ex Vivo Tissue Repair of the Degenerated Bovine Disc

### 7.1 Introduction

The mutual effects of MSCs and resident disc cells on one another have been well characterized. In vitro studies showed that proliferation and ECM expression of disc cells are enhanced when co-cultured with MSCs in direct contact [349,350,351,352,353]. Further, MSCs stimulate degenerate disc cells to regain a healthy phenotype through the upregulation of trophic factors and downregulation of catabolic signaling molecules [353,467]. Concomitantly, resident disc cells alter MSC phenotype and induce differentiation by releasing their own soluble factors [355,356,358]. Direct in vitro co-culture with NP [349,354] or AF [357] cells elevate MSC gene expression levels for ACAN, COL1, COL2, and SOX9. MSCs also differentiate toward NP or AF phenotypes and secrete disc-like ECM when transplanted in vivo [363,468,469,470,471].

Whole disc organ culture offers a cost-effective approach to study the influence of the IVD microenvironment on MSCs and while controlling experimental conditions and evaluating repair. Compared to the human lumbar, caudal bovine discs exhibit similar hydration and ECM gradients of GAG and collagen across the NP and AF [472,473,474,475]. Other characteristics such as swelling pressure [472], cellular density [473], and the lesser presence of notochordal cells [476,477] are also similar to the human lumbar disc. When scaled for differences in geometry, mechanical properties in axial compression and torsion are comparable [474,475]. Based on these findings, the caudal bovine IVD was selected as a model to study ADMSC survival, morphology, and protein expression after delivery to injured IVD tissues.

It is hypothesized that transplanted MSCs will change in phenotype and produce ECM resembling the native composition and structure of the tissue based on their location. MSCs implanted in the NP are expected to produce proteoglycan containing ACAN and COL2 [45,54]. Conversely, MSCs implanted in the outer AF should produce relatively more COL1, minimal COL2, and less proteoglycan [45,61]. MSCs residing within the transition zone between the NP and AF would ideally synthesize mixed quantities of proteoglycans and collagen. Other discogenic proteins such as SOX9 and HIF1α should be ubiquitously expressed by MSCs throughout disc tissue [478,479]. However, MSCs should express higher proportions of KRT19 and FOXF1 in the NP or glypican 3 (GPC3) and fibulin 1 (FBLN1) in the AF [435,480,481]. Morphological changes would also occur, whereby MSCs present a round, chondrocyte-like or elongated, fibroblast-like shape similar to that of NP or AF cells, respectively [40].

In this chapter, an ex vivo organ culture model of caudal bovine IVDs was employed to investigate cell therapy. Our first objective was to establish suitable culturing conditions for free-swelling IVDs by quantifying cellular viability and biochemical composition of the native tissue after 14 days. Our second objective was to develop an injury model using enzymatic digestion. Discs were injected with papain enzyme and cultured for 7 days to create a void space in the NP. Our third objective was to deliver the bioadhesive composite, specifically formulation S-50, with ADMSCs and assess the extent of cellular differentiation and ECM deposition. ADMSC viability, morphology, and protein expression were quantified as a function of location within the injured disc after 14 days of culture.

## 7.2 Methods

**7.2.1 Isolation, debridement, and culturing of bovine IVDs.** Caudal IVDs were dissected from fresh bovine tails (20 months, 3 hours post-mortem) obtained from a local abattoir (Bringhurst Meats, Berlin, NJ). Tails were first disinfected with 10 % povidone-iodine (Fisher Scientific) and dried with sterile gauze. Muscle tissue, tendons, and bony processes were removed using scalpels equipped with blades (#10 and #22) and shears. A histological band saw (Mar-Med, Inc.) was used to isolate IVDs from adjacent vertebrae, leaving behind approximately 1 – 2 mm of thin bone on the superior and inferior endplates. IVDs were wrapped in saline-soaked gauze to prevent dehydration and placed in a 6-well plate on ice to slow cellular metabolism and minimize cell death. Endplates were rinsed thoroughly with a pressurized water system using sterile saline supplemented with 50 mM sodium citrate to remove blood clots and improve diffusion of nutrients. IVDs were cultured under free-swelling conditions with 80 mL of culture media in 100 mL specimen containers (Starplex Scientific, Inc.) and maintained at 37 °C and 5 % $CO_2$. Media was replaced every two days and composed of high glucose DMEM containing 10 % FBS, 100 U/mL penicillin, 100 µg/mL streptomycin, 0.25 µg/mL amphotericin B, and 50 µg/mL ascorbic acid.

**7.2.2 Experimental design.** Bovine discs were subjected to several treatments for analysis (Figure 38). Intact discs were kept in a free-swelling, normoxic environment for 14 days to assess suitable culturing conditions. Changes in native disc cell viability, ECM content, and architecture as a result of dissection technique or ex vivo conditions were compared to intact isolated discs at the beginning of the study.

Disc degeneration was initiated through proteolysis using papain enzyme. Papain suspension (10 mg/mL, 30 U/mg, Sigma Aldrich) was diluted to a final concentration of 100 U/mL in buffer containing 5 mM sodium citrate, 150 mM cysteine hydrochloride, and 5 mM ethylenediaminetetraacetic acid (EDTA). Approximately 100 – 200 µL of papain enzyme was injected into each disc with a 30-gauge needle and proteolytic digestion proceeded for 7 days.

Degenerated discs were treated with carrier containing ADMSCs. PNIPAAm-g-CS was dissolved overnight at 4 °C in ADMSC culture media at a concentration of 5 % w/v. Freeze-dried alginate MPs were immersed in 70 % ethanol, vacuum filtered to remove excess alcohol, and allowed to dry overnight. Aqueous PNIPAAm-g-CS and MPs were sterilized under UV light for a minimum of 5 hours. MPs were blended with 5 % w/v PNIPAA-g-CS at a concentration of 50 mg/mL to form the composite. ADMSCs were detached with trypsin, collected, counted, and labeled with PKH26 red fluorescent dye (Sigma Aldrich) according to the manufacturer's instructions for tracking purposes. Cells were encapsulated within the composite at a density of $5 \times 10^6$ cells/mL. Degenerated discs were injected with as much composite until a resistance to flow was achieved and cultured for an additional 14 days (21 days total). Treated disc tissues were compared to degenerated and intact tissues with respect to native disc cell viability, ECM content, and architecture. Implanted ADMSCs were also characterized for viability, morphology, and protein expression.

**7.2.3 Biochemical assays.** Proteins in NP and AF tissue from intact discs (n = 4) cultured for 14 days were quantified using the Blyscan™ Sulfated Glycosaminoglycan and Sircol™ Soluble Collagen biochemical assay kits (Biocolor, Life Science Assays)

and compared to isolated discs (n = 4) at the beginning of the study. Endplates were removed and biopsied tissue samples were freeze dried to determine their dry masses. To quantify GAG content, buffer composed of 200 mM sodium phosphate, 100 mM sodium acetate, 5 mM cysteine HCl, 10 mM EDTA, and 0.1 mg/mL papain (10 mg/mL, 30 U/mg, Sigma-Aldrich) was used to digest tissue for 24 h at 65 °C. To quantify soluble collagen content, buffer composed of 0.1 mg/mL pepsin (2500 U/mg, Sigma Aldrich) in 0.5 M acetic acid was used to digest tissues for 24 h at 4 °C. Chondroitin sulfate from bovine trachea and collagen from rat tail were used to construct a standard curve for GAG and collagen content, respectively. Absorbance readings were measured at 656 nm and 555 nm using a microplate reader (SpectraMax M2, Molecular Devices) to determine GAG and collagen content, respectively.

**7.2.4 Cellular viability.** Viability of native disc cells and ADMSCs were assessed using the Live/Dead™ Cytotoxicity Kit. Biopsied tissues (n = 3 or 4) from both NP and AF regions were placed into microcentrifuge tubes with DMEM containing 2 µM calcein AM and 4 µM ethidium homodimer-1. Sample incubation occurred for 3 h at 37 °C and 5 % $CO_2$. Tissue samples were washed thrice in PBS, placed on glass coverslips, and viewed on a confocal microscope (Nikon, Model $A1^+$). Superficial edges of tissue samples were excluded in the quantification of cellular viability. Three random depths, approximately 200 µm below the tissue surface, were imaged from each sample to obtain an average viability.

Endplates were removed from treated discs and composites containing PKH26 labeled ADMSCs (n = 3) were inserted into microcentrifuge tubes. Composites were dissolved in citrate buffer consisting of PBS supplemented with 50 mM sodium citrate

(Sigma Aldrich) and 20 mM EDTA (Sigma Aldrich). Suspended cells were pelleted at 300 x g for 5 minutes and the supernatant was discarded. The cell pellet was resuspended in DMEM containing 2 µM calcein AM and incubated for 1 h at 37 °C and 5 % $CO_2$. Suspended cells were pelleted to remove excess reagent, resuspended in PBS, and dispensed in a 48 well plate. Three random regions of living and dead ADMSCs were imaged from each sample to obtain an average viability using an inverted fluorescent light microscope (Zeiss, Axio Vert.A1). Living cells that metabolized calcein AM or dead cells with compromised membranes and nuclei labeled with ethidium homodimer-1 appeared green or red, respectively. ImageJ software was used to estimate cellular viability.

**7.2.5 Protein expression.** Histology was performed to assess cell morphology and proteins present in intact, degenerated, and treated tissues that received composite containing ADMSCs. Discs (n = 3) were fixed with 4 % formaldehyde in PBS for 24 h at 37 °C. Endplates were removed and disc tissues were transferred to cryomolds containing frozen section compound and frozen in methylbutane chilled with liquid nitrogen. Transverse cross sections with a thickness of 30 µm were obtained using a cryostat and placed on positively charged slides. Sections containing PKH26 labeled cells were located and imaged to identify differences in morphology. Hydrogel and microparticle material were removed using sodium citrate-EDTA buffer to identify ECM deposited by ADMSCs. GAGs and collagen were identified by staining with either 1 % w/v alcian blue or 0.1 % w/v picrosirius red, respectively. Cell nuclei were counterstained with Weigert's hematoxylin. Protein expression and morphology of encapsulated ADMSCs in the bioadhesive composite before and after delivery into the degenerated disc were

compared. Cross sections were imaged on an inverted light microscope (Zeiss, AxioVert A.1).

ADMSC differentiation was evaluated as a function of position within the IVD using indirect immunofluorescent staining. Primary and secondary antibodies were purchased from Abcam to confirm the presence of human proteins such as: ACAN, COL1, COL2, HIF1α, FOXF1, KRT19, FBLN1, and GPC3. As described previously, discs injected with composite containing ADMSCs (n = 3) were fixed, sectioned, and rinsed with sodium citrate-EDTA buffer to remove hydrogel and alginate microparticle material. Sections were permeabilized with TBS supplemented with 0.3 % v/v Triton X-100 for 10 minutes. Sections were blocked with TBS containing 10 % v/v goat serum for 10 minutes. Primary antibodies were applied for 1 hour at room temperature. Excess primary antibody was discarded, and sections were rinsed thrice with TBS. Secondary antibodies, conjugated with Alexa Fluor 647, were applied for 30 minutes at room temperature. Excess secondary antibody was discarded, and sections were rinsed thrice with TBS. ADMSCs were identified with the PKH26 fluorescent dye and imaged on a confocal microscope (Nikon, Model A1$^{+}$). Alexa Fluor 647 staining was altered to show green and enhance contrast against cells labeled with PKH26 fluorescent marker. Protein expression of encapsulated ADMSCs in the bioadhesive composite before and after delivery into the degenerated disc were compared.

**7.2.6 Statistical analysis.** Mann-Whitney U Tests were used to identify statistical differences in biochemical composition or cellular viability. Significance was set at the 95 % confidence level ($p < 0.05$). All values are reported as the mean ± SD.

## 7.3 Results

**7.3.1 Intact disc model.** Native disc cell viability was quantified for intact disc tissues (Table 8). Directly after dissection, cells from the NP and AF regions were 74.6 ± 5.7 % and 76.8 ± 6.2 % viable, respectively. After 14 days of free swelling culture, NP and AF cells were 72.4 ± 5.4 % and 74.5 ± 6.0 % viable, respectively. Intact disc tissues exhibited a small, but insignificant drop in cell viability ($p > 0.05$). Native NP cells exhibited a round morphology with dendritic-like processes, as opposed to AF cells which were elongated and aligned. GAG and soluble collagen content of cultured disc tissues (Figure 39) showed no significant differences ($p > 0.05$) to discs tissues sampled prior to culture. Comparatively, NP and AF tissue contained relatively higher concentrations of GAG and soluble collagen, respectively. Histological analysis confirmed the presence and distribution of GAG and collagen throughout the intact disc (Figure 40A/B). Upon gross examination of the discs, no signs of deterioration or morphological changes were observed (Figure 41A/B).

**7.3.2 Degenerative disc model.** Artificial disc degeneration was initiated using proteolytic digestion. Seven days after injection of papain enzyme, a noticeable void formed in the center of the IVD (Figure 40 D and Figure 41D). Degenerated discs were more flexible as a result of tissue digestion compared to discs that did not receive papain injections. Enzymatic digestion caused a complete loss of NP tissue and GAGs residing throughout the AF tissue. Collagen content and architecture of the AF lamellae remained uncompromised.

**7.3.3 Treated disc model.** Native disc cell viability of intact, degenerated, and treated tissues was compared after 21 days (Table 9). Cellular viability of native NP

could not be assessed for degenerated or treated discs as a result of papain digestion, therefore tissue near the periphery of the void was quantified. After 21 days, NP and AF cells from intact discs were 77.0 ± 2.2 % and 79.4 ± 2.0 % viable, respectively. Enzymatic digestion caused a slight significant drop in cellular viability of degenerated discs compared to intact disc tissues ($p < 0.05$). Disc cells along the void periphery and AF in degenerated tissues exhibited a viability of 70.2 ± 4.1 % and 70.6 ± 2.5 %, respectively. Cellular viability of treated disc tissues was not significantly different compared to intact disc tissues ($p > 0.05$). Disc cells along the void periphery and AF in treated tissues were 78.6 ± 2.0 % and 81.2 ± 4.8 % viable, respectively.

ADMSCs stained positively for intracellular staining of GAGs and collagen prior to injection into degenerated discs (Figure 42A/B). Labeling with PKH26 did not significantly affect ADMSC viability and were greater than 95 % viable after encapsulation. Cells exhibited a round morphology with red fluorescently labeled membranes (Figure 42C). After 14 days post-injection into the degenerated disc, isolated ADMSCs that were pooled from the composites were 86.8 ± 4.9 % viable and appeared either round or elongated (Figure 42D). Furthermore, fluorescently labeled cells presented distinct morphologies based on their location within the disc (Figure 43). ADMSCs appeared round at the center of the composite or elongated along the periphery of the composite adjacent to the inner AF.

The carrier was successfully retained within the degenerated disc throughout the culture period and fills the void generated from proteolytic digestion (Figure 40E and Figure 41E). More notable was the diffuse GAG staining surrounding the periphery of the composite, which appeared to have replaced the degraded ECM (Figure 40E). ECM

deposition by ADMSCs was location dependent within the composite. Striations of GAG were identified at the center of the composite; however, collagen staining was not detected (Figure 44A/B). Histological results revealed intense staining of extracellular collagen and GAG along the periphery of the composite (Figure 44C/D).

ADMSCs at the beginning of the study did not show signs of extracellular staining for NP or AF-specific proteins (Figure 45). ACAN, COL1, COL2 and HIF1α proteins produced by ADMSCs were detected in degenerated discs and throughout the carrier at the end of the culture period. At the center of the carrier, COL2 and ACAN were stained positively, whereas COL1 was absent indicating that ADMSCs are producing ECM like the composition of NP tissue. ACAN, COL1, and COL2 were all detected at the periphery of the composite and are typically found in the transition zone (inner AF) between the outer AF and NP. HIF1α was also detected in both regions of the disc. Proteins specific to NP (FOXF1 and KRT19) and AF (FBLN1 and GPC3) tissues were detected in specific regions of the carrier (Figure 46). Positive staining for FOXF1 and KRT19 was identified at the center of the composite and absent along the periphery. In contrast, positive staining for FBLN1 and GPC3 was identified along the periphery and absent at the center. These results suggest that protein expression will vary depending on the location of ADMSCs within the disc.

**7.4 Discussion**

Repairing degenerated disc tissues through cell therapy is one potential alternative that can have important clinical impact. Whole disc organ culture provides a simple approach to studying the repair potential and fate of ADMSCs when injected into the disc environment. Culturing intact caudal bovine discs under free-swelling conditions has

been well established in literature [482,483,484,485]. In this study, we have demonstrated similar findings of sustained cellular viability in both the NP and AF regions for up to three weeks. Additionally, ECM content and morphological tissue structure remained unchanged as evidenced by histology and biochemical assays.

Degeneration models have been established by injecting digestive enzymes into caudal bovine discs [483,486,487]. A papain concentration of 100 U/mL was selected to aggressively degrade proteins with cysteine residues and generate a void space [486]. Naturally occurring disc degeneration is not characterized by a central void, yet this technique allows for carrier injection. Furthermore, papain is not an enzyme present in the human IVD and degrades ECM differently compared to aggrecanases or collagenases. Regardless, this enzyme was effective in causing GAG loss with minor changes in native disc cell viability. When developing a whole disc organ culture model, the type and degree of degeneration should be carefully selected, as these methods will most likely impact the fate of delivered ADMSCs.

Several studies have published findings pertaining to MSC fate when injected into the caudal bovine disc. Chan et al. injected a peptide hydrogel containing encapsulated MSCs into the nucleus pulposi of cryopreserved discs and observed a 20 % viability after 7 days [488]. In a subsequent study, MSCs were injected into mildly degenerate discs using 30 U/mL of papain enzyme and were 40 % viable after two days [486]. These studies have concluded that exogenous factors such as disc health and high intradiscal pressure significantly impact MSC survival, and suggests that viability can be further improved by reducing osmotic pressure via enzymatic degradation and using an adequate cell carrier [486,488]. These hypotheses were supported by Malonzo et al. when

investigators injected a thermosensitive PNIPAAm hydrogel containing encapsulated MSCs into a moderately degenerate disc using 60 U/mL of papain enzyme and reported approximately 70 % viability [489]. A study by Peroglio et al. concluded that hydrogel carriers support MSC viability and an anabolic cellular response [490]. Further, it was demonstrated that the degree of disc degeneration will dictate MSC fate. Significantly higher expression of discogenic markers was observed in MSCs implanted into healthy versus degenerated discs. However, no studies that we are aware of have examined MSC morphology and ECM expression as a function of the local tissue microenvironment within the disc.

We hypothesized that the transplanted ADMSCs would differentiate into the local tissue phenotype, even in the absence of added growth factors or mechanical stimulation. Our results indicate that site-specific differences in the disc microenvironment did indeed affect ADMSC differentiation, morphology, and ECM deposition. Histological, light microscopy, and fluorescent images suggested that transplanted ADMSC morphology and ECM deposition were consistent with observations in intact IVDs. For instance, ADMSCs located along the periphery of the carrier exhibited an elongated morphology and produced ACAN, COL1, and COL2 [40,54,61]. In addition, AF-specific protein markers (FBLN1 and GPC3) were positively identified along the periphery but absent at the center of the carrier [480,481]. These features are characteristic of cells residing within the transition zone or inner AF. In contrast, ADMSCs found at the center of the carrier remained round and produced ACAN and COL2 [40,45,54]. Furthermore, positive staining of NP-specific proteins (FOXF1 and KRT19) was located at the center, but absent along the periphery [435,480,481]. Centrally positioned ADMSCs displayed a

phenotype typical of NP cells. Because these markers were absent at day 0, it is hypothesized that biochemical and biophysical signals produced from both surrounding cells [355,356,358] and ECM [491] within the tissue induced ADMSCs toward region-specific phenotypes. Our findings suggest that direct physical contact between ADMSCs and native disc cells is not required to induce differentiation of the ADMSCs. Overall, these preliminary findings are significant because they suggest that a single biomaterial can be used to support site-specific ECM deposition across the heterogeneous IVD.

### 7.5 Conclusions

This work demonstrates the potential use of a bioadhesive composite as a cell carrier for the encapsulation and delivery of ADMSCs to repair the degenerated IVD. The cell carrier retained viable ADMSCs for up to 14 days in the degenerated disc. ADMSC transplantation improved native IVD cell viability compared to injured discs that were left untreated. Location of the transplanted ADMSCs had an influence ADMSC morphology and protein expression at the end of the culture period. Findings from this work are significant because current therapy for IVD degeneration can be improved with the development of a technology that can support repair of both NP and AF defects.

However, there were limitations to this study. The amount of residual NP tissue was not quantified after enzymatic degradation; therefore, it is difficult to conclude whether cues from the NP or from the adjacent CEPs induced ADMSC differentiation. It must also be considered that carrier composition and stiffness may play a role in guiding cell behavior [492,493], but carrier composition was held constant in this study. It is also important to note that the injury model used in this study mimics the early stages of degeneration [494]. Little is understood about how the timing of the intervention, degree

of tissue degeneration, and inflammatory environment affect tissue engineering outcomes for the IVD. Last, future studies should examine repair in both the inner and outer AF defects. Proper cellular alignment and bridging of newly produced tissue across a defect will be key in sealing annular injuries and restoring biomechanical functionality.

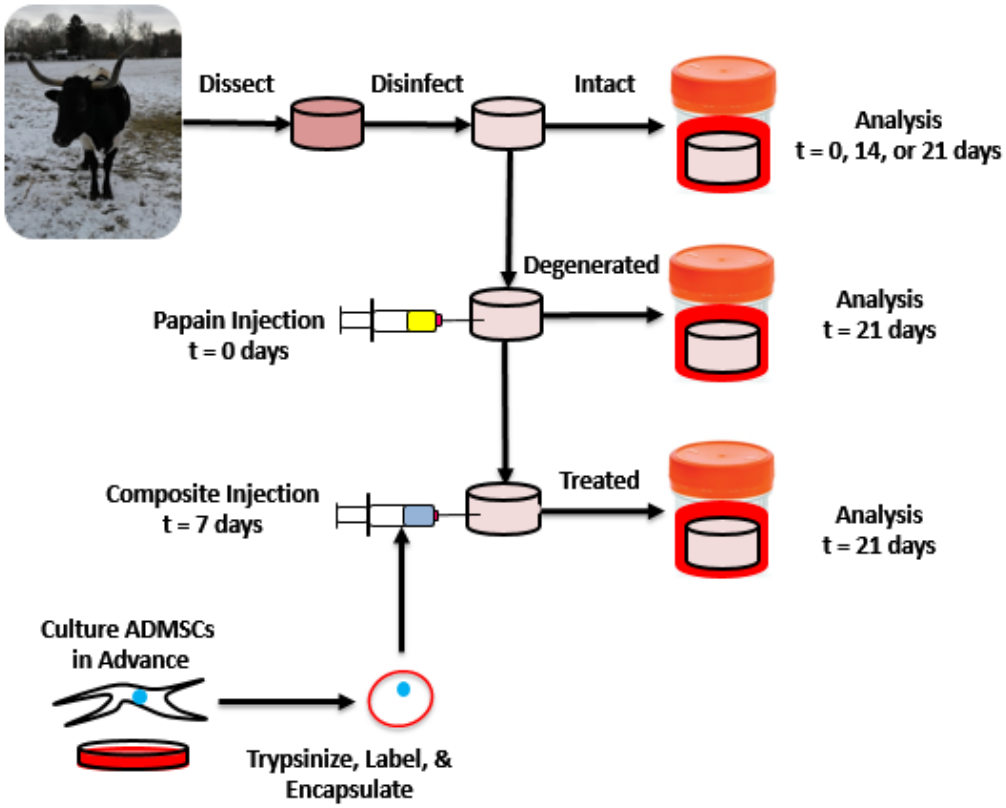


*Figure 38.* Intact bovine discs were first kept in a free-swelling, normoxic environment for 14 days to confirm suitable culturing conditions. Degeneration was then induced with papain enzyme and progressed for 7 days. Degenerated discs were either treated with the bioadhesive composite containing ADMSCs or left untreated and cultured for an additional 14 days. In parallel, intact discs were cultured for a total of 21 days. Discs obtained immediately after dissection were also evaluated for comparison.

Table 8

*Cellular Viability of Intact Disc Tissues*

| Location | NP | NP | AF | AF |
|---|---|---|---|---|
| Time (d) | 0 | 14 | 0 | 14 |
| Viability (%) | 74.6 ± 5.7 % | 72.4 ± 5.4 % | 76.8 ± 6.2 % | 74.5 ± 6.0 % |
| Live/Dead | 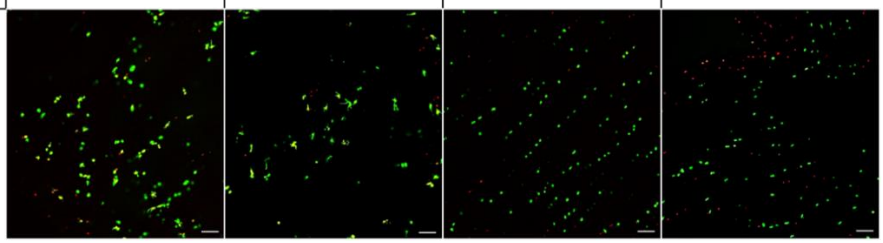 | | | |

*Note.* No significant differences in viability were detected. Scale bars = 100 µm.

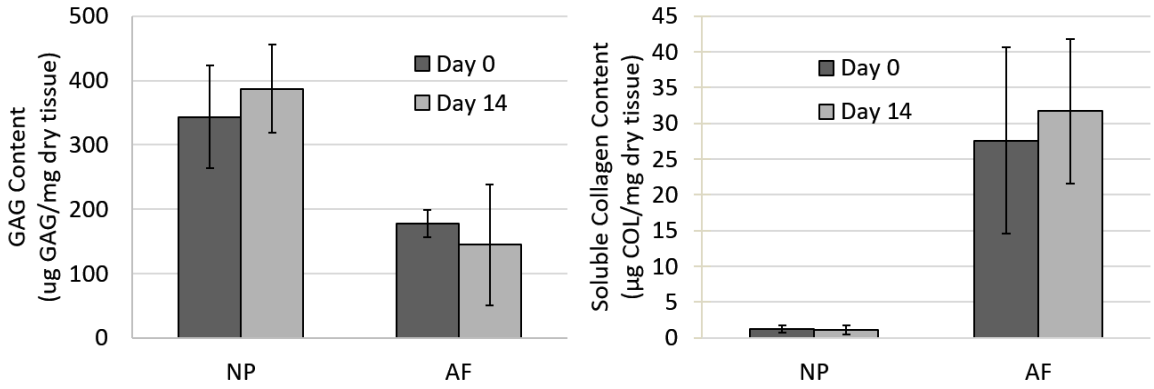


*Figure 39.* GAG and collagen content for intact IVD tissues prior to and after 14 days of culture (n = 4). Samples were normalized to their respective dry masses. No significant differences in GAG or collagen content were observed after 14 days.

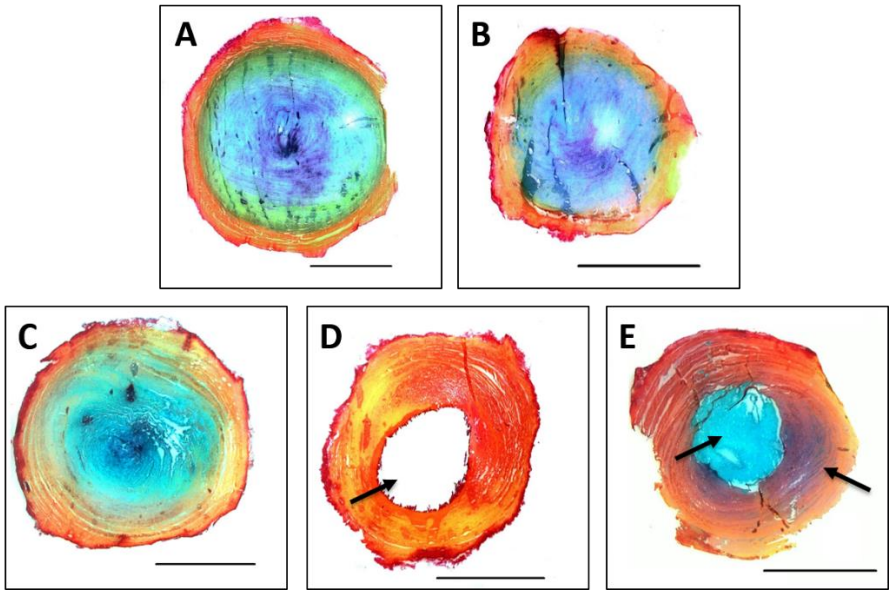


*Figure 40.* Histological staining of transverse IVD cross sections (n = 3). (A) Discs immediately obtained after dissection exhibited similar morphology and ECM content compared to discs cultured after (B) 14 days and (C) 21 days. (D) Artificially degenerated discs contained a void and exhibited a significant loss of GAGs. (E) The carrier filled the void and diffuse GAG was detected throughout the AF. Scale bar = 1 cm.

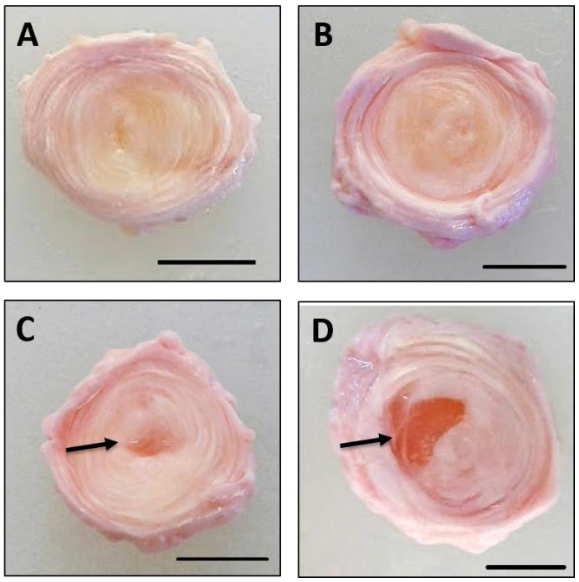


*Figure 41*. Gross morphology of IVDs (n = 3). (A) Discs immediately obtained after dissection were identical to (B) intact discs cultured for 21 days. (C) Papain enzyme was injected into the NP and caused the formation of a void. (D) The carrier filled the void and adhered to native disc tissue. Scale bar = 1 cm.

Table 9

*Cellular Viability of Intact, Degenerated, and Treated Disc Tissues*

| **Disc Model** | Intact | Intact | Degen. | Degen. | Treated | Treated |
|---|---|---|---|---|---|---|
| **Location** | NP | AF | Periphery | AF | Periphery | AF |
| **Viability (%)** | 77.0 ± 2.2 % | 79.4 ± 2.0 % | 70.2 ± 4.1 % | 70.6 ± 2.5 % | 78.6 ± 2.0 % | 81.2 ± 4.8 % |
| **Live/Dead** | 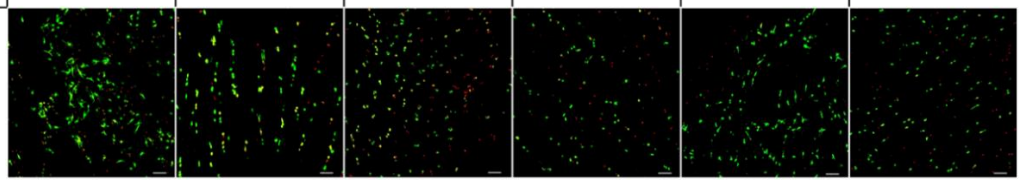 | | | | | |

*Note.* Degenerated tissues showed a slight significant decline in viability compared to intact tissues ($p < 0.05$). Scale bars = 100 µm.

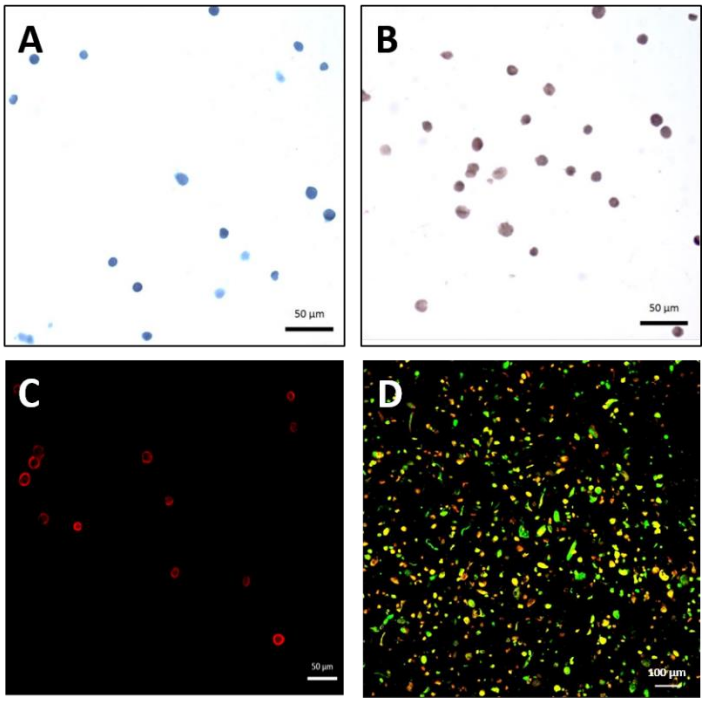


*Figure 42.* Encapsulated ADMSCs in the bioadhesive composite appeared round and exhibited intracellular staining for (A) GAG using alcian blue and (B) collagen using picrosirius red. (C) After labeling with PKH26, cell membranes were clearly distinguished by a fluorescent red color. (D) A representative Live/Dead image of ADMSCs after 14 days of culture in degenerated discs (n = 3). Both round and elongated morphologies were observed. Yellow indicates co-staining of PKH26 and metabolized calcein AM and living transplanted cells. Red and green indicates dead transplanted ADMSCs and alive native IVD cells, respectively.

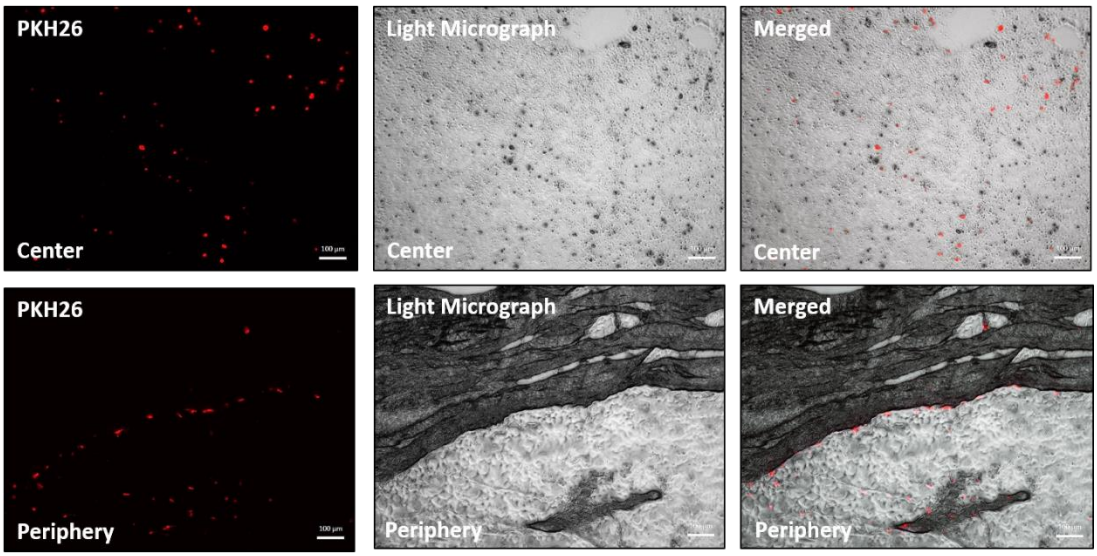


*Figure 43.* Representative fluorescent and light micrograph overlays of ADMSCs located at the center and periphery of the bioadhesive composite in degenerated discs after 14 days of culture (n = 3). ADMSCs in the center of the composite exhibited a round morphology, while those at the periphery were elongated.

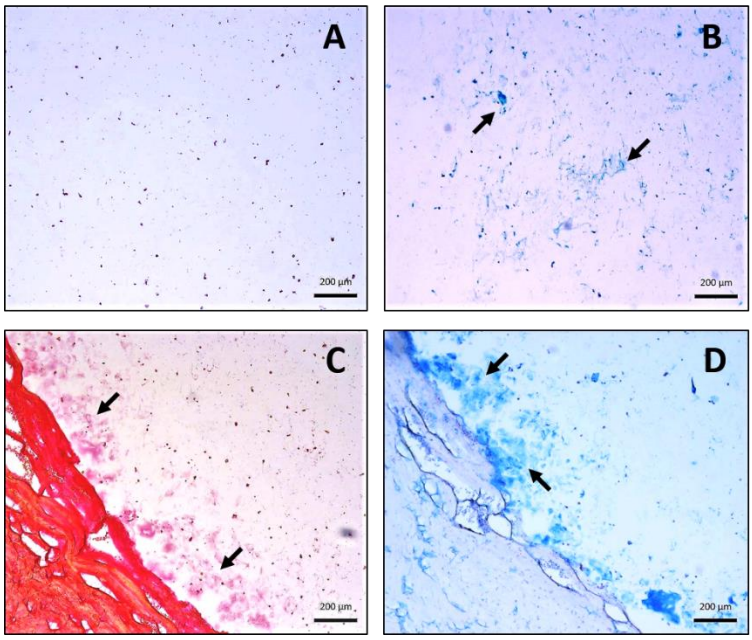


*Figure 44.* Histological images of degenerated discs treated with the bioadhesive composite containing ADMSCs after 14 days (n = 3). The carrier was removed using sodium citrate buffer. At the center of the carrier, (A) collagen staining was absent and (B) small striations of GAG were present. Along the periphery of the carrier, both (C) collagen and (D) GAG staining were evident.

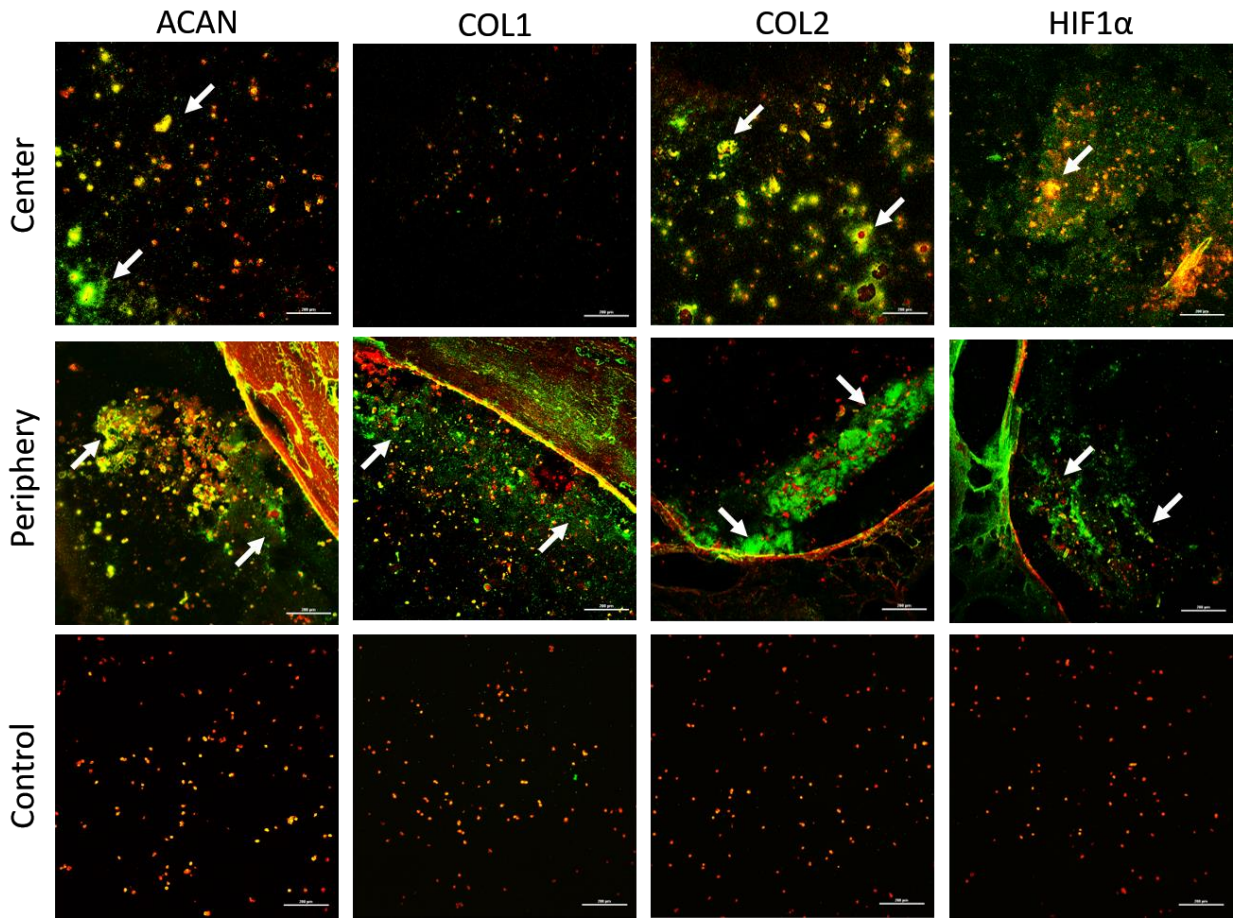


*Figure 45.* Representative images of immunofluorescent staining of ACAN, COL1, COL2, and HIF1α at the center and periphery of the carrier after 14 days (n = 3). Cross-sectional staining of ADMSCs within the bioadhesive composite prior to delivery into the degenerated disc are presented as controls.

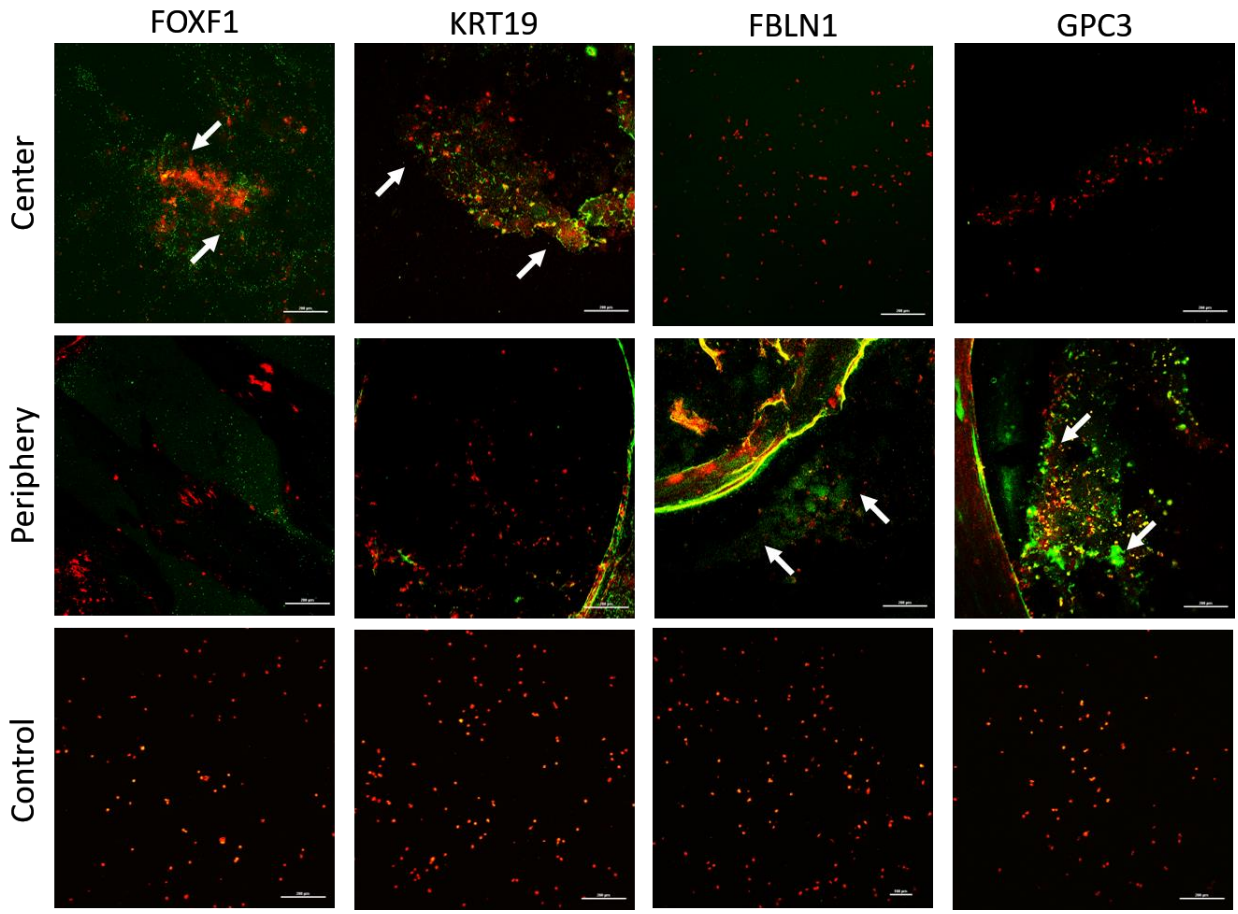


*Figure 46.* Representative images of immunofluorescent staining of FOXF1, KRT19, FBLN1, and GPC3 at the center and periphery of the carrier after 14 days (n = 3). Cross-sectional staining of ADMSCs within the bioadhesive composite prior to delivery into the degenerated disc are presented as controls.

# Chapter 8

# Project Summary

## 8.1 Conclusions

The overall goal of this project was to develop a novel bioadhesive composite cell carrier for the replacement and repair of degenerated IVD tissues. The first specific aim was to develop an injectable composite material that demonstrated adhesion to tissue and requisite mechanical properties for NP replacement. Thermosensitive PNIPAAm-g-CS blended with alginate MPs was viscous, yet injectable and gelled below physiological temperature. It was determined that the addition of 50 mg/mL of 20 µm alginate MPs to PNIPAAm-g-CS significantly increased swelling, viscosity, shear modulus, compressive modulus, and adhesive strength relative to PNIPAAm-g-CS alone. None of the composite formulations exhibited the requisite shear modulus for native NP tissue and must be improved. Adhesion to disc tissue may also be further enhanced to minimize the risk of implant migration upon injection into the disc. The bioadhesive composite was not degraded by enzymes present in the disc such as aggrecanase or collagenase. The inability to degrade allows for the potential long-term retention of MSCs and synthesized ECM within the composite network. Overall, an injectable composite with desirable properties was engineered for NP replacement.

The second specific aim focused on the feasibility of the bioadhesive composite to serve as a three-dimensional culture system for disc regeneration. The differentiation of ADMSCs toward a NP-like phenotype within the bioadhesive composite was induced using GDF6 and characterized in vitro. ADMSCs remained viable over the course of 14 days and exhibited increased metabolic activity. Cell proliferation may have occurred;

however, DNA content was not measured to confirm this hypothesis. Histological findings revealed newly synthesized sulfated GAG and collagen by ADMSCs. Immunostaining further identified the presence of ECM proteins like COL2 and ACAN produced by ADMSCs encapsulated in S-50. In addition, key NP-specific proteins such as KRT19, FOXF1, and PAX1 were positively detected. These proteins were also among the top five most upregulated genes quantified using qRT-PCR. It is important to note that degenerative conditions of ischemia, hypoxia, or low pH were not recapitulated in vitro. Each of these factors can impact MSC survival or differentiation upon transplantation within the degenerated disc. Cell survival, differentiation, and behavior were not fully characterized as a function of composite properties and should be further explored in future work. These results indicate that the bioadhesive composite supports the in vitro differentiation of ADMSCs toward an NP-like phenotype and may serve as a potential delivery vehicle for cell transplantation.

The third specific aim tested the hypothesis that the bioadhesive composite can restore biomechanics after partial nucleotomy and resist extrusion from the injured porcine disc ex vivo. Histology showed that S-50 filled the void remaining after NP tissue removal. Injection of the bioadhesive composite into a partially denucleated and mechanically fatigued porcine disc restored compressive ROM and stiffness relative to the intact condition. The implant was able to resist extrusion under compressive axial loading and lateral bending. The composite's ability to mimic the creep response of the NP, restore disc height, and resist extrusion through a larger annular defect should also be determined. Simultaneous modes of loading such as compression with bending or twisting were not applied in this ex vivo model. If implant extrusion were to occur,

composite properties can be altered to improve stiffness, viscosity, or adhesive strength with tissue. However, modifications to the bioadhesive composite in order to meet mechanical design criteria would consequently affect ADMSC behavior and would warrant further investigation. The bioadhesive composite demonstrated the ability to restore the disc's biomechanical properties through NP augmentation and resisted extrusion during loading.

The last and fourth specific aim tested the hypothesis that the bioadhesive composite supported the differentiation of transplanted ADMSCs toward a discogenic phenotype and deposition of region-specific ECM proteins within a degenerated microenvironment. S-50 retained viable ADMSCs for up to 14 days in the degenerated bovine disc. ADMSC transplantation improved native IVD cell viability compared to untreated, degenerated discs. The local microenvironment induced ADMSC differentiation toward an NP or AF-like phenotype, as evidenced by distinct changes in morphology and protein expression. Residual NP tissue was not quantified after enzymatic digestion; therefore, it is difficult to conclude whether cues from the NP or adjacent CEPs induced differentiation. The degree of disc degeneration and its impact on MSC behavior should be carefully considered and tested. Future work should also include examining the repair and sealing of any AF defects. Sealing annular injuries is key in restoring complete biomechanical functionality and preventing potential implant extrusion. The bioadhesive composite supported the site-specific differentiation and protein synthesis of ADMSCs within the degenerated bovine disc.

In summary, a thermosensitive bioadhesive composite cell carrier was developed for NP replacement. The composite demonstrated both adhesion to disc tissue and

requisite mechanical properties like that of the native NP. Encapsulated ADMSCs were retained, remained viable, differentiated, and produced discogenic proteins in vitro after exposure to GDF6. The composite was able to restore biomechanical properties and resist expulsion from a denucleated and mechanically fatigued porcine disc ex vivo. Finally, ADMSCs were successfully delivered in the bioadhesive composite into a degenerated bovine disc ex vivo, and underwent site-specific differentiation based on cues from the local microenvironment. Findings from this work are significant and will represent a major step forward in improving tissue engineering strategies for the repair of the degenerated IVD.

## References


[1] G.B.J. Andersson. Intervertebral disc herniation: Epidemiology and natural history. In: Weinstein JN, Gordon SL, editors. Low Back Pain: A Scientific and Clinical Overview. Rosemont, IL: American Academy of Orthopaedic Surgeons; 1996. pp. 7 – 21.

[2] N. Bodguk. Clinical anatomy of the lumbar spine and sacrum. Edinburgh: Churchill Livingstone; 1988.

[3] N. Boos, S. Weissbach, H. Rohrbach, et al., "Classification of age-related changes in lumbar intervertebral discs," *Spine (Phila Pa 1976)*, vol. 27, no. 23, pp. 2631 – 2644, Dec. 2002.

[4] A.D. Woolf, B. Pfleger, "Burden of major musculoskeletal conditions," *Bull World Health Organ.*, vol. 81, no. 9, pp. 646 – 656, Nov. 2003.

[5] G.B. Andersson. "Epidemiological features of chronic low-back pain," *Lancet*, vol. 354, no. 9178, pp. 581 – 585, Aug. 1999.

[6] C. Kalb. (2004, May 9). The great back pain debate. [Online]. Available at: http://www.newsweek.com/great-back-pain-debate-127923.

[7] F. Biering-Sorensen, "A prospective study of low back pain in a general population," *Scandinavian Journal of Rehabilitation Medicine*, vol. 15, pp. 71 – 79, 1983.

[8] H. Hurri, J. Karppinen, "Discogenic pain," *Pain*, vol. 112, no. 3, pp. 225 – 228, 2004.

[9] A. Praemer, S. Furner, D.P. Rice, Pain Other Joint. Musculoskeletal Conditions in the United States. Rosemont, IL: American Academy of Orthopaedic Surgeons; 1999. pp. 27 – 33.

[10] D. Hoy, C. Bain, G. Williams, et al., "A systematic review of the global prevalence of low back pain," *Arthritis Rheum.*, vol. 64, no. 6, pp. 2028 – 2037, 2012.

[11] Burden of Musculoskeletal Diseases in the United States: Prevalence, Societal and Economic Cost. Rosemont IL, American Academy of Orthopaedic Surgeons; 2008.

[12] B.P. Klein, R.C. Jensen, L.M. Sanderson, "Assessment of workers' compensation claims for back strains/sprains," *J. Occup. Med.*, vol. 26, no. 6, pp. 443 – 448, 1984.

[13] H.R. Guo, S. Tanaka, L.L. Cameron, et al., "Back pain among workers in the United States: national estimates and workers at high risk," *Am. J. Ind. Med.*, vol. 28, no. 5, pp. 591 – 602, 1995.

[14] V.Y. Ma, L. Chan, K.J. Carruthers, "Incidence, prevalence, costs, and impact on disability of common conditions requiring rehabilitation in the United States: stroke, spinal cord injury, traumatic brain injury, multiple sclerosis, osteoarthritis, rheumatoid arthritis, limb loss, and back pain," *Arch. Phys. Med. Rehabil.*, vol. 95, no. 5, pp. 986 – 995, 2014.

[15] C.J. DeFrances, M.N. Podgornik, "2004 National Hospital Discharge Survey," *Advanced Data*, no. 371, pp. 1 – 19, 2006.

[16] Q.B. Bao, H.A. Yuan, "Artificial disc technology," *Neurosurg Focus*, vol. 9, no. 4, pp. e14, 2000.

[17] A.J. Weiss, A. Elixhauser. (2014, March). Trends in Operating Room Procedures in U.S. Hospitals, 2001—2011. HCUP Statistical Brief #171. [Online]. Available: https://www.hcup-us.ahrq.gov/reports/statbriefs/sb171-Operating-Room-Procedure-Trends.pdf

[18] X. Luo, R. Pietrobon, S.X. Sun, et al., "Estimates and patterns of direct health care expenditures among individuals with back pain in the United States," *Spine (Phila Pa 1976)*, vol. 29, no. 1, pp. 79 – 86, 2004.

[19] J.W. Frymoyer, W.L. Cats-Baril, "An overview of the incidences and costs of low back pain," *Orthop. Clin. North. Am.*, vol. 22, no. 2, pp. 263 – 271, 1991.

[20] R.A. Deyo, A. Nachemson, S.K. Mirza, "Spinal-fusion surgery – The case for restraint," *New England Journal of Medicine*, vol. 350, pp. 722 – 726, 2004.

[21] R.A. Deyo, S.K. Mirza, J.A. Turner, B.I. Martin. "Overtreating chronic back pain: time to back off?" *J. Am. Board. Fam. Med.*, vol. 22, no. 1, pp. 62 – 68, 2009.

[22] H. Gray, T.P. Pick, R. Howden, "Osteology of the Skeleton," in Gray's Anatomy, Philadelphia: Running Press, 1974, pp. 33 – 54.

[23] H. Gray, T.P. Pick, R. Howden, "The Muscles and Fasciae," in Gray's Anatomy, Philadelphia: Running Press, 1974, pp. 338.

[24] J.R. Taylor, L.T. Twomey, "Age changes in lumbar zygapophyseal joints," *Spine (Phila Pa 1976)*, vol. 11, no. 7, pp. 739 – 745, 1986.

[25] N.A. Ebraheim, A. Hassan, M. Lee, X. Rongming, "Functional Anatomy of the Lumbar Spine," *Semin. Pain. Med.*, vol. 2, 131 – 137, 2004.

[26] M.W. Devereaux, "Anatomy and Examination of the Spine," *Neurol. Clin.*, vol. 25, pp. 331 – 351, 2007.

[27] H. Lodish, A. Berk, S.L. Zipursky, et al. Molecular Cell Biology. 4th edition. New York: W. H. Freeman; 2000. Section 22.4, Noncollagen Components of the Extracellular Matrix. Available at: https://www.ncbi.nlm.nih.gov/books/NBK21706/.

[28] T.C. Laurent, J.R. Fraser, "Hyaluronan," *FASEB J.*, vol. 6, no. 7, pp. 2397 – 2404, 1992.

[29] M. Morgelin, D. Heinegard, J. Engel, M. Paulsson, "The cartilage proteoglycan aggregate: assembly through combined protein-carbohydrate and protein-protein interactions," *Biophys. Chem.*, vol. 50, no. (1 – 2), pp. 113 – 128, 1994.

[30] S. Richard-Blum, "The collagen family," *Cold Spring Harb. Perspect. Biol.*, vol. 3, no. 1, pp. a004978, 2011.

[31] M.K. Gordon, R.A. Hahn, "Collagens," *Cell Tiss. Res.*, vol. 339, no. 1, pp. 247 – 257, 2010.

[32] H. Lodish, A. Berk, S.L. Zipursky, et al. Molecular Cell Biology. 4th edition. New York: W. H. Freeman; 2000. Section 22.3, Collagen: The Fibrous Proteins of the Matrix. Available at: https://www.ncbi.nlm.nih.gov/books/NBK21582/.

[33] D.H. Cortes, D.M. Elliot. "The Intervertebral Disc: Overview of Disc Mechanics," in *The Intervertebral Disc*, 1st ed. New York: Springer, 2014, ch. 2, sec. 2.1, pp. 17–32.

[34] L.T. Twomey, J.R. Taylor, "Age changes in lumbar vertebrae and intervertebral discs," *Clin. Orthop.*, no. 224, pp. 97 – 104, 1987.

[35] S. Roberts, J. Menage, J. Urban, "Biochemical and structural properties of the cartilage end-plate and its relation to the intervertebral disc," *Spine (Phila Pa 1976)*, vol. 14, no. 2, pp. 166 – 174, 1989.

[36] M. Cannella, A. Arthur, S. Allen, et al., "The role of the nucleus pulposus in neutral zone human lumbar intervertebral disc mechanics," *J. Biomech.*, vol. 41, no. 10, pp. 2104 – 2111, 2008.

[37] W.J. Virgin, "Experimental investigations into the physical properties of the intervertebral disc," *J. Bone Joint Surg. Br.*, vol. 33-B, no. 4, pp. 607 – 611, 1951.

[38] M. Horst, P. Brinckmann, "1980 Volvo award in biomechanics. Measurements of the distribution of axial stress on the end-plate of the vertebral body," *Spine (Phila Pa 1976)*, vol. 6, no. 3, pp. 217 – 232, 1981.

[39] J. Antoniou, N.M. Goudsouzian, T.F. Heathfield, et al., "The human lumbar endplate. Evidence of changes in biosynthesis and denaturation of the extracellular matrix with growth, maturation, aging, and degeneration," *Spine (Phila Pa 1976)*, vol. 21, no. 21, pp. 1153 – 1161, 1996.

[40] A. Maroudas, R.A. Stockwell, A. Nachemson, J. Urban, "Factors involved in the nutrition of the human lumbar intervertebral disc: cellularity and diffusion of glucose in vitro," *J. Anat.*, vol. 120, no. 1, pp. 113 – 130, 1975.

[41] J. Urban, S. Holm, A. Maroudas, A. Nachemson, "Nutrition of the intervertebral disk. An in vivo study of solute transport," *Clin. Orthop. Relat. Res.*, no. 129, pp. 101 – 114, 1977.

[42] A. Nachemson, T. Lewin, A. Maroudas, M.A. Freeman, "In vitro diffusion of dye through the end-plates and the annulus fibrosus of human lumbar intervertebral discs," *Acta Orthop. Scand.*, vol. 41, no. 6, pp. 589 – 607, 1970.

[43] S. Roberts, J. Urban, H. Evans, S.M. Eisenstein, "Transport properties of the human cartilage endplate in relation to its composition and calcification," *Spine (Phila Pa 1976)*, vol. 21, no. 4, pp. 415 – 420, 1996.

[44] W.E. Gower, V. Pedrini, "Age-Related Variations in Proteinpolysaccharides from Human Nucleus Pulposus, Annulus Fibrosus, and Costal Cartilage," *J. Bone Joint Surg.*, vol. 51, no. 6, pp. 1154 – 1162, 1969.

[45] M.K. Chelberg, G.M. Banks, D.F. Geiger, T.R. Oegema Jr., "Identification of heterogeneous cell populations in normal human intervertebral disc," *J. Anat.*, vol. 186, no. (Pt. 1), pp. 43 – 53, 1995.

[46] S. Roberts, J. Menage, V. Duance, et al., "1991 Volvo Award in basic sciences. Collagen types around the cells of the intervertebral disc and cartilage endplate: an immunolocalization study," *Spine*, vol. 16, no. 9, pp. 1030 – 1038, 1991.

[47] S.S. Sivan, B.V. El, Y. Merkher, et al., "Longevity of elastin in human intervertebral disc as probed by the racemization of aspartic acid," *Biochim. Biophys. Acta*, vol. 1820, no. 10, pp. 1671 – 1677, 2012.

[48] R. Sztrolovics, J. Grover, G. Cs-Szabo, et al., "The characterization of versican and its message in human articular cartilage and intervertebral disc," *J. Orthop. Res.* Vol. 20, no. 2, pp. 257 – 266, 2002.

[49] B. Johnstone, M. Markopoulos, P. Neame, B. Caterson, "Identification and characterization of glycanated and non-glycanated forms of biglycan and decorin in the human intervertebral disc," *Biochem. J.*, vol. 292 (Pt. 3), pp. 661 – 666, 1993.

[50] R.I. Inkinen, M.J. Lammi, S. Lehmonen, et al., "Relative increase of biglycan and decorin and altered chondroitin sulfate epitopes in the degenerating human intervertebral disc," *J. Rheumatol.*, vol. 25, no. 3, pp. 506 – 514, 1998.

[51] N. Ruel, D.Z. Markova, S.L. Adams, et al., "Fibronectin fragments and the cleaving enzyme ADAM-8 in the degenerative human intervertebral disc," *Spine (Phila Pa 1976)*, vol. 39, no. 16, pp. 1274 – 1279, 2014.

[52] J. Chen, L. Jing, C.L. Gilchrist, et al., "Expression of laminin isoforms, receptors, and binding proteins unique to nucleus pulposus cells of immature intervertebral disc," *Connect Tissue Res.*, vol. 50, no. 5, pp. 294 – 306, 2009.

[53] R. Sztrolovics, M. Alini, P.J. Roughley, J.S. Mort, "Aggrecan degradation in human intervertebral disc and articular cartilage," *Biochem. J.*, vol. 326 (Pt. 1), pp. 235 – 241, 1997.

[54] S.S. Sivan, E. Tsitron, E. Wachtel, et al., "Aggrecan Turnover in Human Intervertebral Disc as Determined by the Racemization of Aspartic Acid," *J. Biol. Chem.*, vol. 281, no. 19, pp. 13009 – 13014, 2006.

[55] E.M. Bartels, J.C. Fairbank, C.P. Winlove, J. Urban, "Oxygen and lactate concentrations measured in vivo in the intervertebral discs of patients with scoliosis and back pain," *Spine (Phila Pa 1976)*, vol. 23, no. 1, pp. 1- 7, 1996.

[56] J.J. Trout, J.A. Buckwalter, K.C. Moore, S.K. Landas, "Ultrastructure of the human intervertebral disc: I. Changes in notochordal cells with age," *Tissue and Cell*, vol. 14, no. 2, pp. 359 – 369, 1982.

[57] G. Meachim, M.S. Cornah, "Fine structure of juvenile human nucleus pulposus," *J. Anat.*, vol. 107, no. 2, pp. 337 – 350, 1970.

[58] F. Marchand, A.M. Ahmed, "Investigation of the laminate structure of the lumbar disc annulus fibrosus," *Spine*, vol. 15, pp. 402 – 410, 1990.

[59] S. Ebara, J.C. Iatridis, L.A. Setton, et al., "Tensile properties of nondegenerate human lumbar annulus fibrosus," *Spine*, vol. 21, no. 4, pp. 452 – 461, 1996.

[60] D. Skaggs, et al., "Regional variation in tensile properties and biochemical composition of the human lumbar annulus fibrosus," *Spine (Phila Pa 1976)*, vol. 19, no. 12, pp. 1310 – 1319, 1994.

[61] D.R. Eyre, H. Muir, "Quantitative analysis of types I and II collagens in human intervertebral discs at various ages," *Biochim. Biophys. Acta*, vol. 492, no. 1, pp. 29 – 42, 1977.

[62] C. Hirsch, F. Schajowicz, "Studies on structural changes in the lumbar annulus fibrosus," *Acta Orthopaedica Scandinavica*, vol. 22, pp. 184 – 231, 1952.

[63] K.L. Markolf, J.M. Morris, "The structural components of the intervertebral disc. A study of their contributions to the ability of the disc to withstand compressive forces," *J. Bone Joint Surg. Am.*, vol. 56, no. 4, pp. 675 – 687, 1974.

[64] B.A. Best, F. Guilak, L.A. Setton, et al., "Compressive mechanical properties of the human anulus fibrosus and their relationship to biochemical composition," *Spine (Phila Pa 1976)*, vol. 19, no. 2, pp. 212 – 221, 1994.

[65] P. Brinckmann, W. Frobin, E. Hierholzer, M. Horst, "Deformation of the vertebral end-plate under axial loading of the spine," *Spine*, vol. 8, pp. 851 – 856, 1983.

[66] A.D. Holmes, D.W. Hukins, A.J. Freemont, "End-plate displacement during compression of lumbar vertebra-disc-vertebra segments and the mechanism of failure," *Spine (Phila Pa 1976)*, vol. 18, no. 1, pp. 128 – 135, 1993.

[67] A. Tsantrizos, K. Ito, M. Aebi, T. Steffen, "Internal strains in healthy and degenerated lumbar intervertebral discs," *Spine (Phila Pa 1976)*, vol. 30, no. 19, pp. 2129 – 2137, 2005.

[68] C. Hirsch, A. Nachemson, "New observations on mechanical behavior of lumbar discs," *Acta Orthop. Scand.*, vol. 23, no. 4, pp. 254 – 283, 1954.

[69] A. Nachemson, "Measurement of intradiscal pressure," *Acta Orthop. Scand.*, vol. 28, no. 4, pp. 269 – 289, 1959.

[70] A. Nachemson, "The load on lumbar disks in different positions of the body," *Clin. Orthop. Relat. Res.*, vol. 45, pp. 107 – 122, 1966.

[71] A.L. Nachemson, "Disc pressure measurements," *Spine (Phila Pa 1976)*, vol. 6, no. 1, pp. 93 – 97, 1981.

[72] H.J. Wilke, P. Neef, M. Caimi, et al., "New in vivo measurements of pressures in the intervertebral disc in daily life," *Spine (Phila Pa 1976)*, vol. 24, no. 8, pp. 755 – 762, 1999.

[73] A.R. Tyrrell, T. Reilly, J.D. Troup, "Circadian variation in stature and the effects of spinal loading," *Spine (Phila Pa 1976)*, vol. 10, no. 2, pp. 161 – 164, 1985.

[74] D.S. McNally, M.A. Adams, "Internal intervertebral disc mechanics as revealed by stress profilometry," *Spine (Phila Pa 1976)*, vol. 17, no. 1, pp. 66 – 73, 1992.

[75] B. Johnstone, J. Urban, S. Roberts, J. Menage, "The fluid content of the human intervertebral disc. Comparison between fluid content and swelling pressure profiles of discs removed at surgery and those taken postmortem," *Spine (Phila Pa 1976)*, vol. 17, no. 4, pp. 412 – 416, 1992.

[76] J. Urban, J.F. McMullin, "Swelling pressure of the lumbar intervertebral discs: influence of age, spinal level, composition, and degeneration," *Spine (Phila Pa 1976)*, vol. 13, no. 2, pp. 179 – 187, 1988.

[77] J. Kraemer, D. Kolditz, R. Gowin, "Water and electrolyte content of human intervertebral discs under variable load," *Spine (Phila Pa 1976)*, vol. 10, no. 1, pp. 69 – 71, 1985.

[78] D.J. Botsford, S.I. Essess, D.J. Ogilvie-Harris, "In vivo diurnal variation in intervertebral disc volume and morphology," *Spine (Phila Pa 1976)*, vol. 19, no. 8, pp. 935 – 940, 1994.

[79] A.D. LeBlanc, H.J. Evans, V.S. Schneider, et al., "Changes in intervertebral disc cross-sectional area with bed rest and space flight," *Spine (Phila Pa 1976)*, vol. 19, no. 7, pp. 812 – 817, 1994.

[80] J.A. Miller, A.B. Schultz, D.N. Warwick, D.L. Spencer, "Mechanical properties of lumbar spine motion segments under large loads," *J. Biomech.*, vol. 19, no. 1, pp. 79 – 84, 1986.

[81] M.A. Adams, W.C. Hutton, J.R. Stott, "The resistance to flexion of the lumbar intervertebral joint," *Spine (Phila Pa 1976)*, vol. 5, no. 3, pp. 245 – 253, 1980.

[82] M.A. Adams, P. Dolan, W.C. Hutton, "Diurnal variations in the stresses on the lumbar spine," *Spine (Phila Pa 1976)*, vol. 12, no. 2, pp. 130 – 137, 1987.

[83] M.A. Adams, P. Dolan, "Time-dependent changes in the lumbar spine's resistance to bending," *Clin. Biomech. (Bristol, Avon)*, vol. 11, no. 4, pp. 194 – 200, 1996.

[84] J.J. Costi, I.A. Stokes, M. Gardner-Morse, et al., "Direct measurements of intervertebral disc maxmimum shear strain in sex degrees of freedom: motions that place disc tissue at risk of injury," *J. Biomech.*, vol. 40, no. 11, pp. 2457 – 2466, 2007.

[85] A.A. Espinoza Orias, N.M. Mammoser, J.J. Triano, et al., "Effects of axial torsion on disc height distribution: an in vivo study," *J. Manipulative Physiol. Ther.*, vol. 39, no. 4, pp. 294 – 303, 2016.

[86] H.F. Farfan, J.W. Cossette, G.H. Robertson, et al., "The effects of torsion on the lumbar intervertebral joints: the role of torsion in the production of disc degeneration," *J. Bone Joint Surg. Am.*, vol. 52, no. 3, pp. 468 – 497, 1970.

[87] M.A. Adams, W.C. Hutton, "The relevance of torsion to the mechanical derangement of the lumbar spine," *Spine (Phila Pa 1976)*, vol. 6, no. 3, pp. 241 – 248, 1981.

[88] J.L. Kelsey, P.B. Githens, A.A. White 3rd, et al., "An epidemiologic study of lifting and twisting on the job and risk for acute prolapsed intervertebral disc," *J. Orthop. Res.*, vol. 2, no. 1, pp. 61 – 66, 1984.

[89] D.M. Skrzypiec, K. Nagel, K. Sellenschloh, et al., "Failure of the human lu mbar motion-segments resulting from anterior shear fatigue loading," *Ind. Health*, vol. 54, no. 4, pp. 308 – 314, 2016.

[90] D.K. Sengupta, J.S. Fischgrund, "Lumbar Stenosis," in Spine, Philadelphia: Lippincott Williams & Wilkins, 2004, ch. 16, pp. 132 – 141.

[91] J.M. Beiner et al., "Lumbar Spondylolisthesis," in Spine, Philadelphia: Lippincott Williams & Wilkins, 2004, ch. 18, pp. 146 – 155.

[92] D.B. Allan, G. Waddell, "An historical perspective on low back pain and disability," *Acta Orthop. Scand. Suppl.*, vol. 234, pp. 1 – 23, 1989.

[93] J. Urban, S. Roberts, "Degeneration of the intervertebral disc," *Arthritis Res. Ther.*, vol. 5, no. 3, pp. 120 – 130, 2003.

[94] P.J. Roughley, "Biology of intervertebral disc aging and degeneration: involvement of the extracellular matrix," *Spine*, vol. 29, no. 23, pp. 2691 – 2699, 2004.

[95] J.A. Buckwalter, "Aging and degeneration of the human intervertebral disc," *Spine (Phila Pa 1976)*, vol. 20, no. 11, pp. 1307 – 1314, 1995.

[96] P.A. Vergroesen, I. Kingma, K.S. Emanuel, et al., "Mechanics and biology in intervertebral disc degeneration: a vicious circle," *Osteoarthritis Cartilage*, vol. 23, pp. 1057 – 1070, 2015.

[97] J. Urban, S. Roberts, "Degeneration of the intervertebral disc," *Arthritis Res. Ther.*, vol. 5, no. 3, pp. 120 – 130, 2003.

[98] M.A. Adams, "Biomechanics of back pain," *Acupunct. Med.*, vol. 22, no. 4, pp. 178 – 188, 2004.

[99] G. Lyons, S.M. Eisenstein, M.B. Sweet, "Biochemical changes in intervertebral disc degeneration," *Biochim. Biophys. Acta*, vol. 673, no. 4, pp. 443 – 453, 1981.

[100] W. Frobin, P. Brinckmann, M. Kramer, E. Hartwig, "Height of lumbar discs measured from radiographs compared with degeneration and height classified from MR images," *Eur. Radiol.*, vol. 11, no. 2, pp. 263 – 269, 2001.

[101] S. Holm, A. Maroudas, J. Urban, et al., "Nutrition of the intervertebral disc: solute transport and metabolism," *Connect. Tissue Res.*, vol. 8, no. 2, pp. 101 – 119, 1981.

[102] S-M Kokkonen, M. Kurunlahti, O. Tervonen, et al., "Endplate degeneration observed on magnetic resonance imaging of the lumbar spine: Correlation with pain provocation and disc changes observed on computed tomography diskography," *Spine*, vol. 27, no. 20, pp. 2274 – 2278, 2002.

[103] D. Weishaupt, M. Zanetti, J. Hodler, et al., "Painful lumbar disc derangement: relevance of endplate abnormalities at MR imaging," *Radiology*, vol. 218, no. 2, pp. 420 – 427, 2001.

[104] S. Roberts, J. Menage, M. Eisenstein, "The cartilage end-plate and intervertebral disc in scoliosis: calcification and other sequelae," *J. Orthop. Res.*, vol. 11, no. 5, pp. 747 – 757, 1993.

[105] M.T. Modic, M.A. Weinstein, W. Pavlicek, et al., "Magnetic resonance of intervertebral-disk disease," *Magn. Reson. Med.*, vol. 1, no. 2, pp. 207 – 208, 1984.

[106] H.T. Gilbert, N. Hodson, P. Baird, et al., "Acidic pH promotes intervertebral disc degeneration: Acid-sensing ion channel -3 as a potential therapeutic target," *Sci. Rep.*, vol. 6, pp. 37360, 2016.

[107] H.A. Horner, J. Urban, "2001 Volvo Award Winner in Basic Science Studies: Effect of nutrient supply on the viability of cells from the nucleus pulposus of the intervertebral disc," *Spine (Phila Pa 1976)*, vol. 26, no. 23, pp. 2543 – 2549, 2001.

[108] H. Ishihara, J. Urban, "Effects of low oxygen concentrations and metabolic inhibitors on proteoglycan and protein synthesis rates in the intervertebral disc," *J. Orthop. Res.*, vol. 17, no. 6, pp. 829 – 835, 1999.

[109] H. Ohshima, J. Urban, "The effect of lactate and pH on proteoglycan and protein synthesis rates in the intervertebral disc," *Spine (Phila Pa 1976)*, vol. 17, no. 9, pp. 1079 – 1082, 1992.

[110] J.E. Scott, T.R. Bosworth, A.M. Cribb, J.R. Taylor, "The chemical morphology of age-related changes in human intervertebral disc glycosaminoglycans from cervical, thoracic, and lumbar nucleus pulposus," *Journal of Anatomy*, vol. 184, pp. 73 – 82, 1994.

[111] J. Antoniou, T. Steffen, F. Nelson, et al., "The human lumbar intervertebral disc: evidence for changes in the biosynthesis and denaturation of the extracellular matrix with growth, maturation, ageing, and degeneration," *J. Clin. Invest.*, vol. 98, no. 4, pp. 996 – 1003, 1996.

[112] A.P. Hollander, T.F. Heathfield, J.J. Liu, et al., "Enhanced denaturation of the alpha (II) chains of type-II collagen in normal adult human intervertebral discs compared with femoral articular cartilage," *J. Orthop. Res.*, vol. 4, no. 1, pp. 61 – 66, 1996.

[113] M.A. Adams, D.S. McNally, P. Dolan, "'Stress' distributions inside intervertebral discs. The effects of age and degeneration," *J. Bone Joint Surg. Br.*, vol. 78, no. 6, pp. 965 – 972, 1996.

[114] G.D. O'Connell, E.J. Vresilovic, D.M. Elliot, "Human Intervertebral Disc Internal Strain in Compression: The Effect of Disc Region, Loading Position, and Degeneration." *J. Orthop. Res.*, vol. 29, no. 4, pp. 547 – 555, 2011.

[115] D.S. McNally, I.M. Shackleford, A.E. Goodship, R.C. Mulholland, "In vivo stress measurement can predict on discography," *Spine (Phila Pa 1976)*, vol. 21, no. 22, pp. 2580 – 2587, 1996.

[116] R. Dittmar, M.M. van Rijsbergen, K. Ito, "Moderately Degenerated Human Intervertebral Disks Exhibit a Less Geometrically Specific Collagen Fiber Orientation Distribution," *Global Spine J.*, vol. 6, no. 5, pp. 439 – 446, 2016.

[117] D. Brickley-Parsons, M.J. Glimcher, "Is the chemistry of collagen in intervertebral discs an expression of Wolff's Law? A study of the human lumbar spine," *Spine (Phila Pa 1976)*, vol. 9, no. 2, pp. 148 – 163, 1984.

[118] V.C. Duance, J.K. Crean, T.J. Sims, et al., "Changes in collagen cross-linking in degenerative disc disease and scoliosis," *Spine (Phila Pa 1976)*, vol. 23, no. 23, pp. 2545 – 2551, 1998.

[119] Y. Fujita, N.A. Duncan, J.C. Lotz, "Radial tensile properties of the lumbar annulus fibrosus are site and degeneration dependent," *Journal of Orthopaedic Research*, vol. 15, pp. 814-819, 1997.

[120] Z. Shan, S. Li, J. Liu, et al., "Correlation between biomechanical properties of the annulus fibrosus and magnetic resonance imaging (MRI) findings," *Eur. Spine J.*, vol. 24, no. 9, pp. 1909 – 1916, 2015.

[121] H.A. Guerin, D.M. Elliot, "Degeneration affects the fiber reorientation of human annulus fibrosus under tensile load," *J. Biomech.*, vol. 39, no. 8, pp. 1410 – 1418, 2006.

[122] M.A. Adams, P.J. Roughley, "What is intervertebral disc degeneration, and what causes it?" *Spine (Phila Pa 1976)*, vol. 31, no. 18, pp. 2151 – 2161, 2006.

[123] Y. Kakitsubata, D.J. Theodorou, S.J Theodorou, et al., "Magnetic resonance discography in cadavers: tears of the annulus fibrosus," *Clinc. Orthop. Relat. Res.*, no. 407, pp. 228 – 240, 2003.

[124] O.L. Osti, B. Vernon-Roberts, R. Moore, R.D. Fraser, "Annular tears and disc degeneration in the lumbar spine. A post-mortem study of 135 discs," *J. Bone Joint Surg. Br.*, vol. 74, no. 5, pp. 678 – 682, 1992.

[125] M. Haefeli, F. Kalberer, D. Saegesser, et al., "The course of macroscopic degeneration in the human lumbar intervertebral disc," *Spine (Phila Pa 1976)*, vol. 31, no. 14, pp. 1522 – 1531, 2006.

[126] W.J. Wang, X.H. Yu, C. Wang, et al., "MMPs and ADAMTSs in intervertebral disc degeneration," *Clin. Chim. Acta*, vol. 448, pp. 238 – 246, 2015.

[127] S. Ozkanli, T. Kaner, M. Efendioglu, et al., "The relation of matrix metalloproteinase 1, 2, 3 expressions with clinical and radiological findings in primary and recurrent lumbar disc herniations," *Turk. Neurosurg.*, vol. 25, no. 1, pp. 111 – 116, 2015.

[128] R. Basaran, M. Senol, S. Ozkanli, et al., "Correlation of matrix metalloproteinase (MMP)-1, -2, -3, and -9 expressions with demographic and radiological features in primary lumbar intervertebral disc disease," *J. Clin. Neurosci.*, vol. 41, pp. 46 – 49, 2017.

[129] J.L. Lauer-Fields, D. Juska, G.B. Fields, "Matrix metalloproteinases and collagen catabolism," *Biopolymers*, vol. 66, no. 1, pp. 19 – 32, 2002.

[130] A.J. Pockert, S.M. Richardson, C.L. Le Maitre, et al., "Modified expression of the ADAMTS enzymes and tissue inhibitor of metalloproteinases 3 during human intervertebral disc degeneration," *Arthritis Rheum.*, vol. 60, no. 2, pp. 482 – 491, 2009.

[131] Q. Zhang, M. Huang, X. Wang, et al., "Negative effects of ADAMTS-7 and ADAMTS-12 on endplate cartilage differentiation," *J. Orthop. Res.*, vol. 30, no. 8, pp. 1238 – 1243, 2012.

[132] C.Q. Zhao, Y.H. Zhang, S.D. Jiang, et al., "ADAMTS-5 and intervertebral disc degeneration: the results of tissue immunohistochemistry and in vitro cell culture. *J. Orthop. Res.*, vol. 29, no. 5, pp. 718 – 725, 2011.

[133] K.P. Patel, J.D. Sandy, K. Akeda, et al., "Aggrecanases and aggrecanase-generated fragments in the human intervertebral disc at early and advanced stages of disc degeneration," *Spine (Phila Pa 1976)*, vol. 32, no. 23, pp. 2596 – 2603, 2007.

[134] S. Chen, Y. Huang, Z.J. Zhou, et al., "Upregulation of tumor necrosis factor α and ADAMTS-5, but not ADAMTS-4, in human intervertebral cartilage endplate with modic changes," *Spine (Phila Pa 1976)*, vol. 39, no. 14, pp. E817 – E825, 2014.

[135] S.S. Sivan, E. Wachtel, P. Roughley, "Structure, function, aging and turnover of aggrecan in the intervertebral disc," *Biochim. Biophys. Acta*, vol. 1840, no. 10, pp. 3181 – 3189, 2014.

[136] Z.I. Johnson, Z.R. Schoepflin, H. Choi, et al., "Disc in flames: Roles of TNF-α and IL-1β in intervertebral disc degeneration," *Eur. Cell Mater.*, vol. 30, pp. 104 – 117, 2015.

[137] K.A. Williams, J. Petronis, D. Smith, et al., "Effect of Iyengar yoga therapy for chronic low back pain," *Pain*, vol. 115, no. (1 – 2), pp. 107 – 117, 2005.

[138] P. Tekur, C. Singphow, H.R. Nagendra, N. Raghuram, "Effect of short-term intensive yoga program on pain, functional disability and spinal flexibility in chronic low back pain: a randomized control study," *J. Altern. Complement. Med.*, vol. 14, no. 6, pp. 637 – 644, 2008.

[139] C. Woodyard, "Exploring the therapeutic effects of yoga and its ability to increase quality of life," *Int. J. Yoga*, vol. 4, no. 2, pp. 49 – 54, 2011.

[140] N. Hartfiel, G. Clarke, J. Havenhand, et al., "Cost-effectiveness of yoga for managing musculoskeletal conditions in the workplace," *Occup. Med.*, vol. 67, no. 9, pp. 687 – 695, 2017.

[141] C.M. Jeng, T.C. Cheng, C.H. Kung, H.C. Hsu, "Yoga and disc degenerative disease in cervical and lumbar spine: an MR imaging-based case control study," *Eur. Spine J.*, vol. 20, no. 3, pp. 408 – 413, 2011.

[142] M. Ariyoshi, K. Sonoda, K. Nagata, et al., "Efficacy of aquatic exercises for patients with low-back pain," *Kurume. Med. J.*, vol. 46, no. 2, pp. 91 – 96, 1999.

[143] G. Han, M. Cho, G. Nam, et al., "The effects on muscle strength and visual analog scale pain on aquatic therapy for individuals with low back pain," *J. Phys. Ther. Sci.*, vol. 23, pp. 57 – 60, 2011.

[144] P.A. Baena-Beato, E.G. Artero, M. Arroyo-Morales, et al., "Aquatic therapy improves pain, disability, quality of life, body composition and fitness in sedentary adults with chronic low back pain. A controlled clinical trial," *Clin. Rehabil.*, vol. 24, no. 4, pp. 350 – 360, 2014.

[145] Y.S. Kim, J. Park, J.K. Shim, "Effects of aquatic backward locomotion exercise and progressive resistance exercise on lumbar extension strength in patients who have undergone lumbar discectomy," *Arch. Phys. Med. Rehabil.*, vol. 91, no. 2, pp. 208 – 214, 2010.

[146] M.D. Kane, R.D. Karl, J.H. Swain, "Effects of gravity-facilitated traction on intervertebral dimensions of the lumbar spine," *J. Orthop. Sports Phys. Ther.*, vol. 6, no. 5, pp. 281 – 288, 1985.

[147] H. Vernon, J. Meschino, J. Naiman, "Inversion therapy: a study of physiological effects," *J. Can. Chiropr. Assoc.*, vol. 29, no. 3, pp. 135 – 140, 1985.

[148] G. Gianakopoulos, G.W. Waylonis, P.A. Grant, et al., "Inversion devices: their role in producing lumbar distraction," *Acrh. Phys. Med. Rehabil.*, vol. 66, no. 2, pp. 100 – 102, 1985.

[149] N. Karimi, P. Akbarov, L. Rahnama, "Effects of segmental traction therapy on lumbar disc herniation in patients with acute low back pain measured by magnetic resonance imaging: a single arm clinical trial," *J. Back Musculoskelet. Rehabil.*, vol. 30, no. 2, pp. 247 – 253, 2017.

[150] K.S. Prasad, B.A. Gregson, G. Hargreaves, et al., "Inversion therapy in patients with pure single level lumbar discogenic disease: a pilot randomized trial," *Disabil. Rehabil.*, vol. 34, no. 17, pp. 1473 – 1480, 2012.

[151] R.L. Jones, "Functions of prostaglandins," *Pathobiol. Annu.*, vol. 2, pp. 359 – 380, 1972.

[152] C.J. Hawkey, "COX-1 and COX-2 inhibitors," *Best Pract. Res. Clin. Gastroenterol.*, vol. 15, no. 5, pp. 801 – 820, 2001.

[153] T.L. Coats, D.G. Borenstein, N.K. Nangia, M.T. Brown, "Effects of valdecoxib in the treatment of chronic low back pain: results of a randomized, placebo-controlled trial," *Clin. Ther.*, vol. 26, no. 8, pp. 1249 – 1260, 2004.

[154] C.A. Birbara, A.D. Puopolo, D.R. Munoz, et al., "Etoricoxib Protocol 042 Study Group. Treatment of chronic lower back pain with etoricoxib, a new cyclooxygenase-2 selective inhibitor: improvement in pain and disability – a randomized, placebo-controlled, 3-month trial," *J. Pain*, vol. 4, no. 6, pp. 307 – 315, 2003.

[155] A. Allegrini, L. Nuzzo, D. Pavone, et al., "Efficacy and safety of piroxicam patch versus piroxicam cream in patients with lumbar osteoarthritis. A randomized, placebo-controlled study," *Arzneimittelforschung*, vol. 59, no. 8, pp. 403 – 409, 2009.

[156] E. Bernstein, T.S. Carey, J.M. Garrett, "The use of muscle relaxant medications in acute low back pain," *Spine (Phila Pa 1976)*, vol. 29, no. 12, pp. 1346 – 1351, 2004.

[157] D.C. Cherkin, K.J. Wheeler, W. Barlow, R.A. Deyo, "Medication use for low back pain in primary care," *Spine (Phila Pa 1976)*, vol. 23, no. 5, pp. 607 – 614, 1998.

[158] L.A. DiMarco, B.C. Ramger, G.P. Howell, et al., "Differences in characteristics and downstream drug use among opioid native and prior opioid users with low back pain," *Pain Pract.*, 2018, [Epub ahead of print].

[159] A. Shmagel, L. Ngo, K. Ensrud, R. Foley, "Prescription medication use among community-based U.S. adults with chronic low back pain: a cross-sectional population based study," *J. Pain*, vol. 19, no. 10, pp. 1104 – 1112, 2018.

[160] M.M. Wertli, J. Steurer, "Pain medications for acute and chronic low back pain," *Internist (Berl)*, vol. 59, no. 11, pp. 1214 – 1223, 2018.

[161] H.T. Benzon, "Epidural steroid injections for low back pain and lumbosacral radiculopathy," *Pain*, vol. 24, no. 3, pp. 277 – 295, 1996.

[162] A.H. White, R. Derby, G. Wynne, "Epidural injections for the diagnosis and treatment of low-back pain," *Spine (Phila Pa 1976)*, vol. 5, no. 1, pp. 78 – 86, 1980.

[163] S.K. Rosenberg, A. Grabinsky, C. Kooser, M.V. Boswell, "Effectiveness of transforaminal epidural steroid injections in lower back pain: a one year experience," *Pain Physician*, vol. 5, no. 3, pp. 266 – 270, 2002.

[164] F.E. Sayegh, E.I. Kenanidis, K.A. Papavasiliou, et al., "Efficacy of steroid and nonsteroid caudal epidural injections for low back pain and sciatica: a prospective, randomized, double-blind clinical trial," *Spine (Phila Pa 1976)*, vol. 34, no. 14, pp. 1441 – 1447, 2009.

[165] D.J. Kennedy, P.Z. Zheng, M. Smuck, et al., "A minimum of 5-year follow-up after lumbar transforaminal epidural steroid injections in patients with lumbar radicular pain due to intervertebral disc herniation," *Spine J.*, vol. 18, no. 1, pp. 29 – 35, 2018.

[166] V.B. Vad, A.L. Bhat, G.E. Lutz, F. Cammisa, "Transforaminal epidural steroid injections in lumbosacral radiculopathy: a prospective randomized study," *Spine (Phila Pa 1976)*, vol. 27, no. 1, pp. 11 – 16, 2002.

[167] S. Fukui, N. Iwashita, K. Nitta, et al., “The Results of Percutaneous Intradiscal High-Pressure Injection of Saline in Patients with Extruded Lumbar Herniated Disc: Comparison with Microendoscopic Discectomy,” *Pain Medicine*, vol. 13, pp. 762 – 768, 2012.

[168] A. Blamoutier, “Surgical discectomy for lumbar disc herniation: surgical techniques,” *Orthop. Traumatol. Surg. Res.*, vol. 99, no. 1 Suppl., pp. S187 – 196, 2013.

[169] J.G. Love, “Protruded intervertebral disc (fibrocartilage): section of orthopaedics and section of neurology,” *Proc. R. Soc. Med.*, vol. 32, no. 12, pp. 1697 – 1721, 1939.

[170] W. Caspar, “A new surgical procedure for lumbar disc herniation causing less tissue damage through a microsurgical approach,” *Adv. Neurosurg.*, vol. 4, pp. 74 – 77, 1977.

[171] R.W. Williams, “Microlumbar discectomy: a conservative surgical approach to the virgin herniated lumbar disc,” *Spine (Phila Pa 1976)*, vol. 3, no. 2, pp. 175 – 182, 1978.

[172] P. Kambin, S. Sampson, “Posterolateral percutaneous suction-excision of herniated lumbar intervertebral discs. Report of interim results,” *Clinc. Orthop. Relat. Res.*, no. 207, pp. 37 – 43, 1986.

[173] K. Foley, M. Smith, “Microendoscopic discectomy,” *Oper. Tech. Neurosurg.*, vol. 3, pp. 301 – 307, 1997.

[174] J. He et al., “Microendoscopic discectomy versus open discectomy for lumbar disc herniation: a meta-analysis,” *Eur. Spine J.*, vol. 25, no. 5, pp. 1373 – 1381, 2016.

[175] W. Ruan et al., “Comparison of percutaneous endoscopic lumbar discectomy versus open lumbar microdiscectomy for lumbar disc herniation: a meta-analysis,” *Int. J. Surg.*, vol. 31, pp. 86 – 92, 2016.

[176] B. Zhang et al., “Transforaminal endoscopic discectomy versus conventional microdiscectomy for lumbar disc herniation: a systematic review and meta-analysis,” *J. Orthop. Surg. Res.*, vol. 13, no. 1, pp. 169, 2018.

[177] M.R. Rasouli et al., “Minimally invasive discectomy versus microdiscectomy/open discectomy for symptomatic lumbar disc herniation,” *Cochrane Database Syst. Rev.*, no. 9, pp. CD010328, 2014.

[178] H. Davis, "Increasing rates of cervical and lumbar spine surgery in the United States, 1979-1990,” *Spine (Phila Pa 1976)*, vol. 19, no. 10, pp. 1117 – 1124, 1994.

[179] J.N. Weinstein et al., "United States' trends and regional variations in lumbar spine surgery: 1992 – 2003," *Spine (Phila Pa 1976)*, vol. 31, no. 23, pp. 2707 – 2714, 2006.

[180] V.K. Goel et al., "Kinematics of the whole lumbar spine. Effect of discectomy," *Spine (Phila Pa 1976)*, vol. 10, no. 6, pp. 543 – 554, 1985.

[181] M. Shea et al., "A comparison of the effects of automated percutaneous discectomy and conventional discectomy on intradiscal pressure, disc geometry and stiffness," *J. Spinal Disord.*, vol. 7, no. 4, pp. 317 – 325, 1994.

[182] S. Tibrewal, M.J. Pearcy, I. Portek, J. Spivey, "A prospective study of lumbar spinal movements before and after discectomy using biplanar radiography. Correlation of clinical and radiographic findings," *Spine*, vol. 10. Pp. 455 – 459, 1985.

[183] P. Fransen, "Prevention of scar tissue formation in spinal surgery: state of the art and review of the literature," *J. Neurosurg. Sci.*, vol. 55, no. 3, pp. 277 – 281, 2011.

[184] G.F. Findlay et al., "A 10-year follow-up of the outcomes of lumbar microdiscectomy," *Spine (Phila Pa 1976)*, vol. 23, no. 10, pp. 1168 – 1171, 1998.

[185] P. Gaston, R.W. Marshall, "Survival analysis is a better estimate of recurrent disc herniation," *J. Bone Joint Surg. Br.*, vol. 85, no. 4, pp 535 – 537, 2003.

[186] S.S. Virk et al., "What is the rate of revision discectomies after primary discectomy on a national scale?" *Clin. Orthop. Relat. Res.*, vol. 475, no. 11, pp. 2752 – 2762, 2017.

[187] H. Castillo et al., "Lumbar discectomy is associated with higher rates of lumbar fusion," *Spine J.*, vol. 19, no. 3, pp. 487 – 492, 2019.

[188] R.B. Cloward, "The treatment of ruptured lumbar intervertebral discs by vertebral body fusion. I. Indications, operative technique, after care," *J. Neurosurg.*, vol. 10, no. 2, pp. 154 – 168, 1953.

[189] R.J. Mobbs et al., "Lumbar interbody fusion: techniques, indications and comparison of interbody fusion options including PLIF, TLIF, MI-TLIF, OLIF/ATP, LLIF, and ALIF," *J. Spine Surg.*, vol. 1, no. 1, pp. 2 – 18, 2015.

[190] H.S. Sandhu, H.S. Grewal, H. Parvataneni, "Bone grafting for spinal fusion," *Orthop. Clin. North Amer.*, vol. 30, no. 4, pp. 685 – 698, 1999.

[191] A. Oryan et al., "Bone regenerative medicine: classic options, novel strategies, and future directions," *J. Orthop. Surg. Res.*, vol. 9, no. 1, pp. 18, 2014.

[192] A.M. Jakoi, J.A. Iorio, P.J. Cahill, "Autologous bone graft harvesting: a review of grafts and surgical techniques," *Musculoskelet. Surg.*, vol. 99, no. 3, pp. 171 – 180, 2015.

[193] W. Wang, K.W.K. Yeung, "Bone grafts and biomaterials substitutes for bone defect repair: A review," *Bioact. Mater.*, vol. 2, no. 4, pp. 224 – 247, 2017.

[194] R.J. Hacker, "Comparison of interbody fusion approaches for disabling low back pain," *Spine (Phila Pa 1976)*, vol. 22, no. 6, pp. 660 – 665, 1997.

[195] J.S. Kim et al., "Which lumbar interbody fusion technique is better in terms of level for the treatment of unstable isthmic spondylolisthesis?" *J Neurosurg. Spine*, vol. 12, no. 2, pp. 171 – 177, 2010.

[196] P.C. Hseih et al., "Anterior lumbar interbody fusion in comparison with transforaminal lumbar interbody fusion: implications for the restoration of foraminal height, local disc height, local disc angle, lumbar lordosis, and sagittal balance," *J. Neurosurg. Spine*, vol. 7, pp. 379 – 386, 2007.

[197] S.C. Humphreys et al., "Comparison of posterior and transforaminal approaches to interbody fusion," *Spine (Phila Pa 1976)*, vol. 26, no. 5, pp. 567 – 571, 2001.

[198] J. Park, "Comparison between posterior and transforaminal approaches for lumbar interbody fusion," *J. Korean Neurosurg. Soc.*, vol. 37, pp. 340 – 344, 2005.

[199] Z. Audat, "Comparison of clinical and radiological results of posterolateral fusion, posterior lumbar interbody fusion and transforaminal lumbar interbody fusion techniques in the treatment of degenerative lumbar spine," *Singapore Med. J.*, vol. 53, no. 3, pp. 183 – 187, 2012.

[200] N. Sakeb, K. Ahsan, "Comparison of the early results of transforaminal lumbar interbody fusion and posterior lumbar interbody fusion in symptomatic lumbar instability," *Indian J. Orthop.*, vol. 47, no. 3, pp. 255 – 263, 2013.

[201] S.N. Salzmann, J. Shue, A.P. Hughes, "Lateral lumbar interbody fusion-outcomes and complications," *Curr. Rev. Musculoskelet. Med.*, vol. 10, no. 4, pp. 539 – 546, 2017.

[202] J.N. Sembrano et al., "Radiographic comparison of lateral lumbar interbody fusion versus traditional fusion approaches: analysis of sagittal contour change," *Int. J. Spine Surg.*, vol. 9, pp. 16, 2015.

[203] J.X. Li, K. Phan, and R. Mobbs, "Oblique lumbar interbody fusion: technical aspects, operative outcomes, and complications," *World Neurosurg.*, vol. 98, pp. 113 – 123, 2017.

[204] C.S. Lee, C.J. Hwang, S.W. Lee, et al., "Risk factors for adjacent segment disease after lumbar fusion," *Eur. Spine J.*, vol. 18, no. 11, pp. 1637 – 1643, 2009.

[205] Y. Heo, J.H. Park, H.Y. Seong, et al., "Symptomatic adjacent segment degeneration at the L3-4 level after fusion surgery at the L4-5 level: evaluation of the risk factors and 10-year incidence," *Eur. Spine J.*, vol. 24, no. 11, pp. 2474 – 2480, 2015.

[206] S.F. Suh, Y.H. Jo, H.W. Jeong, et al., "Outcomes of Revision Surgery Following Instrumented Posterolateral Fusion in Degenerative Lumber Spinal Stenosis: A Comparative Analysis between Pseudarthrosis and Adjacent Segment Disease," *Asian Spine J.*, vol. 11, no. 3, pp. 464 – 471, 2017.

[207] F. Stief, A. Meurer, J. Wienand, et al., "Has a Mono- or Bisegmental Lumber Spinal Fusion Surgery an Influence on Self-Assessed Quality of Life, Trunk Rage of Motion, and Gait Performance?" *Spine (Phila Pa 1976)*, vol. 40, no. 11, pp. E618 – E626, 2015.

[208] H. Wang, T. Wang, Q. Wang, W. Ding, "Incidence and risk factors of persistent low back pain following posterior decompression and instrumented fusion for lumbar disk herniation," *J. Pain Res.*, vol. 10, pp. 1019 – 1025, 2017.

[209] J. Bai, W. Zhang, X. Zhang, et al., "A Clinical Investigation of Contralateral Neurological Symptom after Transforaminal Lumbar Interbody Fusion (TLIF)," *Med. Sci. Monit.*, vol. 21, pp. 1831 – 1838, 2015.

[210] W.J. Elias et al., "Complications of posterior lumbar interbody fusion when using a titanium threaded cage device," *J. Neurosurg.*, vol. 93, no. 1 Suppl., pp. 45 – 52, 1993.

[211] A. Çakmak et al. "Colon perforation caused by migration of a bone graft Following a posterior lumbosacral interbody fusion operation," *Spine*, vol. 35, no. 3, pp. E84 – E85, 2010.

[212] B. Garg, A. Singla, S. Batra, S. Kumar, "Early migration of bone graft causing sigmoid colon perforation after trans-foraminal lumbar interbody fusion," *J. Clin. Orthop. Trauma*, vol. 8, no. 2, pp. 165 – 167, 2017.

[213] Y. Tokuahashi, Y. Ajiro, N. Umeazawa, "Subsidence of metal interbody cage after posterior lumbar interbody fusion with pedicle screw fixation," *Orthopedics*, vol. 32, no. 4, 2009.

[214] D. Abi-Hanna et al., "Lumbar disk arthroplasty for degenerative disk disease: literature review," *World Neurosurg.*, vol. 109, pp. 188 – 196, 2018.

[215] H.D. Link, "History, design and biomechanics of the LINK SB Charité artificial disc," *Eur. Spine J.*, vol. 11, no. Suppl. 2, pp. S98 – S105, 2002.

[216] F.H. Geisler, "The Charité Artificial Disc: design history, FDA IDE study results, and surgical technique," *Clin. Neurosurg.*, vol. 53, pp. 223 – 228, 2006.

[217] S.L. Griffith, A.P. Shelokov, K. Büttner-Janz, et al., "A multicenter retrospective study of the clinical results of the LINK SB Charité intervertebral prosthesis. The initial European experience," *Spine (Phila Pa 1976)*, vol. 19, no. 16, pp. 1842 – 1849, 1994.

[218] G. Cinotti, T. David, F. Postacchini, "Results of disc prosthesis after a minimum follow-up period of 2 years," *Spine (Phila Pa 1976)*, vol. 21, no. 8, pp. 995 – 1000, 1996.

[219] J.P. Lemaire, H. Carrier, el-H. Sariali, et al., "Clinical and radiological outcomes with the Charité artificial disc: a 10-year minimum follow-up," *J. Spinal Disord. Tech.*, vol. 18, no. 4, pp. 353 – 359, 2005.

[220] T. David, "Long-term results of one-level lumbar arthroplasty: minimum q0-year follow-up of the Charité artificial disc in 106 patients," *Spine (Phila Pa 1976)*, vol. 32, no. 6, pp. 661 – 666, 2007.

[221] M. Putzier, J.F. Funk, S.V. Schneider, et al., "Charité total disc replacement – clinical and radiographical results after an average follow-up of 17 years," *Eur. Spine J.*, vol. 15, no. 2, pp. 183 – 195, 2006.

[222] R.D. Guyer, P.C. McAfee, R.J. Banco, et al., "Prospective, randomized, multicenter Food and Drug Administration investigational device exemption study of lumbar total disc replacement with the Charité artificial disc versus lumbar fusion: five-year follow-up," *Spine J.*, vol. 9, no. 5, pp. 374 – 386, 2009.

[223] S. Lu, S. Sun, C. Kong, et al., "Long-term clinical results following Charité III lumbar total disc replacement," *Spine J.*, vol. 18, no. 6, pp. 917 – 925, 2018.

[224] M.N. Scott-Young, M.J. Lee, D.E.A. Nielsen, et al., "Clinical and radiological mid-term outcomes of lumbar single-level total disc replacement, *Spine (Phila Pa 1976)*, vol. 43, no. 2, pp. 105 – 113, 2018.

[225] T. Marnay, "Lumbar disc replacement: 7 to 11-year results with Prodisc," *Spine J.*, vol. 2, no. 5, pp. 94, 2002.

[226] P. Tropiano, R.C. Huang, F.P. Girardi, et al., "Lumbar total disc replacement. Seven to eleven-year follow-up," *J. Bone Joint Surg. Am.*, vol. 87, no. 3, pp. 490 – 496, 2005.

[227] R.C. Huang, F.P. Giraradi, F.P. Cammisa Jr., et al., "The implications of constraint in lumbar total disc replacement," *J. Spinal Disord. Tech.*, vol. 16, no. 4, pp. 412 – 417, 2003.

[228] R.B. Delamarter, D.M. Fribourg, L.E. Kanim, et al., "ProDisc artificial total lumbar disc replacement: introduction and early results from the United States clinical trial," *Spine (Phila Pa 1976)*, vol. 28, no. 20, pp. S167 – S175, 2003.

[229] J. Zigler, "Lumbar spine arthroplasty using the ProDisc II," *Spine J.*, vol. 4, no. 6 Suppl., pp. 260S – 267S, 2004.

[230] J. Zigler, R. Delamarter, J.M. Spivak, et al., "Results of the prospective, randomized, multicenter Food and Drug Administration investigational device exemption study of the ProDisc-L total disc replacement versus circumferential fusion for the treatment of 1-level degenerative disc disease," *Spine (Phila Pa 1976)*, vol. 32, no. 11, pp 1155 – 1162, 2007.

[231] J.E. Zigler, R.B. Delamarter, "Five-year results of the prospective, randomized, multicenter Food and Drive Administration investigational device exemption study of the ProDisc-L total disc replacement versus circumferential arthrodesis for the treatment of single-level degenerative disc disease," *J. Neurosurg. Spine*, vol. 17, no. 6, pp. 493 – 501, 2012.

[232] R. Delamarter, J. Zigler, R.A. Balderston, et al., "Prospective, randomized, multicenter Food and Drug Administration investigational device exemption study of the ProDisc-L total disc replacement compared with circumferential arthrodesis for the treatment of two-level lumbar degenerative disc disease: results at twenty-four months," *J. Bone Joint Surg. Am.*, vol. 93, no. 8, pp. 705 – 715, 2011.

[233] J.R. Balderston, Z.M. Gertz, T. McIntosh, et al., "Long-term outcomes of 2-level total disc replacement using ProDisc-L: nine- to 10-year follow-up," *Spine (Phila Pa 1976)*, vol. 39, no. 11, pp. 906 – 910, 2014.

[234] A. Rasouli, J.M. Cuellar, L. Kanim, et al., "Multiple-level lumbar total disk replacement: a prospective clinical and radiographic analysis of motion preservation at 24 – 72 months," *Clin. Spine Surg.*, vol. 32, no. 1, pp. 38 – 42, 2019.

[235] C.J. Siepe, F. Heider, K. Wiechert, et al., "Mid- to long-term results of total lumbar disc replacement: a prospective analysis with 5- to 10-year follow-up," *Spine J.*, vol. 14, no. 8, pp. 1417 – 1431, 2014.

[236] S. Trincat, G. Edgard-Rosa, G. Geneste, et al., "Two-level lumbar total disc replacement: functional outcomes and segmental motion after 4 years," *Orthop. Traumatol. Surg. Res.*, vol. 101, no. 1, pp. 17 – 21, 2015.

[237] J.J. Yue, R. Garcia Jr., L.E. Miller, "The activL® Artificial Disc: a next-generation motion-preserving implant for chronic lumbar discogenic pain," *Med. Devices (Auckl.)*, vol. 9, pp. 75 – 84, 2016.

[238] R. Garcia, J.J. Yue, S. Blumenthal et al., "Lumbar total disc replacement for discogenic low back pain: two-year outcomes of the activL multicenter randomized controlled IDE clinical trial," *Spine (Phila Pa 1976)*, vol. 40, no. 24, pp. 1873 – 1881, 2015.

[239] J.S. Hans, V.K. Goel, J.Y. Ahn, et al., "Loads in the spinal structures during lifting: development of a three-dimensional comprehensive biomechanical model," *Eur. Spine J.*, vol. 4, no. 3, pp. 153 – 168, 1995.

[240] A. Nachemson, "The load on lumbar disks in different positions of the body," *Clin. Orthop. Relat. Res.*, vol. 45, pp. 107 – 122, 1966.

[241] M.M. Panjabi, A.A. White 3rd, "Basic biomechanics of the spine," *Neurosurgery*, vol. 7, no. 1, pp. 76 – 93, 1980.

[242] M.A. Adams, P. Dolan, W.C. Hutton, et al., "Diurnal changes in spinal mechanic and their clinical significance," *J. Bone Joint Surg. Br.*, vol. 72, no. 2, pp. 266 – 270, 1990.

[243] A. Di Martino et al., "Nucleus pulposus replacement: basic science and indications for clinical use," *Spine (Phila Pa 1976)*, vol. 30, no. 16 Suppl., pp. S16 – S22, 2005.

[244] M.L. Goins et al., "Nucleus pulposus replacement: an emerging technology," *Spine J.*, vol. 5, no. 6 Suppl., pp. 317S – 324S, 2005.

[245] R. Bertagnoli, A. Karg, S. Voigt, "Lumbar partial disc replacement," *Orthop. Clin. North Am.*, vol. 36, no. 3, pp. 341 – 347, 2005.

[246] D. Coric, P.V. Mummaneni, "Nucleus replacement technologies: Invited submission from the Joint Section Meeting on Disorders of the Spine and Peripheral Nerves, March 2007," *J. Neurosurg. Spine*, vol. 8, pp. 115 – 120, 2008.

[247] G. Lewis, "Nucleus pulposus replacement and regeneration/repair technologies: present status and future prospects," *J. Biomed. Mater. Res. B Appl. Biomater.*, vol. 100, no. 6, pp. 1702 – 1720, 2012.

[248] N.R. Ordway et al., “Biomechanical assessment and fatigue characteristics of an articulating nucleus implant,” *Int. J. Spine Surg.*, vol. 7, pp. e109 – e117, 2013.

[249] N.J. Hallab, Q.B. Bao, T. Brown, “Assessment of epidural versus intradiscal biocompatibility of PEEK implant debris: an in vivo rabbit model,” *Eur. Spine J.*, vol. 22, no. 12, pp. 2740 – 2751, 2013.

[250] Q.B. Bao et al., “Nubac disc arthroplasty: preclinical studies and preliminary safety and efficacy evaluations,” *SAS J.*, vol. 1, no. 1, pp. 36 – 45, 2007.

[251] M. Balsano et al., “Nucleus disc arthroplasty with the NUBAC ™ device: 2-year clinical experience,” *Eur. Spine J.*, vol. 20 Suppl. 1, pp. S36 – S40, 2011.

[252] P.M. Klara, C.D. Ray, “Artificial nucleus replacement: clinical experience,” *Spine (Phila Pa 1976)*, vol. 27, no. 12, pp. 1374 – 1377, 2002.

[253] C.D. Ray, “The PDN® prosthetic disc-nucleus device,” *Eur. Spine J.*, vol. 11, pp. S137 – S142, 2002.

[254] R. Bertagnoli, E. Schonmayr, “Surgical and clinical results with the PDN® prosthetic disc-nucleus device,” *European Spine Journal*, vol. 11, pp. S143 – S148, 2002.

[255] P. Eysel et al., “Biomechanical behaviour of a prosthetic lumbar nucleus,” *Acta. Neurochir. (Wien)*, vol. 141, no. 10, pp. 1083 – 1087, 1999.

[256] R. Schönmayr et al., “Prosthetic Disc Nucleus Implants: The Wiesbaden Feasibility Study: 2 Years Follow-up in Ten Patients,” vol. 12, no. 1 Suppl., *Riv. Neuroradiol.*, pp. 163 – 170, 1999.

[257] N.R. Ordway et al., “Failure properties of the intervertebral disc with a hydrogel nucleus,” *Trans. Orthop. Res. Soc.*, vol. 23, pp. 685, 1998.

[258] M.J. Allen et al., “Preclinical evaluation of a poly (vinyl alcohol) hydrogel implant as a replacement for the nucleus pulposus,” *Spine (Phila Pa 1976)*, vol. 29, no. 5, pp. 515 – 523, 2004.

[259] A. Korge et al., “A spiral implant as nucleus prosthesis in the lumbar spine,” *Eur. Spine J.*, vol. 11, pp. S149 – S153, 2002.

[260] J.L. Husson et al., “A memory coiling spiral as nucleus pulposus prosthesis: concept, specifications, bench testing, and first clinical results,” *J. Spinal Disord. Tech.*, vol. 16, no. 4, pp. 405 – 411, 2003.

[261] R. Bertagnoli et al., "Mechanical testing of a novel hydrogel nucleus replacement implant," *Spine J.*, vol. 5, no. 6, pp. 672 – 681, 2005.

[262] A. Tsantrizos et al., "Mechanical and biomechanical characterization of a polyurethane nucleus replacement device injected and cured in situ within a balloon," *SAS J.*, vol. 2, no. 1, pp. 28 – 39, 2008.

[263] S.H. Kitchell, J. Cappello, "Injectable biomaterials for augmentation of the nucleus pulposus," *Eur. Spine J.*, vol. 12, no. Suppl. 1, pp. S65 – S66, 2003.

[264] L.M. Boyd, A.J. Carter, "Injectable biomaterials and vertebral endplate treatment for repair and regeneration of the intervertebral disc," *Eur. Spine J.*, vol. 15 Suppl. 3, pp. S414 – S421, 2006.

[265] U. Berlemann, O. Schwarzenbach, "An injectable nucleus replacement as an adjunct to microdiscectomy: 2 year follow-up in a pilot clinical study," *Eur. Spine J.*, vol. 18, no. 11, pp. 1706 – 1712, 2009.

[266] R. Langer, J.P. Vacanti, "Tissue engineering," *Science*, vol. 260, no. 5110, pp. 920 – 926, 1993.

[267] H.S. An, E.J. Thonar, K. Masuda, "Biological repair of the intervertebral disc," *Spine (Phila Pa 1976)*, vol. 28, no. 15 Suppl., pp. S86 – S92, 2003.

[268] D.M. O'Halloran, A.S. Pandit, "Tissue-engineering approach to regenerating the intervertebral disc," *Tissue Eng.*, vol. 13, no. 8, pp. 1927 – 1954, 2007.

[269] M. Alini, S.M. Eisenstein, K. Ito, et al., "Are animal models useful for studying human disc disorders/degeneration?" *Eur. Spine J.*, vol. 17, no. 1, pp. 2 – 19, 2008.

[270] K. Masuda, H.S. An, "Growth factors and the intervertebral disc," *Spine J.*, vol. 4, no. 6 Suppl., 2004; 4 (6 Suppl): 330S – 340S.

[271] N. Tsumaki, K. Tanaka, E. Arikawa-Hirasawa, et al., "Role of CDMP-1 in skeletal morphogenesis: promotion of mesenchymal cell recruitment and chondrocyte differentiation," *J. Cell Bio.*, vol. 144, no. 1, pp. 161 – 173, 1999.

[272] S.H. Ahn, Y.W. Cho, M.W. Ahn, et al., "mRNA expression of cytokines and chemokines in herniated lumbar intervertebral discs," *Spine (Phila Pa 1976)*, vol. 27, no. 9, pp. 911 – 917, 2002.

[273] J.G. Burke, R.W. Watson, D. Conhyea, et al., "Human nucleus pulposis can respond to a pro-inflammatory stimulus," *Spine (Phila Pa 1976)*, vol. 28, no. 24, pp. 2685 – 2693, 2003.

[274] J.D. Kang, H.I. Georgeescu, L. McIntyre-Larkin, et al., "Herniated lumbar intervertebral discs spontaneously produce matrix metalloproteinases, nitric oxide, interleukin-6, and prostaglandin E2," *Spine (Phila Pa 1976)*, vol. 21, no. 3, pp. 271 – 277, 1996.

[275] C. Weiler, A.G. Nerlich, B.E. Bachmeier, N. Boos, "Expression and distribution of tumor necrosis factor alpha in human lumbar intervertebral discs: a study in surgical specimen and autopsy controls," *Spine (Phila Pa 1976)*, vol. 30, no. 1, pp. 44 – 53, 2005.

[276] C.A. Séguin, R.M. Pilliar, P.J. Roughley, R.A. Kandel, "Tumor necrosis factor-alpha modulates matrix production and catabolism in nucleus pulposus tissue," *Spine (Phila Pa 1976)*, vol. 30, no. 17, pp. 1940 – 1948, 2005.

[277] C.L. Le Maitre, A.J. Freemont, J.A. Hoyland, "The role of interleukin-1 in the pathogenesis of human intervertebral disc degeneration," *Arthritis. Res. Ther.*, vol. 7, no. 4, pp. R732 – R745, 2005.

[278] C.L. Le Maitre, A.J. Freemont, J.A. Hoyland, "Localization of degradation enzymes and their inhibitors in the degenerate human intervertebral disc," *J. Pathol.*, vol. 204, no. 1, pp. 47 – 54, 2004.

[279] S. Roberts, B. Caterson, J. Menage, et al., "Matrix metalloproteinases and aggrecanase: their role in disorders of the human intervertebral disc," *Spine (Phila Pa 1976)*, vol. 25, no. 23, pp. 3005 – 3013, 2000.

[280] R. Sztrolovics, M. Alini, P.J. Roughley, J.S. Mort, "Aggrecan degradation in human intervertebral disc and articular cartilage," *Biochem. J.*, vol. 326, no. Pt. 1, pp. 235 – 241, 1997.

[281] H.E. Gruber, E.C. Fisher Jr., B. Desai, et al., "Human intervertebral disc cells from the annulus: three-dimensional culture in agarose or alginate and responsiveness to TGF-β1," *Exp. Cell Res.*, vol. 235, no. 1, pp. 13 – 21, 1997.

[282] H.E. Gruber, Y. Chow, G.L Hoelscher, et al., "Micromass culture of human annulus cells: morphology and extracellular matrix production," *Spine*, vol. 35, no. 10, pp. 1033 – 1038, 2010.

[283] R.D. Abbott, D. Purmessur, R.D. Monsey, J.C. Iatridis, "Regenerative Potential of TGFβ3 + Dex and Notochordal Cell Conditioned Media on Degenerated Human Intervertebral Disc Cells," *J. Orthop. Res.*, vol. 30, no. 3, pp. 482 – 488, 2012.

[284] K. Haberstroh, A. Enz, M.L. Zenclussen, et al., "Human intervertebral disc-derived cells are recruited by human serum and form nucleus pulposus-like tissue upon stimulation with TGF-β3 or hyaluronan in vitro," *Tissue Cell*, vol. 41, no. 6, pp. 414 – 420, 2009.

[285] A.A. Hegewald, J. Cluzel, J.P. Krüger, et al., "Effects of initial boost with TGF-β1 and grade of intervertebral disc degeneration on 3D culture of human annulus fibrosus cells," *J. Orthop. Surg. Res.*, vol. 9, pp. 73, 2014.

[286] D.J. Kim, S.H. Moon, H. Kim, et al., "Bone morphogenetic protein-2 facilitates expression of chondrogenic, not osteogenic, phenotype of human intervertebral disc cells," *Spine (Phila Pa 1976)*, vol. 28, no. 24, pp. 2679 – 2684, 2003.

[287] H. Kim, J.U. Lee, S.H. Moon, et al., "Zonal responsiveness of the human intervertebral disc to bone morphogenic protein-2," *Spine (Phila Pa 1976)*, vol. 34, no. 17, pp. 1834 – 1838, 2009.

[288] L. Gilbertson, S.H. Ahn, P.N. Teng, et al., "The effects of recombinant human bone morphogenetic protein-2, recombinant human bone morphogenetic protein-12, and adenoviral bone morphogenetic protein-12 on matrix synthesis in human annulus fibrosus and nucleus pulposus cells," *Spine J.*, vol. 8, no. 3, pp. 449 – 456, 2008.

[289] F.C. Bach, A. Miranda-Bedate, F.W.M. van Heel, et al., "Bone Morphogenetic Protein-2, But Not Mesenchymal Stromal Cells, Exert Regenerative Effects on Canine and Human Nucleus Pulposus Cells," *Tissue Engineering (Part A)*, vol. 23, no. 5 nd 6, pp. 233 – 242, 2017.

[290] A. Wei, H. Brisby, S.A. Chung, A.D. Diwan, "Bone morphogenetic protein-7 protects human intervertebral disc cells in vitro from apoptosis," *Spine J.*, vol. 8, no. 3, pp. 466 – 474, 2008.

[291] Z. Wang, W.C. Hutton, S.T. Yoon, "Bone morphogenetic protein-7 antagonizes tumor necrosis factor-α-induced activation of nuclear factor κB and upregulation of the ADAMTS, leading to decreased degradation of disc matrix macromolecules aggrecan and collagen II," *Spine J.*, vol. 14, no. 3, pp. 505 – 512, 2014.

[292] B.G.M. van Dijk, E. Potier, M. van Dijk, et al., "Osteogenic protein 1 does not stimulate a regenerative effect in cultured human degenerated nucleus pulposus tissue," *J. Tissue Eng. Regen. Med.*, vol. 11, no. 7, pp. 2127 – 2135, 2017.

[293] J.C. Kennon et al., "Current insights on use of growth factors as therapy for intervertebral disc degeneration," *Biomol. Concepts*, vol. 9, no. 1, pp. 43 – 52, 2018.

[294] K.Y. Huang et al., "The in vivo biological effects of intradiscal recombinant human bone morphogenetic protein-2 on the injured intervertebral disc: an animal experiment," *Spine (Phila Pa 1976)*, vol. 32, no. 11, pp. 1174 – 1180, 2007.

[295] H. Inoue et al., "The effect of bone morphogenetic protein-2 injection at different time points on intervertebral disk degeneration in a rat tail model," *J. Spinal Disord. Tech.*, vol. 28, no. 1, pp. E35 – E44, 2015.

[296] M. Kawakami et al., "Osteogenic protein-1 (osteogenic protein-1/morphogenetic protein-7) inhibits degeneration and pain-related behavior induced by chronically compressed nucleus pulposus in the rat," *Spine (Phila Pa 1976)*, vol. 30, no. 17, pp. 1933 – 1939, 2005.

[297] H.S. An et al., "Intradiscal administration of osteogenic protein-1 increases intervertebral disc height and proteoglycan content in the nucleus pulposus in normal adolescent rabbits," *Spine (Phila Pa 1976)*, vol. 30, no. 1, pp. 25 – 31, 2005.

[298] K. Masuda et al., "Osteogenic protein-1 injection into a degenerated disc induces the restoration of disc height and structural changes in the rabbit anular puncture model," *Spine (Phila Pa 1976)*, vol. 31, no. 7, pp. 742 – 754, 2006.

[299] Y. Imai et al., "Restoration of disc height loss by recombinant human osteogenic protein-1 injection into intervertebral discs undergoing degeneration induced by an intradiscal injection of chondroitinase ABC," *Spine (Phila Pa 1976)*, vol. 32, no. 11, pp. 1197 – 1205, 2007.

[300] A.J. Walsh et al., "In vivo growth factor treatment of degenerated intervertebral discs," *Spine (Phila Pa 1976)*, vol. 29, no. 2, pp. 156 – 163, 2004.

[301] T. Chujo et al., "Effects of growth differentiation factor-5 on the intervertebral disc—in vitro bovine study and in vivo rabbit disc degeneration model study," *Spine (Phila Pa 1976)*, vol. 31, no. 25, pp. 2909 – 2917, 2006.

[302] US National Library of Medicine – Clinical Trials.gov, Available at: https://clinicaltrials.gov/ct2/show/NCT01158924. [Accessed 2017].

[303] US National Library of Medicine – Clinical Trials.gov, Available at: https://clinicaltrials.gov/ct2/show/NCT00813813. [Accessed 2017].

[304] US National Library of Medicine – Clinical Trials.gov, Available at: https://clinicaltrials.gov/ct2/show/NCT01182337. [Accessed 2017].

[305] US National Library of Medicine – Clinical Trials.gov, Available at: https://clinicaltrials.gov/ct2/show/NCT01124006. [Accessed 2017].

[306] F.L. Acosta Jr., J. Lotz, C.P. Ames, "The potential role of mesenchymal stem cell therapy for intervertebral disc degeneration: a critical overview," *Neurosurg. Focus*, vol. 19, no. 3, pp. E4, 2005.

[307] Melton DA, Cowen C. Stemness: definitions, criteria, and standards. In: Lanza R, Gearhart J, Hogan B, Melton D, Pedersen R, Thomas ED, Thomson I, Wilmut I, editors. Essentials of stem cell biology. 2nd ed. San Diego, CA: Academic Press: 2009.

[308] J.A. Ankrum, J.F. Ong, J.M. Karp, "Mesenchymal stem cells: immune evasive, not immune privileged," *Nat. Biotechnol.*, vol. 32, no. 3, pp. 252 – 260, 2014.

[309] D.G. Phinney, "Functional heterogeneity of mesenchymal stem cells: implications for cell therapy," *J. Cell Bioche.*, vol. 113, no. 9, pp. 2806 – 2812, 2012.

[310] U. Lakshmipathy, C. Verfaillie, "Stem cell plasticity," *Blood Rev*., vol. 19, no. 1, pp. 29 – 38, 2005.

[311] A.J. Friedenstein, Piatetzky-Shapiro II, K.V. Petrakova, "Osteogenesis in transplants of bone marrow cells," *J. Embryol. Exp. Morphol.*, vol. 16, no. 3, pp. 381 – 390, 1966.

[312] D.J. Prockop, "Marrow stromal cells as stem cells for nonhematopoietic tissues," *Science*, vol. 276, no. 5309, pp. 71 – 74, 1997.

[313] M.F. Pittenger, A.M. Mackay, S.C. Beck, et al., "Multilineage potential of adult human mesenchymal stem cells," *Science*, vol. 284, no. 5411, pp. 143 – 147, 1999.

[314] P. Hernigou, A. Desroches, S. Queinnec, et al., "Morbidity of graft harvesting versus bone marrow aspiration in cell regenerative therapy," *Int. Orthop.*, vol. 38., no. 9, pp. 1855 – 1860, 2014.

[315] R. Tuli, S. Tuli, S. Nandi, et al., "Characterization of multipotential mesenchymal progenitor cells derived from human trabecular bone," *Stem Cells*, vol. 21, no. 6, pp. 681 – 693, 2003.

[316] A.M. Osyczka, U. Nöth, K.G. Danielson, R.S. Tuan, "Different osteochondral potential of clonal cell lines derived from adult human trabecular bone," *Ann. N. Y. Acad. Sci.*, vol. 961, pp. 73 – 77, 2002.

[317] H.E. Young, M.L. Mancini, R.P. Wright, et al., "Mesenchymal stem cells reside within the connective tissues of many organs," *Dev. Dyn.*, vol. 202, no. 2, pp. 137 – 144, 1995.

[318] P. Bosch, D.S. Musgrave, J.Y. Lee, et al., "Osteoprogenitor cells within skeletal muscle," *J. Orthop. Res.*, vol. 18, no. 6, pp. 933 – 944, 2000.

[319] J.T. Williams, S.S. Southerland, J. Souza, et al., "Cells isolated from adult human skeletal muscle capable of differentiating into multiple mesodermal phenotypes," *Am. Surg.*, vol. 65, no. 1, pp. 22 – 26, 1999.

[320] P.A. Zuk, M. Zhu, P. Ashjian, et al., "Human adipose tissue is a source of multipotent stem cells," *Mol. Biol. Cell*, vol. 13, no. 12, pp. 4279 – 4295, 2002.

[321] G.R. Erickson, J.M. Gimble, D.M. Franklin, et al., "Chondrogenic potential of adipose tissue-derived stromal cells in vitro and in vivo," *Biochem. Biophys. Res. Commun.*, vol. 290, no. 2, pp. 763 – 769, 2002.

[322] S. Alsalameh, R. Amin, T. Gemba, M. Lotz, "Identification of mesenchymal progenitor cells in normal and osteoarthritic human articular cartilage," *Arthritis Rheum.*, vol. 50, no. 5, pp. 1522 – 1532, 2004.

[323] G.P. Dowthwaite, J.C. Bishop, S.N. Redman, et al., "The surface of articular cartilage contains a progenitor cell population," *J. Cell Sci.*, vol. 117, no. Pt 6, pp. 889 – 897, 2004.

[324] T. Tallheden, J.E. Dennis, D.P. Lennon, et al., "Phenotypic plasticity of human articular chondrocytes," *J. Bone Joint Surg. Am.*, vol. 85 – A Suppl 2, pp. 93 – 100, 2003.

[325] J.G. Toma, M. Akhavan, K.J. Fernandes, et al., "Isolation of multipotent adult stem cells from the dermis of mammalian skin," *Nat. Cell Biol.*, vol. 3, no. 9, pp. 778 – 784, 2001.

[326] S. Kern, H. Eichler, J. Stoeve, et al., "Comparative analysis of mesenchymal stem cells from bone marrow, umbilical cord blood, or adipose tissue," *Stem Cells*, vol. 24, no. 5, pp. 1294 – 1301, 2006.

[327] Y. Sakaguchi, J. Sekiya, K. Yagishita, T. Muneta, "Comparison of human stem cells derived from various mesenchymal tissues: Superiority of synovium as a cell source," *Arthritis Rheum.*, vol. 52, no. 8, pp. 2521 – 2529, 2005.

[328] R. Quarto, D. Thomas, C.T. Liang, "Bone progenitor cell deficits and the age-associated decline in bone repair capacity," *Calcif. Tissue. Int.*, vol. 56, no. 2, pp. 123 – 129, 1995.

[329] J.P. Rodríguez, S. Garat, H. Gajardo, et al., "Abnormal osteogenesis in osteoporotic patients is reflected by altered mesenchymal stem cells dynamics," *J. Cell. Biochem.*, vol. 75, no. 3, pp. 414 – 423, 1999.

[330] J.M. Murphy, K. Dixon, S. Beck, et al., "Reduced chondrogenic and adipogenic activity of mesenchymal stem cells from patients with advanced osteoarthritis," *Arthritis Rheum*., vol. 46, no. 3, pp. 704 – 713, 2002.

[331] P.A. Zuk, M. Zhu, H. Mizuno, et al., "Multilineage cells from human adipose tissue: implications for cell-based therapies," *Tissue Eng*., vol. 7, no. 2, pp. 211 – 228, 2001.

[332] J.M. Gimble, A.J. Katz, B.A. Bunnell, "Adipose-derived stem cells for regenerative medicine," *Circ. Res.*, vol. 100, no. 9, pp. 1249 – 1260, 2007.

[333] M. Tobita, H. Orbay, H. Mizuno, "Adipose-derived stem cells: current findings and future perspectives," *Disco. Med.*, vol. 11, no. 57, pp. 160 – 170, 2011.

[334] B.G. Jeon, B.M. Kumar, E.J. Kang, et al., "Characterization and comparison of telomere length, telomerase and reverse transcriptase activity and gene expression in human mesenchymal stem cells and cancer cells of various origins," *Cell Tissue Res*., vol. 345, no. 1, pp. 149 – 161, 2011.

[335] B. Puissant, C. Barreau, P. Bourin, et al., "Immunomodulatory effect of human adipose tissue-derived adult stem cells: comparison with bone marrow mesenchymal stem cells," *Br. J. Haematol*., vol. 129, no. 1, pp. 118 – 129, 2005.

[336] A.C. Boquest, A. Shahdadfar, J.E. Brinchmann, P. Collas, "Isolation of stromal cells from human adipose tissue," *Methods Mol. Biol*., vol. 325, pp. 35 – 46, 2006.

[337] B.M. Strem, K.C. Hicok, M. Zhu, et al., "Multipotential differentiation of adipose tissue-derived stem cells," *Keio. J. Med.*, vol. 54, no. 3, pp. 132 – 141, 2005.

[338] C.A. Brayfield, K.G. Marra, J.P. Rubin, "Adipose tissue regeneration," *Curr. Stem Cell Res. Ther.*, vol. 5, no. 2, pp. 116 – 121, 2010.

[339] M. Cherubino, K.G. Marra, "Adipose-derived stem cells for soft tissue reconstruction," *Regen. Med.*, vol. 4, no. 1, pp. 109 – 117, 2009.

[340] J.P. Rubin, K.G. Marra, "Soft tissue reconstruction," *Method Mol. Biol*., vol. 702, pp. 395 – 400, 2011.

[341] J.L. Dragoo, B. Samimi, M. Zhu, et al., "Tissue-engineered cartilage and bone using stem cells from human infrapatellar fat pads," *J. Bone Joint Surg. Br.*, vol. 85, no. 5, pp. 740 – 747, 2003.

[342] B.T. Estes, B.O. Diekman, J.M. Gimble, F. Guilak, “Isolation of adipose-derived stem cells and their induction to a chondrogenic phenotype,” *Nat. Protoc.*, vol. 5, no. 7, pp. 1294 – 1311, 2010.

[343] B.T. Estes, F. Guilak, “Three-dimensional culture systems to induce chondrogenesis of adipose-derived stem cells,” *Methods Mol. Biol.*, vol. 702, pp. 201 – 217, 2011.

[344] W.C. Lee, J.L. Sepulveda, J.P. Rubin, K.G. Marra, “Cardiomyogenic differentiation potential of human adipose precursor cells,” *Int. J. Cardiol.*, vol. 133, no. 3, pp. 399 – 401, 2009.

[345] V. Planat-Benard, C. Menard, M. André, et al., “Spontaneous cardiomyocyte differentiation from adipose tissue stroma cells,” *Circ. Res.*, vol. 94, no. 2, pp. 223 – 229, 2004.

[346] J. Rehman, D. Traktuev, J. Li, et al., “Secretion of angiogenic and antiapoptotic factors by human adipose stromal cells,” *Circulation*, vol. 109, no. 10, pp. 1292 – 1298, 2004.

[347] M. Cherubino, J.P. Rubin, N. Miljkovic, et al., “Adipose-derived stem cells for wound healing applications,” *Ann. Plast. Surg.*, vol. 66, no. 2, pp. 210 – 215, 2011.

[348] K.M. Safford, S.D Safford, J.M. Gimble, et al., “Characterization of neuronal/glial differentiation of murine adipose-derived adult stromal cells,” *Exp. Neurol.*, vol. 187, no. 2, pp. 319 – 328, 2004.

[349] S. Strassburg, S.M. Richardson, A.J. Freemont, J.A. Hoyland, “Co-culture of mesenchymal stem cell differentiation and modulation of the degenerate human nucleus pulposus cell phenotype,” *Regen. Med.*, vol. 5, no. 5, pp. 701 – 711, 2010.

[350] S.M. Naqvi, C.T. Buckley, “Differential response of encapsulated nucleus pulposus and bone marrow stem cells in isolation and coculture in alginate and chitosan hydrogels,” *Tissue Eng. Part A*, vol. 21, no. (1 – 2), pp. 288 – 299, 2015.

[351] T. Watanabe, D. Sakai, Y. Yamamoto, et al., “Human nucleus pulposus cells significantly enhanced biological properties in a coculture system with direct cell-to-cell contact with autologous mesenchymal stem cells,” *J. Orthop. Res.*, vol. 28, no. 5, pp. 623 – 630, 2010.

[352] Y. Xu, X.J. Zhang, L. Fang, T.B. Zhao, «Co-culture of annulus fibrosus cells and bone marrow mesenchymal stem cells,” *Genet. Mol. Res.*, vol. 14, no. 2, pp. 3932 – 3938, 2015.

[353] E.K. Shim, J.S. Lee, D.E. Kim, et al., "Autogenous mesenchymal stem cells from the vertebral body enhance intervertebral disc regeneration via paracrine interaction: an in vitro pilot study," *Cell Transplant.*, vol. 25, no. 10, pp. 1819 – 1832, 2016.

[354] S.M. Richardson, R.V. Walker, S. Parker, et al., "Intervertebral disc cell-mediated mesenchymal stem cell differentiation," *Stem Cells*, vol. 24, no. 3, pp. 707 – 716, 2006.

[355] Z.F. Lu, B. Zandieh Doulabi, P.I. Wuisman, et al., "Differentiation of adipose stem cells by nucleus pulposus cells: configuration effect," *Biochem. Biophys. Res. Commun.*, vol. 359, no. 4, pp. 991 – 996, 2007.

[356] Z.F. Lu, B.Z. Doulabi, P.I. Wuisman, et al., "Influence of collagen type II and nucleus pulposus cells on aggregation and differentiation of adipose tissue-derived stem cells," *J. Cell. Mol. Med.*, vol. 12, no. 6B, pp. 2812 – 2822, 2008.

[357] Y. Zhou, X. Hu, X. Zheng, et al., "Differentiation potential of mesenchymal stem cells derived from adipose tissue vs bone marrow toward annulus fibrosus cells in vitro," *Curr. Stem Cell Res. Ther.*, vol. 12, no. 5, pp. 432 – 439, 2017.

[358] H. Tapp, R. Deepe, J.A. Ingram, et al., "Adipose-derived mesenchymal stem cells from the sand rat: transforming growth factor beta and 3D co-culture with human disc cells stimulate proteoglycan and collagen type I rich extracellular matrix," *Arthritis Res. Ther.*, vol. 10, no. 4, pp. R89, 2008.

[359] G. Feng, X. Zhao, H. Liu, et al., "Transplantation of mesenchymal stem cells and nucleus pulposus cells in a degenerative disc model in rabbits: a comparison of 2 cell types as potential candidates for disc regeneration," *Journal of Neurosurgery: Spine*, vol. 14, pp. 322 – 329, 2011.

[360] F. Cai, X. Wu, X. Xie, et al., "Evaluation of intervertebral disc regeneration with implantation of bone marrow mesenchymal stem cells (BMSCs) using quantitative T2 mapping: a study in rabbits," *International Orthopaedics*, vol. 39, pp. 149 – 159, 2015.

[361] A. Wei, H. Tao, S.A. Chung, et al., "The Fate of Transplanted Xenogeneic Bone Marrow-Derived Stem Cells in Rat Intervertebral Discs," *Journal of Orthopaedic Research*, vol. 27, pp. 373 – 379, 2009.

[362] J.H. Jeong, J.H. Lee, E.S. Jin, et al., "Regeneration of intervertebral discs in a rat disc degeneration model by implanted adipose-tissue-derived stromal cells," *Acta Neurochirugica*, vol. 152, pp. 1771 – 1777, 2010.

[363] S. Sobajima, G. Vadala, A. Shimer, et al., "Feasibility of a stem cell therapy for intervertebral disc regeneration," *The Spine Journal*, vol. 8, pp. 888 – 896, 2008.

[364] G. Ho, Y.L. Leung, and K.M.C. Cheung, "Effect of Severity of Intervertebral Disc Injury on Mesenchymal Stem Cell-Based Regeneration," *Connective Tissue Research*, vol. 49, pp. 15 – 21, 2008.

[365] G. Vadala, G. Sowa, M. Huben, et al., "Mesenchymal stem cells injection in degenerated intervertebral disc: cell leakage may induce osteophyte formation," *Journal of Tissue Engineering and Regenerative Medicine,* vol. 6, pp. 348 – 355, 2011.

[366] G. Marfia, R. Campanella, S.E. Navone, et al., "Potential use of human adipose mesenchymal stromal cells for intervertebral disc regeneration: a preliminary study on biglycan-deficient murine model of chronic disc degeneration," *Arthritis Research and Therapy*, vol. 16, pp. 1 – 13, 2014.

[367] S.M.W. Haufe, A.R. Mork, "Intradiscal Injection of Hematopoietic Stem Cells in an Attempt to Rejuvenate the Intervertebral Discs," *Stem Cells and Development*, vol. 15, pp. 136 – 137, 2006.

[368] L. Orozco, R. Soler, C. Morera, et al., "Intervertebral disc repair by autologous mesenchymal bone marrow cells: a pilot study," *Transplantation*, vol. 92, no. 7, pp. 822 – 828, 2011.

[369] K.A. Pettine, M.B. Murphy, R.K. Suzuki, T.T. Sand, "Percutaneous Injection of Autologous Bone Marrow Concentrate Cells Significantly Reduces Lumbar Discogenic Pain Through 12 Months," *Stem Cells*, vol. 33, pp. 146 – 156, 2014.

[370] J. Mochida, D. Sakai, Y. Nakamura, T. Watanabe, Y. Yamamoto, S. Kato, "Intervertebral Disc Repair with Activated Nucleus Pulposus Cell Transplantation: A Three-Year, Prospective Clinical Study on Its Safety," *European Cells and Materials*, vol. 29, pp. 202 – 212, 2015.

[371] C. Elabd, C.J. Centeno, J.R. Schultz, et al., "Intra-discal injection of autologous, hypoxic cultured bone marrow-derived mesenchymal stem cells in five patients with chronic lower back pain: a long-term safety and feasibility study," *Journal of Translational Medicine*, vol. 14, pp. 1 – 9, 2016.

[372] G. Crevensten, A.J.L Walsh, D. Ananthakeishnan, P. Page, G.M. Wahba, J.C. Lotz, S. Berven, "Intervertebral Disc Cell Therapy for Regeneration: Mesenchymal Stem Cell Implantation in Rat Intervertebral Discs," *Annals of Biomedical Engineering*, vol. 32, pp. 430 – 434, 2004.

[373] P.A. Revell, E. Damien, L. Di Silvio, et al., "Tissue engineering intervertebral disc repair in the pig using injectable polymers," *Journal of Materials Science: Materials in Medicine*, vol. 18, pp. 303 – 308, 2007.

[374] T. Ganey, W.C. Hutton, T. Moseley, et al., "Intervertebral disc repair using adipose tissue-derived stem and regenerative cells: experiments in a canine model," *Spine (Phila Pa 1976)*, vol. 34, pp. 2297 – 2304, 2009.

[375] P. Ghosh, et al., "Immunoselected STRO-3+ mesenchymal precursor cells and restoration of the extracellular matrix of degenerate intervertebral discs," *J. Neurosurg. Spine*, vol. 16, pp. 479 – 488, 2012.

[376] H.J. Chun, et al., "Transplantation of human adipose-derived stem cells in a rabbit model of traumatic degeneration of lumbar discs," *World Neurosurg.*, vol. 78, pp. 364 – 371, 2012.

[377] S. Reitmaier, L. Kreja, K. Gruchenberg, et al., "In vivo biofunctional evaluation of hydrogels for disc regeneration," *European Spine Journal*, vol. 23, pp. 19 – 26, 2014.

[378] M. Barczewska, et al., "MR monitoring of minimally invasive delivery of mesenchymal stem cells into the porcine intervertebral disc," *PLoS ONE*, vol. 8, pp. e74658, 2013.

[379] G.W. Omlor, J. Fischer, K. Kleinschmitt, et al., "Short-term follow-up of disc cell therapy in a porcine nucleotomy model with an albumin–hyaluronan hydrogel: in vivo and in vitro results of metabolic disc cell activity and implant distribution," *European Spine Journal*, vol. 23, pp. 1837 – 1847, 2014.

[380] D. Sakai, J. Mochida, Y. Yamamoto, et al., "Transplantation of mesenchymal stem cells embedded in Atelocollagen® gel to the intervertebral disc: a potential therapeutic model for disc degeneration," *Biomaterials*, vol. 24, pp. 3531 – 3541, 2003.

[381] D. Sakai, J. Mochida, T. Iwashina, T. Watanabe, et al., "Differentiation of Mesenchymal Stem Cells Transplanted to a Rabbit Degenerative Disc Model," *Spine*, vol. 30, pp. 2379 – 2387, 2005.

[382] D. Sakai, J. Mochida, T. Iwashina, A. Hiyama et al., "Regenerative effects of transplanting mesenchymal stem cells embedded in atelocollagen to the degenerated intervertebral disc," *Biomaterials*, vol. 27, no. 3, pp. 335 – 345, 2006.

[383] Y.Y. Li, H.J. Diao, T.K. Chik, et al., "Delivering Mesenchymal Stem Cells in Collagen Microsphere Carriers to Rabbit Degenerative Disc: Reduced Risk of Osteophyte Formation," *Tissue Engineering: Part A*, vol. 20, pp. 1379 – 1390, 2014.

[384] G.W. Omlor, H. Bertram, K. Kleinschmidt, et al., "Methods to monitor distribution and metabolic activity of mesenchymal stem cells following in vivo injection into nucleotomized porcine intervertebral discs," *European Spine Journal*, vol. 19, pp. 601 – 612, 2010.

[385] A.A. Allon, et al., "Structured coculture of stem cells and disc cells prevent disc degeneration in a rat model," *Spine J.*, vol. 10, pp. 1089 – 1097, 2010.

[386] H. Yang, et al., "Transplanted mesenchymal stem cells with pure fibrinous gelatin-transforming growth factor-β1 decrease rabbit intervertebral disc degeneration," *Spine J.*, vol. 10, pp. 802 – 810, 2010.

[387] H. Wang, et al., "Utilization of stem cells in alginate for nucleus pulposus tissue engineering," *Tissue Eng. Part A*, vol. 20, pp. 908 – 920, 2014.

[388] Y. Zhang, S. Drapeau, S.A. Howard, et al., "Transplantation of goat bone marrow stromal cells to the degenerating intervertebral disc in a goat disc injury model," *Spine (Phila Pa 1976)*, vol. 36, no. 5, pp. 372 – 377, 2011.

[389] H.B. Henriksson, T. Svanvik, M. Jonsson, et al., "Transplantation of human mesenchymal stem cells into intervertebral discs in a xenogenieic porcine model," *Spine (Phila Pa 1976)*, vol. 34, no. 2, pp. 141 – 148, 2009.

[390] M. Bendtsen, C. Bunger, X. Zou, et al., "Autologous stem cell therapy maintains vertebral blood flow and contrast diffusion through the endplate in experimental intervertebral disc degeneration," *Spine (Phila Pa 1976)*, vol. 36, pp. E373 – E379, 2011.

[391] A. Tschugg, F. Michnacs, M. Strowitzki, H.J Meisel, C. Thome, "A prospective multicenter phase I/II clinical trial to evaluate safety and efficacy of NOVOCART Disc plus autologous disc chondrocyte transplantation in the treatment of nucleotomized and degenerative lumbar disc to avoid secondary disease: study protocol for a randomized controlled trial," *Trials*, vol. 17, pp. 1 – 10, 2016.

[392] D. Coric, K. Pettine, A. Sumich, M.O. Boltes, "Prospective study of disc repair with allogeneic chondrocytes presented at the 2012 Joint Spine Section Meeting," *Journal of Neurosurgery Spine*, vol. 18, pp. 85 – 95, 2013.

[393] T. Yoshikawa, Y. Ueda, K. Miyazaki, M. Koizumi, Y. Takakura, "Disc Regeneration Therapy Using Marrow Mesenchymal Cell Transplantation," *Spine*, vol. 35, pp. E475 - E480, 2010.

[394] H. Kumar, D. Ha, E. Lee, et al., "Safety and tolerability of intradiscal implantation of combined autologous adipose-derived mesenchymal stem cells and hyaluronic acid in patients with chronic discogenic low back pain: 1-year follow-up of a phase I study," *Stem Cell Res. Ther.*, vol. 8, no. 1, pp. 262, 2017.

[395] US National Library of Medicine – Clinical Trials.gov, Available at: https://clinicaltrials.gov/ct2/show/NCT01771471, [Accessed 2017].

[396] US National Library of Medicine – Clinical Trials.gov, Available at: https://clinicaltrials.gov/ct2/show/NCT01290367, [Accessed 2017].

[397] US National Library of Medicine – Clinical Trials.gov, Available at: https://clinicaltrials.gov/ct2/show/NCT02412735, [Accessed 2017].

[398] US National Library of Medicine – Clinical Trials.gov, Available at: https://clinicaltrials.gov/ct2/show/NCT01640457, [Accessed 2017].

[399] US National Library of Medicine – Clinical Trials.gov, Available at: https://clinicaltrials.gov/ct2/show/NCT02529566, [Accessed 2017].

[400] US National Library of Medicine – Clinical Trials.gov, Available at: https://clinicaltrials.gov/ct2/show/NCT02338271, [Accessed 2017].

[401] C. Wiltsey, P. Kubinski, T.R. Christiani, et al., "Characterization of injectable hydrogels based on poly(N-isopropylacrylamide)-g-chondroitin sulfate with adhesive properties for nucleus pulposus tissue engineering," *J. Mater. Sci. Mater. Med.*, vol. 24, no. 4, pp. 837 – 847, 2013.

[402] C. Wiltsey, T.R. Christiani, J. Williams, et al., "Thermogelling bioadhesive scaffolds for intervertebral disk tissue engineering: preliminary in vitro comparison of aldehyde-based versus alginate microparticle-mediated adhesion," *Acta Biomater*., vol. 16, pp. 71 – 80, 2015.

[403] T.R. Christiani, K. Toomer, J. Sheehan, et al., "Synthesis of thermogelling poly(N-isopropylacrylamide)-graft-chondroitin sulfate composites with alginate microparticles for tissue engineering," *J. Vis. Exp.*, no. 116, 2016.

[404] T.A. Holland, Y. Tabata, A.G. Mikos, "In vitro release of transforming growth factor-β1 from gelatin microparticles encapsulated in biodegradable, injectable oligo(poly(ethylene glycol) fumarate) hydrogels," *J. Control Release*, vol. 91, no. 3, pp. 299 – 313, 2003.

[405] X. Qi, X. Qin, R. Yang, et al., Intra-articular administration of chitosan thermosensitive in situ hydrogels combined with diclofenac sodium-loaded alginate microspheres," *J. Pharm. Sci.*, vol. 105, no. 1, pp. 122 – 130, 2016.

[406] R.J. DeVolder, I.W. Kim, E.S. Kim, H. Kong, "Modulating the rigidity and mineralization of collagen gels using poly(lactic-co-glycolic acid) microparticles," *Tissue Eng. Part A*, vol. 18, no. (15 – 16), pp. 1642 – 1651, 2012.

[407] A. Serrero, S. Trombotto, Y. Bayon, et al., "Polysaccharide-based adhesive for biomedical applications: correlation between rheological behavior and adhesion," *Biomacromolecules*, vol. 12, no. 5, pp. 1556 – 1566, 2011.

[408] P. Janmey, J.P. Winer, J.W. Weisel, "Fibrin gels and their clinical and bioengineering applications," *Journal of the Royal Society Interface*, vol. 6, no. 30, pp. 1 – 10, 2009.

[409] H. Kjaergard, U.S. Weis-Fogh, "Important factors influencing the strength of autologous fibrin glue; the fibrin concentration and reaction time-- comparison of strength with commercial fibrin glue," *European Surgical Research*, vol. 26, no. 5, pp. 273 – 276, 1994.

[410] K. Siedentop, D.M. Harris, B. Sanchez, "Autologous fibrin tissue adhesive: factors influencing bonding power," *Laryngoscope*, vol. 98, pp. 731 – 733, 1998.

[411] D. Sierra, D.S. Feldman, R. Saltz, S. Huang, "A method to determine shear adhesive strength of fibrin sealants," *Journal of Applied Biomaterials*, vol. 3, pp. 147 – 151, 1992.

[412] A. Colombini, C. Ceriani, G. Banfi, et al., "Fibrin inintervertebral disc tissue engineering," *Tissue Eng. Part B Rev*. vol. 20, no. 6, pp. 713 – 721, 2014.

[413] S.K. Bajpai, S. Sharma, "Investigation of swelling/degradation behaviour of alginate beads crosslinked with $Ca^{2+}$ and $Ba^{2+}$ ions," *React. Funct. Polym.*, vol. 59, pp. 129 – 140, 2004.

[414] M. Pope, M. Magnusson, "Kappa Delta Award. Low back and whole body vibration," *Clinical Orthopaedics & Related Research*, vol. 354, pp. 241 – 248, 1998.

[415] J. Iatridis, L.A. Setton, M. Weidenbaum, "The viscoelastic behavior of the non-degenerate human lumbar nucleus pulposus in shear," *Journal of Biomechanics*, vol. 30, no. 10, pp. 1005 – 1013, 1997.

[416] A. Vicente, M. Peroglio, M. Ernst, et al., "Self-Healing Dynamic Hydrogel as Injectable Shock-Absorbing Artificial Nucleus Pulposus," *Biomacromolecules*, vol. 18, pp. 2360 – 2370, 2017.

[417] P. Malafaya, G.A. Silva, R.L. Reis, "Natural-origin polymers as carriers and scaffolds for biomolecules and cell delivery in tissue engineering applications," *Advanced Drug Delivery Reviews*, vol. 59, pp. 207 – 233, 2007.

[418] H. Osterman, R. Sund, S. Seitsalo, I. Keskimaki, "Risk of Multiple Reoperations After Lumbar Discectomy: A population-based study," *Spine*, vol. 28, pp. 621 – 627, 2003.

[419] P. Heindel, A. Tuchman, P.C. Hsieh, et al., "Reoperation Rates After Single-level Lumbar Discectomy," *Spine*, vol. 42, no. 8, pp. E496 – E501, 2017.

[420] J. Cloyd, N.R. Malhotra, L. Weng, et al., "Material properties in unconfined compression of human nucleus pulposus, injectable hyaluronic acid-based hydrogels and tissue engineering scaffolds," *Eur. Spine J.*, vol. 16, no. 11, pp. 1892 – 1898, 2007.

[421] W. Johannessen, D.M. Elliott, "Effects of degeneration on the biphasic material properties of human nucleus pulposus in confined compression," *Spine (Phila Pa 1976)*, vol. 30, no. 24, pp. E724 – 729, 2005.

[422] C. Lee, J. Shin, J.S. Lee, et al., "Bioinspired, calcium-free alginate hydrogels with tunable physical and mechanical properties and improved biocompatibility," *Biomacromolecules*, vol. 14, no. 6, pp. 2004 – 2013, 2013.

[423] B.M. Minogue, S.M. Richardson, L.A. Zeef, et al., "Characterization of the human nucleus pulposus cell phenotype and evaluation of novel marker gene expression to define adult stem cell differentiation," *Arthritis Rheum.*, vol. 62, no. 12, pp. 3695 – 3705, 2010.

[424] A. Bertolo, M. Mehr, N. Aebli, et al., "Influence of different commercial scaffolds on the in vitro differentiation of human mesenchymal stem cells to nucleus pulposus-like cells," *Eur. Spine J.*, vol. 21 Suppl 6, pp. S826 – 838, 2012.

[425] J.V. Stoyanov, B. Gantenbein-Ritter, A. Bertolo, et al., "Role of hypoxia and growth and diffierentiation factor-5 on differentiation of human mesenchymal stem cells towards intervertebral nucleus pulposus-like cells," *Eur. Cell Mater.*, vol. 21, pp. 533 – 547, 2011.

[426] L.E. Clarke, J.C. Mcconnell, M.J. Sherratt, et al., "Growth differentiation factor 6 and transforming growth factor-beta differentially mediate mesenchymal stem cell differentiation, composition, and micromechanical properties of nucleus pulposus constructs," *Arthritis Res. Ther.*, vol. 16, no. 2, pp. R67, 2014.

[427] F. Mwale, P. Roughley, J. Antoniou, "Distinction between the extracellular matrix of the nucleus pulposus and hyaline cartilage: a requisite for tissue engineering of the intervertebral disc," *Eur. Cell Mater.*, vol. 8, pp. 58 – 63, 2004.

[428] A. Banerjee, M. Arha, S. Choudhary, et al., "The influence of hydrogel modulus on the proliferation and differentiation of encapsulated neural stem cells," *Biomaterials*, vol. 30, no. 27, pp. 4695 – 4699, 2009.

[429] R. Goldshmid, D. Seliktar, "Hydrogel modulus affects proliferation rate and pluripotency of human mesenchymal stem cells grown in three-dimensional culture," *ACS Biomater. Sci. Eng.*, vol. 3, no. 12, pp. 3433 – 3446, 2017.

[430] E. Potier, E. Ferreira, A. Meunier, et al., "Prolonged hypoxia concomitant with serum deprivation induces massive human mesenchymal stem cell death," *Tissue Eng*., vol. 13, no. 6, pp. 1325 – 1331, 2007.

[431] W. Zhu, J. Chen, X. Cong, et al., "Hypoxia and serum deprivation-induced apoptosis in mesenchymal stem cells," *Stem Cells*, vol. 24, no. 2, pp. 416 – 425, 2006.

[432] S.T. Ho, V.M. Tanavde, J.H. Hui, E.H. Lee, "Upregulation of adipogenesis and chondrogenesis in MSC serum-free culture," *Cell Med*., vol. 2, no. 1, pp. 27 – 41, 2011.

[433] H. Park, X. Guo, J.S. Temenoff, et al., "Effect of swelling ratio of injectable hydrogel composites on chondrogenic differentiation of encapsulated rabbit marrow mesenchymal stem cells in vitro," *Biomacromolecules*, vol. 10, no. 3, pp. 541 – 546, 2009.

[434] F. Lv, V.Y. Leung, S. Huang, et al., "In search of nucleus pulposus-specific molecular markers," *Rheumatology (Oxford)*, vol. 53, no. 4, pp. 600 – 610, 2014.

[435] A.A. Thorpe, A.L. Binch, L.B. Creemers, et al., "Nucleus pulposus phenotypic markers to determine stem cell differentiation: fact or fiction," *Oncotarget*, vol. 7, no. 3, pp. 2189 – 2200, 2016.

[436] S. Palomaki, M. Pietila, S. Laitnen S, et al., "HIF-1α is upregulated in human mesenchymal stem cells," *Stem Cells*, vol. 31, no. 9, pp. 1902 – 1909, 2013.

[437] A.A. Thorpe, V.L. Boyes, C. Sammon, C.L. Le Maitre, "Thermally triggered injectable hydrogel, which induces mesenchymal stem cell differentiation to nucleus pulposus cells: potential for regeneration of the intervertebral disc," *Acta Biomater*., vol. 36, pp. 99 – 111, 2016.

[438] H. Li H, C. Liang, Y. Tao, et al., "Acidic pH conditions mimicking degenerative intervertebral discs impair the survival and biological behavior of human adipose-derived mesenchymal stem cells," *Exp. Biol. Med. (Maywood)*, vol. 237, no. 7, pp. 845 – 852, 2012.

[439] D.R. Wagner et al., "Hydrostatic pressure enhance chondrogenic differentiation of human bone marrow stromal cells in osteochondrogenic medium," *Ann. Biomed. Eng.*, vol. 36, no. 5, pp. 813 – 820, May 2008.

[440] R. Ogawa et al., "The effect of hydrostatic pressure on three-dimensional chondroinduction of human adipose-derived stem cells," *Tissue Eng. Part A*, vol. 15, no. 15, pp. 2937 – 2945, Oct. 2009.

[441] D. Pelaez, C.Y. Huang, H.S. Cheung, "Cyclic compression maintains viability and induces chondrogenesis of human mesenchymal stem cells in fibrin gels scaffolds," *Stem Cells Dev.*, vol. 18, no. 1, pp. 93 – 102, 2009.

[442] Z. Li et al., "Chondrogenesis of human bone marrow mesenchymal stem cells in fibrin-polyurethane composites is modulated by frequency and amplitude of dynamic compression and shear stress," *Tissue Eng. Part A*, vol. 16, no. 2, pp. 575 – 584, Feb. 2010.

[443] S.N. Tzouanas, A.K. Ekenseair, F.K. Kasper, A.G. Mikos, "Mesenchymal stem cell and gelatin microparticle encapsulation in thermally and chemically gelling injectable hydrogels for tissue engineering," *J. Biomed. Mater. Res. A*, vol. 102, no. 5, pp. 1222 – 1230, 2014.

[444] S. Lu S, E.J. Lee, J. Lam, et al., "Evaluation of gelatin microparticles as adherent-substrates for mesenchymal stem cells in a hydrogel composite," *Ann. Biomed Eng.*, vol. 44, no. 6, pp. 1894 – 1907, 2016.

[445] P. Brinckmann, M. Horst, "The influence of vertebral body fracture, intradiscal injection, and partial discectomy on the radial bulge and height of human lumbar discs," *Spine (Phila Pa 1976)*, vol. 10, no. 2, pp. 138 – 145, 1985.

[446] A. Arthur, M. Cannella, M. Keane, et al., "Fill of the nuclear cavity affects mechanical stability in compression, bending, and torsion of a spine segment, which has undergone nucleus replacement," *Spine (Phila Pa 1976)*, vol. 35, no. 11, pp. 1128 – 1135, 2010.

[447] M. Cannella, J.L. Isaacs, S. Allen, et al., "Nucleus implantation: the biomechanics of augmentation versus replacement with varying degrees of nucleotomy," *Journal of Biomechanical Engineering*, vol. 136, pp. 051001-1 – 051001-9, 2014.

[448] N.R. Malhotra, W.M. Han, J. Beckstein, et al., "An injectable nucleus pulposus implant restores compressive range of motion in the ovine disc," *Spine*, vol. 37, no. 18, pp. E1099 – 1105, 2012.

[449] D.M. Varma, H.A. Lin, R. Long, et al., "Thermoresponsive, redox-polymerized cellulosic hydrogels undergo in situ gelation and restore intervertebral disc biomechanics post discectomy," *Eur. Cell Mater.*, vol. 35, pp. 300 – 317, 2018.

[450] S.E. Gullbrand, T.P. Schaer, P. Agarwal, et al., "Translation of an injectable triple-interpenetrating-network hydrogel for intervertebral disc regeneration in a goat model," *Acta Biomater.*, vol. 60, pp. 201 – 209, 2017.

[451] G.D. O'Connell, E.J. Vresilovic, D.M. Elliott, "Comparison of animals used in disc research to human lumbar disc geometry," *Spine (Phila Pa 1976)*, vol. 32, no. 3, pp. 328 – 333, 2007.

[452] A. Joshi, G. Fussell, J. Thomas, et al., "Functional compressive mechanics of a PVA/PVP nucleus pulposus replacement," *Biomaterials*, vol. 27, no. 2, pp. 176 – 184, 2006.

[453] B.L. Showalter, D.M. Elliott, W. Chen, N.R. Malhotra, "Evaluation of an in situ gelable and injectable hydrogel treatment to preserve human disc mechanical function undergoing physiologic cyclic loading followed by hydrated recovery," *J. Biomech. Eng.*, vol. 137, no. 8, pp. 081008, 2015.

[454] S. Reitmaier, U. Wolfram, A. Ignatius, et al., "Hydrogels for nucleus replacement—Facing the biomechanical challenge," *Journal of the Mechanical Behavior of Biomedical Materials*, vol. 14, pp. 67 – 77, 2012.

[455] M.H. Pelletier, C.S. Cohen, P. Ducheyne, W.R. Walsh, "Restoring segmental biomechanics through nucleus augmentation: an in vitro study," *Clin. Spine Surg.*, vol. 29, no. 10, pp. 461 – 467, 2016.

[456] C. Balkovec, A.J. Vernengo, S.M. McGill, "The use of a novel injectable hydrogel nucleus pulposus replacement in restoring the mechanical properties of cyclically fatigued porcine intervertebral discs," *J. Biomech. Eng.*, vol. 135, no. 6, pp. 610045 – 61005, 2013.

[457] C. Balkovec, A.J. Vernengo, S.M. McGill, "Disc height loss and restoration via injectable hydrogel influences adjacent segment mechanics in-vitro," *Clin. Biomech. (Bristol Avon)*, vol. 36, pp. 1 – 7, 2016.

[458] S.R. Sloan Jr., D. Galesso, C. Secchieri, et al., "Initial investigation of individual and combined annulus fibrosus and nucleus pulposus repair ex vivo," *Acta Biomater.*, vol. 59, pp. 192 – 199, 2017.

[459] W. Johannesssen, J.M. Cloyd, G.D. O'Connell, et al., "Trans-endplate nucleotomy increases deformation and creep response in axial loading," *Ann. Biomed. Eng.*, vol. 34, no. 4, pp. 687 – 696, 2006.

[460] E.J. Vresilovic, W. Johannessen, D.M. Elliott, "Disc mechanics with trans-endplate partial nucleotomy are not fully restored following cyclic compressive loading and unloaded recovery," *J. Biomech. Eng.*, vol. 128, no. 6, pp. 823 – 829, 2006.

[461] A. Bernkop-Schnurch, C.E. Kast, M.E. Richter, "Improvement in the mucoadhesive properties of alginate by the covalent attachment of cysteine," *J. Control Release*, vol. 71, no. 3, pp. 277 – 285, 2001.

[462] A.J. Michalek, M.R. Buckley, L.J. Bonassar, et al., "The effects of needle puncture injury on microscale shear strain in the intervertebral disc annulus fibrosus," *Spine J.*, vol. 10, no. 12, pp. 1098 – 1105, 2010.

[463] R.M. Schek, A.J. Michalek, J.C. Iatridis, "Genipin-crosslinked fibrin hydrogels as a potential adhesive to augment intervertebral disc annulus repair," *Eur. Cell Mater.*, vol. 21, pp. 373 – 383, 2011.

[464] R. Long, A. Burki, P. Zysset, et al., "Mechanical restoration and failure analyses of a hydrogel and scaffold composite strategy for annulus fibrosus repair," *Acta Biomater.*, vol. 30, pp. 116 – 125, 2016.

[465] M.A. Cruz, W.W. Hom, T.J. DiStefano, et al., "Cell-seeded adhesive biomaterial for repair of annulus fibrosus defects in intervertebral discs," *Tissue Eng. Part A*, vol. 24, no. (3 – 4), pp. 187 – 198, 2018.

[466] O. Guillaume, A. Daly, K. Lennon, et al., "Shape-memory porous alginate scaffolds for regeneration of the annulus fibrosus: effect of TGF-β supplementation and oxygen culture conditions," *Acta Biomater.*, vol. 10, no. 5, pp. 1985 – 1995, 2014.

[467] G.Q. Teixeira, C.L. Pereira, J.R. Ferreira, et al., "Immunomodulation of human mesenchymal stem/stromal cells in intervertebral disc degeneration: insights from a proinflammatory/degenerative ex vivo model," *Spine (Phila Pa 1976)*, vol. 43, no. 12, pp. E673 – E682, 2018.

[468] D. Sakai, J. Mochida, T. Iwashina, et al., "Differentiation of mesenchymal stem cells transplanted to a rabbit degenerative disc model," *Spine (Phila Pa 1976)*, vol. 30, no. 21, pp. 2379 – 2387, 2005.

[469] H.B. Henriksson, T. Svanvik, M. Jonsson, et al., "Transplantation of human mesenchymal stem cells into intervertebral discs in a xenogeneic porcine model," *Spine (Phila Pa 1976)*, vol. 34, no. 2, pp. 141 – 148, 2009.

[470] I. Hussain, S.R. Sloan Jr., C. Wipplinger, et al., "Mesenchymal stem cell-seeded high-density collagen gel for annular repair: 6-week results from in vivo sheep models," *Neurosurgery*, 2018. [Epub ahead of print].

[471] X. Xu, J. Hu, H. Lu, "Histological observation of a gelatin sponge transplant loaded with bone marrow-derived mesenchymal stem cells combined with platelet-rich plasma in repairing an annulus defect," *PLoS One*, vol. 12, no. 2, pp. e0171500, 2017.

[472] H. Oshima, H. Ishihara, J. Urban, H. Tsuji, "The use of coccygeal discs to study intervertebral disc metabolism," *J. Orthop. Res.*, vol. 11, no. 3, pp. 332 – 338, 1993.

[473] C.N. Demers, J. Antoniou, F. Mwale, "Value and limitations of using the bovine tail as a model for the human lumbar spine," *Spine (Phila Pa 1976)*, vol. 29, no. 24, pp. 2793 – 2799, 2004.

[474] J.C. Beckstein, S. Sen, T.P. Schaer, et al., "Comparison of animals discs used in disc research to human lumbar disc: axial compression mechanics and glycosaminoglycan content," *Spine (Phila Pa 1976)*, vol. 33, no. 6, pp. E166 – E173, 2008.

[475] B.L. Showalter, J.C. Beckstein, J.T. Martin, et al., "Comparison of animal discs in disc research to human lumbar disc: torsion mechanics and collagen content," *Spine (Phila Pa 1976)* vol. 37, no. 15, pp. E900 – E907, 2012.

[476] S. Roberts, H. Evans, J. Trivedi, J. Menage, "Histology and pathology of the human intervertebral disc," *J. Bone Joint Surg. Am.*, vol. 88, no. Suppl 2, pp. 10 – 14, 2006.

[477] T. Saggese, P. Redey, S.R. McGlashan, "Same-species phenotypic comparison of notochordal and mature nucleus pulposus cells," *Eur. Spine J.*, vol. 24, no. 9, pp. 1976 – 1985, 2015.

[478] H.E. Gruber, H.J. Norton, J.A. Ingram, E.N. Hanley Jr., "The SOX9 transcription factor in the human disc: decreased immunolocalization with age and disc degeneration," *Spine (Phila Pa 1976)*, vol. 30, no. 6, pp. 625 – 630, 2005.

[479] K.Y. Ha, I.J. Koh, P.A. Kirpalani, et al., "The expression of hypoxia inducible factor-1α and apoptosis in herniated discs," *Spine (Phila Pa 1976)*, vol. 31, no. 12, pp. 1309 – 1313, 2006.

[480] J. Rutges, L.B. Creemers, W. Dhert, et al., "Variations in gene and protein expression in human nucleus pulposus in comparison with annulus fibrosus and cartilage cells: potential associations with aging and degeneration," *Osteoarthritis Cartilage*, vol. 18, no. 3, pp. 416 – 423, 2010.

[481] B.M. Minogue, S.M. Richardson, L.A. Zeef, et al., "Transcriptional profiling of bovine intervertebral disc cells: implications for identification of normal and degenerate human intervertebral disc cell phenotypes," *Arthritis Res. Ther.*, vol. 12, no. 1, pp. R22, 2010.

[482] C.L. Korecki, J.J. MacLean, J.C. Iatridis, "Characterization of an in vitro intervertebral disc organ culture system," *Eur. Spine J.*, vol. 16, no. 7, pp. 1029 – 1037, 2007.

[483] B. Jim, T. Steffen, J. Moir, et al., "Development of an intact intervertebral disc organ culture system in which degeneration can be induced as a prelude to studying repair potential," *Eur. Spine J.*, vol. 20, no. 8, pp. 1244 – 1254, 2011.

[484] M. Grant, L.M. Epure, O. Salem, et al., "Development of a large animal long-term intervertebral disc organ culture model that includes the bony vertebrae for ex vivo studies," *Tissue Eng. Part C Methods*, vol. 22, no. 7, pp. 636 – 643, 2016.

[485] S.C. Chan and B. Gantenbein-Ritter, "Preparation of intact bovine tail intervertebral discs for organ culture," *J. Vis. Exp.*, no. 6, 2012.

[486] S.C. Chan, A. Burki, H.M. Bonel, et al., "Papain-induced in vitro disc degeneration model for the study of injectable nucleus pulposus therapy," *Spine J.*, vol. 13, no. 3, pp. 273 – 283, 2013.

[487] S. Roberts, J. Menage, S. Sivan, J. Urban, "Bovine explant model of degeneration of the intervertebral disc," *BMC Musculoskeletal Disord*, vol. 9, pp. 24, 2008.

[488] S.C. Chan, B. Gantenbein-Ritter, V.Y. Leung, et al., "Cryopreserved intervertebral disc with injected bone marrow-derived stromal cells: a feasibility study using organ culture," *Spine J.*, vol. 10, no. 6, pp. 486 – 496, 2010.

[489] C. Malonzo, S.C. Chan, A. Kabiri, et al., "A papain-induced disc degeneration model for the assessment of thermos-reversible hydrogel-cells therapeutic approach," *J. Tissue Eng. Regen. Med.*, vol. 9, no. 12, pp. E167 – E176, 2015.

[490] M. Peroglio, L.S. Douma, T.S. Caprez, et al., "Intervertebral disc response to stem cell treatment is conditioned by disc state and cell carrier: an ex vivo study," *J. Orthop. Translat.*, vol. 9, pp. 43 – 51, 2017.

[491] N.S. Hwang, S. Varghese, H. Li, J. Elisseeff, "Regulation of osteogenic and chondrogenic differentiation of mesenchymal stem cells in PEG-ECM hydrogels," *Cell Tissue Res.*, vol. 344, no. 3, pp. 499 – 509, 2011.

[492] C.M. Murphy, A. Matsiko, M.G. Haugh, et al., “Mesenchymal stem cell fate is regulated by the composition and mechanical properties of collagen-glycosaminoglycan scaffolds,” *J. Mech. Behav. Biomed. Mater.*, vol. 11, pp. 53 – 62, 2012.

[493] Y. Wu, Z. Yang, J.B. Law, et al., “The combined effect of substrate stiffness and surface topography on chondrogenic differentiation of mesenchymal stem cells,” *Tissue Eng. Part A*, vol. 23, no. (1 – 2), pp. 43 – 54, 2017.

[494] D. Sakai and J. Schol, “Cell therapy for intervertebral disc repair: clinical perspective,” *J. Orthop. Translat.*, vol. 9, pp. 8 – 18, 2017.